Development of Organosilane–Containing Bioorganometallic Compounds Evaluated as Antiparasitic Agents Against *Plasmodium falciparum* and *Trichomonas vaginalis*

Muneebah Adams

University of Cape Town

June 2016

Development of Organosilane–Containing Bioorganometallic Compounds Evaluated as Antiparasitic Agents Against *Plasmodium falciparum* and *Trichomonas vaginalis*

Thesis presented for the degree of

Doctor of Philosophy

by

Muneebah Adams

Department of Chemistry

University of Cape Town

Supervisor: Assoc. Prof. G. S. Smith
Co-supervisor: Prof. K. Chibale

June 2016

DECLARATION

I declare that "**Development of Organosilane–Containing Bioorganometallic Compounds Evaluated as Antiparasitic Agents Against *Plasmodium falciparum* and *Trichomonas vaginalis***" is my own work and has never been submitted for examination for any degree at any university. All sources of information used are acknowledged, cited and completely referenced at the end of each chapter.

Signed by candidate

.....

Muneebah Adams

01/ 06/ 2016

ACKNOWLEDGEMENTS

I would like to express my greatest gratitude to my supervisors Assoc. Prof. Gregory S. Smith and Prof. Kelly Chibale. As a lecturer during my undergraduate years, Assoc. Prof Gregory Smith inspired my interest in organometallic chemistry which has remained to this day. Thus, I am forever grateful to my supervisors for the continued guidance and encouragement during this project.

Special Thanks to the Organometallic Research Group. Being a member of this group has allowed for growth on both an intellectual and personal level, has allowed for an environment of work and fun and it has allowed for collegial relations which may extend to professional relations later in life. I would also like to thank Dr. T. Stringer for taking the time to read chapter drafts and teaching me how to carry out the β–haematin assays and Mr. A. Burgoyne for anticancer screening.

I would like to extend my thanks to Dr. L. Wiesner, Prof. P. J. Smith and the Clinical Pharmacology Group at UCT Medical School for welcoming me into their group and assisting with the pre–clinical working. Thank you to Dr C. de Kock for antimalarial screenings, Prof. H. Hundt for assistance with method development work, as well as Dr L. Gibhard and Mr T. Finch for assistance with the animal work. Thank you to Mr. N. Salie for ensuring that I had all the tools required to complete the study.

I would like to thank the Medical Chemistry Group, as well as Dr. M. Njoroge for assistance with the metabolic stability studies.

I would also like to acknowledge the following people for their assistance during this project, Mr P. Roberts for recording come of the NMR spectra, Mr G. Benincasa for microanalytical analyses and electron impact mass spectral analyses, Dr M. Stander and Mr. F. Hiten (University of Stellenbosch) for electrospray ionisation mass spectral analyses and Dr H. Su for Single-crystal X-ray diffraction analyses. Furthermore, I would also like to thank Associate

Professor K. M. Land and his research group (University of the Pacific) for conducting the *T. vaginalis* studies, Professor D. T. Hendricks and Mrs H. Guzgay (UCT's Division of Medical Biochemistry) for conducting anticancer experiments.

The greatest thanks goes to my parents who have been there right from the start. Their continued encouragement and support throughout the years is the reason that I have managed to reach this point. Thank you for sitting through practice sessions for presentations and for reading chapters drafts.

Thank you to Shakeela Sayed, Shankari Nair, Gadija Akleker, Ashleigh Maart Hartzenberg, Natalie Collop, Ashley Hartzenberg, Chad Willemse and Jeffery Williams for their friendship, encouragement and support both at and off campus. Further thanks to Shakeela for soldiering through the reading of my chapters while completing your own degree.

For funding, I would like to thank the University of Cape Town, the Department of Science and Technology and the National Research Foundation (NRF).

ABSTRACT

Many successful initiatives have been employed to stem the spread of the diseases such as malaria and trichomoniasis. However, in cases where infection has occurred, pharmaceutical treatments are required. A problem seen across the board is the development of resistance to known treatments. An even bigger problem has been the development of resistance to promising compounds during the clinical trial phase. This has led to the need for effective treatments which are able to overcome the resistance problem.

This study investigated the synthesis, characterisation and pharmacological evaluation of new bioorganometallic organosilane–containing compounds based on thiosemicarbazone (TSC), quinoline and benzothiazole scaffolds. Selected thiosemicarbazone–containing ruthenium(II), rhodium(III) and palladium(II) metal complexes were also studied. The compounds were screened for antiplasmodial and antitrichomonal activity, along with their activity against A2780 human ovarian carcinoma and WHCO1 oesophageal cancer cell–lines.

A series of ferrocenyl– and aryl–derived organosilane thiosemicarbazones were synthesised, along with an aryl–derived carbon analogue. Coordination of these thiosemicarbazones with $[Ru(\eta^6\text{-}p\text{-}^{i}PrC_6H_4Me)Cl_2]_2$ and $[Rh(Cp^*)Cl_2]_2$ yielded *N,S*–chelated heterobimetallic ferrocenyl–derived TSC and mononuclear aryl–derived TSC complexes. Furthermore, *ortho*–cyclopalladated complexes were prepared *via* C–H activation of selected thiosemicarbazones by *cis*–$[Pd(PTA)_2Cl_2]$. These compounds were fully characterised using NMR (^{1}H, $^{13}C\{^{1}H\}$, $^{31}P\{^{1}H\}$, COSY, HSQC) spectroscopy, infrared spectroscopy and mass spectrometry [electron impact, electrospray ionisation].

The thiosemicarbazone–based compounds were evaluated for their antiplasmodial activity against the NF54 chloroquine−sensitive (CQS) and Dd2 chloroquine−resistant (CQR) strains of *Plasmodium falciparum*. The aryl–derived cyclopalladated complexes were found to be the most potent, displaying activity below 1 μM against both strains. Furthermore, the organosilane–containing compounds were generally less toxic when screened against the Chinese Hamster Ovarian (CHO) cell–line. One of the biological targets of antimalarial

compounds is haemozoin. Therefore, a metal−free TSC and selected rhodium(III) complexes were screened to investigate their ability to inhibit β–haematin formation (synthetic haemozoin). The rhodium complexes displayed inhibitory effects on the formation of β–haematin. Subsequent to the *in vitro* studies mentioned above, an aryl–derived organosilane–containing cyclopalladated complex was further evaluated in an *in vivo P. berghei* infected mouse model. No significant effect on percentage parasitaemia was observed.

The thiosemicarbazone compounds were also screened against the metronidazole−sensitive G3 strain of *Trichomonas vaginalis* to establish if thiosemicarbazones are selective towards particular parasites. The ruthenium and rhodium complexes were the most effective growth inhibitors of *T. vaginalis* parasites, generally displaying inhibition above 90 %. Following on from the screening against parasites, selected ferrocenyl–derived thiosemicarbazone compounds were evaluated against cisplatin–sensitive (A2780) and cisplatin–resistant (A2780cisR) tumourigenic cell–lines, where the ruthenium complex exhibited the highest cytotoxicity against both cell–lines (IC_{50} = 12.4 and 18.9 μM, respectively). The tested compounds were further tested against the non−tumourigenic KMST-6 human fibroblast cells and displayed similar activities compared to the cancer cell–lines.

A series of ferrocenyl–containing aminoquinolines, consisting of both organosilane and carbon analogues, were prepared and fully characterised using NMR (^{1}H; $^{13}C\{^{1}H\}$; COSY; HSQC) spectroscopy, infrared spectroscopy and electron impact mass spectrometry. The structure of the ferrocenyl–containing aminoquinolines were further confirmed by the molecular structures of two compounds which were determined using single−crystal X−ray diffraction. Both compounds crystallise in a folded conformation due to intramolecular hydrogen bonding between the nitrogen atoms on opposite sides of the ferrocenyl moiety.

Following on from the aminoquinoline compounds, a series of ferrocenyl–containing aminobenzothiazoles, consisting of both organosilane and carbon analogues, were synthesised and fully characterised using NMR (^{1}H; $^{13}C\{^{1}H\}$; COSY) spectroscopy, infrared spectroscopy and mass spectrometry (Electron Impact; Electrospray Ionisation).

The ferrocenyl–containing aminoquinolines and aminobenzothiazoles were screened for their activity against NF54 and Dd2 strains of *P. falciparum*. The aminoquinolines were generally

more effective than the aminobenzothiazoles. However, the aminobenzothiazoles were more selective towards the resistant strain than the sensitive. Additionally, the aminoquinolines were effective inhibitors of β–haematin formation, as opposed to the aminobenzothiazole compound which displayed no inhibitory effects. Metabolic stability studies of the aminoquinolines revealed that the compounds metabolise more quickly than ferroquine. When evaluated against the *T. vaginalis*, the ferrocenyl−containing aminoquinolines and aminobenzothiazoles displayed inhibitory effects of parasite growth with moderate IC_{50} values. Further studies against the WHCO1 oesophageal cancer cell–line revealed that the aminoquinoline and aminobenzothiazole compounds displayed cytotoxicity, with the aminobenzothiazole (IC_{50} = 1.74 μM) displaying good potency.

PUBLICATIONS

Journal Articles

- *Improved antiparasitic activity by incorporation of organosilane entities into half-sandwich ruthenium(II) and rhodium(III) thiosemicarbazone complexes.*
  M. Adams, C. de Kock, P. J. Smith, K. M. Land, N. Liu, M. Hopper, A. Hsiao, A. R. Burgoyne, T. Stringer, M. Meyer, L. Wiesner, K. Chibale and G. S. Smith, *Dalton Transactions*, 2015, **44**, 2456-2468.

- *Cyclopalladated Organosilane–Tethered Thiosemicarbazones: Novel Strategies for Improving Antiplasmodial Activity.*
  M. Adams, Linley Barnard, C. de Kock, P. J. Smith, L. Wiesner, K. Chibale and G. S. Smith, *Dalton Transactions*, 2016,**45**, 5514-5520.

Conferences and Symposia

- **12th European Biological Inorganic Chemistry (EUROBIC) conference:** Zurich, Switzerland, 24th – 28th August 2014, Poster presentation, M. Adams, L. Wiesner, K. Chibale and G. S. Smith − *Evaluation of novel ruthenium(II)- and rhodium(III)-organosilane thiosemicarbazone complexes as potential anti-parasitic agents*.

- **Young Chemists Symposium:** Cape Town, South Africa, 23rd October 2014, Poster presentation, M. Adams, L. Wiesner, K. Chibale and G. S. Smith − *Evaluation of novel ruthenium(II)- and rhodium(III)-organosilane thiosemicarbazone complexes as potential anti-parasitic agents*.

- **INORG2015:** Grahamstown, South Africa, 28th June – 2nd July 2015, Flash Talk and Poster presentation, M. Adams, L. Wiesner, K. Chibale and G. S. Smith − *Exploring the potential antiparasitic properties of Ru(II) and Rh(III) organosilane thiosemicarbazone complexes*.

- **1st International Symposium on Clinical and Experimental Metallodrugs in Medicine:** Honolulu, Hawaii, 12th – 15th December 2015, Poster presentation, M. Adams, H. Guzgay, D. T. Hendricks, K. Chibale, G. S. Smith – *Exploring the potential biological properties of organometallic organosilane heterocyclic compounds.*

ABBREVIATIONS AND SYMBOLS

δ	Chemical shift
ACT	Artemisinin–based Combination Therapy
ADME	Absorption Distribution Metabolism and Excretion
ATR	Attenuated Total Reflectance (IR)
br	Broad (NMR)
CHO	Chinese Hamster Ovarian
COD	1,5-Cyclooctadiene
COSY	Correlation Spectroscopy
Cp	Cyclopentadiene
Cp*	1,2,3,4,5-Pentamethylcyclopentadiene
CQ	Chloroquine
CQDP	Chloroquine Diphosphate
CQR	Chloroquine−Resistant
CQS	Chloroquine−Sensitive
d	Doublet (NMR)
dd	Doublet of Doublets
Decomp.	Decomposition
ED_{50}	Dose that produces an effective response in 50% of the tests
EI	Electron Impact
ESI	Electrospray Ionisation
eq.	Equivalents
FACS	Fluorescence−Activated Cell Sorting
Fc	Ferrocenyl
FDA	Food and Drug Administration
FT	Fourier Transform
GFP	Green Fluorescent Proteins
Hb	Haemoglobin
HPLC	High Pressure Liquid Chromatography
HPMC	Hydroxypropyl Methylcellulose
HSQC	Heteronuclear Single Quantum Coherence
HRMS	High Resolution Mass Spectrometry
Hz	Hertz
IC_{50}	Minimum concentration of test compound to induce 50% cell growth inhibition

ICP−MS	Inductively Coupled Plasma Mass Spectrometry
^{i}Pr	Isopropyl
IP	Intraperitoneally
IR	Infrared
J	Coupling Constant
Lit.	Literature
m	Multiplet (NMR); Medium intensity (IR)
Me	Methyl
MHz	Megahertz
M.P.	Melting Point
MS	Mass Spectrometry
MTT	3-(4,5-Dimethylthiazol-2-yl)-2,5-diphenyltetrazolium bromide
m/z	Mass–to–Charge Ratio (MS)
NMR	Nuclear Magnetic Resonance
NP–40	Nonyl phenoxypolyethoxylethanol
***Pf*CRT**	*P. falciparum* Chloroquine Resistance Transporter
ppm	Parts Per Million
PTA	1,3,5-Triaza-7-phosphaadamantane
q	Quartet (NMR)
RBC	Red Blood Cells
RI	Resistance Index
r.t.	Room temperature
s	Singlet (NMR); Strong Intensity (IR)
SEM	Scanning Electron Microscope
SI	Selectivity Index
t	Triplet (NMR)
***t*½**	Half−Life
t_R	Retention Time
TSC	Thiosemicarbazone
UV	Ultraviolet
vis	Visible
w	Weak Intensity (IR)
w/o	Without
WST-1	4-[3-(4-iodophenyl)-2-(4-nitrophenyl)-2H-5-tetrazolio]-1,3-benzene disulfonate

TABLE OF CONTENTS

CHAPTER 2

Synthesis and Characterisation of Mono– and Binuclear Organosilane Thiosemicarbazone Metal Complexes

CHAPTER 4

Synthesis and Characterisation of Organosilane Derivatives of Heterocyclic Compounds Containing Quinoline and Benzothiazole

CHAPTER 7

Experimental Section

CHAPTER 1

Literature review

1.1 Introduction

Parasites can inhabit organisms such as insects, plants, animals and humans. Parasites may either use the host organism only as a breeding ground (carrier) while waiting for the opportunity to infect another organism, or the organism can be infected as well as affected by the parasite. Overlooking the impact on food supplies when animals such as cattle are infected by parasites, another major concern is the effect parasites have on human beings. The effects of parasitic diseases may range from a simple cold to death, therefore the management and treatment of parasitic diseases is crucial.

1.2 Malaria

Malaria, a disease caused by the *Plasmodium* protozoan parasite, is transmitted by certain types of female *Anopheles* mosquitoes which function as carrier organisms. Five species of plasmodium are reported to infect humans, namely *Plasmodium falciparum*, *P. vivax*, *P. malariae*, *P. ovale* and *P. knowlesi* (originally an ape strain).[1] *P. falciparum* and *P. vivax* are the most prevalent, with *P. falciparum* being the most deadly species.

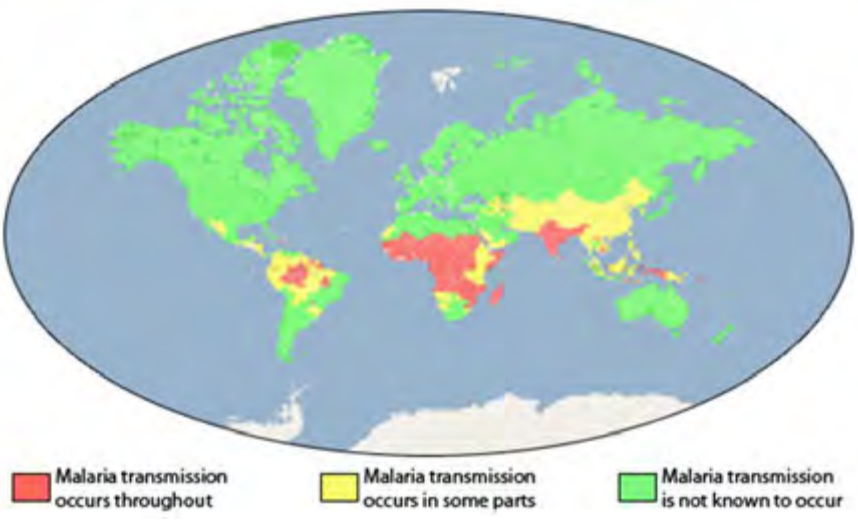

Figure 1.1 A world map illustrating the different regions affected by malaria.[2]

In areas such as the tropical and subtropical regions (Figure 1.1) with ideal climate conditions for parasite reproduction (e.g. humidity), as well as densely populated areas which allow for the

easy transmission from mosquito to human and vice versa, the survival of the parasite is ensured. Therefore, areas which meet these conditions, such as Africa, are affected with 90 % of the 198 million clinical cases reported in 2013.[3] Treatments may aid in reducing the number of reported cases. Therefore, understanding how the parasite reproduces, particularly identifying the stages which can be targeted by potential drugs, is an important aspect to be familiar with.

1.2.1 Life cycle of the parasite

The first step in the life cycle of the malaria parasite involves infection of the human host by a female Anopheles mosquito carrying the malaria-causing parasites, in the form of sporozoites, into the bloodstream (Figure 1.2). The sporozoites travel to the liver *via* the bloodstream and invade liver cells where sporozoites develop into merozoites. However, some malaria parasite species do not immediately start the conversion process from sporozoites to merozoites and instead remain dormant in the liver, causing patient relapses weeks or months later.[4]

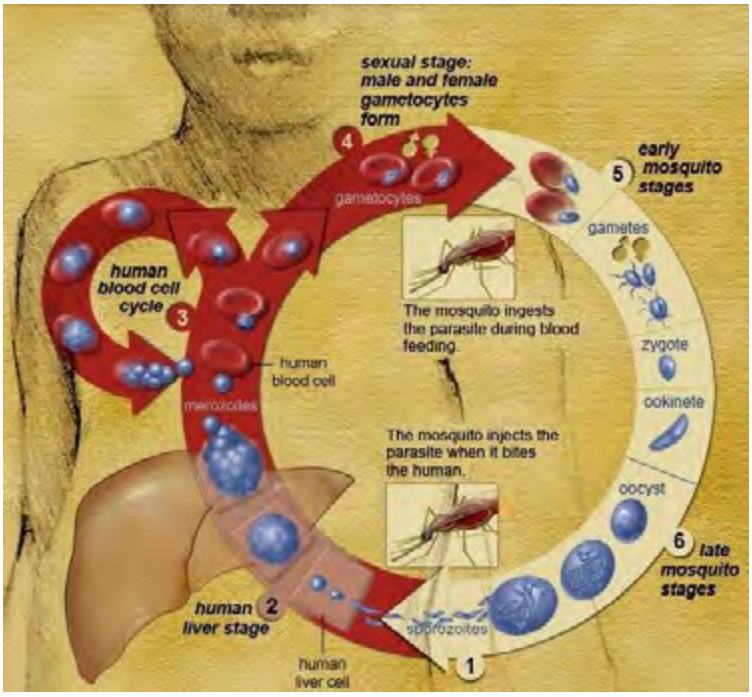

Figure 1.2 Life cycle of the malaria parasite.[5]

Merozoites enter the bloodstream where the red blood cells are invaded, and over the course of 1−3 days of asexual replication, leads to the formation and release of thousands of merozoites which in turn leads to illness if not treated (Figure 1.2). A portion of the merozoite−infected blood cells are involved in the development of the parasite into gametocytes (male and female sexual forms). These merozoite−infected blood cells circulate in the bloodstream and are

available for ingestion by the next mosquito, which bites the infected host, thereby facilitating transmission of the parasite.[4] Further development of the parasite occurs within the gut of the mosquito. Following the bursting of infected blood cells, gametocytes are released and develop into mature sex cells called gametes. The fusing of male and female gametes leads to the formation of diploid zygotes which develop into ookinetes. Further development to oocytes occurs in the midgut wall. After replication of oocytes, sporozoites are formed which are available to be transferred to the next host.[4]

1.2.2 Survival and defence mechanism of the malaria parasite

Infection of the host organism by plasmodium initiates a series of events allowing for parasite survival (Figure 1.3). The first step involves ingestion and transportation of haemoglobin to the parasite's digestive vacuole where various proteases such as the cysteine proteases (falcipains II and III)[6], metalloprotease falcilysin[7] and aspartic proteases plasmepsin[8] are employed in the digestion of haemoglobin to short peptides. These peptides are transported out of the digestive vacuole and converted to amino acids which are the parasite's food source.

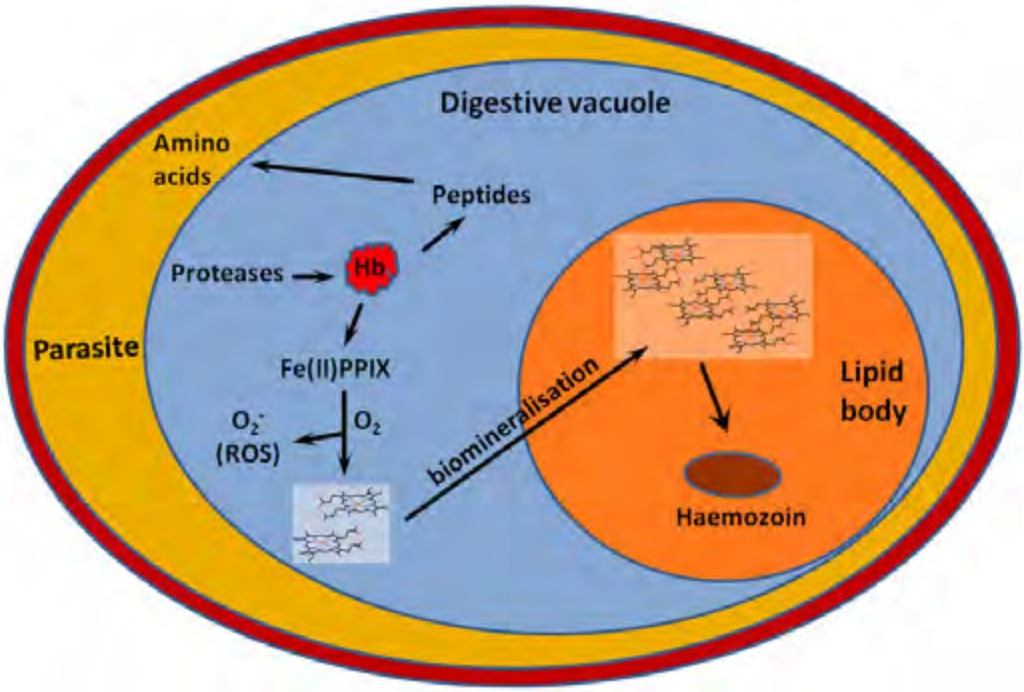

Figure 1.3 The proposed sequence of events following haemoglobin degradation.

Upon degradation of haemoglobin, free haem is released. Oxidation of the iron in free haem, from Fe(II) to Fe(III), by molecular dioxygen produces ferriprotoporphyrin IX (Fe(III)PPIX) and reactive oxygen species (ROS), namely hydroxyl radicals. Hydroxyl radicals are known to be

disruptive to lipid membranes; leading to the death of the parasites.[9] However, the parasite has developed a defence mechanism whereby the cytotoxic haematin is converted to non-toxic haemozoin *via* biomineralisation. Haematin dimers, linked *via* hydrogen bonds between the iron and the propionic acid side chain of the adjacent haem, are able to form chains. The chains, which exist due to the hydrogen bonded propionic acid side chains, form low solubility haemozoin crystals (β−haematin) which accumulate in the food vacuole.[10]

1.2.3 Current and previously used antimalarial treatments

Throughout the years, various compounds have been synthesised and evaluated as antiplasmodial agents, with a select few compounds becoming successful antimalarial drugs. The treatment of malaria using quinoline−based compounds such as quinine and chloroquine became a popular route. However, despite the success of these antimalarial drugs, other classes of compounds were explored to circumvent the parasite developing resistance to the treatments. A method to prevent resistance development is through treatment with compounds which operate *via* a variety of mechanisms. One class of compounds evaluated were artemisinin and its analogues.

Artemisinin and its analogues operate *via* the formation of ROS. Reactive oxygen species are generated by the cleavage of the peroxide bond in the 1,2,4-trioxane core of artemisinin−type compounds (**1.1**; Figure 1.4).[11] In an attempt to slow down the emergence of resistance, artemisinin−based combination therapies (ACTs) were developed.[12] ACTs comprise of two antimalarial drugs, which act *via* different mechanisms, and at different rates, are used in combination to combat resistant strains. The combination involves the use of a fast acting artemisinin derivative and a compound with a longer half−life.[13] Therefore, artemisinin derivatives such as artemether (**1.2**; Figure 1.4) are marketed as combination therapies such as Coartem™ [artemether/lumefantrine (**1.3**; Figure 1.4)].[13] Artemether has a short half−life ($t_{½}$ = 3–7 hr) and quickly kills off a majority of the parasitaemia. Lumefantrine ($t_{½}$ = 4–6 days) on the other hand, has a longer half−life, allowing for removal of any remaining parasites.[13] Other combinations are dihydro-artemisinin/piperaquine and artesunate with either amodiaquine or mefloquine.

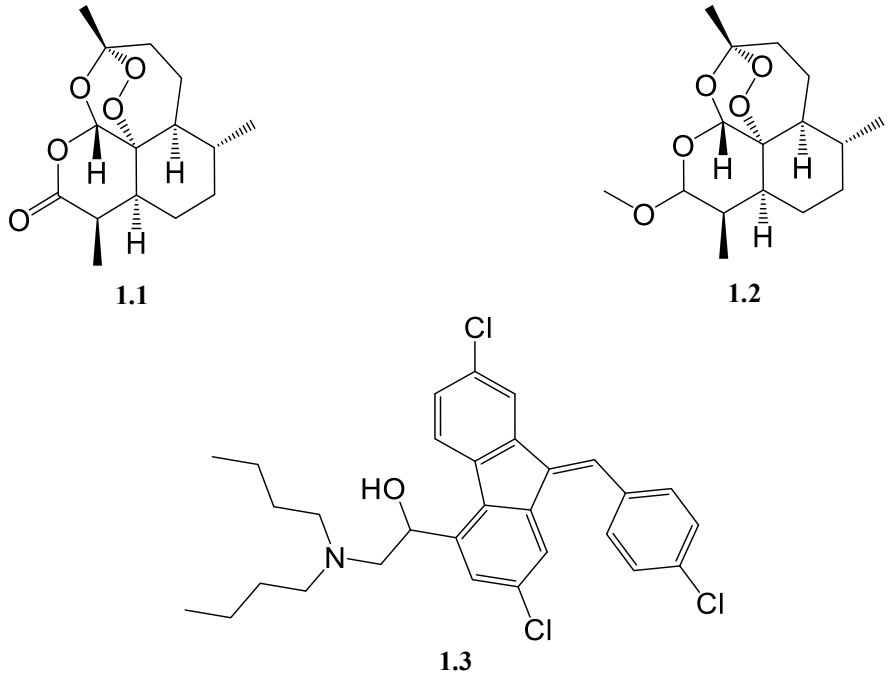

1.1 **1.2** **1.3**

Figure 1.4 Endoperoxide compounds artemisinin (**1.1**) and artemether (**1.2**) [in combination with lumefantrine (**1.3**)] were evaluated as antimalarial agents.[11,13,14]

Additionally, antifolates and protease inhibitors (e.g. cysteine proteases) have also been of interest. Antifolates, for example, target the folic acid cycle (involves the transfer of one−carbon unit during the synthesis of DNA components such as amino acids, nucleotides and other biomolecules). Therefore antifolates such as pyrimethamine [**1.4**, in combination with sulfadoxine (**1.5**); Figure 1.5] inhibit enzymes such as dihydrofolate reductase (DHFR) and dihydropteroate synthase (DHPS), which are involved in parasite folate biosynthesis.[15]

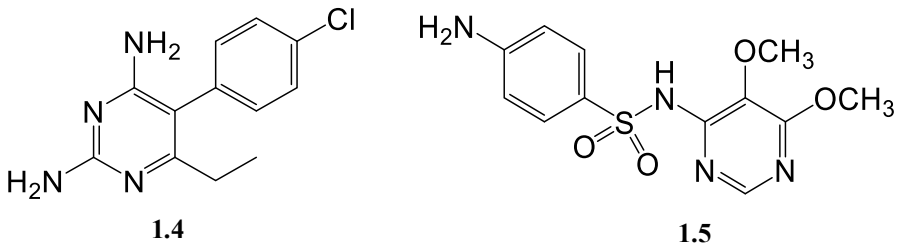

1.4 **1.5**

Figure 1.5 The antimalarial combination treatment Fansidar [pyrimethamine (**1.4**)/sulfadoxine (**1.5**)].[15]

As previously mentioned, drug resistance is a major problem. Due to this, there is a continuous search for new drugs, which has led to the development of a wide range of compounds displaying promising activities *in vitro* and *in vivo*. However, the main difficulty in drug discovery is finding a potential drug which satisfies the requirements for both pre−clinical and clinical trials. Furthermore, malaria is not the only parasitic disease affected by drug resistance. Other parasitic

disease such as leishmaniasis, schistosomiasis and trichomoniasis, to name a few, are also plagued by drug resistance. In particular, the reported number of trichomoniasis cases has steadily been on the rise.

1.3 Trichomoniasis

Trichomoniasis is a parasitic disease, caused by the protozoan *Trichomonas vaginalis*, which is one of the most prevalent sexually transmitted parasitic diseases. The major concern with regard to trichomoniasis is the increased risk of acquiring HIV, cervical cancer and aggressive prostate cancer.[16–18] It is estimated that in 2008, there were 187.0 million people infected with *T. vaginalis* globally, of which 42.8 million were located in Africa.[19]

1.3.1 Life cycle of the parasite

The life cycle of the *Trichomonas vaginalis* parasite is not well understood. The trophozoite (lacking a cystic stage) of the parasite is transferred during sexual intercourse and divides by longitudinal binary fission (cytoplasmic division along the longitudinal axis of the individual). This gives rise to a parasite population in the lumen and on the mucosal surfaces of the urogenital tracts of humans.[20]

1.3.2 Survival and defence mechanism of the T. vaginalis parasite

It is evident from previous studies that the parasite obtains its nutrients *via* the phagocytosis of various host cells (e.g. leucocytes, vaginal epithelial cells).[21] The mechanism by which the parasite evades the host immune system is of significance. It is believed that leucocytes (white blood cells) are phagocytosed to circumvent any immune responses, which is illustrated in Figure 1.6.[21,22] Furthermore, the parasite contains proteases which degrade immunogenic cytokines and antibodies, preventing an immune response.[23,24]

a **b**

Figure 1.6 SEM photos illustrating the idea that the *T. vaginalis* (green) ingests the cells *via* phagocytosis. (**a**) Trichomonad phagocytosing yeast (yellow) and bacteria (pink) cells. (**b**) Cells completely internalised by the parasite.[22]

1.3.3 Current and previously used antitrichomonal treatments

The current treatment of *T. vaginalis* is limited to 5-nitroimidazole compounds, such as metronidazole (**1.6**; Figure 1.7), tinidazole (**1.7**; Figure 1.7), ornidazole, secnidazole and nimorazole to name a few, which are effective drugs against protozoal infections.[16,25–28] Metronidazole, a derivative of azomycin (**1.8**, 2-nitroimidazole; Figure 1.7) which was one of the first antiprotozoal agents, was introduced in 1959 and became one of the first and most successful antitrichomonal drugs. This drug is believed to diffuse into the hydrogenosomes of the parasite, where the nitro group is reduced by the flavin enzyme thioredoxin reductase, resulting in the formation of cytotoxic nitro radical−ion intermediates which are able to interact with DNA.[29] This interaction cleaves the DNA, disrupting mitosis and resulting in cell death. The other end−products are inactive and excreted.[29] However, as mentioned for antimalarial drugs, there is evidence for the emergence of metronidazole−resistant *T. vaginalis* strains.

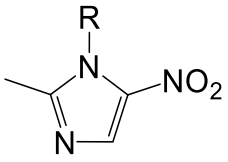

1.6 R = CH_2CH_2OH
1.7 R = $CH_2CH_2SO_2CH_2CH_3$

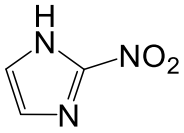

1.8

Figure 1.7 5-Nitroimidazole compounds metronidazole (**1.6**), tinidazole (**1.7**) and azomycin (**1.8**) which are active against *T. vaginalis*.[16]

This led to the synthesis of tinidazole, a derivative of metronidazole. It is proposed that the drug works in a similar manner to metronidazole, though tinidazole ($t_{½}$ = 12–14 hr) has a longer half−life than metronidazole ($t_{½}$ = 6–7 hr) making it more favourable as it reduces the administered dosage.[20] Tinidazole has also exhibited good tissue penetration and with the reduction of tinidazole, a gradient is created which allows for the influx of more tinidazole, providing more prodrug to be reduced and increasing bioavailability.[30] As is the case with malaria, new antitrichomonal compounds based on a scaffold other than nitroimidazole are required in an attempt to overcome the resistance problem.

1.4 The application of metals in the medical field

Metals have been recognised for their medicinal properties and used for the treatment of various diseases.[31–33] Gold compounds have been used for centuries; however the 20th century brought about their use in the treatment of rheumatoid arthritis.[34] Research into the synthesis and

biological evaluation of inorganic and organometallic complexes have significantly increased since the success of complexes such as cisplatin (**1.9**; Figure 1.8).[4,35–41]

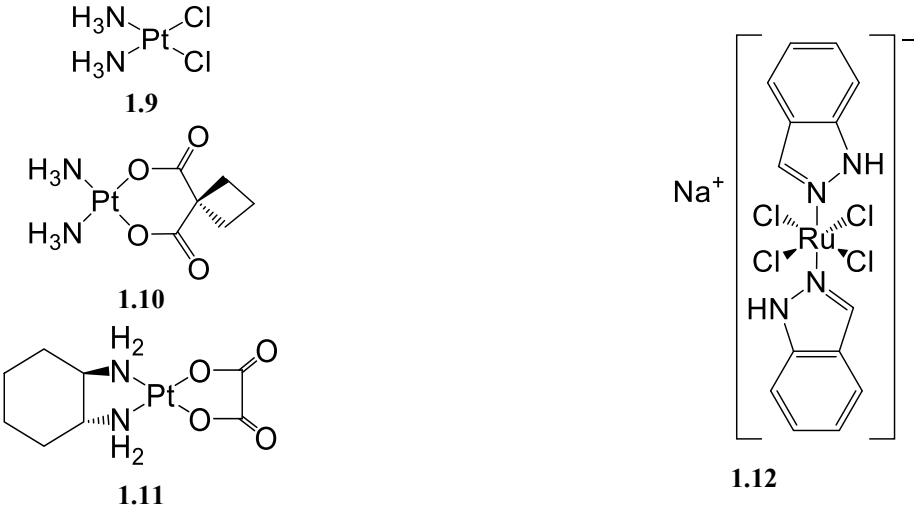

Figure 1.8 Clinically approved platinum−based complexes cisplatin (**1.9**), carboplatin (**1.10**), oxaliplatin (**1.11**) and the ruthenium complex (N)KP1339 (**1.12**) which is currently in clinical trials.[42]

However, due to the cytotoxicity of cisplatin, second generation platinum compounds carboplatin and oxaliplatin (**1.10** and **1.11**, respectively; Figure 1.8) were investigated to overcome the drawbacks of cisplatin. As seen with malaria and trichomoniasis, drug resistance gradually develops and the anticancer drug loses its potency. Therefore, researchers began studies with other platinum group metals, such as ruthenium, which have displayed promising results. (N)KP1339 [**1.12**, sodium *trans*-tetrachlorobis-(1H-indazole)ruthenate(III); Figure 1.8] is an example of a ruthenium complex currently in clinical trials. (N)KP1339 was initially designed to mimic the DNA binding ability of platinum complexes, the mode of action appears to be DNA−independent. Especially the transport through serum protein binding and the activation by reduction only in cancer cells, may contribute to the low side−effects of this compound type.[43]

Hydroxynaphthoquinones, such as atovaquone, have displayed antiplasmodial activities through the altering of mitochondrial membrane potentials.[44] Therefore, Padhye and co−workers prepared transition metal (Cu, Ni, Co, Fe, Mn) complexes of the hydroxynaphthoquinone, buparvaquone, and evaluated them *in vitro* for biological activity against 3D7 (CQS) and K1 (CQR) strains of *P. falciparum*.[45] All the tested complexes displayed activity against the *P. falciparum* strains, with the Cu complex (**1.13**, Figure 1.9) displaying the highest activity [ED_{50}

= 0.0002 (3D7) and 0.01 (K1) μg/mL]. Compound **1.13** exhibited a 1000−fold increase in activity compared to that of the uncoordinated buparvaquone [ED_{50} = 0.18 (3D7) and 0.03 (K1) μg/mL], as well as improved activity over chloroquine and atovaquone.[45] Compound **1.13** was further evaluated *in vivo* in a Peter's four−day suppression test against female mice infected with *P. berghei*. The results of the antimalarial study was promising as compound **1.13** cleared 90 % parasitaemia at a 15 mg/kg dose per day, while chloroquine cleared the parasite at a dose of 10 mg/kg per day.[45]

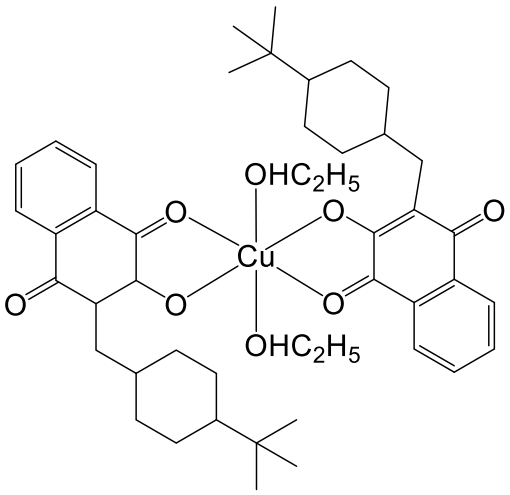

1.13

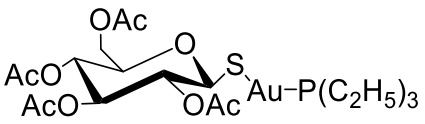

1.14

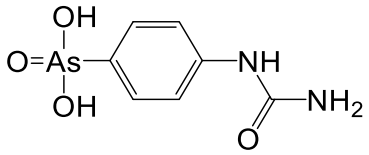

1.15

Figure 1.9 Examples of complexes (**1.13**−**1.15**) evaluated as antiparasitics.[45–47]

The clinically proven antiarthritic drug Auranofin (**1.14**, Figure 1.9) has also been evaluated as an antiplasmodial agent.[46] Auranofin was tested against the 3D7 strain of *P. falciparum* and displayed nearly complete inhibition of *P. falciparum* growth at concentrations in the nanomolar range (IC_{50} = 142 nM).[46]

In terms of antitrichomonal agents, one of the earliest known drugs was the organoarsenic Carbarsone (**1.15**, Figure 1.9).[47] Nevertheless, the evaluation of metal complexes as treatments for other diseases is an ongoing challenge.

1.4.1 The use of organosilanes

Silicon chemistry has attracted a lot of interest due to the ability of silicon to favourably alter the chemical properties of a compound compared to the carbon analogue. Silicon has previously been incorporated into the scaffold of known drugs to either enhance the potency of the drug or

to remodel the drug to treat other diseases. Silicon−containing compounds generally exhibit enhanced pharmacological activity, and reduced cytotoxicity against non−infected cells, when compared to their corresponding non−silicon analogues.[48–51] In cases where a compound enters the cell *via* membrane crossing, silicon−containing compounds have been associated with enhanced cell and tissue penetration.

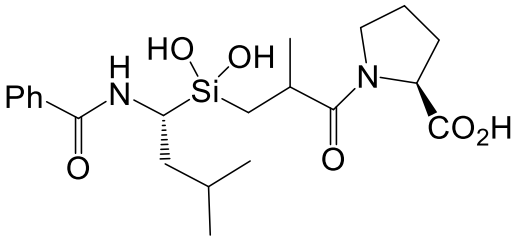

1.16

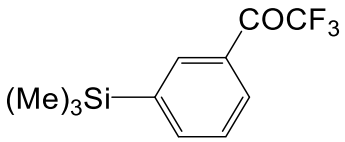

1.18

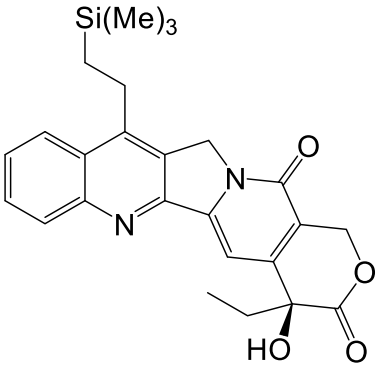

1.17

Figure 1.10 Organosilicon compounds **1.16–1.18** evaluated as biological agents.[50–52]

Compounds **1.16–1.18** (Figure 1.10) are examples of silicon−containing compounds which have exhibited significant biological activities. Compound **1.16**, a silanediol protease inhibitor, has exhibited activity as an angiotensin converting enzyme inhibitor (IC_{50} = 3.8 nM), while compounds **1.17** (Zifrosilone) and **1.18** (Karenitecin) have been evaluated as treatment for Alzheimer's disease and as an anticancer drug, respectively.[48] Organosilane **1.18** was designed as the lipophilic analogue of camptothecin and intended to reduce toxicity. Compound **1.18** is currently undergoing phase III clinical trials in advanced ovarian cancer patients.[51,53]

Organosilicon compounds have displayed not only activities in the nanomolar range, but also favourable pharmacokinetic properties. Coupled with the limited number of compounds which have been tested as antiparasitic agents, the evaluation of organosilanes and their complexes is a viable avenue to explore. Furthermore, the incorporation of pharmacophores, in combination with silane moieties, may further improve the biological properties of the proposed compounds. A pharmacophore is defined as the ensemble of steric and electronic features which are necessary to ensure optimal interactions with a specific biological target and to trigger (or block) its biological response. Therefore, the design of potential drugs would contain one or more pharmacophores.

1.5 Thiosemicarbazones

Schiff base compounds such as thiosemicarbazones (TSCs, Figure 1.11) are formed *via* a condensation reaction between a carbonyl group and an amine group. Thiosemicarbazone systems contain donor atoms which allow for binding or chelation to various metals depending on the softness [Pd(II), Pt(II)] or hardness [Fe(III), Mg(II)] of the metal.[54] The compounds can act as a monodentate (binding *via* the S atom)[55], bidentate (chelate in a *N,S* fashion)[56,57], or tridentate (*N,N,S*[58,59], *O,N,S*[60–62] or *C,N,S*[63–65]) ligands which allows for the formation of a wide range of complexes. Thiosemicarbazones have been tested for biological applications, and displayed pharmacological properties as antitumoural,[56,60,61,64,66–68] antibacterial,[69,70] antiviral[71,72] and antiparasitic[60,63,64,73–77] agents.

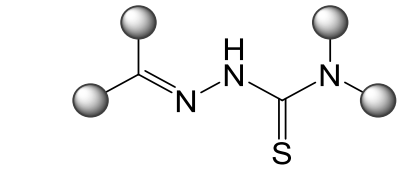

= H, alkyl, aryl or heteroaromatic group

Figure 1.11 The general structure of a thiosemicarbazone compound.

Organic thiosemicarbazone compounds

Studies focused on the evaluation of thiosemicarbazones as antiplasmodial and antitrichomonal agents are scarce in literature.[73–75,78–80] Thiosemicarbazones were first regarded as antiplasmodial agents by Barrett and co-workers in 1965, and then in 1979 by Klayman and co-workers who sought to reintroduce thiosemicarbazones with derivatives of 2-acetylpyridine 4-phenyl-3-thiosemicarbazone.[79–83] They expanded upon their initial work by evaluating the antimalarial activity of 2-acetylpyridine 1-oxide thiosemicarbazone.[84] Compound **1.19** (Figure 1.12) was the only active compound curing one out of five animals at 640 mg/kg. The pyridyl oxides were generally found to be less active than the parent pyridyl compounds.[84]

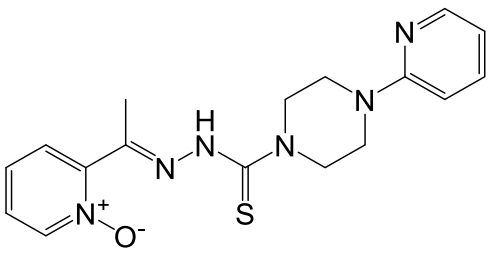

1.19

Figure 1.12 Thiosemicarbazone compound (**1.19**) evaluated as antiplasmodial agent.[84]

More recent work on thiosemicarbazones also focused on testing potential modes of action such as inhibition of cysteine proteases.[75,78] Chiyanzu *et al.* have investigated potential cysteine protease inhibitors in the form of thiosemicarbazone derivatives of isatins.[78] Previous studies on isatins revealed that these compounds inhibit cysteine and serine proteases.[85,86] As mentioned before, inhibition of cysteine proteases has also been suggested as the mode of action for thiosemicarbazones. Therefore, the compounds were evaluated against three parasitic cysteine proteases namely cruzain, falcipain−2 and rhodesain. Compound **1.20** (Figure 1.13) exhibited good activity (IC_{50} = 10.5, 9.4 and 3 μM, respectively) against all three proteases.[78]

Phenolic Mannich bases of benzaldehyde and thiosemicarbazone derivatives were synthesised by Chipeleme *et al.* as potential inhibitors of the cysteine protease falcipain−2, and tested against the CQ−resistant W2 strain of *P. falciparum*.[75] Of the thiosemicarbazone−containing Mannich base compounds, compound **1.21** (Figure 1.13) showed the best overall inhibition of falcipain−2 (IC_{50} value = 2.25 μM) and antiplasmodial activity against W2 (IC_{50} value = 3.75 μM).[75] The presence of the quinoline suggests that the activity is related to haem−binding and the ability of the thiosemicarbazones to chelate endogenous iron in the cell.[75]

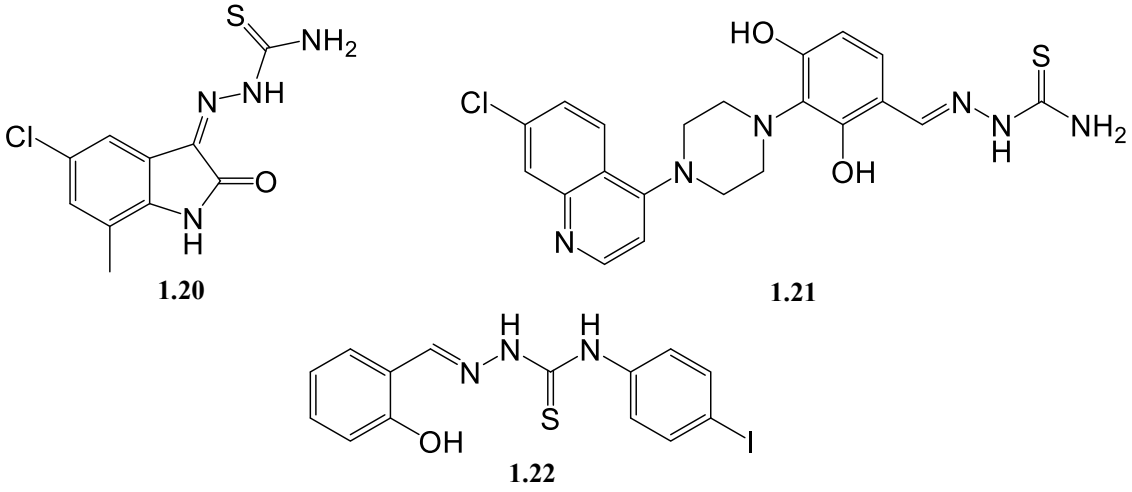

Figure 1.13 Thiosemicarbazone compounds (**1.20**–**1.22**) evaluated as antiplasmodial agents.[75,78,87]

Duan and Zhang explored the activity of aromatic iodide thiosemicarbazone compounds *in vivo* (mice) against *P. falciparum*.[87] Work previously done on iodine containing compounds prompted this work as the compounds exhibited higher activity and lower toxicity than the corresponding chloro compounds. Compound **1.22** [4-(*p*-Iodophenyl)-3-thiosemicarbazone; Figure 1.13] exhibited the best activity with suppression percentages of 88.1, 90.7 and 92.6 at

concentrations of 3, 9 and 27 mg/kg, respectively. The authors concluded that the hydroxyl group was important for antimalarial activity and the iodine analogues were slightly more active than the chloro analogue.[87]

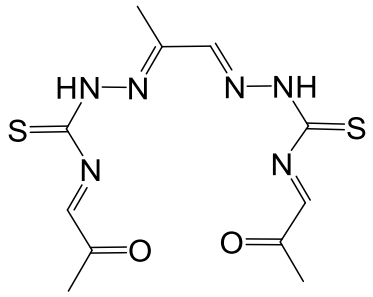

1.23

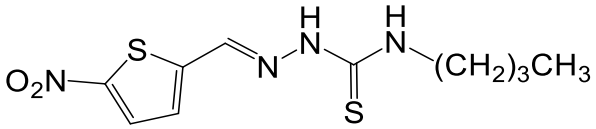

1.24

Figure 1.14 Thiosemicarbazone compounds (**1.23** & **1.24**) evaluated as antitrichomonal agents.[88,89]

Very limited research has focussed on the investigation of thiosemicarbazones as antitrichomonal agents.[88,89] Michaels *et al*. investigated the use of bis(thiosemicarbazones) *in vitro* and *in vivo* as antitrichomonal agents. The *in vitro* tests revealed that the bis(thiosemicarbazone) with the terminal amine methylated is more active than the unsubstituted analogue. Pyruvaldehyde-bis(4-methythiosemicarbazone) [**1.23**; Figure 1.14] displayed 90 % inhibition at 3 ng/mL. *In vivo* tests were conducted on mice and hamsters, which were treated with the compounds orally, *via* injection and applied locally. However, these compounds were not able to cure chronically infected hamsters or the intravaginally infected mice. The authors believed this was due to the lack of local absorption of the compounds.[89]

5-Nitrothiophene-2-carboxaldehyde thiosemicarbazone was evaluated as an antiprotozoal agent by Bharti *et al*. due to the antiprotozoal activity exhibited by previously evaluated thiophene−containing compounds.[88,90,91] As antitrichomonal agents, compound **1.24** (Figure 1.14) was the most active with an IC_{50} value of 1.49 μM (Metronidazole: 1.92 μM).[88]

Metal−based thiosemicarbazone compounds

Thiosemicarbazone complexes containing metals, such as copper[92], nickel[92], iron[92], ruthenium[93–95] , gold[55,57], palladium[60–63,70,96] and platinum[59,64,70,97,98] to name a few, have been investigated for their biological properties.

Some of the first thiosemicarbazone−based complexes evaluated as antimalarials were synthesised in the 1980's. Scovill *et al*. prepared Cu(II), Ni(II), Fe(II) and Mn(II) complexes with 2-acetylpyridine thio− and selenosemicarbazones.[92] The Cu(II), Ni(II) and Fe(II) complexes prepared using 2-acetylpyridine thiosemicarbazone ligands were evaluated *in vivo* against *P. berghei* infected mice. The thiosemicarbazone ligands exhibited activity at dosage levels of 40 to 160 mg/kg, whereby 3/5 infected mice were cured. Upon complexation, the Cu(II) complexes, which includes compound **1.25** (Figure 1.15), were found to be the most active curing 5/5 infected mice at a dose of 160 mg/kg. The Ni(II) complexes were inactive and the Fe(II) complexes were less active than the Cu(II) complexes.[92]

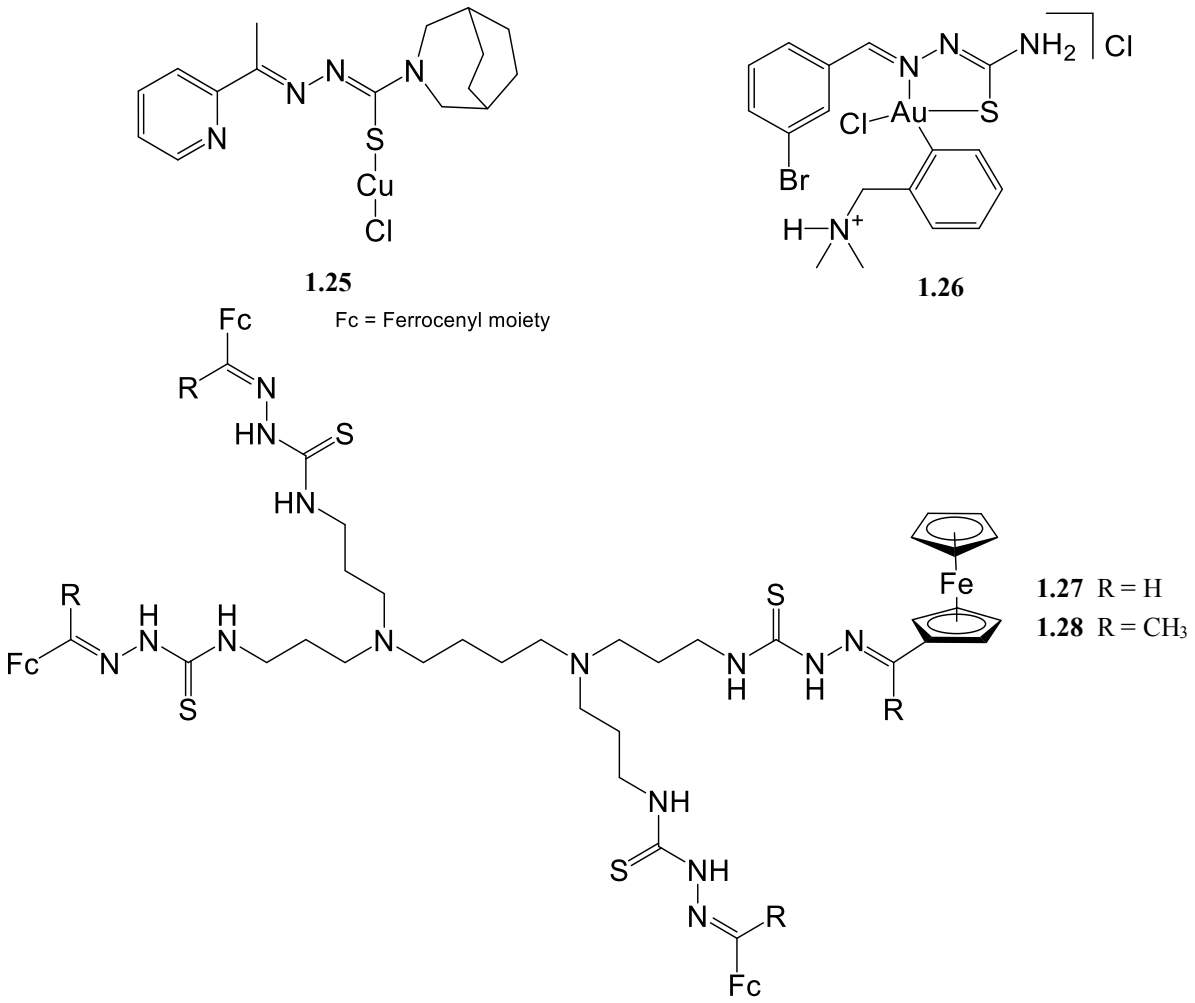

Figure 1.15 Thiosemicarbazone complexes (**1.25**–**1.28**) evaluated as antiparasitic agents.[57,92,99]

Work by Khanye *et al*. focused on the use of Au(I) and Au(III) complexes as antiplasmodial agents.[55,57] The Au(III) compound **1.26** (Figure 1.14) displayed activity (IC_{50} = 3.04 μM) in the

low micromolar range against the CQR W2 strain of *P. falciparum*.[57] Khanye also worked on incorporating ferrocenyl thiosemicarbazones onto a poly(propyleneimine) dendrimer scaffold (Figure 1.15) and evaluated the antiplasmodial activity.[99] There is a significant increase in activity when comparing compounds **1.27** and **1.28**, which contains four ferrocenyl moieties, to the ferrocenyl dithiocarbamates (one ferrocenyl moiety). Compounds **1.27** and **1.28** were tested *in vitro* against the W2 strain of *P. falciparum*, and exhibited activity with IC_{50} values of 6.59 and 1.79 μM, respectively. The other compounds were inactive at the highest tested concentration (20 μM).[99] Compound **1.27** was further evaluated for its antitrichomonal properties against the metronidazole−sensitive G3 strain of *T. vaginalis*.[100] Compound **1.27** displayed moderate inhibition (61.5 %) of parasite growth.

Therefore, due to the potential of these compounds as antiparasitic agents, TSCs are a class of compounds which can further be explored. Other pharmacophores, including heterocycles, may prove to be a useful addition to potential antiplasmodial agents.

1.6 Heterocyclic compounds

1.6.1 Quinoline−based compounds

Quinolines are heterocyclic compounds comprised of a benzene ring fused to a pyridine ring at two adjacent carbons (Figure 1.16). Quinolines have garnered significant attention due to their presence in a large number of natural products, as well as their prevalence in biologically active compounds displaying properties such as antimalarial[14,101–103], antitumoural[104–107] and antimycobacterial[108] activity.

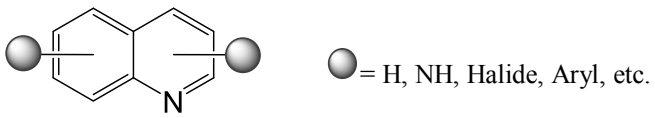

Figure 1.16 The general structure of a quinoline compound.

Organic quinoline compounds

As mentioned in section 1.2, quinine (**1.29**; Figure 1.17) was one of the first quinoline−based compounds used in the treatment of malaria. Quinine−containing materials were used since the 17th century up until the 1940's.[14] The cost effectiveness of chloroquine (CQ, **1.30**; Figure 1.17), and its success against various *plasmodium* strains, allowed for the world−wide use of the drug and the phasing out of quinine. Chloroquine is believed to act by binding to α−haematin through

π–π complexation to slow the rate of conversion to haemozoin, which is a non–toxic crystallised form of haematin.[109] Despite the emergence of resistant strains, chloroquine is still being used to treat the sensitive strains, or in combination therapies, especially in developing countries. However, as chloroquine resistance increased, other quinoline–based compounds such as mefloquine (**1.31**) and amodiaquine (**1.32**) were evaluated with the prospect of different mechanisms of action (Figure 1.17).[14] As with chloroquine, various other quinoline–based compounds such as piperaquine (**1.33**) and naphthoquine (**1.34**) to name a few have been utilised in combination therapies.[110,111] These quinoline based compounds generally inhibit β–haematin formation, while other functional groups either help with other properties such as changing the lipophilicity of the compound and assisting with accumulation in the vacuole.

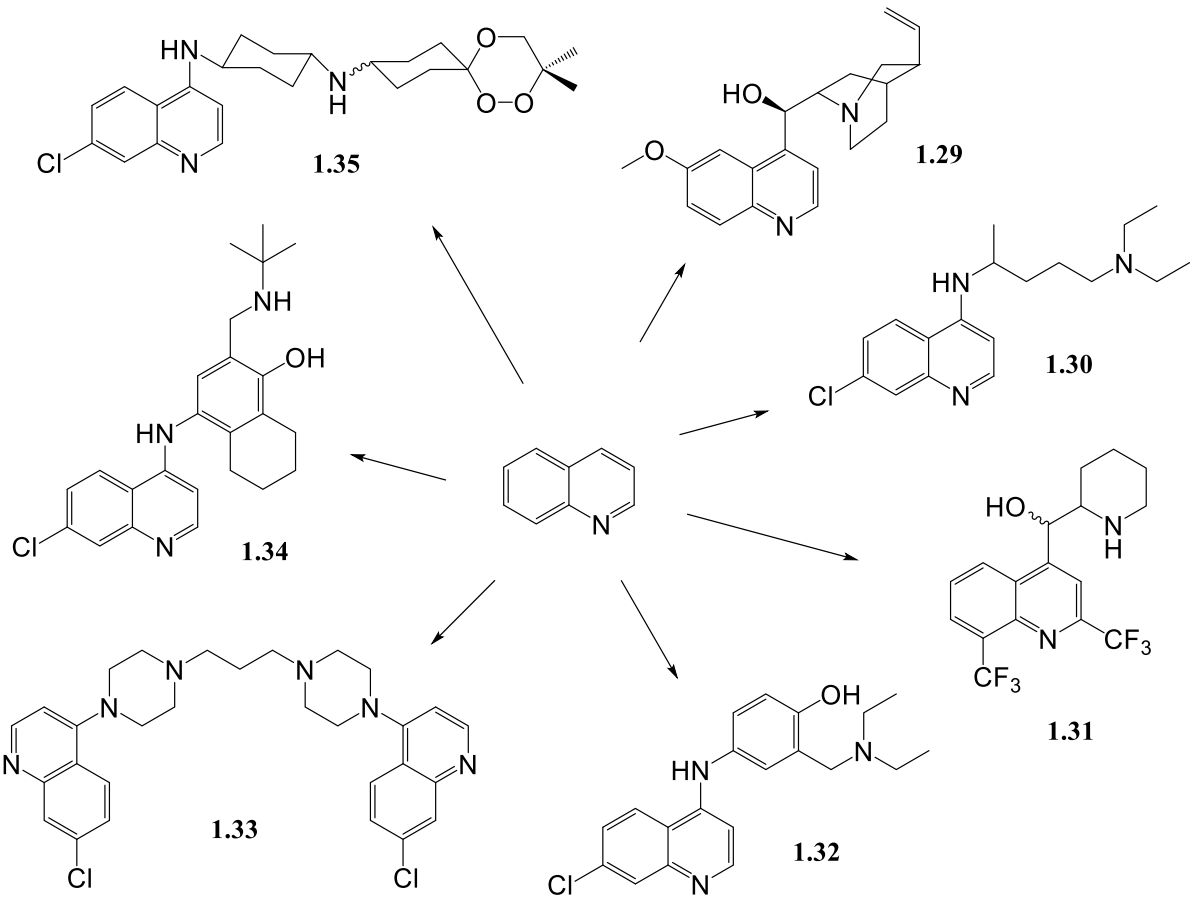

Figure 1.17 Quinoline based antimalarial drugs quinine (**1.29**), chloroquine (**1.30**), mefloquine (**1.31**), amodiaquine (**1.32**), piperaquine (**1.33**), naphthoquine (**1.34**) and trioxane (**1.35**).[14,101,112,113]

Extensive work has been done to derivatise known quinoline-based drugs to afford new effective compounds which may overcome drug resistance.[14,114,115] A method researchers have employed is to focus studies towards the synthesis of hybrid compounds. Coslédan *et al*. developed a series

of compounds which contain the 7-chloro-4-aminoquinoline base for inhibition of haemozoin formation, as well as the 1,2,4-trioxane motif present in artemisinin derivatives. Trioxaquine (**1.35**, PA1103/SAR116242; Figure 1.17) exhibited the best activity against D6 (CQS) and FcM29 (CQR) malaria strains *in vitro* with IC_{50} values of 7 and 10 nM, respectively.[112] *In vivo* studies carried out on mice infected with rodent strains *P. vinckei petteri* (CQS strain) and *P. vinckei vinckei* (CQR strain) demonstrated that the antimalarial activity was similar. Therefore, due to the high antimalarial activity and the low toxicity of the compound, trioxaquine is currently in preclinical trials.[112,116]

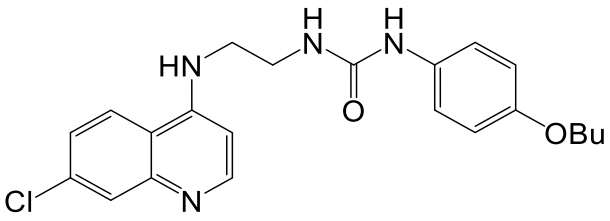

1.36

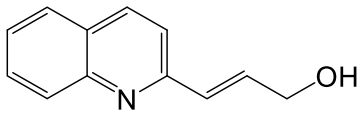

1.37

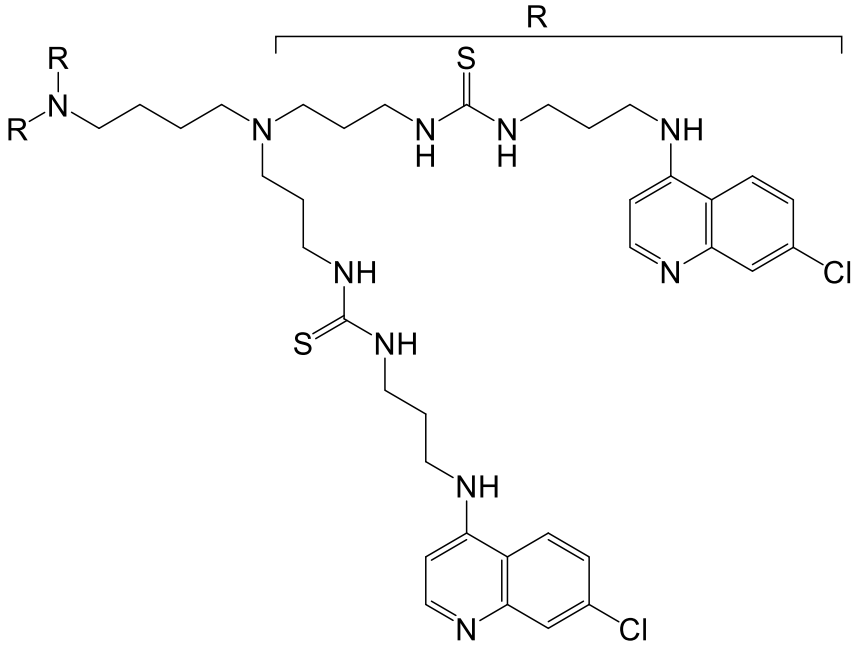

1.38

Figure 1.18 Quinoline−based compounds (**1.36**–**1.38**) evaluated as antitrichomonal agents.[100,117,118]

Not many quinoline−based compounds have been investigated as potential treatment for trichomoniasis.[100,117–119] The work by Nava−Zuazo *et al.* sought to derivatise chloroquine by synthesising hybrids containing the ethylenediamine spacer and phenylurea from ethambutol (first−line TB drug) and isoxyl (displays antimycobacterial activity), respectively.[117] These compounds were tested against parasitic strains such as *G. Intestinalis* and *T. cruzi* to name a

few, but in terms of *T. vaginalis* the tested compounds exhibited moderate activity with compound **1.36** (Figure 1.18) exhibiting the best activity. Compound **1.36** exhibited an IC_{50} value of 8.44 μM, which is more active than chloroquine (30.0 μM) while compared to metronidazole (0.29 μM) the activity was approximately 30−fold less.[117]

2-Alkenylquinoline compounds have exhibited a variety of biological properties and were thus exploited by Martinez−Grueiro *et al*. The observed inhibition of *T. vaginalis* growth was generally above 50 % for the tested compounds at the highest tested concentration (100 μM).[118] Compound **1.37** (Figure 1.18) exhibited the highest inhibition of 99.7 %. However, it was observed for all compounds that the percentage inhibition decreased as the concentration decreased.[118]

Stringer *et al*. prepared a series of quinoline−based compounds conjugated onto a thiourea polyamine scaffold.[100] These compounds were evaluated for their antiparasitic properties as antiplasmodial and antitrichomonal agents.[100] The compounds, which includes the tetrameric **1.38** (Figure 1.18), displayed moderate percentage inhibitions (< 60 %) against the *T. vaginalis* G3 strain.

Metal−based quinoline compounds

In terms of quinoline−based complexes evaluated as antiparasitic agents, research is primarily focused on antimalarial studies. One of the first organometallic complexes evaluated as an antimalarial agent was RhCl(COD)(CQ) [**1.39**, COD = cyclooctadiene; Figure 1.19] which was synthesised by Sánchez−Delgado *et al*.[120] In addition to the rhodium complex, a binuclear ruthenium(II)−chloroquine complex (**1.40**; Figure 1.19) was also synthesised by the Sánchez−Delgado group.[120]

Due to the low toxicity exhibited by ruthenium complexes, further research has gone into the synthesis of ruthenium−chloroquine complexes.[120,121] In the case of the rhodium complex, chloroquine binds to the metal *via* the quinoline nitrogen atom, whilst for **1.40**, the ruthenium is coordinated to two chloroquines, through the quinoline N of one chloroquine molecule and the diethylamine N of another, to form a dimer.[120] Compounds **1.39** and **1.40** exhibited *in vitro* and *in vivo* activity against the rodent strain *P. berghei*. However, the ruthenium complex **1.40** exhibited better activity than **1.39**, as well as chloroquine diphosphate, with IC_{50} = 18 nM (*in*

vitro) and a 94 % reduction of parasitaemia (*in vivo*). Therefore, **1.40** was also evaluated against two chloroquine−resistant strains FcB1 and FcB2 (IC_{50} = 10.5 and 46.5 nM, respectively). The structure and basicity of the complex, as well as the presence of the Ru(II), contributed to the enhanced activity of the complex.[120]

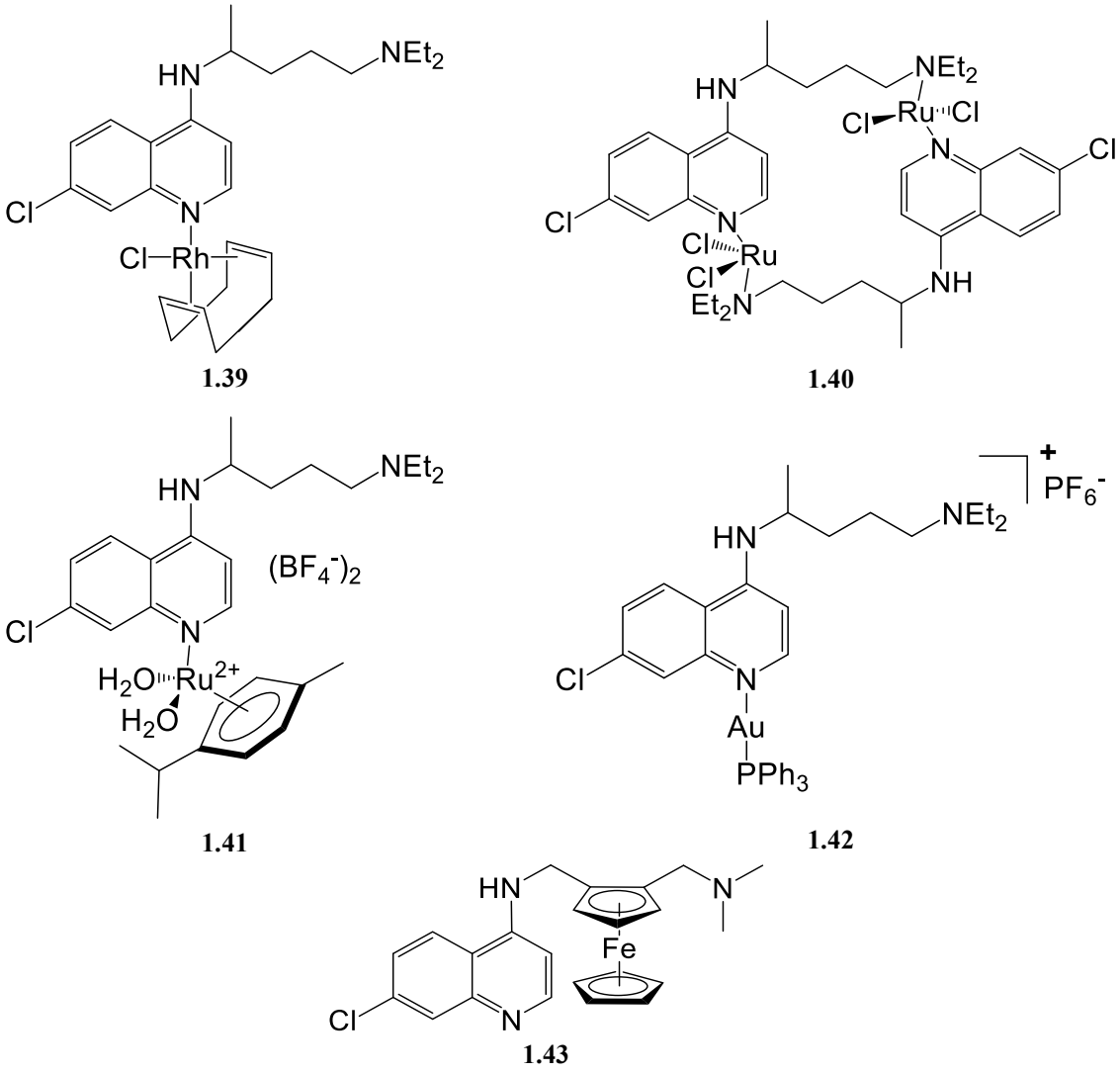

Figure 1.19 Quinoline based metal complexes (**1.39–1.43**) evaluated as antiplasmodial agents.[120–123]

Ruthenium is able to access the oxidation states Ru(II), Ru(III) and Ru(IV) under physiological conditions. Ruthenium(II) complexes are generally more biologically active and lower in toxicity due to their ability to mimic iron. Iron(II) is able to bind to biological molecules and be excreted. Thus, ruthenium is able to reduce its concentration in the body in a similar manner as Fe(II), and is therefore less toxic.[124] Ruthenium(II) ions can also be oxidised in a similar manner to Fe(II), allowing for electron transfer, and generation of reactive oxygen species which may play a role in parasite death.

Following on from the previously mentioned work, Sánchez−Delgado group investigated the activity of half−sandwich ruthenium(II)−chloroquine complexes containing arene moieties.[121] The arene ring is present in order to stabilise the metal, as well as possibly alter the lipophilicity of chloroquine, thus enabling transport of the complex to the active site. The ruthenium(II)−complexes were tested *in vitro*, and showed significant activity against resistant strains. Compound **1.41** (Figure 1.19) exhibited the highest activity with IC_{50} values (234 nM for Dd2) which were significantly lower than chloroquine diphosphate (1184 nM for Dd2).[121]

Due to the medicinal uses of gold, Au(III)−chloroquine complexes were synthesised by Navarro *et al*. and their antiplasmodial activities evaluated.[122] With the coordination of Au(III) to chloroquine, there is a change in the electronic properties of the 7-chloro-4-aminoquinoline base. The complex $[Au(PPh_3)(CQ)]PF_6$ (**1.42**; Figure 1.19) showed good activity against FcB1 and FcB2, with IC_{50} values of 5 and 23 nM, respectively,[122] which was significantly lower than CQDP (47 nM for FcB1[120] and 104.5 nM for FcB2[120]). Derivatives of compound **1.42**, such as $[Au(PEt_3)(CQ)]PF_6$, displayed the highest activity against FcB1 with an IC_{50} value of 10 nM when compared to the activity of chloroquine diphosphate (IC_{50} = 50 nM).[122]

Ferrocene, an iron−containing sandwich structure, has garnered significant interest despite having no inherent cytotoxic activity. The lipophilic properties of ferrocene allow for the effective penetration of cellular membranes and it is believed to act in the same way as the iron in haematin, which produces reactive oxygen species when oxidised from Fe(II) to Fe(III).[123] There has been a significant interest in ferrocenyl−containing compounds especially with the synthesis of ferroquine (**1.43**; Figure 1.19) by the Brocard group.[123] Ferroquine, a chloroquine (**1.30**; Figure 1.17) derivative with a ferrocenyl moiety incorporated into the side chain, has not only shown higher activity against *P. falciparum* than chloroquine, but has also displayed activity against chloroquine−resistant strains.[123] Ferroquine is currently in phase IIb clinical trials.[125]

Further studies were conducted on a variety of ferrocene-containing analogues of other known antimalarials to determine if the incorporation of ferrocene could favourably alter the properties of those antimalarial drugs in a similar manner as seen with ferroquine.[4,126,127] As mentioned in section 1.2, artemisinin compounds contain a 1,2,4-trioxane motif which is largely responsible for the observed antimalarial activity. Ferrocenyl artemisinin derivatives prepared by Delhaes *et al*. were evaluated for their antiplasmodial activity against CQS (HB2, SGE2) and CQR (Dd2)

strains of *P. falciparum*.[126] The activities were compared to that of the parent artemisinin compounds. Compound **1.44** (Figure 1.20) displayed the highest activity with IC_{50} values of 12, 11 and 14 nM against the tested strains HB3, SGE2 and Dd2, respectively. A loss of activity was observed for the ferrocenyl compounds; however, the compounds still displayed significant cytotoxic effects.[126]

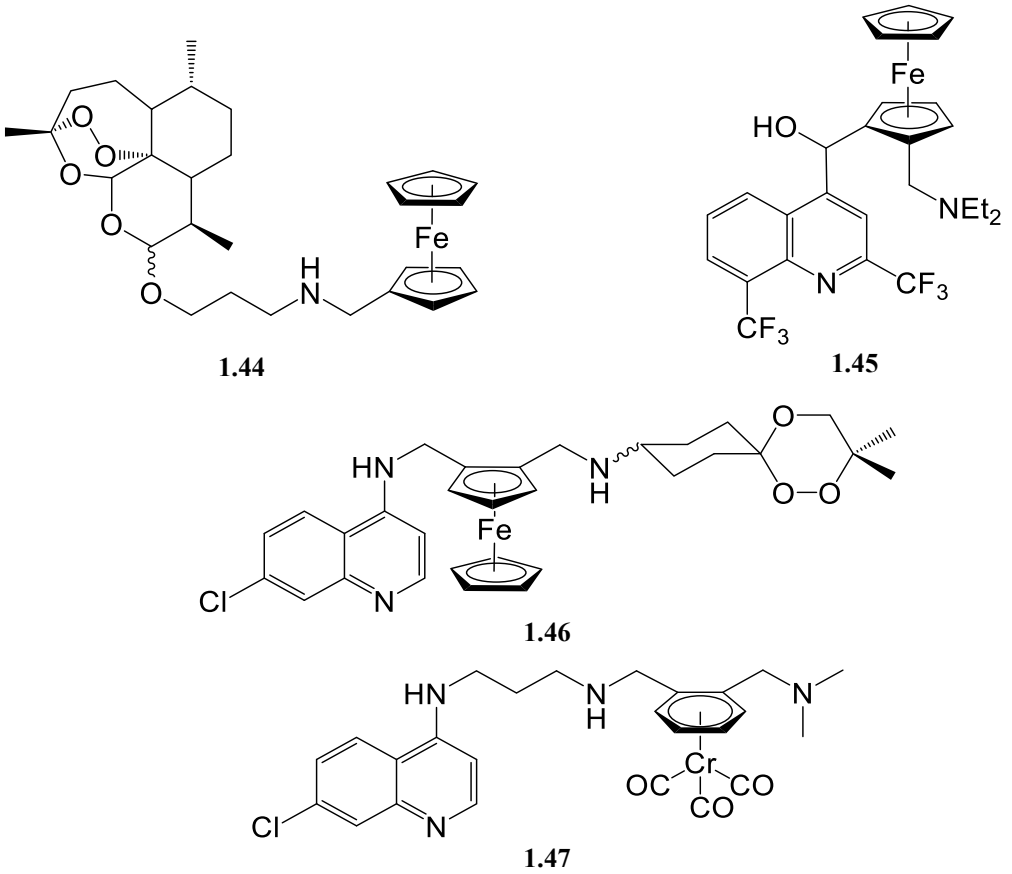

Figure 1.20 Sandwich (**1.44–1.46**) and half−sandwich (**1.47**) quinoline complexes evaluated as antiplasmodial agents.[126–129]

A similar study was carried out by Biot *et al*. who synthesised ferrocenyl analogues of mefloquine (**1.31**; Figure 1.17) and quinine (**1.29**; Figure 1.17), and tested the compounds against CQS (HB2) and CQR (Dd2) strains of *P. falciparum*.[127] Of the tested compounds, compound **1.45** (Figure 1.20) displayed the highest activity. As seen with the artemisinin derivatives, the ferrocenyl analogues were less active than the parent compound.[127]

Similarly trioxaferroquine (**1.46**; Figure 1.20), a ferrocenyl analogue of trioxane (**1.35**; Figure 1.17), was prepared by Bellot *et al*.[128] The trioxaferroquines and trioxaferrocenes (compounds which lack the 7-chloro-4-aminoquinoline) were tested against the FcB1 and FcM29 strains.[128]

The authors reported that all the trioxaferroquines displayed activity similar to that of artemisinin and ferroquine, whilst they were more active than chloroquine. The trioxaferroquines displayed significantly higher activity than trioxaferrocenes, which suggests that in this instance the 7-chloro-4-aminoquinoline is required for activity. Trioxaferroquine **1.46** displayed the highest activity with IC_{50} values 20 and 17 nM against FcB1 and FcM29, respectively.[128]

On the other hand, half−sandwich rhenium and chromium compounds have been prepared to determine if the oxidation of the ferrocenyl moiety is partially responsible for the antimalarial activity.[129,130] The tricarbonylchromium complex **1.47** (Figure 1.20) along with the organic ligand, and the dimethylaminomethyl tricarbonylchromium intermediate compounds prepared by Glans *et al*. were evaluated for their antiplasmodial activity against CQS (D10) and CQR (Dd2) strains of *P. falciparum*.[129] The two intermediates were also tested to determine if the tricarbonylchromium fragment possessed any inherent antiplasmodial activity. The intermediates had no significant effect on the parasites [> 1000 nM (D10)], which led the authors to conclude that any activity observed for compound **1.47** is not related to chromium toxicity. IC_{50} values of 3.8 and 33.9 nM were recorded for compound **1.47** against D10 and Dd2, respectively. Compound **1.47** displayed enhanced activity compared to chloroquine [IC_{50} = 22 nM (D10)], especially against the chloroquine−resistant Dd2 strain, where an IC_{50} value of 109.5 nM was observed for chloroquine.[129]

1.6.2 Benzothiazole−based compounds

Benzothiazoles are heterocyclic compounds comprised of a thiazole ring fused onto a benzene ring at two adjacent carbons (Figure 1.21). Benzothiazoles have extensively been used as biological agents since the 1950's, initially as muscle relaxants, and since then as antitumour[131–134], antimicrobial[133,134], antifungal[135] and antiparasitic[134,136–138] agents to name a few.

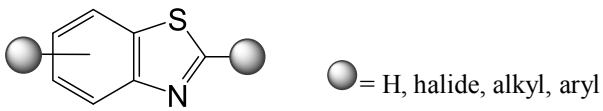

Figure 1.21 The general structure of a benzothiazole compound.

Organic benzothiazole compounds

Hout *et al*. tested three series of compounds *in vitro* against healthy human cells and the W2 strain of *P. falciparum*.[137] Compounds **1.48** and **1.49** (Figure 1.22) exhibited the highest activity

against the parasite with IC_{50} values of 0.7 and 1.8 μM, respectively, and displayed the lowest cytotoxicity against the healthy cells. Compounds **1.48** and **1.49** were further evaluated against the 3D7 strain, as well as clinical isolates. Compound **1.48** (IC_{50} = 1 μM) was more active than compound **1.49** (IC_{50} = 4.1 μM) against 3D7, as well as against the clinical isolates.[137] The mechanism of action for these compounds was evaluated using a range of tests and assays. The compounds were found to have an effect on the mitochondrial membrane potential; dropping the potential resulted in changes in the respiratory chain length and ultimately parasite death. Only compound **1.49** had a slight effect on the inhibition of haem crystallisation. Compound **1.49** had no effect on free radical production, and appeared to have no effect on DNA as no changes in structure were observed.[137]

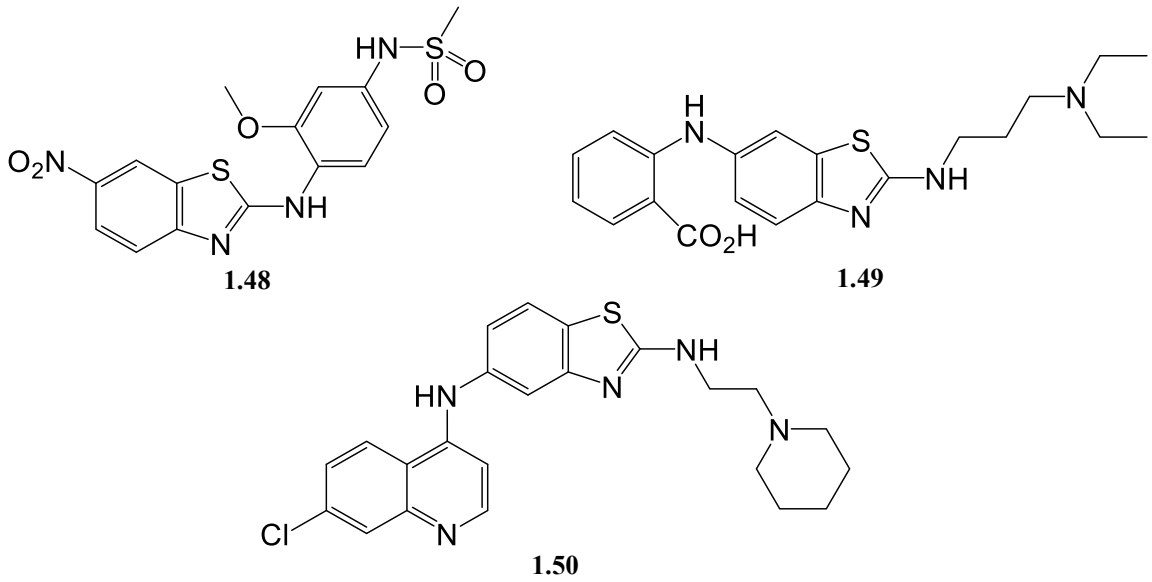

Figure 1.22 Benzothiazole−based compounds (**1.48**–**1.50**) exhibiting antimalarial properties.[137,138]

The derivatisation of known antimalarials continued in work done by Ongarora *et al*. whereby amodiaquine was altered by replacing the phenyl group with heteroaromatic ring systems, as well as altering the attached amine groups.[138] The tested compounds generally exhibited good activity against the W2 and K1 strains of *P. falciparum*. Compound **1.50** (Figure 1.22), a benzothiazole−containing compound, was one of the compounds which exhibited the best activity with IC_{50} values of 0.013 (W2) and 0.007 (K1) μM. The cytotoxicity of the compounds was also determined and found to be moderate against the rat mycoplast L6 cells.[138]

Delmas *et al*. prepared and evaluated 6-nitro-, 6-amino and anthranilic benzothiazole derivatives as antitrichomonal agents. Compounds **1.51** and **1.52** (Figure 1.23) were the only compounds in

the three series which displayed activity below 10 μM. Compound **1.51** and **1.52** gave IC_{50} values of 1.6 and 2.9 μM, respectively, which was also more active than metronidazole (3.2 μM).[136]

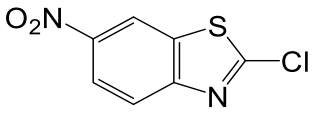

1.51

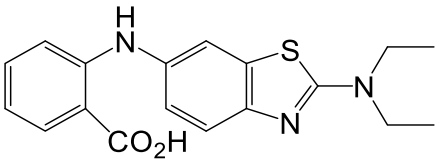

1.52

Figure 1.23 Benzothiazole compounds (**1.51** & **1.52**) exhibiting antitrichomonal properties.[136]

Platinum group metal benzothiazole−containing complexes have been tested against tumoural cell−lines and bacterial strains.[95,139,140] However, no benzothiazole−containing complexes have been tested as antiplasmodial or antitrichomonal agents.

1.7 Aims and objectives

1.7.1 General aims

Identifying potential lead compounds based on pharmacophores such as thiourea, quinoline and benzothiazole are of interest for the development of new bioorganometallic antiparasitic agents. Therefore, the overall aims of the project were as follows:

i. To prepare organosilane−containing thiosemicarbazones, which were further reacted with metal precursors, to prepare mono− and binuclear complexes (Figure 1.24).
ii. To prepare organosilane−based ferrocenyl−containing compounds comprised of aminoquinolines (Figure 1.25) or aminobenzothiazoles (Figure 1.26).
iii. To evaluate the prepared compounds for their pharmacological activity as antiparasitic agents.
iv. To investigate potential mechanisms of action responsible for any observed pharmacological activity.

1.7.2 Specific objectives

a) Synthetic objectives

- Ferrocenyl− and aryl−derived organosilane thiosemicarbazones (Figure 1.24a) were prepared *via* a nucleophilic acyl substitution reaction between Schiff base compounds (dithiocarbamates) and amine−terminated silanes. Groups R_1−R_3 of the thiosemicarbazones were modified as listed in Figure 1.24. The organosilicon TSC

compounds were used to prepare mono− or heterobimetallic *N,S*−chelated TSC ruthenium(II) and rhodium(III) complexes containing arenes as the ancillary ligands (Figure 1.24b). The presence of the arene assists in stabilising the metal centre. Additionally, selected cyclopalladated *C,N,S*−chelated thiosemicarbazone complexes were also prepared which contained the water soluble 1,3,5-triaza-7-phosphaadamantane (PTA) ligand in the fourth position around the Pd(II) metal ion.

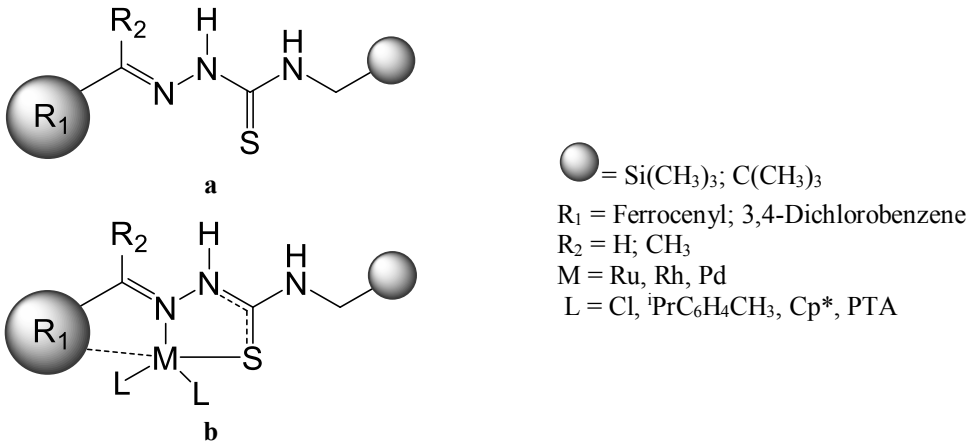

Figure 1.24 Representation of the organosilane thiosemicarbazones and corresponding complexes.

- Ferrocenyl−containing aminoquinolines (Figure 1.25) were synthesised *via* the nucleophilic substitution of the trimethylammonium group of quaternised ferroquine[141] by amine−terminated organosilanes, and the corresponding carbon analogue.

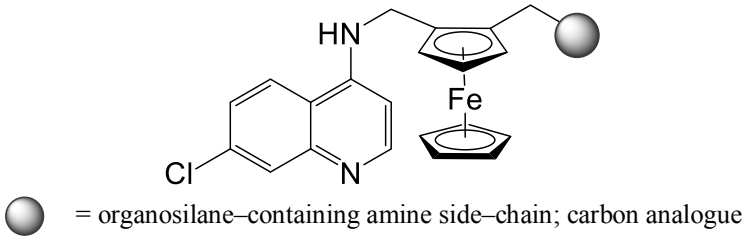

Figure 1.25 Representation of ferrocenyl−containing quinoline−based compounds.

- Ferrocenyl−containing aminobenzothiazoles (Figure 1.26) were prepared in a similar manner to the aminoquinolines illustrated in Figure 1.25, which began with the nucleophilic substitution of a halide (6-chloro-2-iodobenzothiazole) by 2-[(*N,N*-dimethylamino)methyl]-ferrocenylmethylamine. Quaternisation of the resulting

compound was followed by the nucleophilic substitution of the trimethylammonium group by amine−terminated organosilanes, and the corresponding carbon analogue.

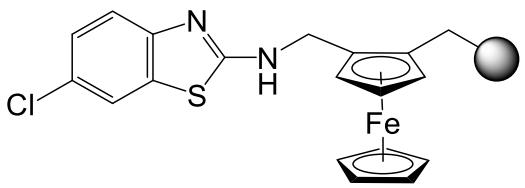

= organosilane–containing amine side–chain; carbon analogue

Figure 1.26 Representation of ferrocenyl−containing benzothiazole−based compounds.

b) Characterisation

The compounds were fully characterised using the required techniques such as Nuclear Magnetic Resonance (NMR) [^{1}H, ^{13}C{^{1}H}, ^{31}P{^{1}H}, COSY (correlation spectroscopy), HSQC (Heteronuclear Single Quantum Coherence)] spectroscopy, Infrared (IR) spectroscopy and mass spectrometry [electron impact (EI), electrospray ionisation (ESI)]. The molecular structure of selected compounds was confirmed using single−crystal X−ray diffraction.

c) Pharmacological studies

Following the preparation of the desired compounds, *in vitro* screening against parasitic strains of *Plasmodium falciparum* and *Trichomonas vaginalis* was carried out, along with cytotoxicity studies. As a potential mechanism of action, selected compounds were evaluated for their ability to inhibit the formation of β−haematin. Furthermore, based on promising *in vitro* data, a complex was selected for *in vivo* evaluation in a *P. berghei* infected mouse model. Another important aspect to consider when identifying potential lead compounds, is how long it takes the compound of interest to metabolise and what it metabolises to. Therefore, the metabolic stability of ferrocenyl−containing aminoquinoline compounds were assessed in liver microsomes.

1.8 References

1 C. Biot and D. Dive, *Top. Organomet. Chem.*, 2010, **32**, 155–193.

2 World Health Organisation
http://www.who.int/malaria/media/world_malaria_report_2014/en/
(Accessed January 2016).

3 Malaria map
http://www.cdc.gov/malaria/about/distribution.html

(Accessed January 2016).

4 C. Biot, W. Castro, C. Botté and M. Navarro, *Dalton Trans.*, 2012, **41**, 6335–6349.

5 Life cycle of the malaria parasite
http://www.niaid.nih.gov/topics/malaria/pages/lifecycle.aspx
(Accessed March 2015).

6 P. J. Rosenthal, *Int. J. Parasitol.*, 2004, **34**, 1489–1499.

7 K. K. Eggleson, K. L. Duffin and D. E. Goldberg, *J. Biol. Chem.*, 1999, **274**, 32411–32417.

8 G. H. Coombs, D. E. Goldberg, M. Klemba, C. Berry, J. Kay and J. C. Mottram, *Trends Parasitol.*, 2001, **17**, 532–537.

9 N. Chavain, H. Vezin and D. Dive, *Mol. Pharm.*, 2008, 239–244.

10 T. J. Egan, *Mol. Biochem. Parasitol.*, 2008, **157**, 127–136.

11 S. R. Meshnick, *Int. J. Parasitol.*, 2002, **32**, 1655–1660.

12 P. M. O'Neill and G. H. Posner, *J. Med. Chem.*, 2004, **47**, 2945–2964.

13 T. M. Davis, H. A. Karunajeewa and K. F. Ilett, *Med. J. Aust.*, 2005, **182**, 181–185.

14 J. N. Burrows, K. Chibale and T. N. C. Wells, *Curr. Top. Med. Chem.*, 2011, **11**, 1226–1254.

15 J. Swarbrick, P. Iliades, J. S. Simpson and I. Macreadie, *Open Enzym. Inhib. J.*, 2008, **1**, 12–33.

16 D. Petrin, K. Delgaty, R. Bhatt and G. Garber, *Clin. Microbiol. Rev.*, 1998, **11**, 300–317.

17 C. M. Ryan, N. De Miguel and P. J. Johnson, *Essays Biochem.*, 2011, **51**, 161–175.

18 S. Sutcliffe, E. Giovannucci, J. F. Alderete, T.-H. Chang, C. A. Gaydos, J. M. Zenilman, A. M. De Marzo, W. C. Willett and E. A. Platz, *Cancer Epidemiol. Biomarkers Prev.*, 2006, **15**, 939–945.

19 World Health Organisation
http://www.who.int/reproductivehealth/publications/rtis/2008_STI_estimates.pdf
(Accessed January 2016).

20 J. R. Schwebke and D. Burgess, *Clin. Microbiol. Rev.*, 2004, **17**, 794–803.

21 J. G. Rendón-Maldonado, M. Espinosa-Cantellano, A. González-Robles and A. Martínez-Palomo, *Exp. Parasitol.*, 1998, **89**, 241–250.

22 A. Pereira-Neves and M. Benchimol, *Biol. Cell*, 2007, **99**, 87–101.

23 D. Provenzano and J. F. Alderete, *Infect. Immun.*, 1995, **63**, 3388–3395.

24 H. M. Hernández, R. Marcet and J. Sarracent, *Parasite*, 2014, **21**, 54–62.

25 P. Sucharit, A. Uthaischant, T. Chintana, W. Suphadtanapongs, P. Eamsobhana and P.

Prasomsitti, *Southeast Asian J Trop Med Public Health*, 1979, **10**, 556–561.

26 P. Fugere, G. Verschelden and M. Caron, *Obstet. Gynecol.*, 1983, **62**, 502–505.

27 D. Videau, G. Niel, A. Siboulet and F. Catalan, *Br. J. Vener. Dis.*, 1978, **54**, 77–80.

28 M. J. Hayward and R. B. Roy, *Br. J. Vener. Dis.*, 1976, **52**, 63–64.

29 M. Müller, *Biochem. Pharmacol.*, 1986, **35**, 37–41.

30 H. B. Fung and T. Doan, *Clin. Ther.*, 2005.

31 S. P. Fricker, *Dalton Trans.*, 2007, 4903–4917.

32 S. Medici, M. Peana, V. M. Nurchi, J. I. Lachowicz, G. Crisponi and M. A. Zoroddu, *Coord. Chem. Rev.*, 2014, **284**, 329–350.

33 K. H. Thompson and C. Orvig, *Science*, 2003, **300**, 936–939.

34 C. Shaw, *Chem. Rev.*, 1999, **99**, 2589–2600.

35 M. Navarro, W. Castro and C. Biot, *Organometallics*, 2012, **31**, 5715–5727.

36 G. S. Smith and B. Therrien, *Dalton Trans.*, 2011, **40**, 10793–10800.

37 P. Govender, B. Therrien and G. S. Smith, *Eur. J. Inorg. Chem.*, 2012, 2853–2862.

38 P. F. Salas, C. Herrmann and C. Orvig, *Chem. Rev.*, 2013, **113**, 3450–3492.

39 M. A. L. Blackie and K. Chibale, *Met. Based. Drugs*, 2008, **2008**, 495123–495133.

40 P. Martins, M. Marques, L. Coito, A. Pombeiro, P. Baptista and A. Fernandes, *Anticancer. Agents Med. Chem.*, 2014, **14**, 1199–1212.

41 K. D. Mjos and C. Orvig, *Chem. Rev.*, 2014, **114**, 4540–4563.

42 B. Lippert, *Cisplatin: Chemistry and Biochemistry of a Leading Anticancer Drug*, VCHA & Wiley-VCH, Zurich, 1999.

43 R. Trondl, P. Heffeter, C. R. Kowol, M. A. Jakupec, W. Berger and B. K. Keppler, *Chem. Sci.*, 2014, **5**, 2925–2932.

44 D. C. Schuck, S. B. Ferreira, L. N. Cruz, D. R. da Rocha, M. Moraes, M. Nakabashi, P. J. Rosenthal, V. F. Ferreira and C. R. Garcia, *Malar. J.*, 2013, **12**, 234–239.

45 N. H. Gokhale, S. B. Padhye, S. L. Croft, H. D. Kendrick, W. Davies, C. E. Anson and A. K. Powell, *J. Inorg. Biochem.*, 2003, **95**, 249–258.

46 A. R. Sannella, A. Casini, C. Gabbiani, L. Messori, A. R. Bilia, F. F. Vincieri, G. Majori and C. Severini, *FEBS Lett.*, 2008, **582**, 844–847.

47 N. A. David, H. H. Anderson and D. A. Koch, *Proc. Soc. Exp. Biol. Med.*, 1932, **29**, 125–128.

48 A. K. Franz and S. O. Wilson, *J. Med. Chem.*, 2013, **56**, 388–405.

49 S. M. Sieburth and C.-A. Chen, *Eur. J. Org. Chem.*, 2006, **2006**, 311–322.

50 N. R. Cutler, R. D. Seifert, M. M. Schleman, J. J. Sramek, O. J. Szylleyko, D. R. Howard, A. Barchowsky, T. S. Wardle and E. P. Brass, *Clin. Pharmacol. Ther.*, 1995, **58**, 54–61.

51 A. H. Van Hattum, H. M. Pinedo, H. M. M. Schlüper, F. H. Hausheer and E. Boven, *Int. J. Cancer*, 2000, **88**, 260–266.

52 M. Blunder, N. Hurkes, S. Spirk, M. List and R. Pietschnig, *Bioorg. Med. Chem. Lett.*, 2011, **21**, 363–365.

53 V. J. Venditto and E. E. Simanek, *Mol. Pharm.*, 2010, **7**, 307–349.

54 R. G. Pearson, *J. Am. Chem. Soc.*, 1963, **85**, 3533–3539.

55 S. D. Khanye, G. S. Smith, C. Lategan, P. J. Smith, J. Gut, P. J. Rosenthal and K. Chibale, *J. Inorg. Biochem.*, 2010, **104**, 1079–1083.

56 T. T. Tavares, D. Paschoal, E. V. S. Motta, a. G. Carpanez, M. T. P. Lopes, E. S. Fontes, H. F. Dos Santos, H. Silva, R. M. Grazul and a. P. S. Fontes, *J. Coord. Chem.*, 2014, **67**, 956–968.

57 S. D. Khanye, B. Wan, S. G. Franzblau, J. Gut, P. J. Rosenthal, G. S. Smith and K. Chibale, *J. Organomet. Chem.*, 2011, **696**, 3392–3396.

58 C. R. Kowol, R. Berger, R. Eichinger, A. Roller, M. A. Jakupec, P. P. Schmidt, V. B. Arion and B. K. Keppler, *J. Med. Chem.*, 2007, **50**, 1254–1265.

59 D. Kovala-Demertzi, A. Papageorgiou, L. Papathanasis, A. Alexandratos, P. Dalezis, J. R. Miller and M. A. Demertzis, *Eur. J. Med. Chem.*, 2009, **44**, 1296–1302.

60 P. Chellan, N. Shunmoogam-Gounden, D. T. Hendricks, J. Gut, P. J. Rosenthal, C. Lategan, P. J. Smith, K. Chibale and G. S. Smith, *Eur. J. Inorg. Chem.*, 2010, 3520–3528.

61 T. Stringer, P. Chellan, B. Therrien, N. Shunmoogam-Gounden, D. T. Hendricks and G. S. Smith, *Polyhedron*, 2009, **28**, 2839–2846.

62 P. Chellan, T. Stringer, A. Shokar, P. J. Dornbush, G. Vazquez-Anaya, K. M. Land, K. Chibale and G. S. Smith, *J. Inorg. Biochem.*, 2011, **105**, 1562–1568.

63 P. Chellan, S. Nasser, L. Vivas, K. Chibale and G. S. Smith, *J. Organomet. Chem.*, 2010, **695**, 2225–2232.

64 P. Chellan, K. M. Land, A. Shokar, A. Au, S. H. An, C. M. Clavel, P. J. Dyson, C. de Kock, P. J. Smith, K. Chibale and G. S. Smith, *Organometallics*, 2012, **31**, 5791–5799.

65 H. Weiss and F. Mohr, *J. Organomet. Chem.*, 2011, **696**, 3150–3154.

66 A. I. Matesanz and P. Souza, *Mini Rev. Med. Chem.*, 2009, **9**, 1389–1396.

67 R. Brockman, J. Thomson, M. Bell and H. Skipper, *Cancer Res.*, 1956, **16**, 167–170.

68 A. I. Matesanz, C. Hernández, A. Rodríguez and P. Souza, *J. Inorg. Biochem.*, 2011, **105**,

1613–1622.

69 S. A. Khan and M. Yusuf, *Eur. J. Med. Chem.*, 2009, **44**, 2270–2274.

70 R. Arancibia, C. Quintana, C. Biot, M. E. Medina, S. Carrère-Kremer, L. Kremer and A. H. Klahn, *Inorg. Chem. Commun.*, 2015, **55**, 139–142.

71 P. Genova, T. Varadinova, A. I. Matesanz, D. Marinova and P. Souza, *Toxicol. Appl. Pharmacol.*, 2004, **197**, 107–112.

72 C. Shipman Jr, S. H. Smith, J. C. Drach and D. L. Klayman, *Antimicrob. Agents Chemother.*, 1981, **19**, 682–685.

73 D. C. Greenbaum, Z. Mackey, E. Hansell, P. Doyle, J. Gut, C. R. Caffrey, J. Lehrman, P. J. Rosenthal, J. H. McKerrow and K. Chibale, *J. Med. Chem.*, 2004, **47**, 3212–3219.

74 R. B. de Oliveira, E. M. de Souza-Fagundes, R. P. P. Soares, A. A. Andrade, A. U. Krettli and C. L. Zani, *Eur. J. Med. Chem.*, 2008, **43**, 1983–1988.

75 A. Chipeleme, J. Gut, P. J. Rosenthal and K. Chibale, *Bioorg. Med. Chem.*, 2007, **15**, 273–282.

76 C. Sarniguet, J. Toloza, M. Cipriani, M. Lapier, M. Vieites, Y. Toledano-Magaña, J. C. García-Ramos, L. Ruiz-Azuara, V. Moreno, J. D. Maya, C. O. Azar, D. Gambino and L. Otero, *Biol. Trace Elem. Res.*, 2014, **159**, 379–392.

77 A. Marella, M. Shaquiquzzaman, M. Akhter, G. Verma and M. M. Alam, *J. Enzyme Inhib. Med. Chem.*, 2015, **30**, 597–606.

78 I. Chiyanzu, E. Hansell, J. Gut, P. J. Rosenthal, J. H. McKerrow and K. Chibale, *Bioorg. Med. Chem. Lett.*, 2003, **13**, 3527–3530.

79 D. L. Klayman, J. F. Bartosevich, T. S. Griffin, C. J. Mason and J. P. Scovill, *J. Med. Chem.*, 1979, **22**, 855–862.

80 D. L. Klayman, J. P. Scovill, J. F. Bartosevich and J. Bruce, *J. Med. Chem.*, 1983, **26**, 35–39.

81 P. A. Barrett, E. Beveridge, P. L. Bradley, C. G. D. Brown, S. R. M. Bushby, M. L. Clarke, R. A. Neal, R. Smith and J. K. H. Wilde, *Nature*, 1965, **206**, 1340–1341.

82 D. Klayman and J. Scovill, *J. Med. Chem.*, 1979, **22**, 1367–1373.

83 C. Lambros, G. E. Childs, J. D. Notsch, J. P. Scovill, D. L. Klayman and D. E. Davidson Jr, *Antimicrob. Agents Chemother.*, 1982, **22**, 981–984.

84 J. P. Scovill, D. L. Klayman, C. Lambros, G. E. Childs and J. D. Notsch, *J. Med. Chem.*, 1984, **27**, 87–91.

85 S. E. Webber, J. Tikhe, S. T. Worland, S. A. Fuhrman, T. F. Hendrickson, D. A. Matthews,

R. A. Love, A. K. Patick, J. W. Meador, R. A. Ferre, E. L. Brown, D. M. Delisle, C. E. Ford and S. L. Binford, *J. Med. Chem.*, 1996, **39**, 5072–5082.

86 S. J. Shuttleworth, D. Nasturica, C. Gervais, M. A. Siddiqui, R. F. Rando and N. Lee, *Bioorg. Med. Chem. Lett.*, 2000, **10**, 2501–2504.

87 L. P. Duan and H. B. Zhang, *Arab. J. Chem.*, 2011, **4**, 231–234.

88 N. Bharti, K. Husain, M. T. G. Garza, D. E. Cruz-Vega, J. Castro-Garza, B. D. Mata-Cardenas, F. Naqvi and A. Azam, *Bioorg. Med. Chem. Lett.*, 2002, **12**, 3475–3478.

89 R. M. Michaels, L. J. Peterson and G. L. Stahl, *J. Parasitol.*, 1962, **48**, 891–897.

90 J. Valderrama, A. Fournet, C. Valderrama, S. Bastias, C. Astudillo, A. Rojas de Arias, A. Inchausti and G. Yaluff, *Chem. Pharm. Bull.*, 1999, **47**, 1221–1226.

91 F. Delmas, M. Gasquet, P. Timon-David, N. Madadi, P. Vanelle, A. Vaille and J. Maldonado, *Eur. J. Med. Chem.*, 1993, **28**, 23–27.

92 J. P. Scovill, D. L. Klayman and C. F. Franchino, *J. Med. Chem.*, 1982, **25**, 1261–1264.

93 M. Adams, Y. Li, H. Khot, C. de Kock, P. J. Smith, K. Land, K. Chibale and G. S. Smith, *Dalton Trans.*, 2013, **42**, 4677–4685.

94 T. Stringer, B. Therrien, D. T. Hendricks, H. Guzgay and G. S. Smith, *Inorg. Chem. Commun.*, 2011, **14**, 956–960.

95 K. Sampath and C. Jayabalakrishnan, *Arab. J. Chem.*, 2013.
DOI: 10.1016/j.arabjc.2013.12.017.

96 S. Halder, S.-M. Peng, G.-H. Lee, T. Chatterjee, A. Mukherjee, S. Dutta, U. Sanyal and S. Bhattacharya, *New J. Chem.*, 2008, **32**, 105–114.

97 A. A. El-Asmy, O. A. El-Gammal and H. S. Saleh, *Spectrochim. Acta. A. Mol. Biomol. Spectrosc.*, 2008, **71**, 39–44.

98 R. M. El-Shazly, G. A. A. Al-Hazmi, S. E. Ghazy, M. S. El-Shahawi and A. A. El-Asmy, *J. Coord. Chem.*, 2008, **59**, 845–859.

99 S. D. Khanye, J. Gut, P. J. Rosenthal, K. Chibale and G. S. Smith, *J. Organomet. Chem.*, 2011, **696**, 3296–3300.

100 T. Stringer, D. Taylor, C. de Kock, H. Guzgay, A. Au, S. H. An, B. Sanchez, R. O'Connor, N. Patel, K. M. Land, P. J. Smith, D. T. Hendricks, T. J. Egan and G. S. Smith, *Eur. J. Med. Chem.*, 2013, **69**, 90–98.

101 C. Teixeira, N. Vale, B. Pe, A. Gomes, J. R. B. Gomes and P. Gomes, *Chem. Rev.*, 2014, **14**, 11164–11220.

102 J. N. Burrows, E. Burlot, B. Campo, S. Cherbuin, S. Jeanneret, D. Leroy, T. Spangenberg,

D. Waterson, T. N. Wells and P. Willis, *Parasitology*, 2014, **141**, 128–139.

103 K. Kaur, M. Jain, R. P. Reddy and R. Jain, *Eur. J. Med. Chem.*, 2010, **45**, 3245–3264.

104 L. H. Huang, H. De Xu, Z. Y. Yang, Y. F. Zheng and H. M. Liu, *Steroids*, 2014, **82**, 1–6.

105 B. Heiniger, G. Gakhar, K. Prasain, D. H. Hua and T. A. Nguyen, *Anticancer Res.*, 2010, **30**, 3927–3932.

106 V. V. Kouznetsov, F. A. R. Ruiz, L. Y. Vargas Mendez and M. P. Gupta, *Lett. Drug Des. Discov.*, 2012, **9**, 680–686.

107 V. R. Solomon and H. Lee, *Curr. Med. Chem.*, 2011, **18**, 1488–1508.

108 P. Senthilkumar, M. Dinakaran, P. Yogeeswari, D. Sriram, A. China and V. Nagaraja, *Eur. J. Med. Chem.*, 2009, **44**, 345–358.

109 T. J. Egan, W. W. Mavuso, D. C. Ross and H. M. Marques, *J. Inorg. Biochem.*, 1997, **68**, 137–145.

110 T. M. E. Davis, T. Hung, I. Sim, H. A. Karunajeewa and K. F. Ilett, *Drugs*, 2005, **65**, 75–87.

111 J. Y. Wang, W. C. Cao, C. Q. Shan, M. Zhang, G. F. Li, D. Ben Ding, Y. L. Shi and B. A. Wu, *Acta Trop.*, 2004, **89**, 375–381.

112 F. Coslédan and L. Fraisse, *Proc. Natl. Acad. Sci.*, 2008, **105**, 17579–17584.

113 M. A. Biamonte, J. Wanner and K. G. Le Roch, *Bioorg. Med. Chem. Lett.*, 2013, **23**, 2829–43.

114 F. A. R. Ruiz, R. N. Garcia-Sanchez, S. V. Estupinan, A. Gomez-Barrio, D. F. T. Amado, B. M. Perez-Solorzano, J. J. Nogal-Ruiz, A. R. Martinez-Fernandez and V. V. Kouznetsov, *Bioorg. Med. Chem.*, 2011, **19**, 4562–4573.

115 M. Tukulula, S. Little, J. Gut, P. J. Rosenthal, B. Wan, S. G. Franzblau and K. Chibale, *Eur. J. Med. Chem.*, 2012, **57**, 259–267.

116 F. Benoit-Vical, J. Lelièvre, A. Berry, C. Deymier, O. Dechy-Cabaret, J. Cazelles, C. Loup, A. Robert, J. F. Magnaval and B. Meunier, *Antimicrob. Agents Chemother.*, 2007, **51**, 1463–1472.

117 C. Nava-Zuazo, S. Estrada-Soto, J. Guerrero-Alvarez, I. León-Rivera, G. M. Molina-Salinas, S. Said-Fernández, M. J. Chan-Bacab, R. Cedillo-Rivera, R. Moo-Puc, G. Mirón-López and G. Navarrete-Vazquez, *Bioorg. Med. Chem.*, 2010, **18**, 6398–6403.

118 M. Martínez-Grueiro, C. Giménez-Pardo, A. Gómez-Barrio, X. Franck, A. Fournet, R. Hocquemiller, B. Figadère and N. Casado-Escribano, *Farmaco*, 2005, **60**, 219–224.

119 V. V Kouznetsov, L. Y. V. Méndez, B. Tibaduiza, C. Ochoa, D. M. Pereira, J. J. N. Ruiz,

C. F. Portillo, S. M. Serrano, A. Gómez Barrio, A. Bahsas and J. Amaro-Luis, *Arch. Pharm.*, 2004, **337**, 127–132.

120 R. A. Sánchez-Delgado, M. Navarro, H. Pérez and J. A. Urbina, *J. Med. Chem.*, 1996, **39**, 1095–1099.

121 C. S. K. Rajapakse, A. Martínez, B. Naoulou, A. A. Jarzecki, L. Suárez, C. Deregnaucourt, V. Sinou, J. Schrével, E. Musi, G. Ambrosini, G. K. Schwartz and R. A. Sánchez-Delgado, *Inorg. Chem.*, 2009, **48**, 1122–1131.

122 M. Navarro, F. Vásquez, R. A. Sánchez-Delgado, H. Pérez, V. Sinou and J. Schrével, *J. Med. Chem.*, 2004, **47**, 5204–5209.

123 C. Biot, G. Glorian, L. A. Maciejewski and J. S. Brocard, *J. Med. Chem.*, 1997, **40**, 3715–3718.

124 B. C. S. Allardyce and P. J. Dyson, *Platin. Met. Rev.*, 2001, 62–69.

125 C. Biot, F. Nosten, L. Fraisse, J. Khalife and D. Dive, *Parasite*, 2011, **18**, 207–214.

126 L. Delhaes, C. Biot, L. Berry, L. A. Maciejewski, D. Camus, J. S. Brocard and D. Dive, *Bioorg. Med. Chem.*, 2000, **8**, 2739–2745.

127 C. Biot, L. Delhaes, L. A. Maciejewski, M. Mortuaire, D. Dive and J. S. Brocard, *Eur. J. Med. Chem.*, 2000, **35**, 707–714.

128 F. Bellot, F. Coslédan, L. Vendier, J. Brocard, B. Meunier and A. Robert, *J. Med. Chem.*, 2010, **53**, 4103–4109.

129 L. Glans, D. Taylor, C. de Kock, P. J. Smith, M. Haukka, J. R. Moss and E. Nordlander, *J. Inorg. Biochem.*, 2011, **105**, 985–990.

130 R. Arancibia, F. Dubar, B. Pradines, I. Forfar, D. Dive, A. H. Klahn and C. Biot, *Bioorg. Med. Chem.*, 2010, **18**, 8085–8091.

131 S. N. Manjula, N. Malleshappa Noolvi, K. Vipan Parihar, S. A. Manohara Reddy, V. Ramani, A. K. Gadad, G. Singh, N. Gopalan Kutty and C. Mallikarjuna Rao, *Eur. J. Med. Chem.*, 2009, **44**, 2923–2929.

132 M. N. Noolvi, H. M. Patel and M. Kaur, *Eur. J. Med. Chem.*, 2012, **54**, 447–462.

133 S. Saeed, N. Rashid, P. G. Jones, M. Ali and R. Hussain, *Eur. J. Med. Chem.*, 2010, **45**, 1323–1331.

134 R. S. Keri, M. R. Patil, S. A. Patil and S. Budagumpi, *Eur. J. Med. Chem.*, 2015, **89**, 207–251.

135 R. J. Alaimo, S. S. Pelosi, C. J. Hatton and J. E. Gray, *J. Med. Chem.*, 1974, **17**, 775–776.

136 F. Delmas, C. Di Giorgio, M. Robin, M. Gasquet, C. Detang, M. Costa, N. Azas, P. Timon-

David and J.-P. Galy, *Antimicrob. Agents Chemother.*, 2002, **46**, 2588–2594.

137 S. Hout, N. Azas, a. Darque, M. Robin, C. Di Giorgio, M. Gasquet, J. Galy and P. Timon-David, *Parasitology*, 2004, **129**, 525–535.

138 D. S. B. Ongarora, J. Gut, P. J. Rosenthal, C. M. Masimirembwa and K. Chibale, *Bioorg. Med. Chem. Lett.*, 2012, **22**, 5046–5050.

139 N. A. Pulina, F. V. Sobin, T. A. Yushkova, T. F. Odegova and A. I. Krasnova, *Pharm. Chem. J.*, 2014, **48**, 505–508.

140 S. Sathiyaraj, K. Sampath, R. J. Butcher and C. Jayabalakrishnan, *Transit. Met. Chem.*, 2013, **38**, 291–298.

141 C. Biot, L. Delhaes, C. M. N'Diaye, L. A. Maciejewski, D. Camus, D. Dive and J. S. Brocard, *Bioorg. Med. Chem.*, 1999, **7**, 2843–2847.

CHAPTER 2

Synthesis and Characterisation of Mono– and Binuclear Organosilane Thiosemicarbazone Metal Complexes

2.1 Introduction

Thiosemicarbazones (TSC), are thiourea–based compounds known for their ability to chelate to metals by means of electron–rich donor atoms. The thiourea moiety is found in biologically active compounds,[1–4] making TSCs attractive systems to work with in terms of metal complex preparation and biological evaluation thereof.

Several bonding modes such as monodentate, bidentate or tridentate modes (Figure 2.1) have been observed for thiosemicarbazones.[5–8] In the case of monodentate complexes, the metal ion generally coordinates *via* the thione sulfur atom. The metal ion coordinates *via* the imine nitrogen atom and the thione/thiolate sulfur atom when the TSC chelates in a bidentate manner. Tridentate complexes are formed *via* the coordination of the metal ion to the imine nitrogen atom, the thiolate/thione sulfur atom and an additional atom which is usually either part of a ring system (e.g. pyridyl, thiophene, phenyl) or attached to the ring system (e.g., deprotonated hydroxyl group).[5–8]

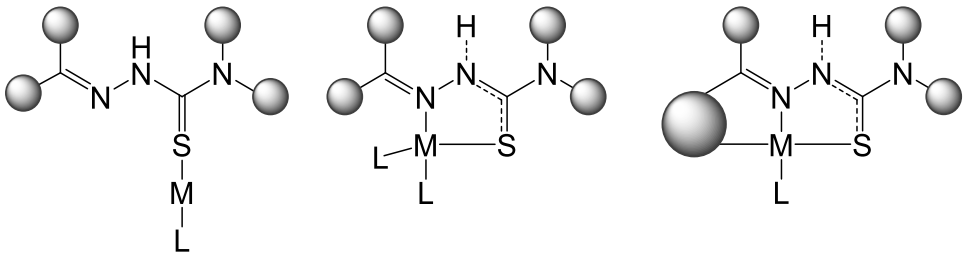

Figure 2.1 Monodentate (**I**), bidentate (**II**) and tridentate (**III**) coordination modes.[5]

Thiosemicarbazones and their complexes have previously been evaluated within our research group for their biological activities.[9–16] Smith and co–workers investigated cycloplatinated, cyclopalladated, palladium(II) salicylaldiminato and ruthenium−arene TSC complexes *in vitro* as antiplasmodial and/or antitrichomonal agents.[9,10,16,17] It was found that the compounds containing chlorines on the aromatic ring generally displayed better activity against the *Plasmodium falciparum* and *Trichomonas vaginalis* parasitic strains than the compounds with

unsubstituted aromatic rings.[16] In the studies involving the cycloplatinated and cyclopalladated TSC complexes, the incorporation of a 1,3,5-triaza-7-phosphaadamantane (PTA) ligand generally led to improved activity.[9,17] The cycloplatinated complex **IV** displayed moderate biological activities against *P. falciparum* strains, giving IC_{50} values of 21.42 (D10) and 24.90 μM (Dd2). Against the parasite *T. vaginalis* (T1 strain), compound **IV** displayed 92.5 % inhibition of parasite growth at 100 μM and an IC_{50} value of 21.1 μM (Metronidazole: IC_{50} = 0.72 μM).[9] The cyclopalladated complexes **V** was screened against the NF54 and Dd2 strains and displayed low micromolar IC_{50} values of 1.93 and 2.69 μM, respectively.[17] Compound **V** was not tested against the parasite *T. vaginalis*.

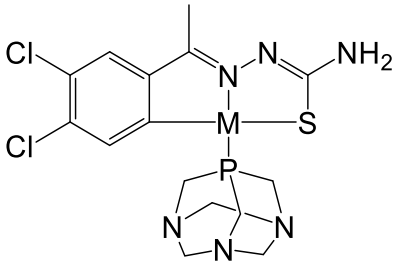

IV: M = Pt; **V:** M = Pd

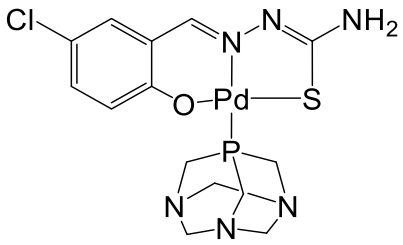

VI

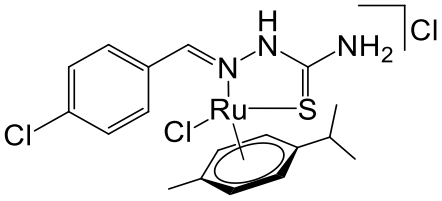

VII

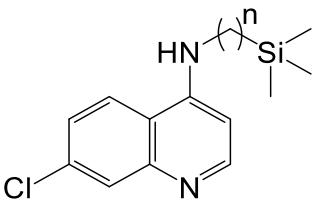

VIII: n = 1; **IX**: n = 3

Figure 2.2 Compounds **IV**–**IX** were evaluated as antiparasitic agents. [9,10,16–18]

In another study, the palladium(II) salicylaldiminato TSC complexes were evaluated against the T1 strain of *T. vaginalis*.[10] The tested complexes displayed varying percentages of parasite growth inhibition ranging from 14–97 %, with compound **VI** (Figure 2.2), the most potent inhibitor, displaying the lowest IC_{50} values of 17 μM (Metronidazole: IC_{50} = 0.72 μM).[10]

Another metal of interest in antiparasitic research has been ruthenium, which led to the evaluation of ruthenium(II)−arene complexes such as compound **VII** (Figure 2.2) which displayed IC_{50} values of 2.9 μM (NF54) and 3.8 μM (Dd2). Moderate activity was observed against the G3 strain of *T. vaginalis*, with an IC_{50} value of 7.56 μM.[16] Additionally, the compounds containing a ferrocenyl moiety displayed moderate potency which may be improved upon.

In addition to the pharmacologically active thiourea–containing compounds, organosilanes are of significant interest. As mentioned in Chapter 1 (Section 1.4.1), the idea of enhancing the pharmacological properties of a drug, or the repurposing of the drug for treatment of an alternate disease may be achieved through incorporation of organosilanes.[19–21] Silicon–containing compounds have been associated with enhanced cell and tissue penetration, provided a suitable balance between hydrophilicity and lipophilicity exists.[19] Additionally, the lipophilicity, as well as electropositive nature of silicon, may alter the selectivity of the organosilane compounds compared to their carbon analogues. These properties of the silicon–containing compounds have made organosilanes an attractive field to pursue.

In terms of TSCs and silicon, coordination complexes involving the chelation of TSC to silicon(IV) are found in literature.[22,23] None of the TSC compounds involve the formation of organosilane (C–Si) bonds, which are then chelated to selected transition metals. As seen in Figure 2.2, TSCs previously evaluated as antiparasitic agents contained an unsubstituted terminal amine. This led to the idea of altering the structure of previously evaluated TSC compounds through incorporation of organosilanes in order to improve pharmacological effects.

In another study, non–TSC compounds containing organosilanes of interest were synthesised. Li *et al*. prepared silicon–containing 7-chloro-4-aminoquinoline compounds which were evaluated as antitumour, antimycobacterial and antiplasmodial agents.[18] In terms of the *in vitro* *P. falciparum* studies, compounds **VIII** and **IX** (Figure 2.2) displayed activities in the nanomolar range, with IC_{50} values of 248 and 98 nM, respectively, against the NF54 strain. Additionally, compound **IX** also exhibited higher activity against the Dd2 (270 nM) strain of *P. falciparum*.[18]

For this study, compounds with increased potency and an ability to circumvent antiparasitic drug resistance are of interest. The scarcity of research on organosilicon TSCs as antiparasitic agents provides an avenue worthy of exploration. In this project, organosilane TSCs with bidentate [*N,S* (thione)] and tridentate [*C,N,S* (thiolate)] systems were studied.

2.2 Results and Discussion

2.2.1 Synthesis and Characterisation of Schiff base Dithiocarbamates and Organosilane Thiosemicarbazones

Synthesis

Methyl hydrazinecarbodithioate was synthesised by means of a published method.[24] Schiff base dithiocarbamates (**2.1** and **2.2**) were prepared by the procedure illustrated in Scheme 2.1. The dithiocarbamates were synthesised *via* a Schiff base condensation reaction between the respective aldehyde (ferrocenecarboxaldehyde and 3,4-dichlorobenzaldehyde) or ketone (acetylferrocene and 3,4-dichoroacetophenone) and methyl hydrazinecarbodithioate.

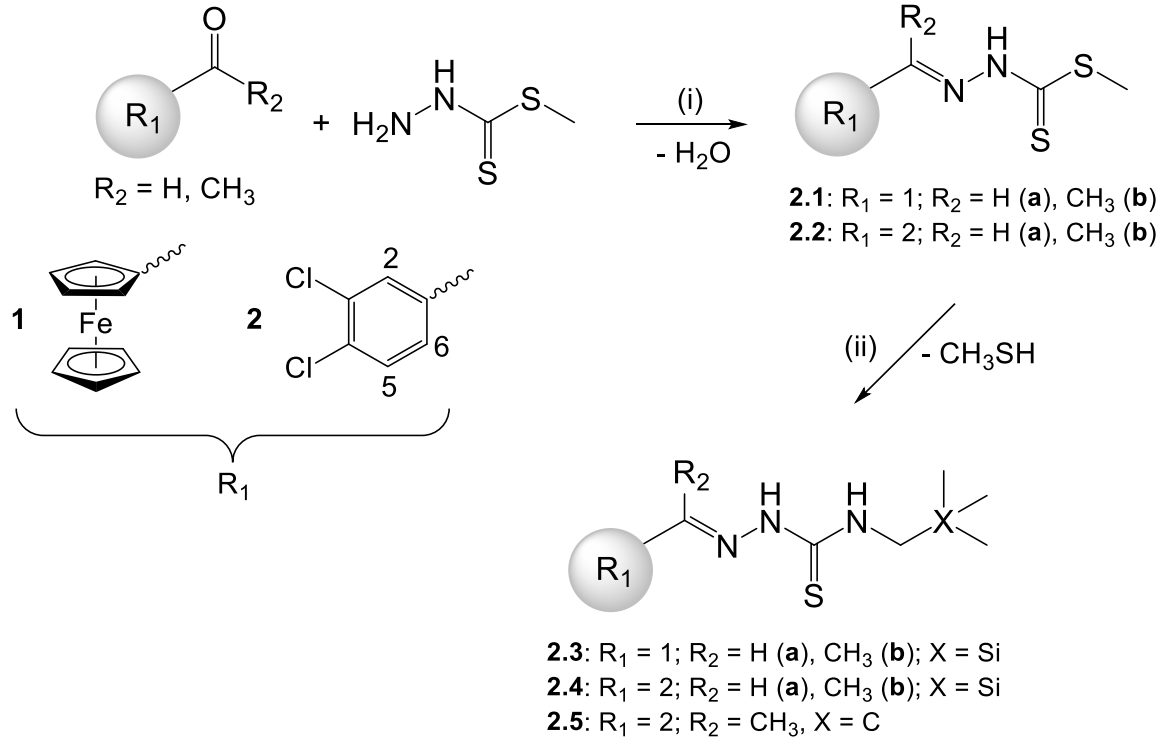

Scheme 2.1 The synthesis of the Schiff base dithiocarbamates (**2.1a–b** and **2.2a–b**) and the corresponding thiosemicarbazones (**2.3a–b**, **2.4a–b** and **2.5**).
Reagents and conditions: (i) 2-Propanol, 70 ˚C, 24 hr; (ii) (aminomethyl)trimethylsilane (**2.3**, **2.4**) or 2,2'-dimethylpropan-1-amine (**2.5**), Ethanol, 70 ˚C, 22 hr (**2.3a**); 7 hr (**2.3b**); 24 hr (**2.4a**, **2.4b**, **2.5**).

Motivation for the choice of the R_1 group

Cohen and co–workers screened a wide range of thiosemicarbazones for their ability to inhibit cysteine proteases.[25] The thiosemicarbazones which contained a 3,4-dichloroaryl group were amongst the most active compounds. In addition to this, TSCs prepared within our group, which contained the above mentioned 3,4-dichloro-substituted aryl group, have displayed good antiplasmodial activities.[12] Furthermore, as mentioned in Chapter 1 (Section 1.6.1), the

incorporation of ferrocenyl moieties is believed to assist with membrane penetration and redox properties.

Compounds **2.1a**–**b** and **2.2b** have previously been synthesised.[26–28] Compound **2.2a** is a new compound, which was isolated as an off–white powder in moderate yield (68 %) with a melting point range of 200.9–201.4 ˚C. The compound is soluble in most organic solvents and insoluble in water and non–polar organic solvents.

Five new thiosemicarbazones were synthesised following the procedure described in Scheme 2.1. The organosilane compounds were prepared *via* a nucleophilic acyl substitution reaction between the Schiff base dithiocarbamates and an amine, as illustrated in Figure 2.3. The nucleophilic amine attacks the electrophilic thiocarbonyl carbon of the dithiocarbamate to form an unstable tetrahedral intermediate. Reforming the thiocarbonyl double bond and proton transfer (PT) results in the elimination of methanethiol gas and formation of the desired TSC. Additionally, a carbon analogue of compound **2.4b** was synthesised, using 2,2'-dimethylpropan-1-amine, to determine if the Si atom is significant for biological activity.

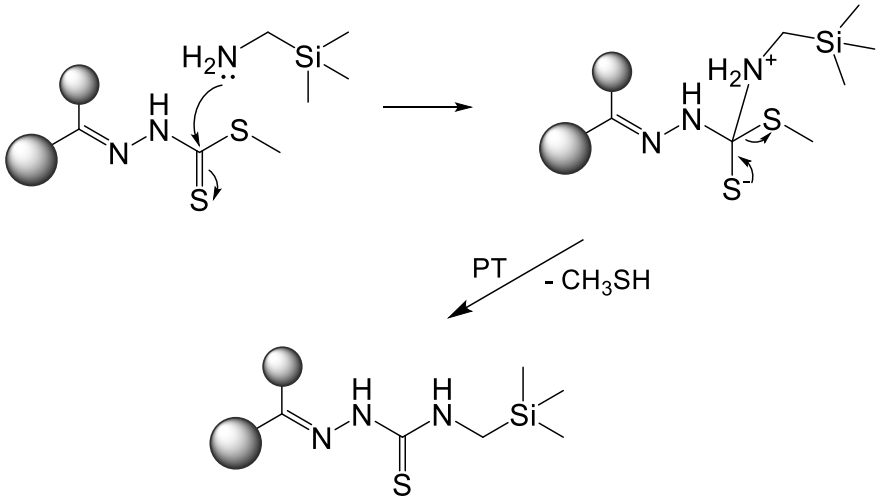

Figure 2.3 Formation of organosilane thiosemicarbazones *via* a nucleophilic acyl substitution reaction.

Compounds **2.3a**–**b** were isolated as brown powders and compounds **2.4a**–**b** and **2.5** were isolated as white powders in low to high yields (34–83 %). Compounds **2.3**–**2.5** are soluble in most organic solvents such as dichloromethane, chloroform, diethyl ether and dimethyl sulfoxide. Not surprisingly, the compounds are not soluble in water or non-polar solvents such as hexane and pentane.

Characterisation

Compounds **2.2a**, **2.3a**–**b**, **2.4a**–**b** and **2.5** were fully characterised using NMR (^{1}H; ^{13}C{^{1}H}) spectroscopy, infrared (IR) spectroscopy and electron impact mass spectrometry (EI–MS).

NMR Spectroscopy

The ^{1}H NMR spectrum of compound **2.2a** was recorded in DMSO–d_6. The compound displays a singlet corresponding to the imine proton at 8.21 ppm. Formation of the Schiff base shields the SCH_3 protons, resulting in a small upfield shift of the peak (2.53 ppm) compared to that observed for methyl hydrazinecarbodithioate (2.63 ppm). The peak corresponding to the hydrazinic proton is observed downfield at 13.4 ppm. The peaks for the aromatic protons H–5 and H–6 overlap, while a broad signal is observed for H–2.

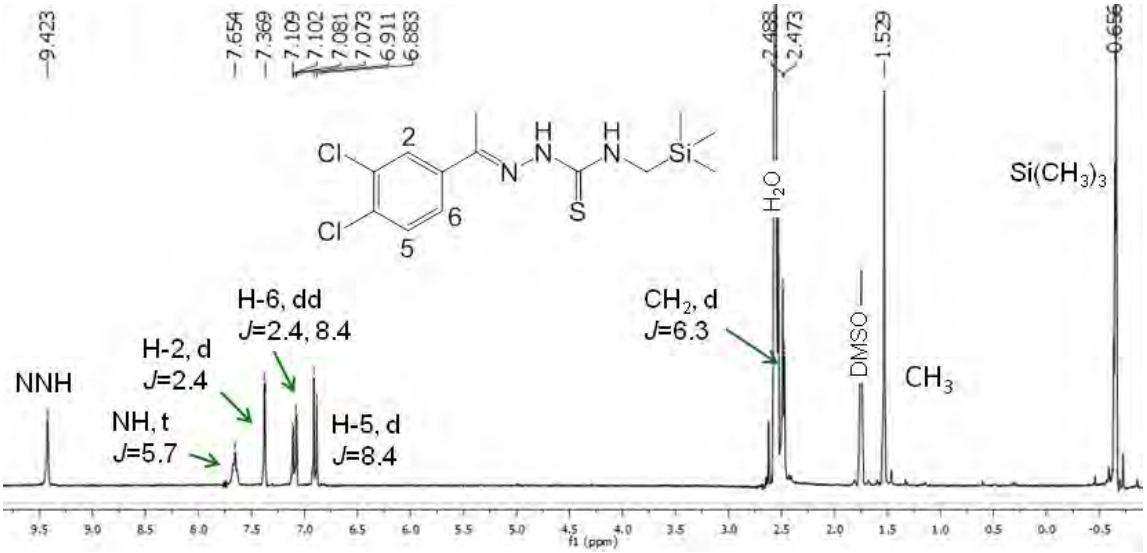

Figure 2.4 ^{1}H NMR spectrum of 3,4-dichlorophenylethylidene-((trimethylsilyl)methyl) TSC (**2.4b**).

Compounds **2.3a**, **2.4a** and **2.5** were recorded in $CDCl_3$ and compounds **2.3b** and **2.4b** in DMSO–d_6. It was evident from the ^{1}H NMR spectra that the organosilane TSCs had been synthesised. The absence of a singlet for the methanethiol protons and the appearance of a signal for the newly incorporated amine confirm this. In addition to the presence of a singlet in the range 0.10–0.18 ppm for the $Si(CH_3)_3$ protons[18], it was also observed that the CH_2 protons couple to the proton of the adjacent secondary amine. A doublet is observed at approximately 3.30 ppm ($^{3}J_{HH}$ ~ 5.90 Hz) for the CH_2 protons of the TSC compounds. For the carbon analogue **2.5**, the $C(CH_3)_3$ protons resonate as a singlet at 1.04 ppm.

The hydrazinic proton is more deshielded than the other secondary amine proton, and resonates in the range 8.46–10.1 ppm. In $CDCl_3$, the peak for the second amine proton is observed as a broad signal in the range 7.31–7.74 ppm. However, in DMSO–d_6 (**2.3b**, **2.4b**) the peak for the amine proton is observed as a triplet ($^3J_{HH}$ = 5.70 Hz; Figure 2.4) at 7.95 and 8.41 ppm, respectively. As mentioned before, the amine proton couples to the adjacent CH_2 protons resulting in the observed triplet. For compounds **2.3a** and **2.4a**, the peak associated with the imine proton is observed at 7.65 and 7.78 ppm, respectively. The protons of the methyl group situated on the azomethine carbon atom resonate as a singlet between 2.14–2.26 ppm for compounds **2.3b**, **2.4b** and **2.5**.

Similar trends are seen for the ferrocenyl (**2.3a**−**b**) and aromatic (**2.4a–b**, **2.5**) TSC compounds. Three peaks corresponding to the ferrocenyl protons are observed between 4.15 and 4.74 ppm. Two triplets ($^3J_{HH}$ = 2.00 Hz) corresponding to the protons on the substituted cyclopentadienyl (Cp) ring and one singlet associated with the unsubstituted Cp ring are observed.[29] The H–2, H–5 and H–6 protons of the aryl ring resonate as a doublet, doublet and doublet of doublets, respectively, in the range 7.41–8.13 ppm.

The $^{13}C\{^1H\}$ NMR spectrum of compound **2.2a** was recorded in DMSO–d_6. The $^{13}C\{^1H\}$ NMR spectrum of compound **2.2a** displays peaks at 199.0 and 143.4 ppm which correspond to the thiocarbonyl and azomethine carbon atoms, respectively. The aromatic carbon atoms resonate in the range 127–134 ppm and the carbon atom of the methyl group (SCH_3) resonates upfield at 16.7 ppm.

The $^{13}C\{^1H\}$ NMR spectra of compounds **2.3a–b**, **2.4a** and **2.5** were recorded in $CDCl_3$ and compound **2.4b** in DMSO–d_6. With the formation of the organosilane TSCs (**2.3a–b**, **2.4a–b**), two additional peaks are observed in the $^{13}C\{^1H\}$ NMR spectra. The CH_2 carbon atom resonates at around 35.0 ppm, while the methyl carbon atoms of the $Si(CH_3)_3$ group resonates as a singlet in the range –1.84 to –2.50 ppm for organosilane TSCs (**2.3a–b**, **2.4a–b**).[18] In addition to the CH_2 carbon atom (55.8 ppm), and the methyl carbon atom of the $C(CH_3)_3$ group (27.4 ppm), the carbon analogue displays an additional peak at 32.2 ppm which correspond to the quaternary carbon atom of the $C(CH_3)_3$ group.

Formation of the thiosemicarbazones (**2.3**–**2.5**) occurs *via* the substitution of the methanethiol group with the amine. This resulted in a more shielded thiocarbonyl carbon atom which resonates at ~178 ppm [199.0 ppm (**2.2a**)]. Amines are stronger bases than thiols, and thus the newly incorporated amine group has a larger electron donating effect, resulting in a more shielded thiocarbonyl carbon atom. No significant shift is observed for the peak of the imine carbon atom, which resonates between 143.1 and 148.0 ppm. As with the imine carbon, no significant change is observed for the peak associated with the CH_3 carbon atom ($\underline{C}H_3C{=}N$) upon formation of the TSC compounds (**2.3**–**2.5**). The ferrocenyl carbon atoms resonate between 66.8 and 82.5 ppm, with the quaternary carbon atoms being the most deshielded. The peaks for the aromatic carbon atoms are observed in the range 125.1–138.4 ppm.

Infrared Spectroscopy

Infrared analysis of compounds **2.3a**, **2.4a**–**b** and **2.5** was carried out using KBr pellets, while ATR was used for **2.2a** and **2.3b**. In the infrared spectrum of compound **2.2a**, the absorption bands observed at 1586 and 812 cm^{-1} corresponds to C=N imine and C=S bond, respectively.

Table 2.1 The C=N and C=S stretching vibrations for compounds **2.2**–**2.5**.

Compound	C=N ν (cm^{-1})	C=S ν (cm^{-1})	Si-CH_3 ν (cm^{-1})
2.2a	1586	812	–
2.3a	1606	856	1245
2.3b	1600	851	1243
2.4a	1602	854	1250
2.4b	1616	846	1252
2.5	1615	858	–

A comparison of the infrared spectra of the dithiocarbamates and TSCs (**2.3**–**2.5**) reveals a significant shift, which is expected for the absorption band of the C=S bond. An absorption band is observed in the range 846−858 cm^{-1} (Table 2.1), which is at a higher wavenumber than the Schiff base dithiocarbamates. As mentioned before, the incorporation of the amine results in a higher electron density on the carbon of the new C−N bond, shifting the absorption band to a lower wavenumber. The absorption bands for the imine bond are observed in the range 1600–1616 cm^{-1}. Furthermore, incorporation of the organosilane is confirmed by the presence of the absorption band between 1243 and 1252 cm^{-1}, which corresponds to the Si−CH_3 bond.

Mass Spectrometry

Compounds **2.2a** and **2.3**–**2.5** were analysed using electron impact mass spectrometry. The mass spectrum of compound **2.2a** displays the molecular ion peak at *m/z* 277.94 (Theoretical: 277.9504 g.mol^{-1}), once again confirming formation of the desired dithiocarbamate. For compounds **2.3**–**2.5**, the estimated molecular masses were calculated to be 373.0724, 387.07, 333.00, 347.04 and 331.0672 g.mol^{-1}, which is consistent with the molecular ion peaks observed at *m/z* 373.07, 387.04, 333.00, 347.02 and 330.98, respectively.

2.2.2 Synthesis and Characterisation of Organosilane Thiosemicarbazone Half–Sandwich Ruthenium(II) Complexes

As previously discussed in Chapter 1, a strategy to improve the biological activity of a compound involves the incorporation of transition metals. Therefore, in this project we sought to prepare organosilane TSC ruthenium(II) complexes for evaluation as antiparasitic agents.

Synthesis

The bridge–splitting reaction of the ruthenium dimer $[Ru(\eta^6\text{-}p\text{-}^iPrC_6H_4Me)Cl_2]_2$ by two equivalents of TSC (**2.3a**–**b**, **2.4a**–**b**, **2.5**) was used to prepare five new chiral ruthenium(II) complexes, as outlined in Scheme 2.2.

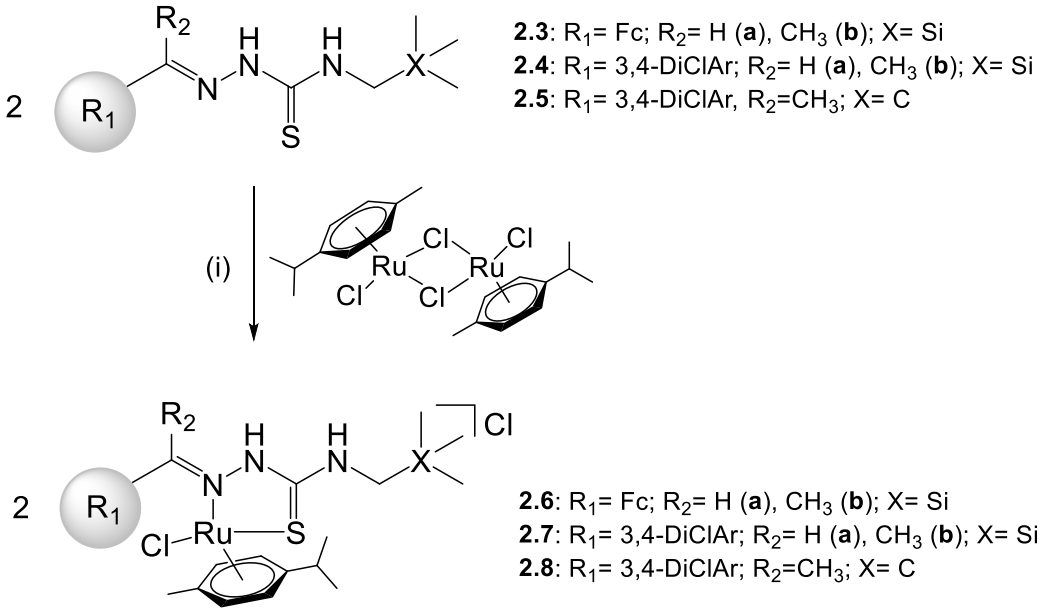

Scheme 2.2 The synthesis of organosilane thiosemicarbazone ruthenium(II) complexes **2.6**–**2.8**.
Reagents and conditions: (i) Dichloromethane, r.t., 4 hr.

Compounds **2.6**–**2.8** were isolated as orange to red solids in moderate yields (61−84 %), and relatively stable to temperatures above 100 ˚C. The complexes are soluble in most polar organic solvents (e.g. chlorinated solvents, alcoholic solvents, etc.), and as expected insoluble in non-polar solvents and water.

Characterisation

The racemic mixtures of the ruthenium complexes were characterised using NMR (^{1}H, ^{13}C{^{1}H}, COSY, HSQC) spectroscopy, infrared (IR) spectroscopy and high resolution electrospray ionisation (ESI) mass spectrometry.

NMR Spectroscopy

The ^{1}H NMR spectra of the ruthenium(II) complexes (**2.6**–**2.8**) were recorded in $CDCl_3$. Due to the orientation around the ruthenium centre, the arene ring losses its two–fold symmetry, resulting in protons being observed in different environments.[14,16,30] The aromatic *p*–cymene protons (Figure 2.5) are observed in the range 4.10–5.52 ppm ($^{3}J_{HH}$ ~ 6.00 Hz) as a set of four doublets each accounting for one aromatic proton, as opposed to the two doublets observed for the starting material. Additionally, the two methyl groups (isopropyl) are observed as two doublets between 1.08–1.21 ppm ($^{3}J_{HH}$ ~ 6.80 Hz). The remaining *p*–cymene protons, CH (multiplet) and CH_3 (singlet) are observed between 2.57–2.66 and 2.06−2.15 ppm, respectively.

The ruthenium metal coordinates to the imine nitrogen, and due to back–donation, the environment of the imine proton and the methyl protons (CH_3C=N) are altered. The peak associated with the methyl protons (CH_3C=N) of TSC compounds **2.6b**, **2.7b** and **2.8** have shifted downfield upon complexation, from around 2.20 to approximately 3.00 ppm. Similarly, the imine proton is also more deshielded upon complexation, resonating at 8.60 and 8.79 ppm (ligands: ~7.70 ppm), respectively, for **2.6a** and **2.7a**.

While the $Si(CH_3)_3$ protons have been deshielded (shift from ~0.13 to ~0.22 ppm), the CH_2 protons have been slightly shielded (from ~3.23 to ~3.05 ppm). The same effect is observed for compound **2.8**, where the $C(CH_3)_3$ protons are slightly deshielded upon formation of the complex [1.04 (**2.5**) to 1.08 ppm], while the CH_2 protons are more shielded [3.60 (**2.5**) to 3.41 ppm]. Binding of the ruthenium arene fragment has also had a deshielding effect on the amine

protons. Both the hydrazinic proton and the other secondary amine proton resonate downfield in comparison with the free TSC. As seen with other ruthenium arene complexes containing a ferrocenyl ligand, one of the protons of the substituted Cp ring is significantly more deshielded than the other three protons on the ring.[16] The proton resonates at approximately 6.10 ppm, whilst the remaining ferrocenyl protons resonate in the expected region between 4.00 and 5.00 ppm.

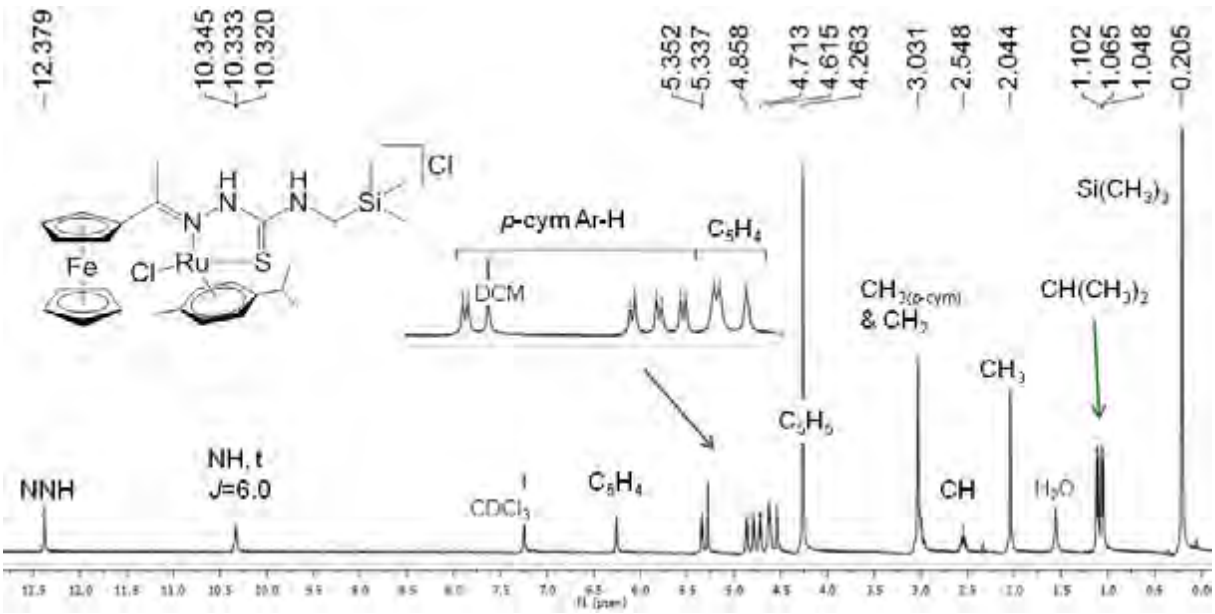

Figure 2.5 ^{1}H NMR spectrum of the ruthenium(II) complex **2.6b**.

The $^{13}C\{^{1}H\}$ NMR spectra of compounds **2.6a**–**b**, **2.7a**–**b** and **2.8** were recorded in $CDCl_3$. No significant change is observed for the thiocarbonyl carbon (~178 ppm). As previously mentioned, coordination of the ruthenium metal ion to the imine nitrogen affects the environment around the imine bond due to back–donation. Therefore, the imine carbon atom is more deshielded as it resonates at approximately 163 ppm (ligand: ~144 ppm).

Similarly, the carbon of the CH_3 attached to the imine carbon atom of compounds **2.6b**, **2.7b** and **2.8** is also significantly deshielded and observed at ~27.0 ppm (ligand: ~14.0 ppm). The presence of the newly incorporated *p*–cymene ring carbon atoms are also observed in the $^{13}C\{^{1}H\}$ NMR spectra. Decomposition of **2.6a** is observed after 2 hours, which may explain why the peaks for the ferrocenyl carbon atoms were not resolved (broad hump).

Infrared Spectroscopy

Infrared analysis of compounds **2.6a**, **2.6b** and **2.7b** were carried out using KBr pellets, while **2.7a** and **2.8** was analysed using ATR. As seen in the infrared spectra of similar cationic complexes, upon chelation of the TSC to the ruthenium centre, a high energy shift was expected for the absorption band of the C=N bond.[14] The absorption band for the imine bond is observed as a weak shoulder in the range 1624−1633 cm^{-1}, which was at a higher wavenumber than found for the TSCs (1600−1616 cm^{-1}).

Mass Spectrometry

The ruthenium complexes **2.6**−**2.8** were analysed using high resolution electrospray ionisation mass spectrometry. Complexes **2.6**−**2.8** were calculated to have theoretical molecular masses of 678.9866, 693.0392, 638.9808, 654.0042 and 638.0242 $g.mol^{-1}$, respectively. The mass spectra of the ruthenium complexes (**2.6a**–**b**, **2.7a**–**b**, **2.8**) revealed a peak at *m/z* 304.5437, 311.5522, 284.5207, 291.5291 and 284.5441, respectively. These peaks correspond to the fragment $[M–Cl]^{2+}$ (M refers to the complex cation excluding the Cl counter-ion). A peak corresponding to the fragment $[M–H–Cl]^{+}$ has also been observed for the compounds (**2.6a**–**b**, **2.7a**–**b**, **2.8**) at *m/z* 608.0793, 622.0960, 568.0345, 582.0500 and 568.0828, respectively. The mass spectra further confirm the successful preparation of the desired ruthenium complexes.

Molecular Structure

Crystals suitable for single−crystal X−ray diffraction were grown by slowly diffusing pentane into a solution of compound **2.6b** dissolved in chloroform. The compound crystallised as red blocks with a molecule of chloroform in a monoclinic crystal system with space group $P2_1/c$. Selected bond lengths and angles are listed in Table 2.2 and selected crystallographic data in Table 2.3.

As seen in Figure 2.6, as well as bond angles around the metal centre, the complex has a pseudo−tetrahedral geometry around the ruthenium centre. The structure confirms that the thiosemicarbazone chelates to the ruthenium centre in a *N,S*−bidentate manner. The bond length of C(5)−S [1.701(4) Å] was compared to that of previously reported complexes, as well as similar thiosemicarbazone ligands, and found to be comparable. This suggest that the ligand chelates in the thione form (Table 2.2) and not the thiolate form.[14,16,31–33] This is also confirmed

by the bond length of N(2)−C(5) [1.346 Å] which is longer than the imine bond N(3)−C(6) [1.303 Å]. This implies that the single bond character of the N(2)−C(5) bond is retained.

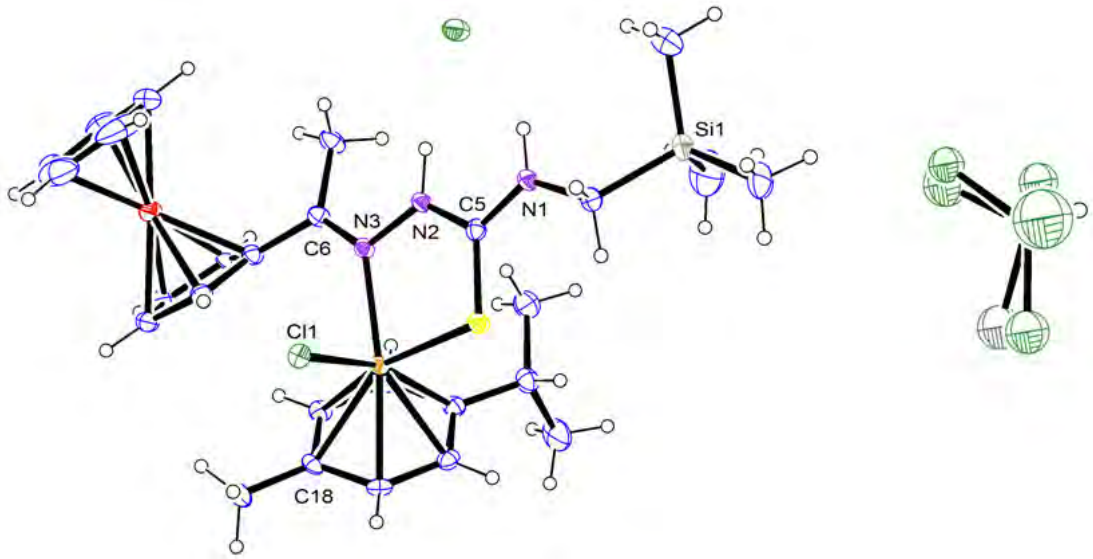

Figure 2.6 ORTEP representation of compound **2.6b** with ellipsoids drawn at the 50 % probability level.

Due to differences in atom sizes, the alkyl C–Si σ–bonds should be longer than alkyl C–C σ–bonds. This is evident from the crystal data, whereby C(3)–Si(1) has an observed bond length of 1.859(9) Å, which is longer than that observed for C(25)-C(26) [1.530(8) Å]. As seen in Figure 2.6, and from the data listed in Table 2.2, a chlorido ligand occupies one of the sites around the ruthenium metal centre. Additionally, preparation of a *N,S*−chelated ruthenium (II) complex results in a cationic complex, which is confirmed by the presence of a chloride counter−ion (Figure 2.6).

Table 2.2 Selected bond lengths (Å) and angles (˚).

Bond lengths (Å)			
Ru–N(3)	2.158(4)	N(2)–C(5)	1.346
Ru–S	2.3497(11)	N(1)–C(5)	1.333
Ru–Cl(1)	2.4134(12)	C(5)–S	1.701(4)
Ru–C(18)	2.273(4)	C(3)–Si(1)	1.859(9)
N(3)–C(6)	1.303	C(25)-C(26)	1.530(8)
Bond angles (˚)			
N(3)–Ru–S	82.11(10)	Cl(1)–Ru–S	86.07(4)
N(3)–Ru–Cl(1)	88.04(11)	Ru–S–C(5)	99.19(16)

Table 2.3 Tabulation of the crystal data of **2.6b**

	2.6b.$CHCl_3$
Chemical formula	$C_{27}H_{39}Cl_2FeN_3RuSSi.CHCl_3$
Formula weight	812.96
Crystal system	Monoclinic
Space group	$P2_1/c$
Crystal size (mm)	0.04 x 0.16 x 0.17
a, b, c (Å)	13.8986(3), 22.6091(4), 11.4831(3)
α, β, γ (°)	90, 103.4820(10), 90
V/Å^3	3508.95(13)
Z	4
T/K	173(2)
D_c/g.cm^{-3}	1.539
μ/mm^{-1}	1.341
Scan range/°	$3.5 < \theta < 27.5$
Unique reflections	8016
Reflections used [I > 2σ(I)]	6426
R_{int}	0.061
R indices (all data)	0.0519, wR2 0.1587, S 1.06
Goodness-of-fit	1.012
Max, Min Δρ/e Å	−1.96, 2.26

2.2.3 Synthesis and Characterisation of Organosilane Thiosemicarbazone Half−Sandwich Rhodium(III) Complexes

As with the ruthenium complexes, it is believed that the activity of a compound may be enhanced with the incorporation of the rhodium. Additionally, the effect of a more electron−deficient metal centre was to be evaluated. Therefore, in this project we sought to prepare organosilane thiosemicarbazone rhodium(III) complexes to be evaluated as antiparasitic agents.

Synthesis

The rhodium dimer $[Rh(Cp^*)Cl_2]_2$ was cleaved in a bridge−splitting reaction by two equivalents of the thiosemicarbazone (**2.3a**–**b**, **2.4a**–**b**, **2.5**) to prepare five new rhodium(III) complexes, as outlined in Scheme 2.3. The rhodium complexes were isolated in moderate to high yields (78−93 %) as orange or red powders. The compounds exhibit thermal stability

above 100 ˚C and are soluble in most polar organic solvents such as dichloromethane, ethanol, diethyl ether and dimethyl sulfoxide.

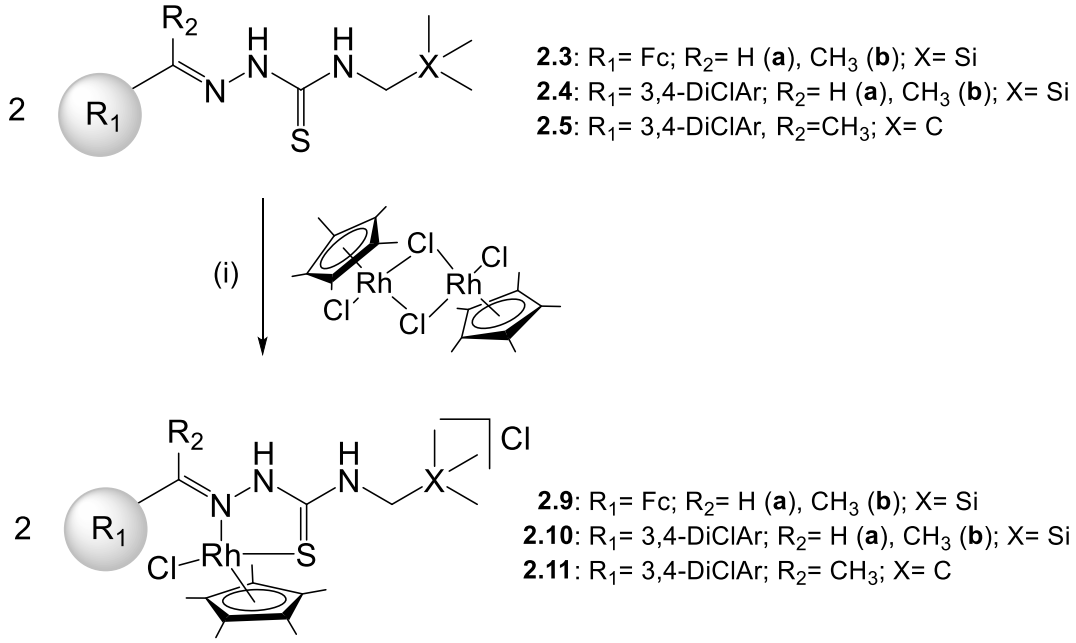

2.3: R_1= Fc; R_2= H (**a**), CH_3 (**b**); X= Si
2.4: R_1= 3,4-DiClAr; R_2= H (**a**), CH_3 (**b**); X= Si
2.5: R_1= 3,4-DiClAr, R_2=CH_3; X= C

2.9: R_1= Fc; R_2= H (**a**), CH_3 (**b**); X= Si
2.10: R_1= 3,4-DiClAr; R_2= H (**a**), CH_3 (**b**); X= Si
2.11: R_1= 3,4-DiClAr; R_2= CH_3; X= C

Scheme 2.3 The synthesis of organosilane thiosemicarbazone rhodium(III) complexes **2.9–2.11**.
Reagents and conditions: Dichloromethane, r.t., 4 hr.

Characterisation

The rhodium complexes were characterised using NMR (^{1}H, ^{13}C{^{1}H}, COSY, HSQC) spectroscopy, infrared (IR) spectroscopy and high resolution electrospray ionisation (ESI) mass spectrometry.

NMR Spectroscopy

The ^{1}H NMR spectra of compounds **2.9a**, **2.10a–b** and **2.11** were recorded in $CDCl_3$ and compound **2.9b** was recorded in acetone–d_6. Formation of the rhodium complexes is confirmed by the appearance of a singlet in the region 1.51–1.70 ppm. The signal corresponds to the methyl protons on the cyclopentadienyl ring coordinated to the rhodium centre. In addition to the appearance of the aforementioned singlet, a similar pattern is observed for the ferrocenyl protons of **2.9a** as compounds **2.6a–b** (Section 2.2.2). The signal for one of the protons of the substituted ferrocenyl ring is observed downfield at 6.25 ppm due to the new orientation brought about by the incorporated metal fragment. The signals for the remaining ferrocenyl protons and the aromatic protons are observed in the expected regions.

A singlet for the azomethine proton is, as expected, observed downfield at 8.62 and 7.94 ppm for compounds **2.9a** and **2.10a**, respectively, when compared to the free ligand [7.68 ppm (**2.3a**); 7.78 ppm (**2.4a**)]. Additionally, a singlet in the range 2.40 and 2.53 ppm corresponds to the CH_3 protons (attached to the imine carbon) of compounds **2.9b**, **2.10b** and **2.11**, which is observed downfield compared to the ligands.

The $^{13}C\{^1H\}$ NMR spectra of compounds **2.9a**, **2.10a–b** and **2.11** were recorded in $CDCl_3$, while **2.9b** was recorded in acetone–d_6. The formation of the complexes is confirmed by the appearance of two additional peaks in the NMR spectra. A singlet at ~9.00 ppm, and a doublet ($^3J_{HH}$ = 7.84 Hz) at approximately 96.0 ppm, corresponds to the carbon atoms of the cyclopentadienyl methyl groups and the quaternary carbons. The quaternary carbon atoms resonate as a doublet due to coupling with the spin active rhodium centre. The aromatic and ferrocenyl carbon atoms resonate in the expected regions.

Infrared Spectroscopy

Infrared analysis of compounds **2.9a–b** and **2.10a–b** were carried out using KBr pellets, while **2.11** was analysed using ATR. As seen in the infrared spectra of the ruthenium complexes (Section 2.2.2) and similar cationic complexes, upon chelation of the TSC to the metal centre, a high energy shift is observed for the absorption band of the C=N bond.[14] The absorption band for the imine bond of compounds **2.9–2.11** is observed between 1624 and 1638 cm^{-1} (Table 2.4), which is at a higher wavenumber than the rhodium–free TSCs (1600–1616 cm^{-1}).

Table 2.4 The C=N and C=S stretching vibrations for compounds **2.9–2.11**.

Compound #	C=N ν (cm^{-1})	C=S ν (cm^{-1})
2.9a	1636	856
2.9b	1638	856
2.10a	1638	856
2.10b	1629	858
2.11	1624	853

Mass Spectrometry

Complexes **2.9–2.11**, which was further characterised using mass spectrometry, were estimated to have theoretical molecular masses of 681.0254, 695.0480, 640.9886, 655.0042 and 639.0272 $g.mol^{-1}$, respectively. In the mass spectra of the rhodium complexes (**2.9a–b**, **2.10a–b**, **2.11**),

peaks corresponding to the fragment $[M–Cl]^{2+}$ (M refers to the cationic portion excluding the Cl counter–ion) are observed at *m/z* 305.5477, 312.5549, 285.5261, 292.5339 and 283.5399, respectively. A peak corresponding to the fragment $[M–H–Cl]^{+}$ is also observed for compounds **2.9a**–**b**, **2.10a**–**b** and **2.11** at *m/z* 610.0873, 624.1039, 570.0446, 584.0607 and 568.0739, respectively.

2.2.4 Synthesis and Characterisation of Organosilane Thiosemicarbazone Cyclopalladated Complexes

As seen in Section 2.1, previously synthesised *C,N,S*–chelated cyclopalladated complexes have exhibited low to moderate antiplasmodial activities.[12,17] Therefore, this study included the preparation of cyclopalladated complexes containing an organosilane moiety, in an attempt to improve on the previously observed biological activities.

Synthesis

The organosilane thiosemicarbazone can chelate in either a bidentate (*N,S*) or tridentate (*C,N,S*) manner to the palladium(II) metal ion. The cyclopalladated complexes were prepared by the procedure outlined in Scheme 2.4. The palladium complexes (**2.12**–**2.14**) were synthesised by reacting the TSCs with the palladium precursor $Pd(PTA)_2Cl_2$ [PTA = 1,3,5-triaza-7-phosphaadamantane] in the presence of triethylamine as the base. Compound **2.12** is a chiral compound; this is due to the planar chirality brought about by the 1,2−disubstitution of the cyclopentadienyl ring of the ferrocenyl moiety.

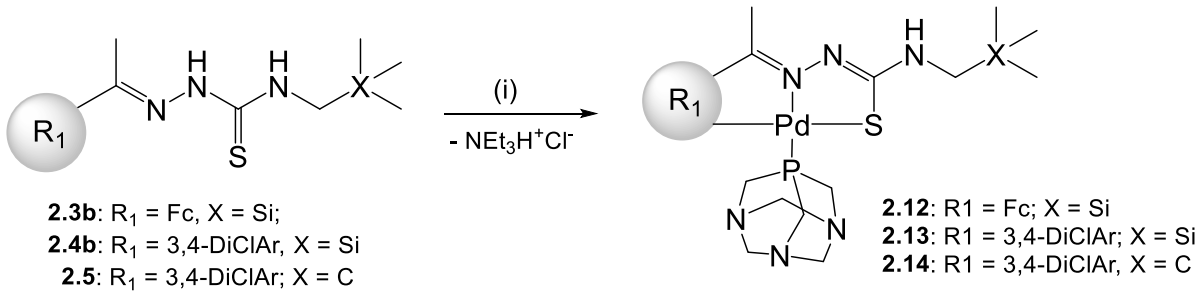

2.3b: R_1 = Fc, X = Si;
2.4b: R_1 = 3,4-DiClAr, X = Si
2.5: R_1 = 3,4-DiClAr; X = C

2.12: R1 = Fc; X = Si
2.13: R1 = 3,4-DiClAr; X = Si
2.14: R1 = 3,4-DiClAr, X = C

Scheme 2.4 Synthesis of *ortho*–cyclopalladated complexes **2.12**–**2.14**.
Reagents and conditions: (i) $Pd(PTA)_2Cl_2$, Ethanol, Triethylamine, 85 ˚C, 24 hr.

In the absence of a base, the direct reaction of the TSC with $Pd(PTA)_2Cl_2$ forms the *N,S*-chelated palladium complex. Furthermore, formation of the *N,S*–chelated palladium complexes are sluggish and resulted in low yields even after refluxing for 4 days. The *ortho*–metallated

complexes (**2.12**–**2.14**) were prepared *via* C–H activation[6,8,34,35], where the palladium(II) acts as a soft Lewis acid in an electrophilic substitution reaction (Figure 2.7). The substituted cyclopentadienyl ring (**2.12**) and the aromatic ring (**2.13**, **2.14**) acts as the nucleophile which attacks the electrophilic palladium(II) metal centre. Incorporation of a methyl substituent on the imine carbon changes the electronic and steric properties of the aromatic ring, which in turn assists in bringing about cyclopalladation. In comparison to the direct method mentioned above, the presence of a base such as triethylamine facilitates deprotonation of the ring, which yields the desired *C,N,S*–chelated complex (Figure 2.7).

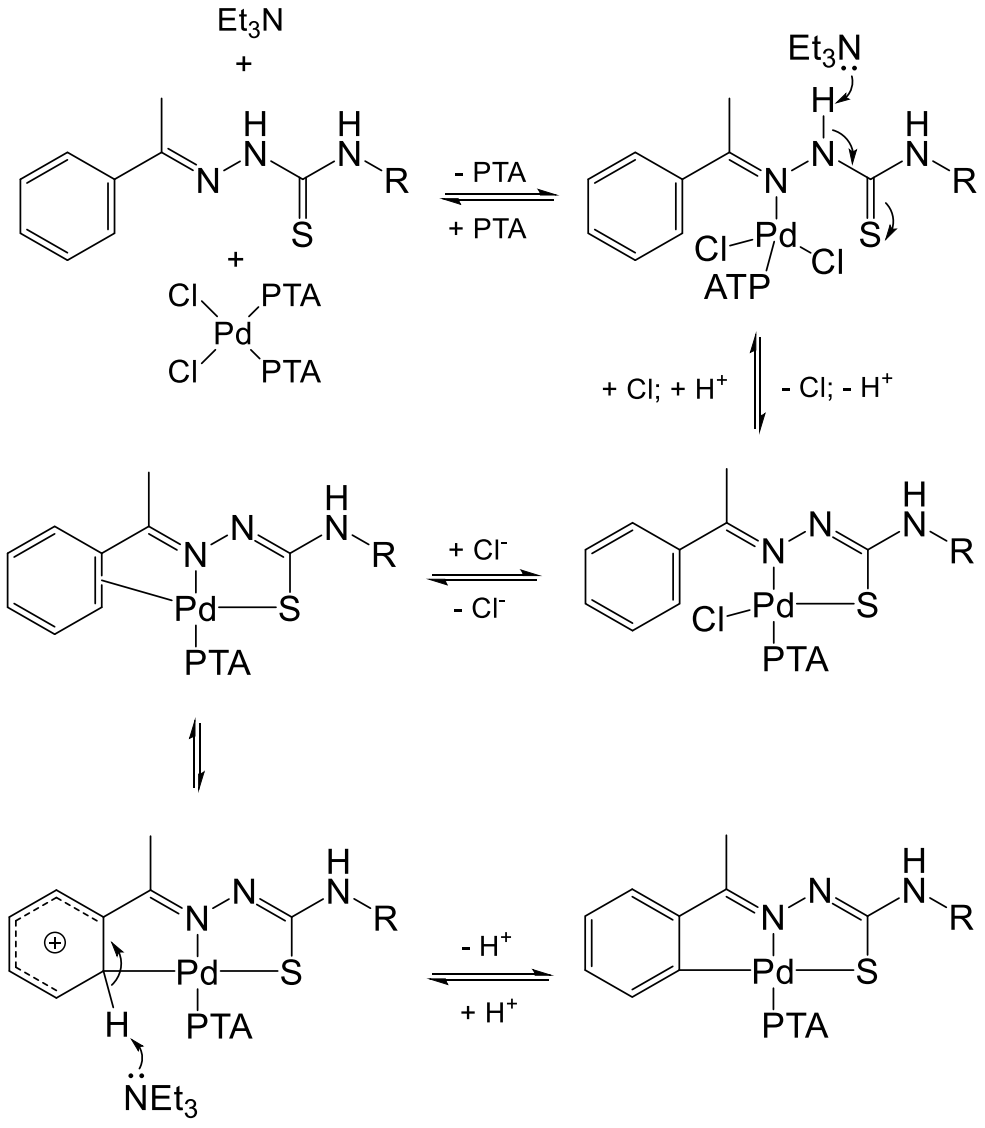

Figure 2.7 A proposed mechanism for the C−H activated formation of cyclopalladated complexes.

Compound **2.12** was isolated as a red powder, whereas compounds **2.13** and **2.14** were isolated as yellow powders, in moderate yields (45–52 %). The compounds are thermally stable and decompose at temperatures above 240 ˚C. The silicon−containing compounds (**2.12** and **2.13**) are slightly more soluble than compound **2.14** in ethyl acetate and methanol. The compounds are soluble in dimethyl sulfoxide, chlorinated solvents, sparingly soluble in alcoholic solvents and insoluble in water.

Characterisation

The palladium complexes were characterised using NMR (^{1}H, ^{13}C{^{1}H}, ^{31}P{^{1}H}, COSY, HSQC) spectroscopy, infrared (IR) spectroscopy and electron impact mass spectrometry (EI−MS).

NMR Spectroscopy

The ^{1}H NMR spectra of compounds **2.12**–**2.14** were recorded in DMSO–d_6. Synthesis of the cyclopalladated complexes is evident by the absence of a signal for a proton of the substituted cyclopentadienyl ring, as seen in Figure 2.8, and the C–6 position on the aromatic ring.

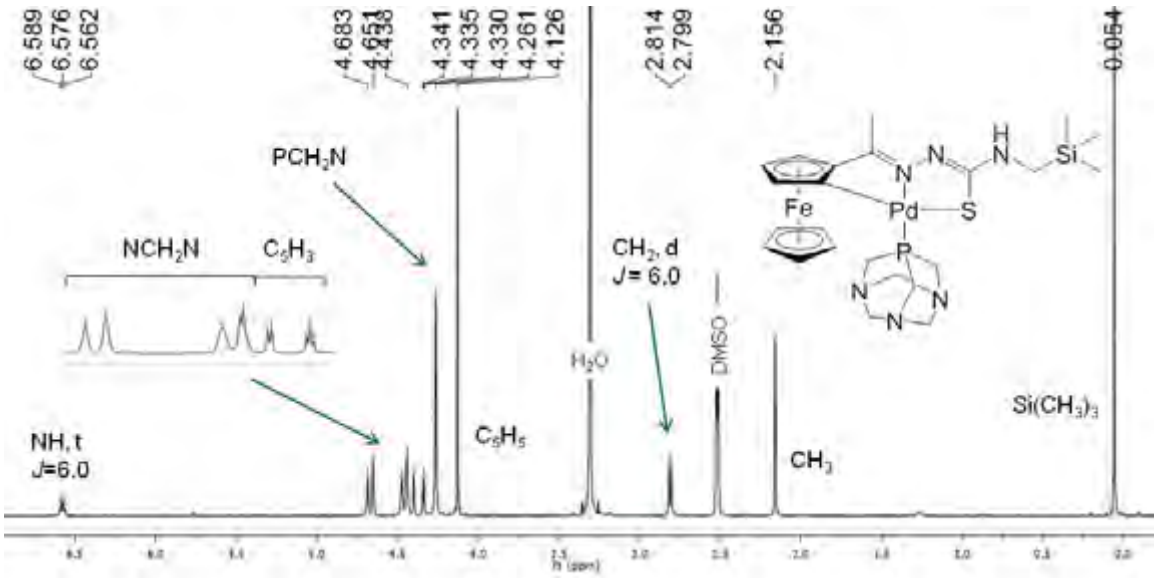

Figure 2.8 ^{1}H NMR spectrum of the cyclopalladated complex **2.12**.

In the ^{1}H NMR spectrum of compound **2.12**, there are only three signals for the protons of the substituted Cp ring observed in the range 4.32–4.44 ppm. For compounds **2.13** and **2.14** a doublet ($^{4}J_{HP}$ = 3.60 Hz) is observed for the aromatic proton H–5, which experiences long-range (four bond) coupling to phosphorus. The H–2 proton of compounds **2.13** and **2.14** is now

observed as a singlet, as opposed to the doublet observed for the ligand when H–2 coupled to the now absent H–6.

Formation of the palladacycle is further confirmed by the absence of the hydrazinic proton. The splitting pattern expected for the PTA ligand is observed. A singlet observed at ~4.26 ppm corresponds to the PCH_2N protons (Figure 2.8). The NCH_2N protons are in an AB spin system which should result in two doublets corresponding to the different environments experienced by the axial and equatorial NCH_2N protons. In the ^1H NMR spectra of **2.12**–**2.14**, a doublet ($^2J_{PH}$ ~ 12.7 Hz) is observed for the equatorial protons (NCH_2N). For compounds **2.13** and **2.14** the axial protons are also observed as a doublet, whereas the signals for compound **2.12** overlap with the signal for a proton of the substituted Cp ring resulting in a multiplet.

The $^{13}C\{^1H\}$ NMR spectra of compounds **2.12** and **2.13** were recorded in DMSO-d_6 and compound **2.14** was recorded in $CDCl_3$. Coordination of the palladium metal to the imine nitrogen, deshields the imine carbon atom which resonates downfield at approximately 163 ppm (Ligand: ~145 ppm). In the case of the aryl complexes (**2.13**, **2.14**), the imine carbon atom resonates as a doublet ($^2J_{CP}$ = 7.45 Hz). The quaternary ferrocenyl and aromatic carbon atoms to which the palladium metal is coordinated is also observed as a doublet due to coupling with phosphorus. The remaining aromatic and ferrocenyl carbon atoms resonate in the expected ranges 126–153 ppm and 66–100 ppm, respectively.

As seen with similar complexes, the carbon atoms of the PTA ligand couples to phosphorus and resonate as doublets at approximately 52.0 (PCH_2N) and 72.4 (NCH_2N) ppm.

The $^{31}P\{^1H\}$ NMR spectra displayed a singlet at –41.6, –49.6 and –49.6 ppm for compounds **2.12**–**2.14**, respectively, which is upfield from –24.59 ppm for the precursor $PdCl_2(PTA)_2$. This corresponds to the expected chemical shift for the phosphorus (PTA) of the cyclopalladated complexes.[12,17]

Infrared (IR) Spectroscopy and Mass Spectrometry

Infrared spectral analyses of compounds **2.12**–**2.14** were carried out using ATR. Upon formation of the cyclopalladated complexes **2.12**–**2.14**, the absorption band for the imine bond chelated to the metal is found at a lower wavenumber (1530–1560 cm^{-1}) when compared to the

thiosemicarbazones (Table 2.1). As previously mentioned, the thiosemicarbazone chelates in the thiolate form which is confirmed by the appearance of an absorption band for a C–S bond, instead of the thione C=S bond, at a lower wavenumber (801–807 cm^{-1}). The shift to a lower wavenumber is indicative of the loss of double bond character and formation of a single bond. Additionally, chelation in the thiolate form is confirmed by the appearance of a second absorption band in the range 1570–1582 cm^{-1} for the newly formed C=N bond (Table 2.5).

Table 2.5 The C=N and C=S stretching vibrations for **2.12**–**2.14**.

Compound #	C=N ν (cm^{-1})	C–S ν (cm^{-1})
2.12	1570, 1530	807
2.13	1578, 1560	807
2.14	1582, 1558	801

The mass spectra for compounds **2.12**–**2.14**, which have theoretical masses of 648.0520, 608.0082 and 592.0312 $g.mol^{-1}$, displayed molecular ion peaks at *m/z* 647.97, 607.99 and 592.09, respectively.

The ligands and complexes mentioned above were screened as potential antiparasitic agents against parasitic strains *Plasmodium falciparum* and *Trichomonas vaginalis*. The results of the biological studies are outlined in Chapter 3.

2.3 Summary

Thiosemicarbazone dithiocarbamates **2.1a**–**b** and **2.2a**–**b** were prepared *via* a Schiff base condensation reaction between methyl hydrazinecarbodithioate with either an aldehyde or ketone, respectively. The thiosemicarbazone dithiocarbamates were then reacted in a nucleophilic acyl substitution reaction with an amine–terminated silane [(aminomethyl)trimethylsilane] to synthesise the organosilane thiosemicarbazones **2.3a**–**b** and **2.4a**–**b**. Compound **2.2b** was also reacted with 2,2'-dimethylpropanamine to prepare compound **2.5**, the carbon analogue of **2.4b**. These compounds were fully characterised using NMR (^{1}H; $^{13}C\{^{1}H\}$) spectroscopy, infrared (IR) spectroscopy and electron impact mass spectrometry (EI–MS).

The aforementioned ligands (**2.3a**–**b**, **2.4a**–**b**, **2.5**) were then used in the preparation of a series of ruthenium(II)–, rhodium(III)– and palladium(II) complexes. Two equivalents of the thiosemicarbazone was reacted in a bridge–splitting reaction with the ruthenium dimer $[Ru(\eta^6\text{-}p\text{-}^{i}PrC_6H_4Me)Cl_2]_2$ to yield heterobimetallic complexes **2.6a**–**b** and mononuclear complexes **2.7a**–**b** and **2.8**. The molecular structure of **2.6b** was determined using single–crystal X–ray diffraction and shown to have a pseudo-tetrahedral geometry around the ruthenium metal centre. Following the ruthenium series, the rhodium series was synthesised in a similar manner by reacting the rhodium dimer $[Rh(Cp^*)Cl_2]_2$ with the ligand to yield two heterobimetallic complexes **2.9a**–**b** as well as the mononuclear complexes **2.10a**–**b** and **2.11**. These ruthenium and rhodium complexes were fully characterised using NMR (^1H, $^{13}C\{^1H\}$, COSY, HSQC) spectroscopy, infrared (IR) spectroscopy and electrospray ionisation mass spectrometry (ESI–MS).

Three *C,N,S*–chelated cyclopalladated complexes (**2.12**–**2.14**) were prepared *via* the C–H activation of the thiosemicarbazones by the palladium precursor $Pd(PTA)_2Cl_2$, in the presence of triethylamine. These compounds were fully characterised using NMR (^1H, $^{13}C\{^1H\}$, $^{31}P\{^1H\}$, COSY, HSQC) spectroscopy, infrared (IR) spectroscopy and electron impact mass spectrometry (EI–MS).

2.4 References

1 D. C. Schroeder, *Chem. Rev.*, 1955, **55**, 181–228.

2 A. Shakeel, A. A. Altaf, A. M. Qureshi and A. Badshah, *J. Drug Des. Med. Chem.*, 2016, **2**, 10–20.

3 Jaesool Shim, N. R. Jyothi and N. A. M. Farook, *Asian J. Chem.*, 2013, **25**, 5838–5840.

4 K. Harrouche, J.-F. Renard, P. de Tullio, E. Goffin, P. Lebrun, G. Faury, B. Pirotte and S. Khelili, *Eur. J. Med. Chem.*, 2016, **115**, 352–360.

5 G. Pelosi, *Open Crystallogr. J.*, 2010, **3**, 16–28.

6 T. S. Lobana, *RSC Adv.*, 2015, **5**, 37231–37274.

7 T. S. Lobana, R. Sharma, G. Bawa and S. Khanna, *Coord. Chem. Rev.*, 2009, **253**, 977–1055.

8 P. Paul, P. Sengupta and S. Bhattacharya, *J. Organomet. Chem.*, 2013, **724**, 281–288.

9 P. Chellan, K. M. Land, A. Shokar, A. Au, S. H. An, C. M. Clavel, P. J. Dyson, C. de

Kock, P. J. Smith, K. Chibale and G. S. Smith, *Organometallics*, 2012, **31**, 5791–5799.

10 P. Chellan, T. Stringer, A. Shokar, P. J. Dornbush, G. Vazquez-Anaya, K. M. Land, K. Chibale and G. S. Smith, *J. Inorg. Biochem.*, 2011, **105**, 1562–1568.

11 T. Stringer, P. Chellan, B. Therrien, N. Shunmoogam-Gounden, D. T. Hendricks and G. S. Smith, *Polyhedron*, 2009, **28**, 2839–2846.

12 P. Chellan, S. Nasser, L. Vivas, K. Chibale and G. S. Smith, *J. Organomet. Chem.*, 2010, **695**, 2225–2232.

13 P. Chellan, N. Shunmoogam-Gounden, D. T. Hendricks, J. Gut, P. J. Rosenthal, C. Lategan, P. J. Smith, K. Chibale and G. S. Smith, *Eur. J. Inorg. Chem.*, 2010, 3520–3528.

14 T. Stringer, B. Therrien, D. T. Hendricks, H. Guzgay and G. S. Smith, *Inorg. Chem. Commun.*, 2011, **14**, 956–960.

15 T. Stringer, D. T. Hendricks, H. Guzgay and G. S. Smith, *Polyhedron*, 2012, **31**, 486–493.

16 M. Adams, Y. Li, H. Khot, C. de Kock, P. J. Smith, K. Land, K. Chibale and G. S. Smith, *Dalton Trans.*, 2013, **42**, 4677–4685.

17 M. Adams, C. de Kock, P. J. Smith, K. Chibale and G. S. Smith, *J. Organomet. Chem.*, 2013, **736**, 19–26.

18 Y. Li, C. de Kock, P. J. Smith, H. Guzgay, D. T. Hendricks, K. Naran, V. Mizrahi, D. F. Warner, K. Chibale and G. S. Smith, *Organometallics*, 2013, **32**, 141–150.

19 A. K. Franz and S. O. Wilson, *J. Med. Chem.*, 2013, **56**, 388–405.

20 M. Blunder, N. Hurkes, S. Spirk, M. List and R. Pietschnig, *Bioorg. Med. Chem. Lett.*, 2011, **21**, 363–365.

21 I. Segal, A. Zablotskaya and E. Lukevics, *Chem. Heterocycl. Compd.*, 2005, **41**, 713–725.

22 S. Sonika, M. Meenakshi and R. Malhotra, *Phosphorus. Sulfur. Silicon Relat. Elem.*, 2010, **185**, 1875–1885.

23 Q. Wang, R. Ding, X. Wen and F. Yin, *Phosphorus. Sulfur. Silicon Relat. Elem.*, 2013, **188**, 895–903.

24 D. L. Klayman, J. F. Bartosevich, T. S. Griffin, C. J. Mason and J. P. Scovill, *J. Med. Chem.*, 1979, **22**, 855–862.

25 X. Du, C. Guo, E. Hansell, P. S. Doyle, C. R. Caffrey, T. P. Holler, J. H. McKerrow and F. E. Cohen, *J. Med. Chem.*, 2002, **45**, 2695–2707.

26 G. Zhao and C. Yuan, *Transit. Met. Chem.*, 1994, **19**, 218–220.

27 B. K. Srivastava, S. K. Srivastava, O. P. Pandey and S. K. Sengupta, *Indian J. Chem. A Inorg. Bioinorg. Phys. Theor. Anal. Chem.*, 1996, **35A**, 57–59.

28 C. Biot, B. Pradines, M.-H. Sergeant, J. Gut, P. J. Rosenthal and K. Chibale, *Bioorg. Med. Chem. Lett.*, 2007, **17**, 6434–6438.

29 M. Mariño, E. Gayoso, J. M. Antelo, L. A. Adrio, J. J. Fernández and J. M. Vila, *Polyhedron*, 2006, **25**, 1449–1456.

30 L. Glans, A. Ehnbom, C. de Kock, A. Martínez, J. Estrada, P. J. Smith, M. Haukka, R. A. Sánchez-Delgado and E. Nordlander, *Dalton Trans.*, 2012, **41**, 2764–2773.

31 F. Beckford, D. Dourth, M. Shaloski, J. Didion, J. Thessing, J. Woods, V. Crowell, N. Gerasimchuk, A. Gonzalez-Sarrías and N. P. Seeram, *J. Inorg. Biochem.*, 2011, **105**, 1019–1029.

32 F. Beckford, G. Leblanc, J. Thessing, M. Shaloski, B. J. Frost, L. Li and N. P. Seeram, *Inorg. Chem. Commun.*, 2009, **12**, 1094–1098.

33 P. Bourosh and M. Revenko, *J. Struct. Chem.*, 2009, **50**, 532–535.

34 J. Dupont, C. S. Consorti and J. Spencer, *Chem. Rev.*, 2005, **105**, 2527–2571.

35 T. S. Lobana, P. Kumari, R. J. Butcher, T. Akitsu, Y. Aritake, J. Perles, F. J. Fernandez and M. C. Vega, *J. Organomet. Chem.*, 2012, **701**, 17–26.

CHAPTER 3

Pharmacological Evaluation of Organosilane Thiosemicarbazone Compounds as Antiparasitic Agents

3.1 Introduction

The development of a potential antiparasitic lead compound derived from whole–cell phenotypic screening may involve the following:

In Vitro Evaluation

The first course of action involves testing drug efficacy *in vitro*. For example, in terms of *Plasmodium falciparum*, the asexual erythrocytic stage human *P. falciparum* parasites are cultured and dosed with a control drug (usually chloroquine and artesunate) and the tested compounds. The *in vitro* antiplasmodial assay protocols are generally based on either microscopic detection of ^{3}H-hypoxanthine uptake inhibition, Giemsa–stained slides, flow cytometry, fluorescence or the determination of parasite lactate dehydrogenase (pLDH) activity.[1–3] These detection methods can be used to quantitatively assess the antiplasmodial activity of the compound. Of course the assay protocol and detection method may change depending on the microbe of interest.

Cytotoxicity Studies

After a compound is identified as being effective against parasitic cells, further testing is done to identify compounds which are cytotoxic overall. Cytotoxicity studies involve the *in vitro* evaluation of compounds against a mammalian cell–line. A common method to assess cell growth is the colorimetric MTT–assay.[4,5]

The selectivity index of a compound is determined:

$$\text{Selectivity index (SI)} = \frac{Cytotoxicity}{Antiplasmodial\ activity}$$

A compound with a large SI value displays selectivity towards parasitic cells.

In Vivo Evaluation

Compounds selected for *in vivo* evaluations are subject to efficacy studies. These studies assess the ability of a compound to elicit a pharmacological response, thus eliminating ineffective compounds in the early stages of pre–clinical studies. Promising lead compounds identified as having *in vivo* pharmacological effects are subsequently studied to determine the associated pharmacokinetic and pharmacodynamic factors.

Pharmacokinetics studies the changes in drug concentration as it moves through the body (Figure 3.1) in terms of the rate at which the drug is absorbed, distributed, metabolised and excreted (ADME).[6–8]

Absorption is the process of a drug before it enters systemic circulation. It considers factors such as blood flow, total surface area and contact time at the absorption site.

Distribution considers the passage of a drug, after entering systemic circulation, from the plasma to tissues and active sites. The distribution of the drug is dependent on factors such as the size of the drug, lipid solubility (polarity), the degree of ionisation at physiological pH (non−ionised compounds are lipid soluble), the blood flow and the extent of binding to tissue proteins and plasma.

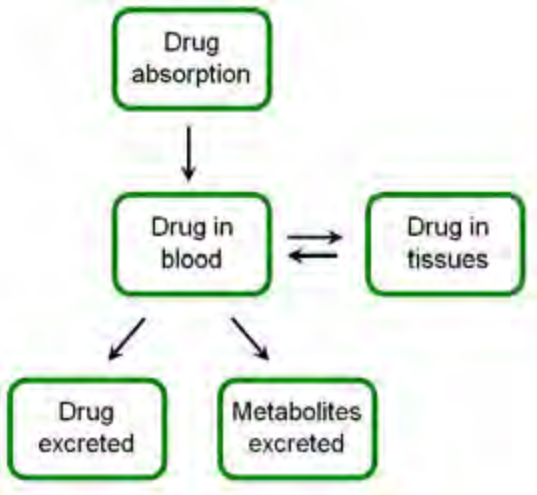

Figure 3.1 Flow diagram illustrating the journey of the drug through the body.

Metabolism (Biotransformation) is the irreversible process of transforming the administered compound into metabolites. Metabolism generally occurs in the liver before reaching the

systemic circulation thus reducing the amount of the administered compound in the system. Administered compounds may be metabolised to their active forms (prodrugs) or the drugs/active metabolites may be metabolised further to an inactive non–toxic form. The process of metabolism may alter compounds, making them more soluble and easily excreted/secreted.

Elimination is one of the most important stages in the drug's journey, as accumulation without any means of elimination could lead to severe toxicity. The drug/metabolites can be removed from the body *via* excretion or secretion. Removal of metabolites may occur using renal (kidney) or biliary excretion, or removal may occur *via* sweat, saliva or exhalation of metabolites (secretion).

Pharmacodynamics looks at how the drug affects the body, as well as the potency and efficacy of the drug in relation to the active site.

Pharmacokinetics and pharmacodynamics are used to determine the time course, therapeutic window, the dose selection and adverse effects. This is done by evaluating the tested compound in terms of the rate of reaction (metabolism or elimination), and basic parameters such as the area under the curve (AUC), maximum plasma concentration (c_{max}), time of maximum concentration (t_{max}), volume of distribution (V_d), half-life ($t_{1/2}$), bioavailability (F %) and clearance (CL) are taken into consideration when monitoring the progress of a drug within the body.[6–8]

Animal models

Compounds are considered for *in vivo* testing if they are found to be effective during *in vitro* screening, low toxicity and good metabolic stability. The purpose of pre–clinical work is to develop sufficient data on the drug's safety to support the decision to proceed to clinical trials. Therefore, animal testing is used to measure drug bioavailability, the toxicity of the drug, to monitor its metabolism and how quickly the drug and its metabolites are excreted from the body. *In vivo* screening progressively moves from smaller models, such as rodents, to larger models if favourable pharmacokinetic properties are established.[1]

Animal pharmacokinetic studies are usually performed in mice due to availability of inbred mice, and provide information on the behaviour of host immune cells in the presence of the tested compound. *In vivo* screenings may be conducted to test compounds on erythrocytic or liver stage malaria.[9] Mouse models are generally infected with rodent malaria strains *P. berghei*, *P. chabaudi*, *P. vinckei* or *P. yoelii*. These strains of rodent parasites have different red blood cell growth that is used as experimental models for human disease.

The differences in rodent and human parasite strains mean that the data collected does not model the human pharmacodynamics exactly. Nevertheless, this is still a good approximation for pre–clinical trials. In recent years, humanised mouse models have become the model of choice for researchers. Immunocompromised mice are grafted with either human erythrocyte or hepatocytes, thus enabling the mouse to accommodate the human *P. falciparum* parasite in the asexual blood or hepatic stage.[10–12] However, this model is still relatively new and thus expensive.

3.2 Pharmacological Evaluation of Thiosemicarbazone−Containing Compounds

The pharmacological activities of the synthesised thiosemicarbazone compounds (Figure 3.2) were evaluated through *in vitro* screening. The compounds were screened against NF54 chloroquine–sensitive and Dd2 chloroquine–resistant strains of *Plasmodium falciparum*, and their cytotoxicity evaluated against the Chinese Hamster Ovarian (CHO) cell–line. Selected compounds were also tested for their ability to inhibit β−haematin formation as a possible mechanism of action. The antiparasitic activity of these compounds was also tested against the metronidazole–sensitive G3 strain of *Trichomonas vaginalis*. Furthermore, selected ferrocenyl–derived TSC compounds were evaluated for their antitumour activity against the A2780 cisplatin–sensitive and A2780cisR cisplatin–resistant human ovarian carcinoma cell–lines, as well as non–tumourigenic KMST–6 human fibroblast skin cell–line. This was to determine the selectivity of these compounds towards parasitic and tumourigenic cell–lines. Furthermore, a selected compound was also evaluated in a preliminary *in vivo* efficacy study in a *P. berghei* mouse model.

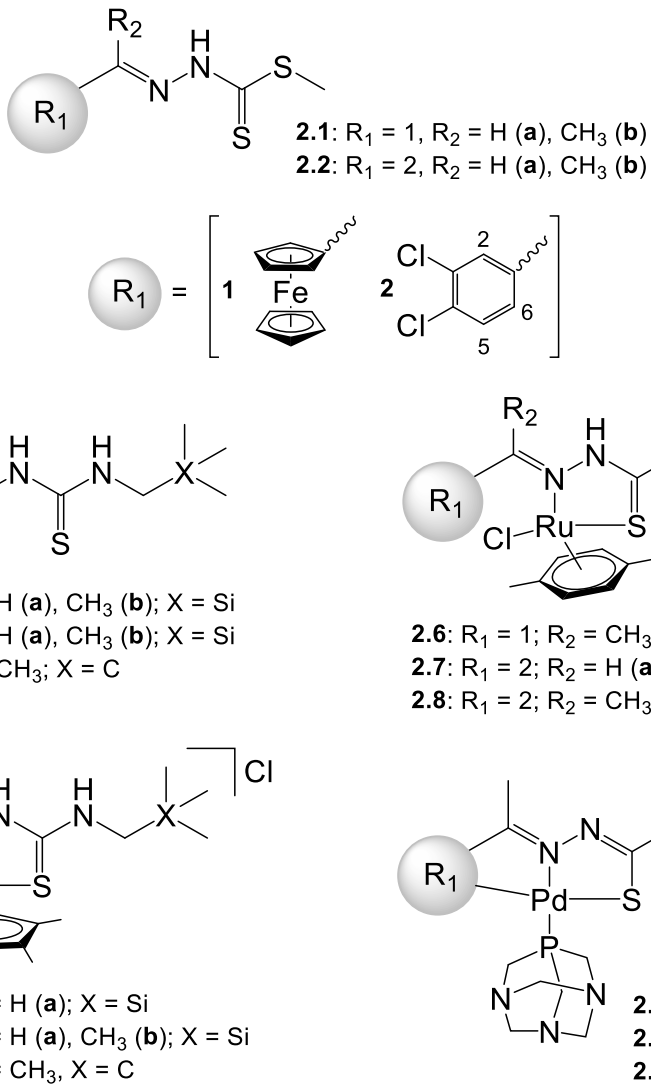

Figure 3.2 Illustration of the screened thiosemicarbazone compounds (**2.1**–**2.14**).

3.2.1 Predicting Lipophilicity

The incorporation of silicon into the framework of these compounds was carried out on the basis that an enhancement of the compound's lipophilicity may lead to an enhancement of pharmacological activity. The log*P* values of the ferrocenyl– and aryl–derived dithiocarbamates and thiosemicarbazones were calculated to determine if a relationship existed between lipophilicity and the pharmacological activity observed.

These calculations were carried out by first determining the clog*P* values of the aryl–derived dithiocarbamates and thiosemicarbazones using ChemBioDraw Ultra v13.0. The ferrocenyl–derived compounds could not be calculated directly using the aforementioned method. Instead the ferrocenyl–derived compounds were calculated using a method combining

data from ChemBioDraw and the fragmental approach proposed by Rekker *et al.*[13] and Lanez *et al.*[14–16]

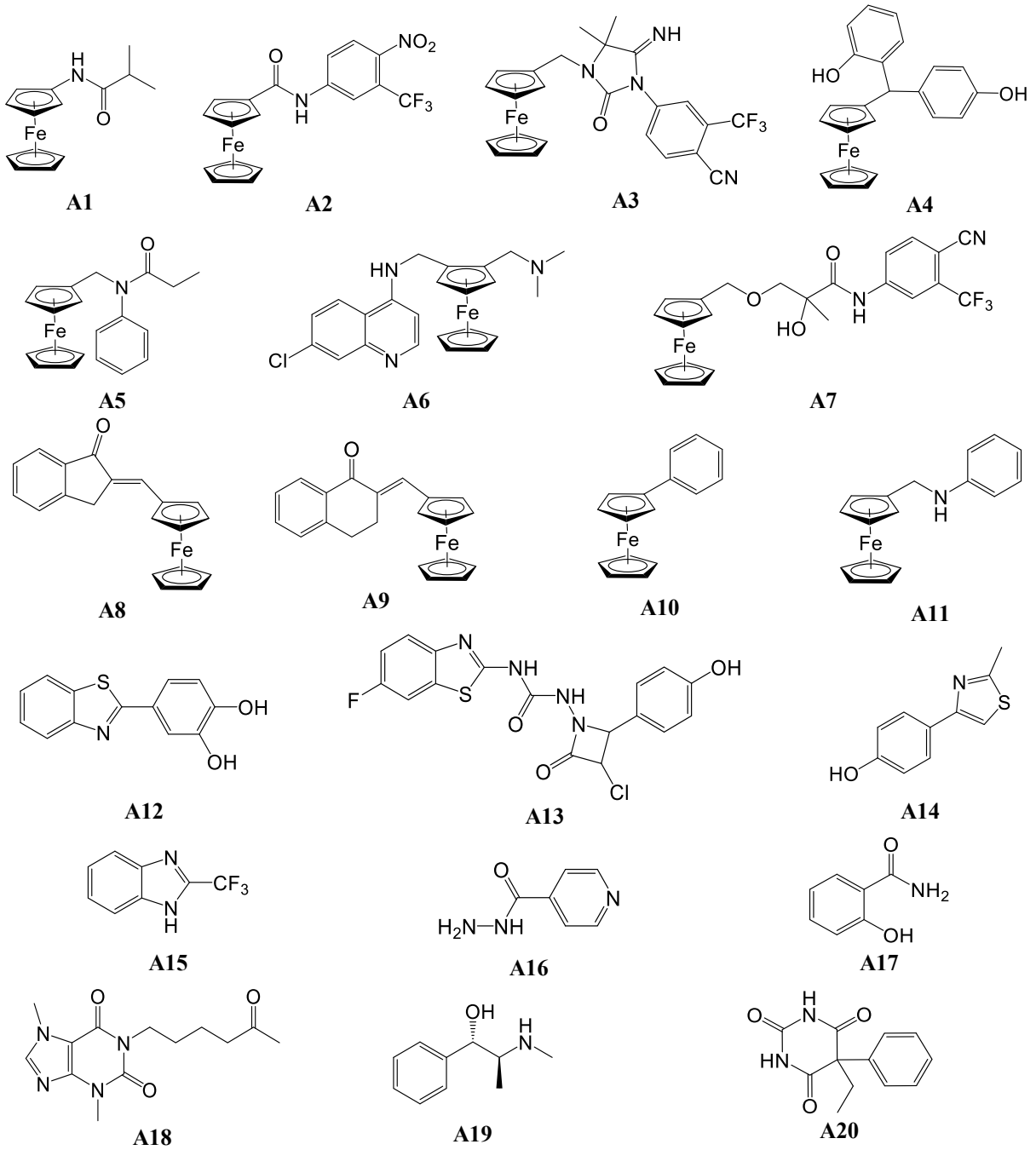

Figure 3.3 Reference compounds (**A1**–**A20**) used to validate the method.

The fragmental approach, which involved the generation of fragmental constants associated with each atom (aliphatic or aromatic), was produced from experimental log*P* values.[13] In addition to fragmental constants, this method also considers various characteristics of the compounds, such as resonances, hydrogen bonding, etc. The log*P* value calculated using the

fragmental approach is adjusted with a correction factor which depends on the relevant features present.[13] However, this method cannot be applied to metal containing compounds. For ferrocenyl–containing compounds, the log*P* value of ferrocene (Fc) was assumed to be the same as the experimental value which is 2.66.[14,17] In this particular study, Fc-H (ferrocene less one hydrogen atom) was calculated by subtracting the fragmental constant for hydrogen, which results in a value of 2.456.[14]

The data was used in the following equation:

$\text{Log}P_{(\text{Fc derivative})} = \text{Log}P_{(\text{benzene derivative})} - f_{(C6H5)} + f_{(\text{Fc-H})}$

Where: $\text{Log}P_{(\text{benzene derivative})}$ calculated using ChemBioDraw

$f_{(C6H5)}$ is obtained from fragmental approach[13]

$f_{(\text{Fc-H})}$ is obtained from Lanez *et al.* reference[15]

to predict the Log*P* values for the ferrocenyl compounds.

However, before applying this method to the compounds evaluated herein, the method had to be validated. A set (n=20) of both ferrocenyl−containing and organic compounds (Figure 3.3) with reported experimental log*P* values were selected to validate this method.

Representative calculation

A representative calculation was carried out on compound **A1**, whereby the clog*P* value was determined for the benzene–derivative (right) using ChemBioDraw. The log*P* value was then determined for the ferrocenyl–derivative (left) using the equation below.

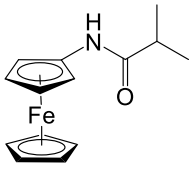

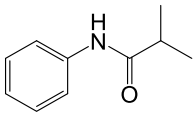

$\text{Log}P_{(\text{Fc derivative})} = \text{Log}P_{(\text{benzene derivative})} - f_{(C6H5)} + f_{(\text{Fc-H})}$

$= 1.999 - [6\text{xC} + 5\text{xH}] + 2.456$

$= 1.999 - [6(0.110) + 5(0.204)] + 2.456$

$= 2.775$

The above calculation was used to determine the theoretical values for compounds **A1**–**A11**, whereas the clog*P* values were taken directly from ChemBioDraw for compounds **A12**–**A20**

(Table 3.1). The regression analysis function in Microsoft Excel was used to determine how well the experimental log*P* values for the twenty reference compounds **A1**–**A20** compared to the estimated values. The data was plotted to produce the graph in Figure 3.4.

Table 3.1 Experimental and estimated log*P* values for compounds **A1**−**A20**.

Compound	Experimental Log*P*	Estimated Log*P*
A1	2.64[18]	2.78
A2	4.42[18]	4.76
A3	4.68[19]	4.74
A4	4.90[20]	4.89
A5	4.38[21]	4.18
A6	5.10[22]	5.32
A7	4.63[18]	4.31
A8	4.77[23]	4.38
A9	5.27[23]	4.93
A10	4.59[15]	4.81
A11	3.82[21]	3.86
A12	2.98[24]	3.33
A13	2.44[25]	2.21
A14	2.68[24]	2.62
A15	2.39[26]	2.63
A16 (Isoniazid)	-0.70[27]	-0.67
A17 (Salicylamide)	1.28[27]	1.28
A18 (Pentoxifylline)	0.29[27]	0.12
A19 (Pseudoephedrine)	0.89[28]	0.89
A20 (Phenobarbital)	1.47[27]	1.36

As seen in Figure 3.4, there is a good correlation between the experimental and estimated values, where the slope of the graph (=0.9907) is close to 1 and 98.48 % of the compounds fit the model. Furthermore, the p–value (8.262×10^{-18}) is considerably smaller than 0.05, which suggests that there is no significant difference between the two sets of data. Therefore, no correction is required.

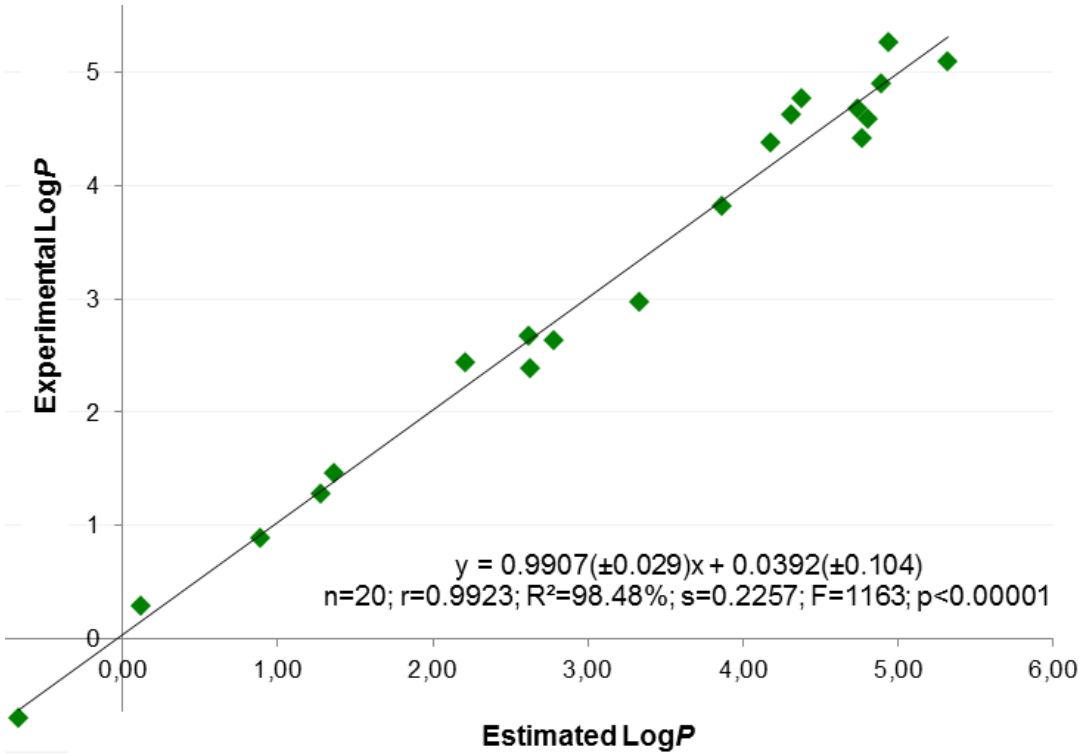

Figure 3.4 Relationship between the experimental and theoretical log*P* values.

Predicting the logP values for the thiosemicarbazones

The log*P* values for the Schiff base dithiocarbamates and thiosemicarbazones were determined using the method described above. The clog*P* values obtained for the benzene– and 3,4-dichlorobenzene–derivatives are listed in Table 3.2 and Table 3.3, respectively.

Table 3.2 The clog*P* values calculated using ChemBioDraw.

Compound	clog*P*
Benzene-derivative of 2.1a	2.68
Benzene-derivative of 2.1b	3.436
Benzene-derivative of 2.3a	4.292
Benzene-derivative of 2.3b	4.708

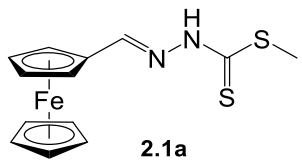

2.1a

Prediction:

$$Log P_{(Fc\ derivative)} = Log P_{(benzene\ derivative)} - f_{(C6H5)} + f_{(fc\text{-}H)}$$

$$= 2.68 - [1.68] + 2.456 = \mathbf{3.456}$$

The log*P* values for compounds **2.1b**, **2.3a**, **2.3b** and the ferrocenylTSC were calculated using the above method.

Table 3.3 Compilation of the estimated log*P* values for compounds **1**–**5**.

Compound	Log*P*	Compound	Log*P*
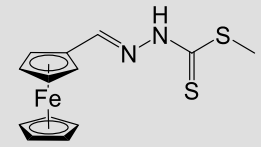 **2.1a**	3.456	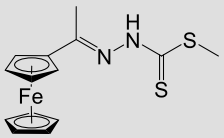 **2.1b**	4.212
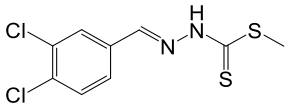 **2.2a**	3.986	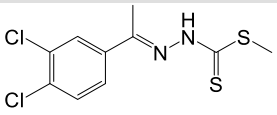 **2.2b**	4.742
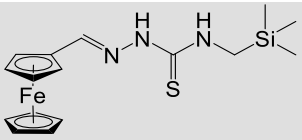 **2.3a**	5.068	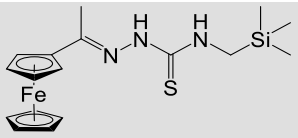 **2.3b**	5.484
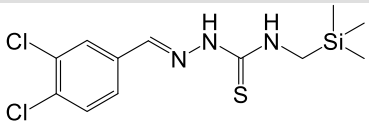 **2.4a**	5.598	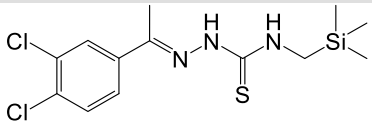 **2.4b**	6.127
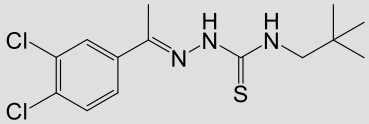 **2.5**	5.562	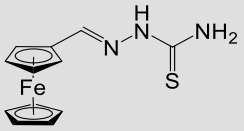 **FerrocenylTSC**[29]	3.177[a]
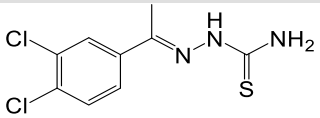 **3,4-DichloroacetophenoneTSC**[30]	3.820[a]		

[a]Calculated following procedure described above.

A comparison of the log*P* values for ferrocenyl– and 3,4-dichloroaryl–dithiocarbamates and their corresponding TSC reveals that the TSC compounds are more lipophilic (Table 3.3). As seen in Table 3.3, a comparison of the organosilane TSC **2.4b** (log*P* = 6.127) and its carbon analogue **2.5** (log*P* = 5.562) demonstrates that the silicon–containing compound has a higher log*P* value, as expected. Furthermore, the log*P* values of two non–silicon thiosemicarbazones (FerrocenylTSC; 3,4-DichloroacetophenoneTSC) which are analogous to compounds **2.3a** and **2.4b**, and contain a terminal primary amine, were also calculated. The log*P* values for the previously prepared TSC compounds were significantly lower than the corresponding TSCs (**2.3a**, **2.4b**) evaluated in this study.

The log*P* values of the ruthenium(II)–, rhodium(III)– and palladium(II) complexes could not be calculated using the same method as the non–coordinated compounds. However, inclusion

of the arene and cyclopentadienyl fragments of the ruthenium and rhodium complexes, respectively, are expected to enhance the lipophilicity of the compounds to which they are coordinated. On the other hand, the palladium complexes are not expected to be as lipophilic as the ruthenium and rhodium complexes due to the presence of the hydrophilic PTA ligand. As previously mentioned, pharmacological evaluation of these compounds may reveal whether or not a relationship exists between lipophilicity and potency.

3.2.2 In Vitro Antiplasmodial and Cytotoxicity Studies

The *in vitro* antiplasmodial activity of the Schiff base dithiocarbamates (**2.1**; **2.2**) and their corresponding organosilane (**2.3**; **2.4**) and non–silicon (**2.5**) thiosemicarbazones was evaluated against the NF54 (CQS) strain of *P. falciparum*. The corresponding ruthenium– (**2.6b**; **2.7**; **2.8**), rhodium– (**2.9a**; **2.10**; **2.11**) and palladium– (**2.12**–**2.14**) complexes were also screened against this strain. Chloroquine diphosphate (CQDP) and artesunate were used as the control drugs in this study. The IC_{50} values are listed in Table 3.4 and illustrated in Figure 3.5 and 3.6, while the resistance and selectivity indices are listed in Table 3.5.

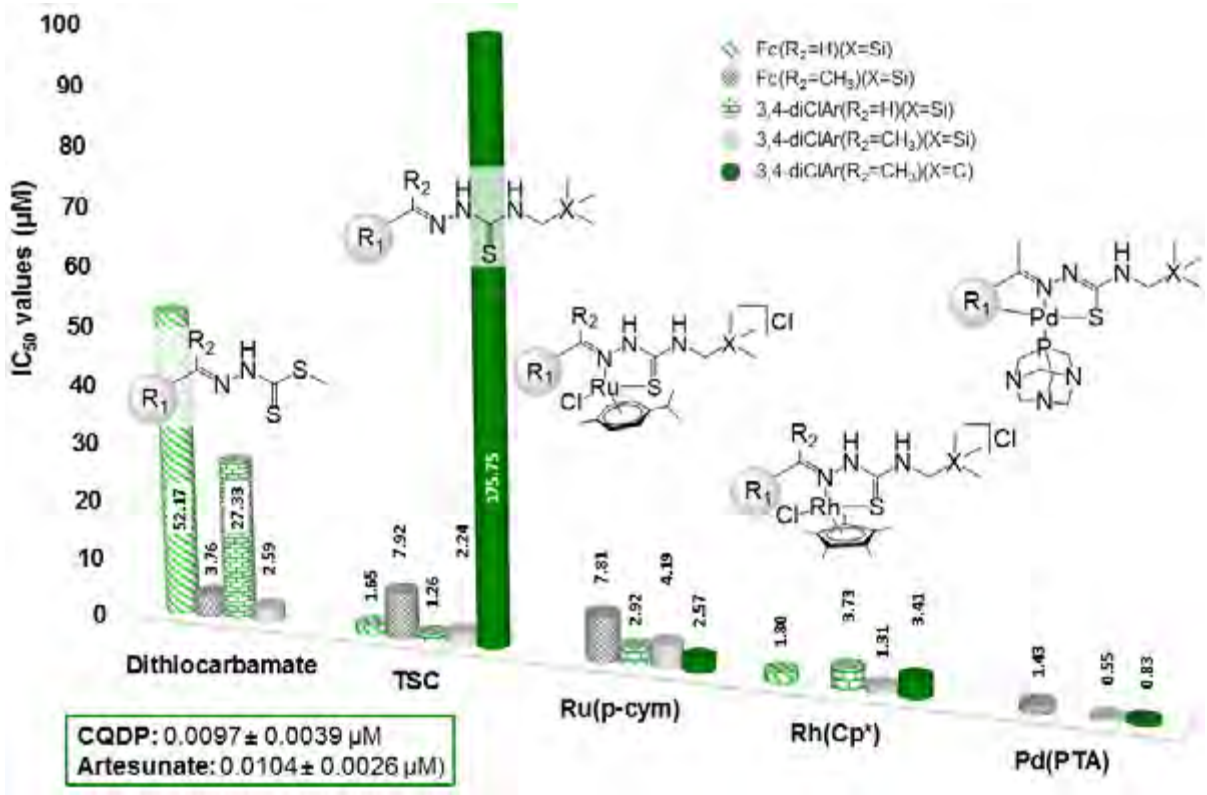

Figure 3.5 Antiplasmodial evaluation against the NF54 strain of *P. falciparum*.

Table 3.4 Antiplasmodial data for compounds **2.1**–**2.14**.

Compound		IC_{50} (μM)		
		NF54	**Dd2**	**CHO**
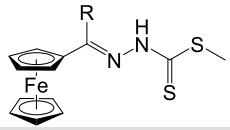	**2.1a** (R=H)	52.17±11.69	ND	ND
	2.1b (R=CH_3)	3.76±1.35	13.70±1.32	0.49±0.21
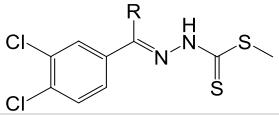	**2.2a** (R=H)	27.33±7.85	ND	ND
	2.2b (R=CH_3)	2.59±0.89	10.95±1.06	1.20±0.41
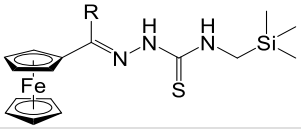	**2.3a** (R=H)	1.65±0.37	2.62±0.29	> 267.81
	2.3b (R=CH_3)	7.92±1.99	ND	ND
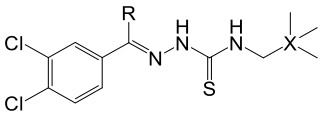	**2.4a** (R=H; X=Si)	1.26±0.69	6.91±0.48	25.10±1.23
	2.4b (R=CH_3; X=Si)	2.24±0.26	2.40±0.57	29.28±0.89
	2.5 (R=CH_3; X=C)	175.74±43.03	ND	ND
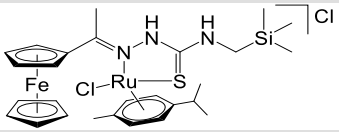	**2.6b**	7.81±0.56	ND	ND
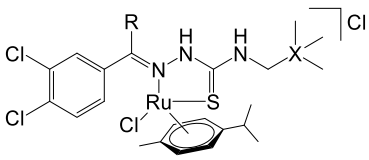	**2.7a** (R=H; X=Si)	2.92±0.33	4.28±0.33	71.82±18.11
	2.7b (R=CH_3; X=Si)	4.19±0.12	6.66±2.58	21.54±3.80
	2.8 (R=CH_3; X=C)	2.57±0.99	2.29±0.25	3.65±0.63
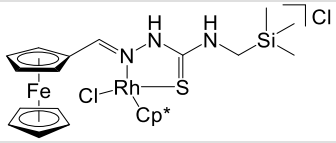	**2.9a**	1.80±0.04	2.27±0.10	53.49±1.45
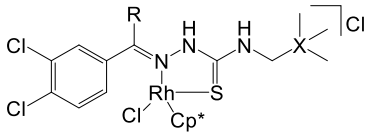	**2.10a** (R=H; X=Si)	3.73±0.96	3.11±0.58	14.89±0.37
	2.10b (R=CH_3; X=Si)	1.31±0.29	1.18±0.09	10.85±1.00
	2.11 (R=CH_3; X=C)	3.41±0.41	1.01±0.16	4.10±0.19
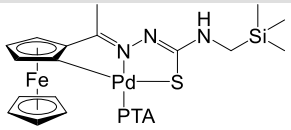	**2.12**	1.43±0.29	1.26±0.03	3.93±0.26
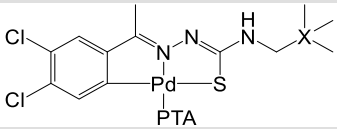	**2.13** (X=Si)	0.55±0.10	0.29±0.05	3.54±0.21
	2.14 (X=C)	0.83±0.12	0.34±0.08	2.73±0.34
Chloroquine		0.0097±0.0039	0.19±0.06	ND
Artesunate		0.0104±0.0026	0.05±0.02	ND
Emetine		ND	ND	0.13±0.0062

ND = Not determined

When comparing the data for the Schiff base dithiocarbamates (**2.1**; **2.2**), it is observed that **2.1b** and **2.2b** are the most active with IC_{50} values of 3.76 and 2.59 μM, respectively. Incorporation of the organosilane moiety generally led to the enhancement of activity for the TSCs (Figure 3.5). Compound **2.5**, a non–silicon analogue of compound **2.4b**, was tested in order to determine the impact of introducing silicon. Compound **2.5** (175.74 μM) was found to be significantly less potent compared to its silicon counter–part **2.4b** (2.24 μM), which suggests that the incorporation of the silicon atom plays a role in moderating antiplasmodial activity.

Returning to the previously calculated log*P* values, thiosemicarbazones **2.3a**, **2.4a** and **2.4b** had the highest log*P* values of 5.07, 5.60 and 6.13, respectively (Table 3.3), and generally displayed the lowest IC_{50} values. Furthermore, previously evaluated ferrocenylTSC [3.4 μM (NF54); 6.4 μM (Dd2)] and 3,4-dichloroacetophenone TSC [14.1 μM (NF54); 9.82 μM (Dd2)] are comparable in activity to the organosilane TSCs **2.3a** and **2.4b**, respectively.[30,31] As seen in Table 3.3, the ferrocenyl– and 3,4-dichloroactophenone–derived TSC compounds have low log*P* values of 3.18 and 3.82, respectively. This suggests that the activity of these compounds may be related to their lipophilicity.

The ruthenium complexes were found to be slightly less active than the corresponding TSCs. However, the potency of the non–silicon compound (**2.5**) is significantly enhanced upon complexation with ruthenium (**2.8**; 2.57 μM, NF54). This may be related to an enhancement in lipophilicity, or the interaction of the complex with the target. The rhodium complexes **2.9a** and **2.10a** were less potent when compared to the organosilane TSC (**2.3a**; **2.4a**, Table 3.4). Compound **2.10b** was found to be more active than the corresponding free TSC (**2.4b**) and a significant enhancement in activity was once again observed for the non–silicon complex (**2.11**). However, the non–silicon rhodium complex (**2.11**) was less potent than its silicon counter–part **2.10b**. At this stage, a larger series of compounds need to be evaluated before a conclusive statement can be made with regards to the use of ruthenium(II) versus rhodium(III). The cyclopalladated complexes **2.12**–**2.14** were significantly more active than the TCSs (Figure 3.5) and more potent when compared to the ruthenium and rhodium complexes. A comparison of similarly structured complexes **2.13** (IC_{50} = 0.55 μM) and **2.14** (IC_{50} = 0.83 μM) shows a slight enhancement of activity for the silicon–containing complex.

Further testing was done on the compounds which exhibited antiplasmodial activity below 5 μM. The compounds were specifically tested for their antiplasmodial activity against the Dd2 (CQR) strain of *P. falciparum*. The cytotoxicity of these compounds was also evaluated against a Chinese Hamster Ovarian cell–line, using Emetine as the control drug (Figure 3.6). The Schiff base dithiocarbamates [**2.1b**; **2.2b**] were significantly less active against the Dd2 strain when compared to the NF54 strain (Figure 3.5 and 3.6). The same loss of activity was observed for the organosilane TSCs (**2.3a**; **2.4a**; **2.4b**), the ruthenium complexes (**2.7a**; **2.7b**) and the rhodium complexes (**2.9a**; **2.10b**). The non–silicon complex **2.11** was more potent against the Dd2 strain (1.01 μM) than the NF54 strain (3.41 μM). The potency of the cyclopalladated complexes **2.12**–**2.14** against the Dd2 strain was higher than that against the NF54 strain, with IC_{50} values of 1.26, 0.29 and 0.34 μM, respectively.

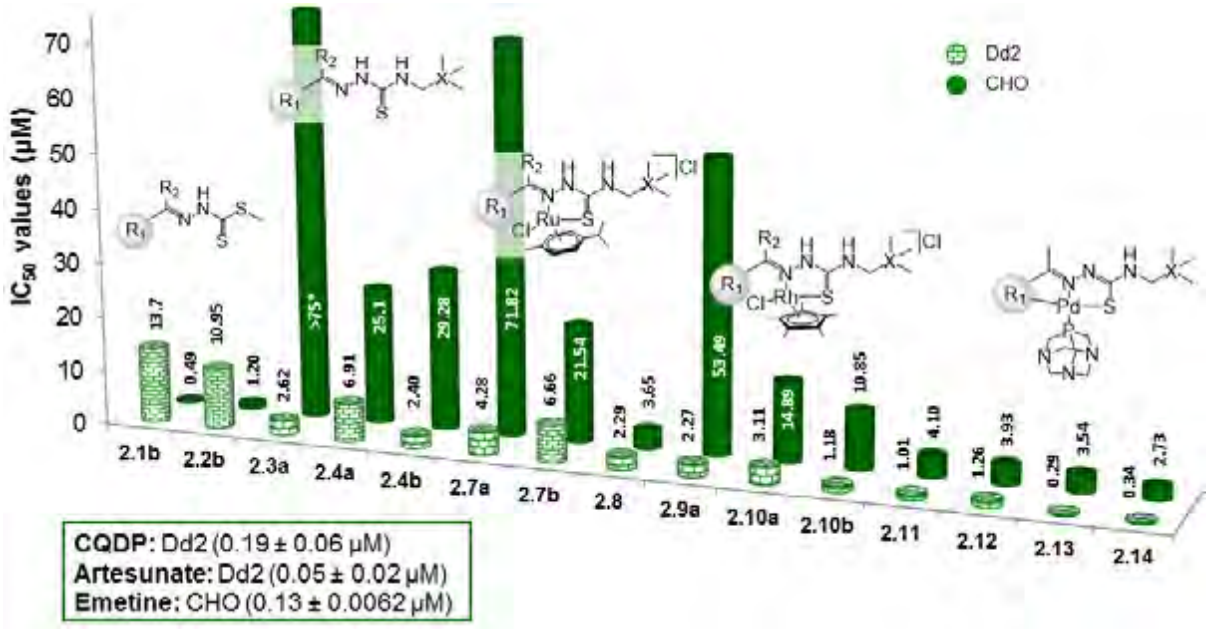

Figure 3.6 Antiplasmodial evaluation against the Dd2 strain of *P. falciparum* and the cytotoxicity studies tested on the Chinese Hamster Ovarian cell–line. *not active at the tested concentration.

Resistance indices [$RI = \frac{IC50\ (Dd2)}{IC50\ (NF54)}$] were calculated for the TSC compounds which displayed activity against the Dd2 strain and plotted in the graph seen in Figure 3.7. The data points either positioned around or below the line correspond to RI values equal to 1 or less than, respectively. Compounds displaying low RI values are of interest as this suggests that such compounds may be active against a broader range of sensitive and resistant strains. The tested compounds generally displayed low RI values in comparison to chloroquine (19.59) and artesunate (4.81). The non–silicon ruthenium– (**2.8**), rhodium– (**2.11**) and palladium complexes

(**2.14**), as well as organosilane rhodium (**2.10a–b**) and palladium (**2.12**; **2.13**) complexes had RI values below 1 (Figure 3.7). This suggests that they are likely to be active against resistant strains and that the incorporation of a metal may be important in overcoming drug–resistance.

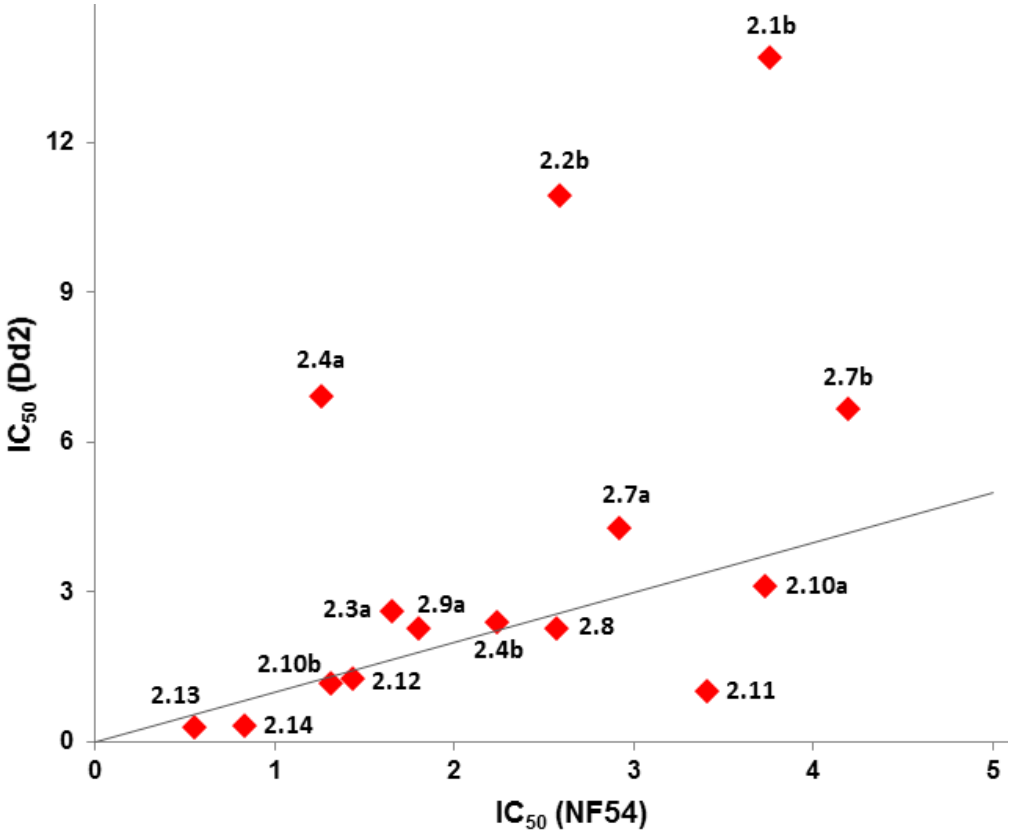

Figure 3.7 Resistance index (RI) correlation between CQR Dd2 and CQS NF54 strains of *P. falciparum*.

In addition to the resistance index, the selectivity indices [$SI_{1\text{ or }2} = \frac{IC50\ (CHO)}{IC50\ (NF54)\text{ or }(Dd2)}$] were also calculated to determine if the tested compounds were more selective towards the parasite strains or mammalian cells. Overall, the organosilane thiosemicarbazones (**2.4a**; **2.4b**), the ruthenium– (**2.7a**) and rhodium– (**2.9a**) complexes were the least cytotoxic, and thus significantly more selective for the parasitic cells (Table 3.5). The SI_1 values for the previously mentioned compounds ranged between 13 and 30 for the NF54 strain and 4 and 24 for the Dd2 strain. As highlighted before, the cyclopalladated complexes were the most potent of the tested compounds and show good selectivity indices (Table 3.5), though not to the same extent as mentioned for the compounds above.

Table 3.5 The resistance and selectivity indices for selected compounds.

Compound		SI_1[a]	SI_2[b]
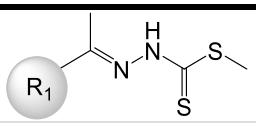	**2.1b**	0.13	0.036
	2.2b	0.46	0.11
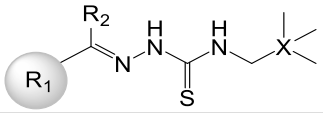	**2.4a** (X=Si)	19.92	3.63
	2.4b (X=C)	13.07	12.20
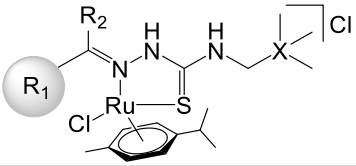	**2.7a** (R=H; X=Si)	24.60	16.78
	2.7b (R=CH_3; X=Si)	5.14	3.23
	2.8 (R=CH_3; X=C)	1.42	1.59
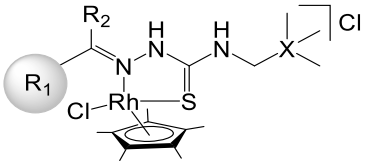	**2.9a** (R=H; X=Si)	29.72	23.56
	2.10a (R=H; X=Si)	3.99	4.79
	2.10b (R=CH_3; X=Si)	8.28	9.19
	2.11 (R=CH_3; X=C)	1.20	4.06
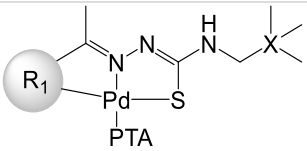	**2.12** (X=Si)	2.75	3.12
	2.13 (X=Si)	6.44	12.21
	2.14 (X=C)	3.29	8.03

[a]SI_1 = IC_{50}(CHO)/IC_{50}(NF54); [b]SI_2 = IC_{50}(CHO)/IC_{50}(Dd2)

Previously reported ruthenium(II) *p*–cymene complexes displayed low to moderate activity against *P. falciparum*, in the range observed for the ruthenium complexes (**2.6**–**2.8**) reported herein.[29] A comparison of the cyclopalladated complexes (**2.12**–**2.14**) with previously reported cyclopalladated complexes reveal an enhancement of activity for the compounds reported herein.[30,32] Unfortunately there are no rhodium TSC complexes to which the rhodium complexes (**2.9**–**2.11**) reported herein can be compared. Furthermore, no comment can be made on the selectivity of the previously reported TSCs towards parasitic strains due to a lack of data.

The thiosemicarbazone compounds evaluated in this study generally display improved activity compared to the previously evaluated thiosemicarbazone compounds.

3.2.3 β−Haematin Inhibition Studies

The NP–40 detergent mediated assay[33,34] was used to establish if selected thiosemicarbazone compounds (**2.4b**, **2.9a** and **2.10b**), along with chloroquine as the control, inhibits β–haematin (synthetic haemozoin) formation. Table 3.6 gives the IC_{50} values obtained for this study.

The organosilane thiosemicarbazone ligand **2.4b** did not exhibit activity at the tested concentration. On the other hand, the rhodium(III) complexes **2.9a** (IC_{50} = 150.3 μM) and **2.10b** (IC_{50} = 38.1 μM) displayed inhibitory effects. The superior activity of the rhodium(III) complex **2.10b** relative to chloroquine (IC_{50} ~ 74 μM) is noteworthy.

Table 3.6 β–haematin inhibition activity of **2.4b**, **2.9a**, **2.10b** and **CQ**

Compound		IC_{50} (μM) [95% confidence interval]
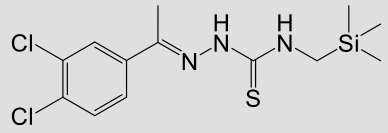	**2.4b**	n.a.[a]
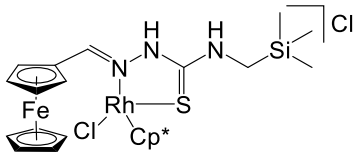	**2.9a**	150.3 [144.9 to 155.8]
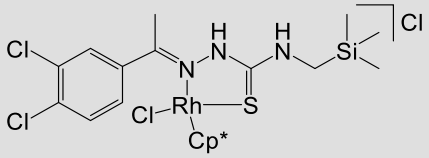	**2.10b**	38.09 [35.94 to 40.38]
CQ		73.76 [71.32 to 76.28]

[a]n.a. = not active at the tested concentration

No direct correlation could be drawn between the β–haematin inhibition data and the *in vitro* antiplasmodial data reported in Section 3.2.2. The difference in antiplasmodial activity observed for compounds **2.4b**, **2.9a** and **2.10b** was not as pronounced as seen for the corresponding β–haematin inhibition data. However, a relationship does exist between the antiplasmodial activity and the ability of the rhodium compounds to inhibit β–haematin formation. Furthermore, a larger number of diverse rhodium compounds would have to be tested before a conclusive statement can be made about the mode of action of these compounds.

3.2.4 In Vitro Antitrichomonal Studies

The synthesised compounds (50 μM solutions) were screened to determine general growth inhibition against the G3 strain of *Trichomonas vaginalis*. DMSO and metronidazole were employed as controls for the screening, and the antitrichomonal activity data is illustrated in Figure 3.8 and listed in Table 3.6.

The Schiff base dithiocarbamates (**2.1**; **2.2**) and thiosemicarbazones (**2.3**; **2.4**; **5**) generally displayed poor inhibitory effects (< 50 %, Figure 3.8). The ruthenium (**2.6b**; **2.7**) and rhodium (**2.9a**; **2.10**; **2.11**) complexes, on the other hand, were significantly more potent. The complexes generally display inhibitory effects above 90 %, with the ferrocenyl−derived TSC rhodium complex (**2.9a**) displaying 100 % inhibition.

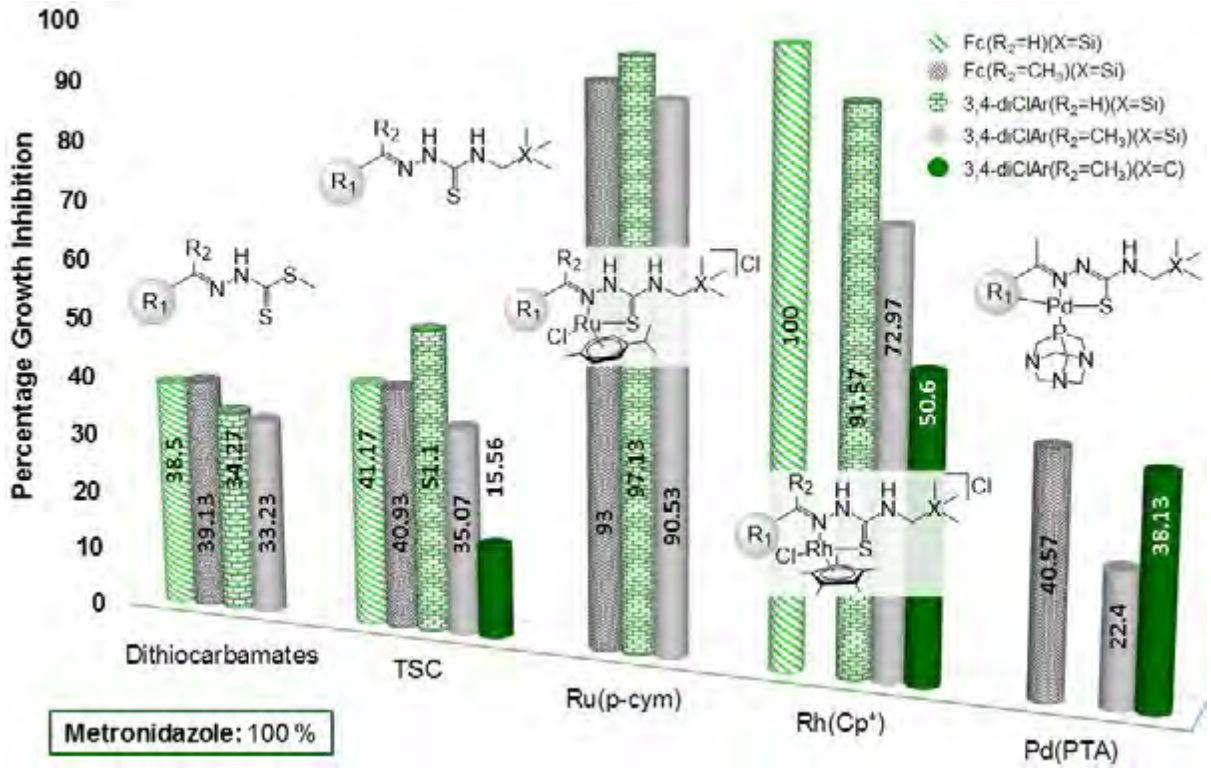

Figure 3.8 Percentage growth inhibition of *T. vaginalis* (G3 strain) at a test concentration of 50 μM.

The non–silicon containing TSC ligand (**2.5**) and rhodium complex (**2.11**) displayed the lowest inhibitory effects when compared to the silicon containing TSCs and the rhodium complexes, respectively (Figure 3.8). The cyclopalladated complexes (**2.12**–**2.14**) were significantly less active than the ruthenium and rhodium complexes, exhibiting inhibitory effects (< 41 %, Figure 3.8) comparable to that of the dithiocarbamates and TSCs.

Table 3.7 Antitrichomonal inhibition data for the tested compounds against the G3 strain.

Compound		IC_{50} (μM)
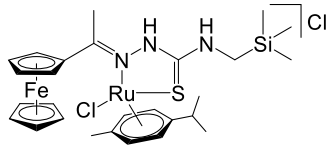	**2.6b**	35.21 ± 0.22
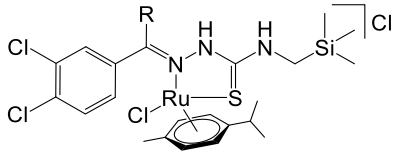	**2.7a** (R=H)	17.53 ± 0.88
	2.7b ($R=CH_3$)	12.55 ± 0.61
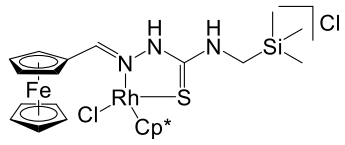	**2.9a**	7.51 ± 0.81
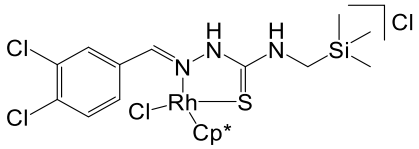	**2.10a**	7.28
Metronidazole		0.72

Dose–response curves were constructed for the thiosemicarbazone compounds displaying inhibition above 90 %, and used to determine the IC_{50} values, which are listed in Table 3.7. The ferrocenyl–derived TSC ruthenium complex **2.6b** (IC_{50} = 35.21 μM) was less active than its 3,4-dichloroaryl–derived TSC ruthenium counterparts **2.7a** (IC_{50} = 17.53μM) and **2.7b** (IC_{50} = 12.55 μM). Rhodium complexes **2.9a** and **2.10a** exhibited similar activity with IC_{50} values of 7.51 μM and 7.28 μM, respectively. The rhodium complexes were generally more effective in inhibiting G3 parasite growth compared to the ruthenium complexes.

As previously mentioned in Chapter 1 (Section 1.5) and Chapter 2 (Section 2.1), research on the use of metal–containing compounds for antitrichomonal treatment is scarce. Within our group we have evaluated TSC–containing palladium–, platinum– and ruthenium–complexes for their antitrichomonal activity against either the T1 or G3 strains of *T. vaginalis*.[29,35,36] The complexes were weak growth inhibitors of the *T. vaginalis* parasite.

Overall, the silicon–containing TSC ruthenium(II)– and rhodium(III)–complexes reported herein were the most effective parasite growth inhibitors., albeit not as effective as the FDA approved drug Metronidazole.

3.2.5 In Vitro Antitumour Studies

Ferrocenyl compounds such as ferrocifen and its analogues have displayed significant antiproliferative effects on human cancer cell–lines.[37,38] Preliminary cytotoxicity studies were carried out on selected ferrocenyl compounds, which were screened against the cisplatin–sensitive (A2780) and cisplatin–resistant (A2780cisR) human ovarian carcinoma cell–lines, as well as non–tumourigenic human fibroblast cells (KMST–6). The IC_{50} values are listed in Table 3.8.

Table 3.8 Antitumour data for ferrocenyl–derived compounds **2.1**, **2.3**, **2.6b** and **2.12**.

Compound		IC_{50} (μM)			SI_1[a]	SI_1[b]
		A2780	A2780CisR	KMST-6		
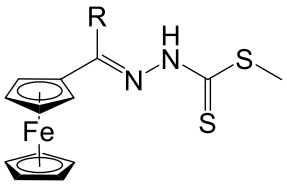	**2.1a**	42.67 ± 5.0	76.52 ± 4.1	73.86 ± 5.2	1.73	0.96
	2.1b	120.7 ± 2.9	150.2 ± 3.8	85.83 ± 5.0	0.71	0.57
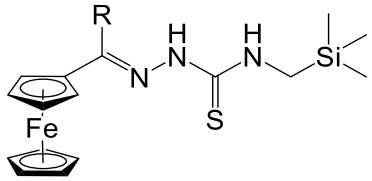	**2.3a**	111.1 ± 5.9	110.2 ± 10.5	104.6 ± 8.7	0.94	0.95
	2.3b	82.14 ± 12.1	113.4 ± 4.0	132.3 ± 5.9	1.61	1.17
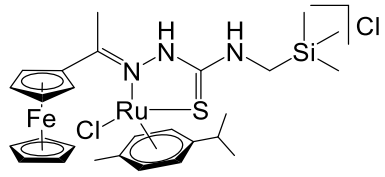	**2.6b**	12.45 ± 2.5	18.91 ± 3.6	17.23 ± 2.6	1.38	0.91
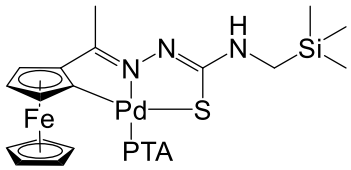	**2.12**	111.6 ± 5.0	134.1 ± 5.7	85.17 ± 4.9	0.76	0.63
Cisplatin		1.97 ± 3.4	18.90 ± 0.8	44.04 ± 0.8	22.35	2.33

[a]SI_1 =IC_{50}(KMST-6)/IC_{50}(A2780); [b]SI_2 = IC_{50}(KMST-6)/IC_{50}(A2780cisR)

The Schiff base dithiocarbamates **2.1a** appears to be slightly more active than compound **2.1b** against both the A2780 and A2780cisR cell–lines (Table 3.8). A loss of activity is observed for the organosilane TSC **2.3a**, whilst **2.3b** [82.13 μM (A2780); 113.4 μM (A2780cisR)] displays a slight improvement in activity. On the other hand, a significant improvement in activity is observed for the ruthenium complex [**2.6b**; 12.45 μM (A2780); 18.91 μM (A2780cisR)] when

compared to the corresponding TSC **2.3b**. The activity against the resistant strain is comparable to the activity of cisplatin (18.90 μM).

A loss in activity was observed for the palladium complex [111.6 μM (A2780); 134.1 μM (A2780cisR)] when compared to the corresponding TSC **2.3b** [82.14 μM (A2780); 113.4 μM (A2780cisR)]. Additionally, the TSC **2.3b** was also less toxic towards the non–tumourigenic cell–line KMST–6 than the cyclopalladated complex **2.12** (Table 3.8). Rhodium complex **2.9a** did not display any activity at the highest tested concentration.

In general, the tested compounds exhibited similar cytotoxicities against the tumourigenic and the non–tumourigenic cell–lines, and thus displayed no selectivity.

3.2.6 Evaluation using a Plasmodium Berghei infected Mouse Model

As mentioned in Section 3.1, pre–clinical mouse studies are practical models for the experimental study of human malaria. Rodent *Plasmodium* species are analogues to human malaria parasites in terms of structure, physiology and life cycle, and thus relatively good models for initial studies.[39] Compound **2.13**, which displayed good antiplasmodial activity [IC_{50} = 0.55 (NF54) and 0.29 (Dd2) μM] along with good selectivity [SI_1 = 6.44 (NF54) and SI_2 = 12.21 (Dd2)] was chosen for *in vivo* evaluation (project no. 013/028).

*Stability of Compound **2.13***

When evaluating the biological activity of a particular compound, it is important to ensure that the metal–based compounds proposed as being biologically active are in fact responsible for the observed activity. Therefore, it is important to monitor metal–based compounds in solution in order to either ensure stability of the compound or identify the active species. Therefore, as a model system the stability of complex **2.13** was investigated and monitored by ^{1}H NMR spectroscopy over a 72 hr period at 37 °C. The ^{1}H NMR spectra (Figure 3.9) of complex **2.13** were recorded in (**a**) DMSO–d_6 and (**b**) DMSO–d_6:D_2O (9:1, v/v). The spectra remain unchanged over the study period.

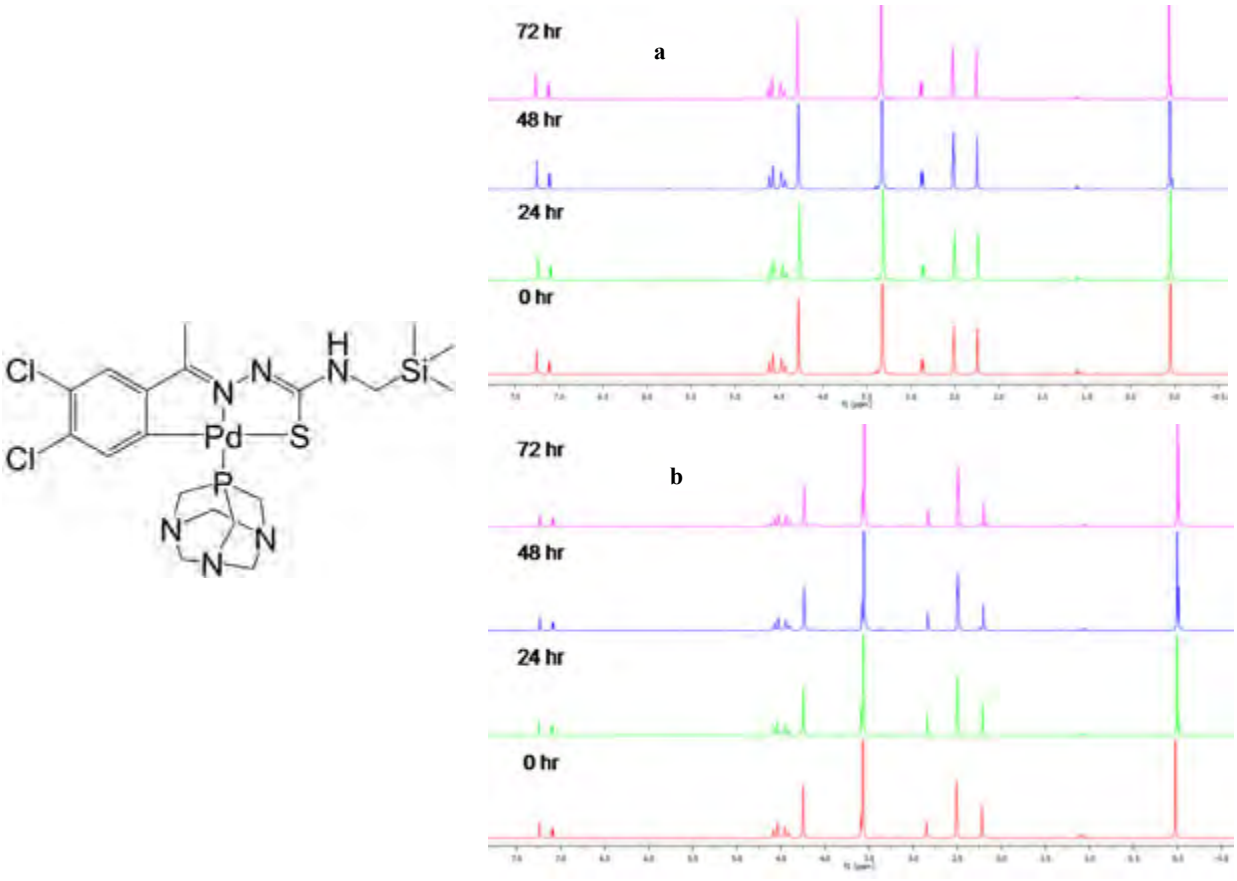

Figure 3.9 ^{1}H NMR spectra of a solution of compound **2.13** in (**a**) DMSO−d_6 and (**b**) DMSO−d_6:D_2O heated at 37 ˚C over 72 hr.

The dosing formulation for compound **2.13** was prepared as a suspension in a hydroxypropyl methylcellulose (HPMC) and dimethyl sulfoxide (9:1, v/v) vehicle. Hydroxypropyl methylcellulose is an inert polymer, which has been used in the pharmaceutical industry to control the release of an orally administered compound in the digestive tract, and is not toxic to animals such as mice.[40] In this study, doses were delivered *via* intragastric administration (oral gavage) to healthy male C57BL/6 mice.

Toxicity study

In a preliminary study, compound **2.13** was administered orally at three different concentrations [50, 30 and 10 mg/kg dose; to one mouse each (**M**$_{1\text{-}3}$); Table 3.9] once a day for four days. The weight of the mice and general behaviour was used as an indication of health and monitored continuously throughout the experimentation period. As per protocol, the experiment would be stopped if a 15 % loss in initial body weight was observed.

Table 3.9 Dosage information for mice **M_1–M_3**.

	M_1	**M_2**	**M_3**
Dose (mg/kg)	50	30	10
Final Concentration[a] (mg/mL)	6.25	3.75	1.25
Volume Administered[a] (µL)	270	280	250

[a] Calculated for an average mouse weight of 35 grams.

Over the course of four days no visible discomfort or the maximum weight loss (15 %) was observed. Therefore, no significant toxicity was observed at the tested concentrations.

Efficacy study

An efficacy study similar to a Peter's four–day suppressive test was carried out in mice infected with the CQS *P. berghei* ANKA strain to evaluate the blood schizontocidal activity of the formulations. Three groups (negative control; positive control; test compound) consisting of three mice each were studied (Table 3.9). Groups A and C were the negative and positive control groups, respectively. They were administered either as a blank formulation vehicle (Group A) or 20 mg/kg chloroquine (Group C) *via* oral gavage (Table 3.10; Figure 3.10). Group B was administered as a suspension of compound **2.13** (50 mg/kg in DMSO:HPMC) *via* oral gavage.

Table 3.10 Formulations for Groups A–C.

	Group A	**Group B** Compound **2.13**	**Group C** Chloroquine
Dose (mg/ kg)	-[a]	50	20
Final concentration (mg/ml)	-	6.25	2.5
Delivery Vehicle	DMSO : HPMC (1:9)	DMSO : HPMC (1:9)	H_2O
Volume Administered (µL)	200	200[b]	240[c]

[a] not applicable; [b] Calculated for an average mouse weight of 25 grams; [c] Calculated for an average mouse weight of 30 grams.

The mice received the first dose two hours after infection on day 0, followed by the second, third and fourth dose at intervals of 24 hours (Figure 3.10). The weight of the mice was monitored (Figure 3.11) and a change of less than 15 % suggested no significant negative effects during the testing period. Blood samples were collected on day 4 and analysed using flow cytometry.

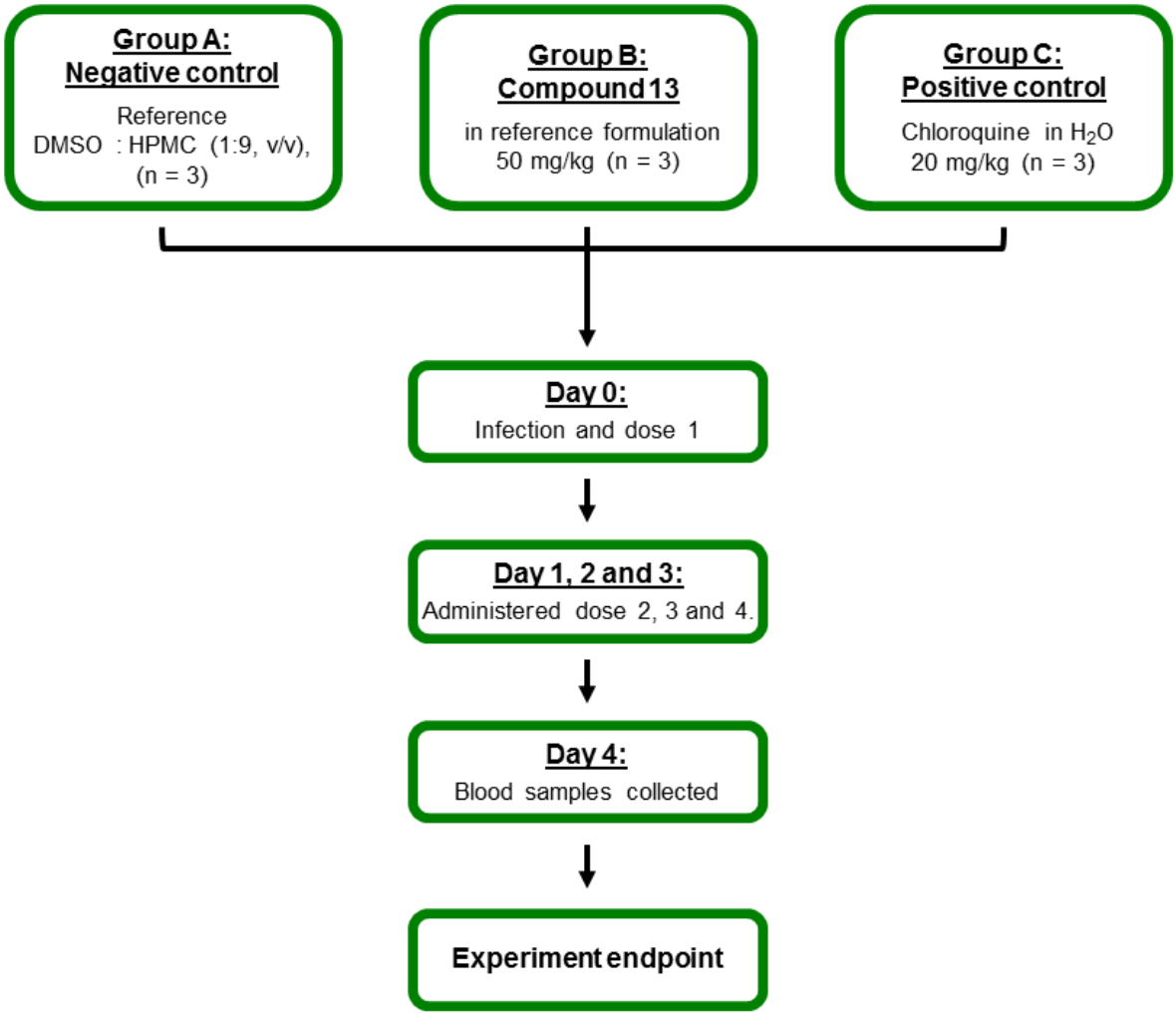

Figure 3.10 Diagram showing the experimental design of the efficacy study.

Transgenic parasitic strains, such as *P. berghei* ANKA strain, express green fluorescent proteins (GFP), which enables fluorescence–activated cell sorting (FACS) using flow cytometry. FACS is a specialised flow cytometry method for the sorting of mixtures of biological cells based on differences in light scattering and fluorescent characteristics. Therefore, red blood cells infected with the parasite expressing GFP can be distinguished from uninfected red blood cells, and thus detected by flow cytometry. The percentage parasitaemia determined using flow cytometry is listed in Table 3.11.

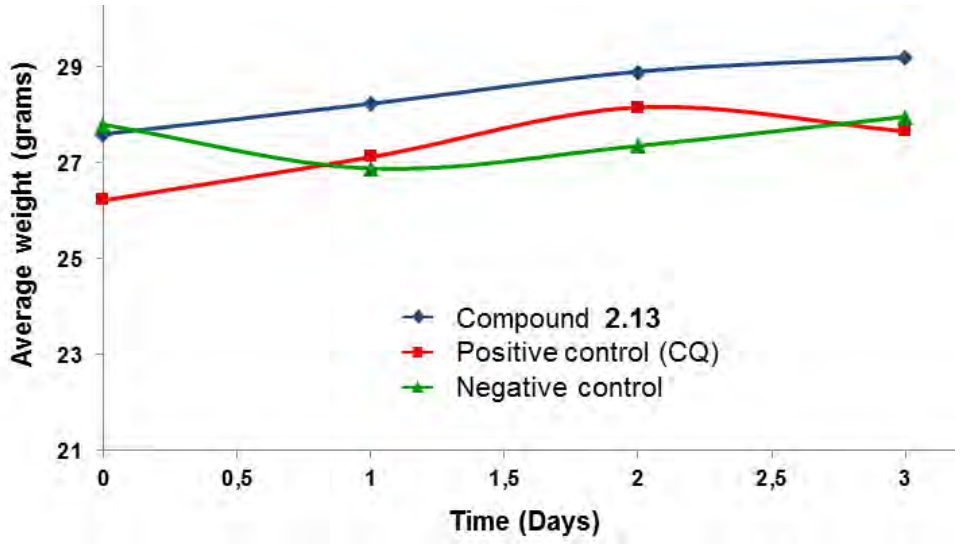

Figure 3.11 Graph showing the average body weight versus time for the mice infected with *P. berghei* and treated with compound **2.13** in a Peter's four–day suppressive test, along with positive (chloroquine) and negative controls.

As seen in Table 3.11, a comparison of the overall average percentage parasitaemia revealed that Group B (Compound **2.13**) had a similar value to that of Group A (negative control). Group C, which received the control drug chloroquine, displayed a significant clearance of parasitaemia (Table 3.11). Therefore, the test compound had no effect on the percentage parasitaemia.

Table 3.11 Percentage parasitaemia detected for Groups A–C.

	Group A			Group B			Group C		
	A1	**A2**	**A3**	**B1**	**B2**	**B3**	**C1**	**C2**	**C3**
Regional stats	10.37	9.70	11.03	14.11	10.56	10.58	0.25	0.20	0.17
Histogram stats	10.43	9.78	11.10	14.28	10.64	10.67	0.28	0.22	0.19
Individual Average	10.40	9.74	11.06	14.19	10.60	10.62	0.26	0.21	0.18
Overall average		10.40			10.61*			0.22	

*Calculated using **B2** and **B3**.

Attempts were made to develop an HPLC–UV method to analyse compound **2.13**. Blood samples spiked with compound **2.13** were subjected to either protein precipitation or liquid–liquid extraction methods.

Protein precipitation involves the additional of an organic solvent (such as acetonitrile) to the spiked blood sample to extract the compound. This is followed by centrifugation and collection of the supernatant.[41] The supernatant was then analysed by HPLC–UV after a suitable reverse–phase C18 column, wavelength (from UV–vis studies) and solvent system gradients [acetonitrile: H_2O (0.1% formic acid)] were selected.

When analysing a specified concentration of the tested compound, at a particular wavelength, the chromatogram would ideally display a peak with a specific intensity (and area) at a specific retention time. Therefore, analysis of the supernatant collected after protein precipitation was based on the intensity of the peak at the identified retention time for compound **2.13**. However, analysis of the supernatant from protein precipitation gave chromatograms with varying peak intensities for spiked samples of the same concentration. Therefore, the recovery of compound **2.13** was not consistent.

Following on from these results, the liquid–liquid extraction method was used. The liquid–liquid extraction method uses a buffer in combination with the spiked blood sample and immiscible organic solvent.[41] The buffer is used to ensure the presence of the largest amount of unionised complex, which can then be extracted with the organic solvent. Therefore, Britton Robinson Universal buffer solutions with a pH range between 3 and 11 were used to determine at which pH the largest amount of unionised complex was extracted. However, despite initial results identifying pH 9 as the ideal pH, reproducibility studies failed and the recovery of compound **2.13** was not consistent.

One problem with these extraction methods is the possibility of protein binding, which may be the case in this work. Therefore, future studies involving either inductively coupled plasma mass spectrometry (ICP–MS) analysis of the precipitated proteins or protein binding studies may prove or disprove that idea.

Unfortunately no useful information was obtained from this study. However, determining if compound **2.13** was indeed interacting with proteins may assist with future ADME studies for other metal complexes, and may shed light on the fate of compound **2.13** in the mouse model. As mentioned above, compound **2.13** was administered orally as a suspension. Therefore,

determining the bioavailability, as well as potential metabolism products, may also contribute to why the tested compound did not display any effect on the percentage parasitaemia.

3.3 Summary

The Schiff base dithiocarbamates (**2.1**; **2.2**) and thiosemicarbazone compounds (**2.3**–**2.14**) were screened as potential antiparasitic agents against parasitic strains *Plasmodium falciparum* and *Trichomonas vaginalis*.

The compounds (**2.1**−**2.14**) were evaluated for their antiplasmodial activity against the CQ–sensitive NF54 and CQ–resistant Dd2 strains of *P. falciparum*. The compounds generally displayed antiplasmodial activity in the low micromolar range. The cyclopalladated complexes (**2.12**−**2.14**) were found to be the most potent, with the 3,4-dichloroaryl derivatives (**2.13**; **2.14**) displaying activity below 1 μM against both strains. Selected compounds were also evaluated for their cytotoxicity against the Chinese Hamster Ovarian (CHO) cell–line. As proposed, compounds containing the incorporated organosilane moiety have reduced cytotoxicity compared to the dithiocarbamates and non–silicon compounds.

Selected compounds (**2.4b**, **2.9b**, **2.10b**) were evaluated for their ability to inhibit the formation of β–haematin. The rhodium complexes **2.9b** and **2.10b** had a moderate inhibition effect on the formation of β–haematin, whereas the metal−free thiosemicarbazone **2.4b** had no effect.

The antitrichomonal activity of the TSC compounds was also evaluated against the metronidazole–sensitive G3 strain of *T. vaginalis*. The ruthenium and rhodium complexes displayed growth inhibitions above 90 %, whereas the dithiocarbamates, thiosemicarbazones and the cyclopalladated complexes had no significant effects. The IC_{50} values were determined for complexes displaying inhibitions above 90 %. The ruthenium (**2.6b**; **2.7a**; **2.7b**) and rhodium (**2.9a**; **2.10a**) complexes displayed moderate IC_{50} values (7–35 μM), with the rhodium complexes appearing to be more effective inhibitors of G3 parasite growth compared to the ruthenium complexes.

Preliminary antitumour activities of selected ferrocenyl compounds were determined against cisplatin–sensitive (A2780) and cisplatin–resistant (A2780*cis*R) human ovarian carcinoma cell–lines, as well as non–tumourigenic human fibroblast skin cells (KMST–6). The

compounds displayed moderate activities (18–150 μM), but did not show any selectivity between the tumourigenic and non–tumourigenic cell–lines.

Cyclopalladated complex **2.13**, which displayed good *in vitro* antiplasmodial activity, was chosen for *in vivo* evaluation in a mouse model. This compound did not display any signs of toxicity at the highest tested concentration (50 mg/kg). Compound **2.13** was evaluated for *in vivo* efficacy in a *P. berghei* mouse model and was found to be inactive.

3.4 References

1 B. Kalra, S. Chawla, P. Gupta and N. Valecha, *Indian J. Pharmacol.*, 2006, **38**, 5–12.

2 D. A. Fidock, P. J. Rosenthal, S. L. Croft, R. Brun and S. Nwaka, *Nat. Rev. Drug Discov.*, 2004, **3**, 509–520.

3 M. T. Makler, J. M. Ries, J. A. Williams, J. E. Bancroft, R. C. Piper, B. L. Gibbins and D. J. Hinrichs, *Am. Soc. Trop. Med. Hyg.*, 1993, **48**, 739–741.

4 T. Mosmann, *J. Immunol. Methods*, 1983, **65**, 55–63.

5 L. V. Rubinstein, R. H. Shoemaker, K. D. Paull, R. M. Simon, S. Tosini, P. Skehan, D. A. Scudiero, A. Monks and M. R. Boyd, *J. Natl. Cancer Inst.*, 1990, **82**, 1113–1118.

6 J. Lin and A. Lu, *Pharmacol. Rev.*, 1997, **49**, 403–449.

7 R. Urso, P. Blardi and G. Giorgi, *Eur. Rev. Med. Pharmacol. Sci.*, 2002, **6**, 33–44.

8 C. Gunaratna, *Curr. Sep.*, 2001, **3**, 87–92.

9 J. N. Burrows, E. Burlot, B. Campo, S. Cherbuin, S. Jeanneret, D. Leroy, T. Spangenberg, D. Waterson, T. N. Wells and P. Willis, *Parasitology*, 2014, **141**, 128–139.

10 E. Badell, C. Oeuvray, A. Moreno, S. Soe, N. van Rooijen, A. Bouzidi and P. Druilhe, *J. Exp. Med.*, 2000, **192**, 1653–1660.

11 A. Moreno, E. Badell, N. van Rooijen and P. Druilhe, *Antimicrob. Agents Chemother.*, 2001, **45**, 1847–1853.

12 K. Sunita, M. Rajyalakshmi, K. Kalyan Kumar, M. Sowjanya, P. V. V Satish and D. Madhu Prasad, *Indian J. Exp. Biol.*, 2014, **52**, 67–72.

13 R. Mannhold and R. Rekker, *Perspect. Drug Discov. Des.*, 2000, **18**, 1–18.

14 R. Ahmedi and T. Lanez, *Asian J Chem*, 2010, **22**, 299–306.

15 R. Ahmedi and T. Lanez, *Int. J. Pharm. Pharm. Sci.*, 2009, **1**, 182–189.

16 R. Ahmedi and T. Lanez, *J. Fundam. Appl. Sci.*, 2011, **3**, 183–193.

17 A. J. Leo and C. Hansch, *Perspect. Drug Discov. Des.*, 1999, **17**, 1–25.

18 O. Payen, S. Top, A. Vessières, E. Brulé, A. Lauzier, M.-A. Plamont, M. J. McGlinchey, H. Müller-Bunz and G. Jaouen, *J. Organomet. Chem.*, 2011, **696**, 1049–1056.

19 O. Payen, S. Top, A. Vessières, E. Brulé, M. A. Plamont, M. J. McGlinchey, H. Müller-Bunz and G. Jaouen, *J. Med. Chem.*, 2008, **51**, 1791–1799.

20 E. Hillard, A. Vessieres, F. Le Bideau, D. Plazuk, D. Spera, M. Huché and G. Jaouen, *Chem. Med. Chem.*, 2006, **1**, 551–559.

21 R. Ahmedi and T. Lanez, *1SNEMA*, 2014, **1**, 131–140.

22 C. Biot, D. Taramelli, I. Forfar-Bares, L. A. Maciejewski, M. Boyce, G. Nowogrocki, J. S. Brocard, N. Basilico, P. Olliaro and T. J. Egan, *Mol. Pharm.*, 2005, **2**, 185–193.

23 P. Perjési, K. Takács-Novák, Z. Rozmer, P. Sohár, R. E. Bozak and T. M. Allen, *Cent. Eur. J. Chem.*, 2012, **10**, 1500–1505.

24 B. Sadek, M. M. Al-Tabakha and K. M. S. Fahelelbom, *Molecules*, 2011, **16**, 9386–9396.

25 N. Siddiqui, A. Rana, S. A. Khan, S. E. Haque, M. S. Alam, W. Ahsan and M. F. Arshad, *Acta Chim. Slov.*, 2009, **56**, 462–469.

26 C. Hansch and A. Leo, *Substituent Constants for Correlation Analysis in Chemistry and Biology*, Wiley, New York, 1979.

27 A. Pyka, M. Babuśka and M. Zachariasz, *Acta Pol. Pharm.*, 2006, **63**, 159–67.

28 M. B. Kril and H. L. Fung, *J. Pharm. Sci*, 1990, **79**, 440–443.

29 M. Adams, Y. Li, H. Khot, C. de Kock, P. J. Smith, K. Land, K. Chibale and G. S. Smith, *Dalton Trans.*, 2013, **42**, 4677–4685.

30 M. Adams, C. de Kock, P. J. Smith, K. Chibale and G. S. Smith, *J. Organomet. Chem.*, 2013, **736**, 19–26.

31 M. Adams, C. de Kock, P. J. Smith, P. Malatji, A. T. Hutton, K. Chibale and G. S. Smith, *J. Organomet. Chem.*, 2013, **739**, 15–20.

32 P. Chellan, S. Nasser, L. Vivas, K. Chibale and G. S. Smith, *J. Organomet. Chem.*, 2010, **695**, 2225–2232.

33 R. D. Sandlin, M. D. Carter, P. J. Lee, J. M. Auschwitz, S. E. Leed, J. D. Johnson and D. W. Wright, *Antimicrob. Agents Chemother.*, 2011, **55**, 3363–3369.

34 K. K. Ncokazi and T. J. Egan, *Anal. Biochem.*, 2005, **338**, 306–319.

35 P. Chellan, T. Stringer, A. Shokar, P. J. Dornbush, G. Vazquez-Anaya, K. M. Land, K. Chibale and G. S. Smith, *J. Inorg. Biochem.*, 2011, **105**, 1562–1568.

36 P. Chellan, K. M. Land, A. Shokar, A. Au, S. H. An, C. M. Clavel, P. J. Dyson, C. de Kock, P. J. Smith, K. Chibale and G. S. Smith, *Organometallics*, 2012, **31**, 5791–5799.

37 I. Zanellato, J.-M. Heldt, A. Vessières, G. Jaouen and D. Osella, *Inorg. Chim. Acta*, 2009, **362**, 4037–4042.

38 D. Plazuk, A. Vessières, E. A. Hillard, O. Buriez, E. Labbé, P. Pigeon, M.-A. Plamont, C. Amatore, J. Zakrzewski and G. Jaouen, *J. Med. Chem.*, 2009, **52**, 4964–4967.

39 R. Carter and C. L. Diggs, in *Parasitic protozoa*, ed. J. P. Kreier, Academic Press, New York, 1977, pp. 359–465.

40 E. A. Thackaberry, S. Kopytek, P. Sherratt, K. Trouba and B. McIntyre, *Toxicol. Sci.*, 2010, **117**, 485–492.

41 R. J. Flanagan, A. Taylor, I. D. Watson and R. Whelpton, *Fundamentals of Analytical Toxicology*, John Wiley & Sons, Ltd, West Sussex, 2007.

CHAPTER 4

Synthesis and Characterisation of Organosilane Derivatives of Heterocyclic Compounds Containing Quinoline and Benzothiazole

4.1 Introduction

Heterocycles, such as quinolines, benzothiazoles, benzimidazoles, benzoxazoles, imidazoles to name a few, form part of another class of pharmacologically significant compounds in medicinal chemistry.[1] Thus, the identification of heterocyclic compounds among naturally occurring biologically active compounds led to a boom in the synthesis of derivatives thereof. In this project quinoline– and benzothiazole–based compounds were explored.

As mentioned in Chapter 1 (Section 1.2.3) chloroquine was one of the most widely–used antimalarial drugs, and thus its mechanism of action has been thoroughly studied. Neutral chloroquine (CQ) is transported into the digestive vacuole *via* simple diffusion, and protonated under the acidic conditions of the digestive vacuole. However, due to marked difference in the biology of parasite strains, compounds with various physico-chemical properties are tolerated differently. Mutations of various *Plasmodium falciparum* genes and proteins have been associated with drug resistance, for example the development of *P. falciparum* CQ resistance transporter (*Pf*CRT), which is present only in CQ–resistant strains.[2,3] Due to the presence of these transporters, the protonated form of CQ is transported out of the vacuole, resulting in a marked decrease in accumulated CQ and thus a decrease in activity.

Therefore, identifying compounds which are able to circumvent the above mentioned resistance mechanism is of great importance. Ferroquine (**I**, Figure 4.1), which was briefly mentioned in Chapter 1 (Section 1.6.1), is an analogue of chloroquine containing a ferrocenyl moiety in the side–chain and has received a lot of attention due to enhanced potency against chloroquine–resistant strains of *P. falciparum*.[4,5] Studies have also shown that the activity of ferroquine is unrelated to mutations in *P. falciparum* genes.[6,7] Additionally, the differences in basicity and lipophilicity of ferroquine and chloroquine at cytosolic and digestive vacuole pH results in more efficient accumulation of ferroquine than chloroquine.[8] Furthermore, the folded conformation brought about as a result of a noncovalent intramolecular interaction, is also believed to contribute to the accumulation of the ferroquine.[5,9]

The role of the ferrocenyl moiety present in ferroquine includes influencing the lipophilicity and redox properties of the compound.[5,8] This has led to the investigation of a range of quinoline–based analogues containing a metal fragment.[10–17] The position of the ferrocenyl moiety was varied in these analogues[14,15,18] (**II**, Figure 4.1), aminoquinoline nitrogen alkylated[5] (**III**, Figure 4.1), changed the substituent on the terminal nitrogen[16,17,19–21] (**IV** & **V**, Figure 4.1), and incorporation of metal–containing structures based on ruthenocene[5], rhenium[22] and chromium compounds[23] (**VI**, Figure 4.1).

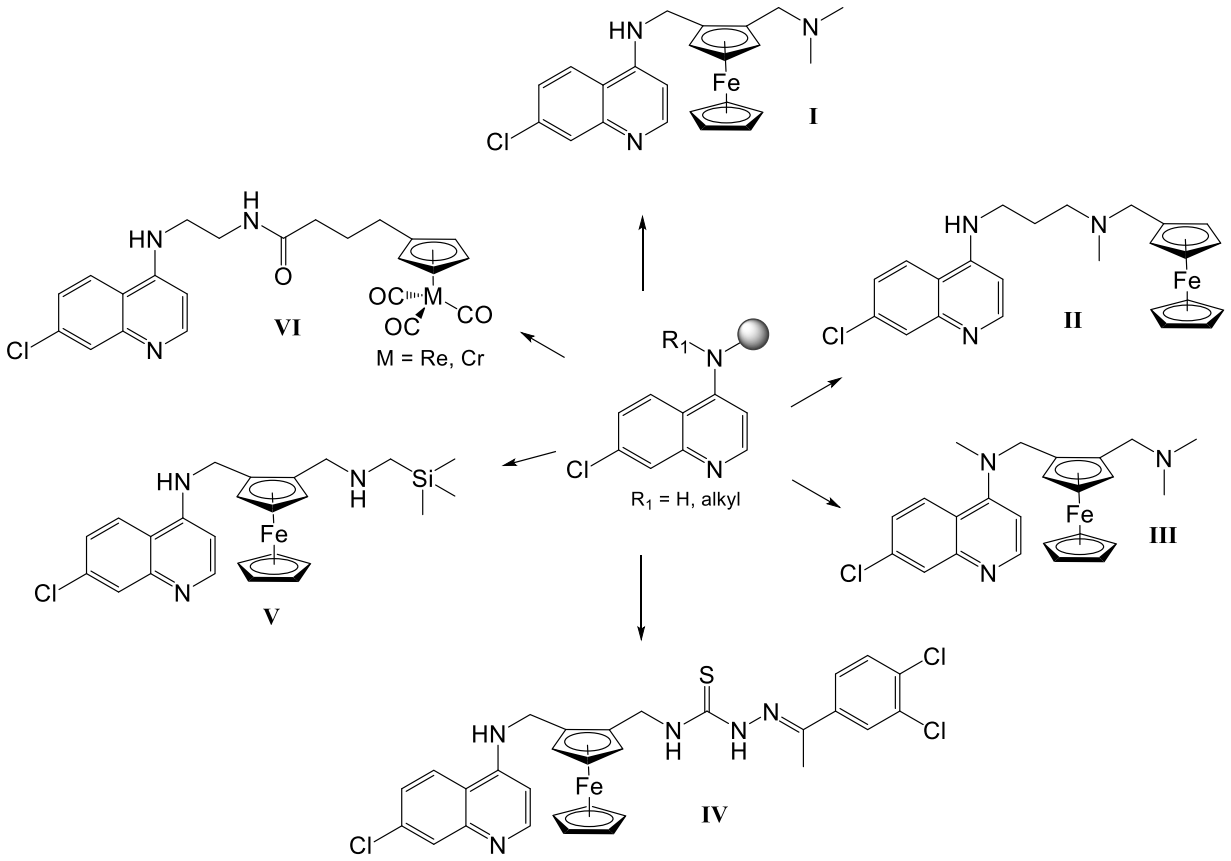

Figure 4.1 Metallo–compounds (**I**–**VI**) displaying antiplasmodial activity.[4,5,14,16,17,22,23]

The majority of the literature published on metal–containing compounds has related to their activity against *P. falciparum*, with a limited number of complexes screened against parasitic strains of *Trichomonas vaginalis*. However, a report on the evaluation of ferroquine against the metronidazole–sensitive CMP (Chatenay–Malabry Parasitology) strain of *T. vaginalis*, has been published, but no activity was noted.[24] In another study, the inhibitory effects of binuclear rhodium(I) complexes of quinoline-based compounds were evaluated with the complexes found to display promising results against the G3 strain of *T. vaginalis*.[25]

As mentioned in Chapter 1 (Section 1.3.3), 5-nitroimidazole compounds such as metronidazole or tinidazole produce cytotoxic nitro radical–ion intermediates from the reduction of the nitro groups.[26] These reactive nitrogen species act similar to ROS, and thus the presence of an oxidisable ferrocenyl moiety may be important for potential antitrichomonal agents. On the other hand, the mechanism of action and antiparasitic (antiplasmodial and antitrichomonial) activity of benzothiazole–based compounds have not been as thoroughly explored.[27–30] There have been a few publications relating to the activity of the benzothiazole–based compounds to their interactions with DNA and enzymes, or the effect they have on mitochondria.[29,31,32] However, no conclusive targets have been identified. Perhaps further evaluation of benzothiazole–based compounds will reveal potent antiparasitic and antitrichomonal agents which are able to circumvent the parasite resistance mechanism.

Unlike ferrocenyl–containing quinoline compounds, research focussed on ferrocenyl–containing benzothiazole–based compounds does not feature as prominently in literature. The only examples of ferrocenylbenzothiazoles are thiosemicarbazone–based compounds (Figure 4.2) evaluated as antitumour agents.[33,34]

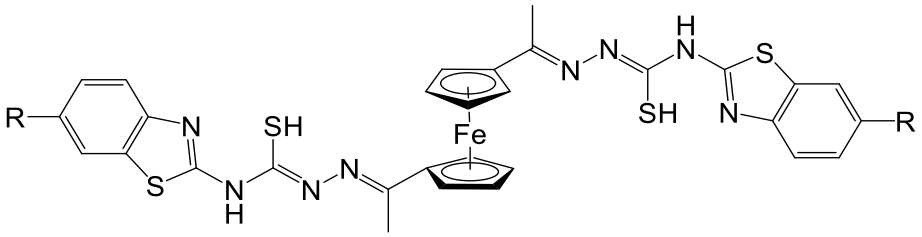

Figure 4.2 Ferrocenylbenzothiazole connected *via* a thiosemicarbazone.[34]

As mentioned in Chapter 1 (Section 1.4.1) and Chapter 2 (Section 2.1), there was an interest in exploring whether or not incorporation of silicon would favourably alter the pharmacological activity and selectivity of the compounds studied in this project. A previous study conducted within our research group investigated the preparation and evaluation of an organosilane ferroquine derivative (**V**, Figure 4.1). This compound displayed promising *in vitro* activity with IC_{50} values of 7.32 and 53.87 nM against the *P. falciparum* strains NF54 and Dd2, respectively.[17] Chloroquine displayed IC_{50} values of 5.43 nM (NF54) & 108.36 nM (Dd2).

The promising pharmacological results observed with compound **V** (Figure 4.1) prompted further investigation into ferrocenyl–containing quinoline– and benzothiazole−based compounds, with respect to activity against *P. falciparum* and *T. vaginalis*.

4.2 Results and Discussion

4.2.1 Synthesis and Characterisation of Ferrocenyl–Containing Aminoquinolines

Synthesis

Ferroquine and its quaternised form were prepared using published methods set forth by Biot *et al*. as illustrated in Scheme 4.1.[4,35] 2-[(*N*,*N*-dimethylamino)methyl]-ferrocenylmethylamine was prepared from the starting material 2-[(*N*,*N*-dimethylamino)methyl]ferrocene. This was achieved *via* aldehyde and oxime intermediates. The 2-[(*N*,*N*-dimethylamino)methyl]-ferrocenylmethylamine was reacted with 4,7-dichloroquinoline in a nucleophilic aromatic substitution reaction to prepare ferroquine, which in turn was quaternised using iodomethane.[4,35]

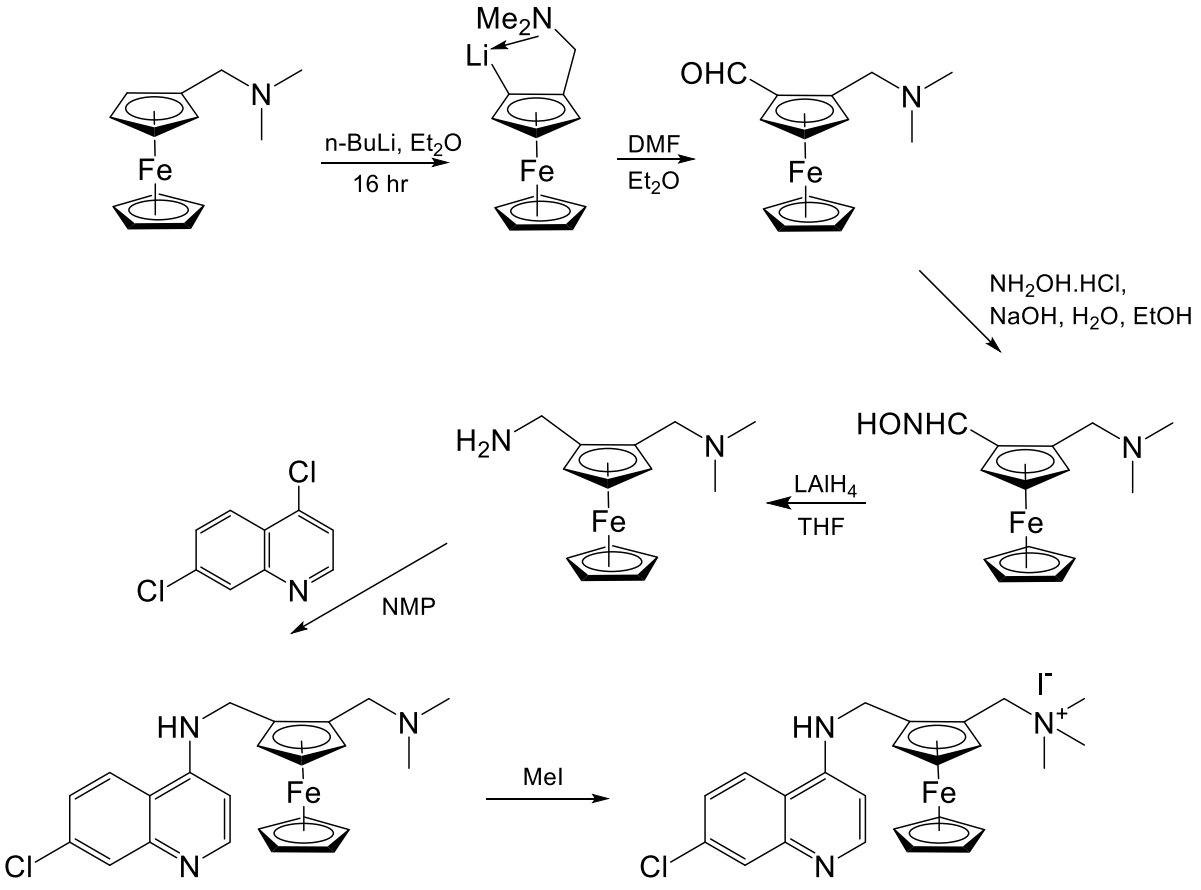

Scheme 4.1 Preparation of ferroquine and its quaternised form.[4,35]

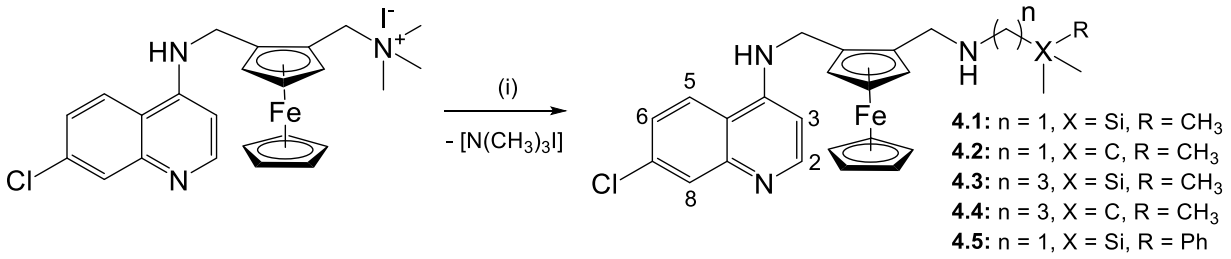

Scheme 4.2 The synthesis of ferrocenyl–containing aminoquinolines (**4.1**–**4.5**).
Reagents and conditions: 8 eq. of (aminomethyl)trimethylsilane (**4.1**), 2,2'-dimethylpropan-1-amine (**4.2**), (3-aminopropyl)trimethylsilane (**4.3**), 4,4'-dimethylpentan-1-amine (**4.4**) or (aminomethyl)dimethylphenylsilane (**4.5**); CH_3CN, K_2CO_3, reflux, 3 days.

The ferrocenyl–containing aminoquinolines (**4.1**–**4.5**) were prepared by the procedure outlined in Scheme 4.2. Nucleophilic substitution of the trimethylammonium group by amine–terminated organosilanes (aminomethyl)trimethylsilane, (3-aminopropyl)trimethyl-silane or (aminomethyl)dimethylphenylsilane, as well as the corresponding carbon analogues 2,2'-dimethylpropan-1-amine and 4,4'-dimethylpentan-1-amine, yielded the desired compounds. Previously published compound **4.1**[17] was prepared following the method described herein.

Compounds **4.1**–**4.5** were isolated in moderate yields (48 – 85 %) as orange or yellow solids. The compounds were thermally stable, melting at around 150 ˚C. Compounds **4.1**–**4.5** were soluble in most organic solvents, such as chlorinated and alcoholic solvents.

Characterisation

Compounds **4.1**–**4.5** were fully characterised using NMR (^{1}H, ^{13}C{^{1}H}, COSY, HSQC) spectroscopy, infrared (IR) spectroscopy and electron impact (EI) mass spectrometry.

NMR Spectroscopy

The ^{1}H NMR spectra of compounds **4.1**–**4.5** were recorded in $CDCl_3$. The protons of the aromatic quinoline ring were observed in the expected region 6.46–8.56 ppm. The ferrocenyl protons of the substituted and unsubstituted cyclopentadienyl rings resonate between 4.10 and 4.30 ppm (Figure 4.4).

The methylene protons H−11 and H−12 of compounds **4.1**–**4.5** are diastereotopic protons due to the planar chirality of the ferrocenyl moiety, brought about as a result of 1,2-disubstitution of the cyclopentadienyl ring. The same applies to the methylene protons H−13 of compounds

4.1, **4.2** and **4.5**. The signal for one H−11 proton appears as a doublet at ~4.3 ppm (J = 13.2 Hz) and the signal for the other H−11 proton overlaps with the signal of the unsubstituted ferrocenyl ring (confirmed using COSY). The H−12 protons resonate as two doublets at around 3.5 and 3.7 ppm (J ~ 12.3 Hz). The observed doublets were due to geminal coupling of the methylene protons.

The formation of the proposed compounds was also confirmed by the presence of signals for the incorporated amine side–chain. Two doublets were observed for the methylene protons H−13 of compounds **4.1**, **4.2** and **4.5**, whereas three upfield signals corresponding to the propyl spacer of compounds **4.3** and **4.4** were observed (Figure 4.4). Furthermore, the methyl protons [$Si(CH_3)_3$ or $C(CH_3)_3$] of compounds **4.1**−**4.5** resonate as singlets at 0.046, 0.91, −0.036, 0.85 and 0.34 ppm, respectively. The protons of the methyl groups for $Si(CH_3)_3$ are more shielded than $C(CH_3)_3$ due to the electropositive silicon.

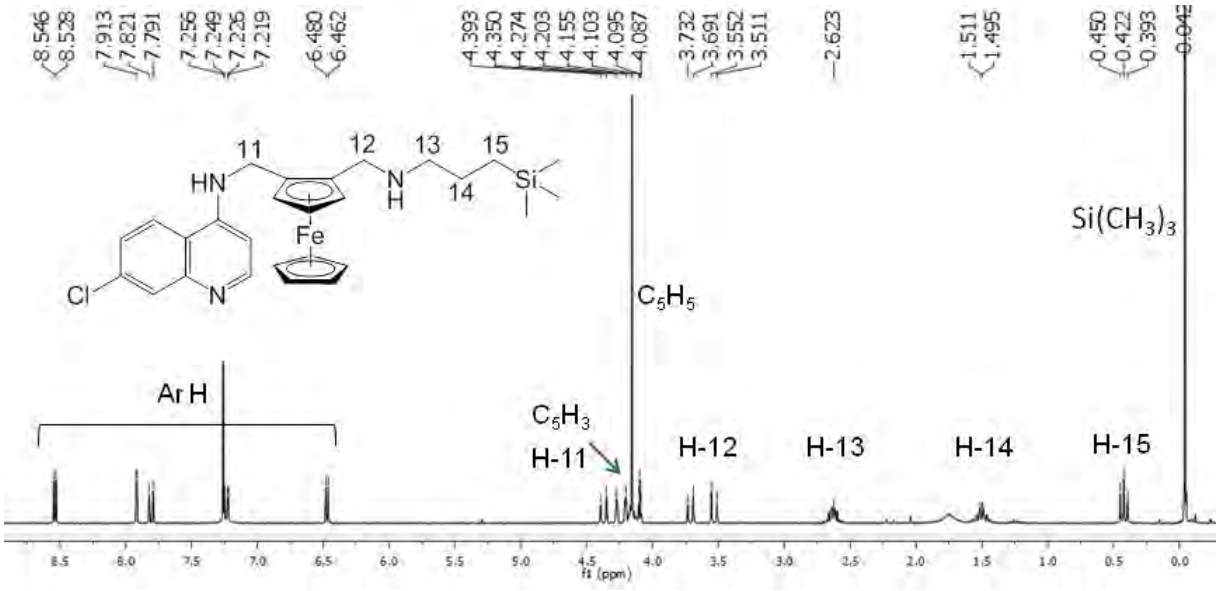

Figure 4.4 The ^{1}H NMR spectrum of compound **4.3**.

The $^{13}C\{^{1}H\}$ NMR spectra for compounds **4.1**–**4.5** were recorded in $CDCl_3$. The quinoline carbon atoms resonate between 98.6 and 152.1 ppm. The peaks for the ferrocenyl carbon atoms were observed in the range 66.1 to 86.1 ppm, with the quaternary carbon atoms being the most deshielded (identified using HSQC).

In addition to the above mentioned carbon atoms, the three methylene carbon atoms of compounds **4.1**, **4.2** and **4.5** resonate as three peaks in the range 38.8–62.5 ppm, whilst the

spectra for compounds **4.3** and **4.4** displayed the expected five signals (14.2–53.4 ppm). The most shielded methylene carbon atoms were those situated closest to the electropositive silicon. The methyl carbon atoms of the ($Si(CH_3)_3$) group of compounds **4.1**, **4.3** and **4.5** were heavily shielded, and the signal was observed at −2.29, −1.74 and –3.99 ppm, respectively. As expected, the methyl carbon atoms [$C(CH_3)_3$] were more deshielded than the signals observed for the silicon–containing compounds. The methyl carbon atoms resonate at 27.9 and 29.3 ppm, whilst the quaternary carbon atom [$\underline{C}(CH_3)_3$] was observed at 31.5 and 30.1 ppm for compounds **4.2** and **4.4**, respectively.

Infrared Spectroscopy and Mass Spectrometry

Infrared analysis of compounds **4.1**–**4.5** was carried out using attenuated total reflection (ATR). The absorption band corresponding to the stretching frequency of the C=N (quinoline ring) bond was observed at 1611 cm^{-1} (**4.1**–**4.4**) and 1609 cm^{-1} (**4.5**) for the compounds analysed.

The identity of compounds **4.2**−**4.5**, which have molecular masses of 475.1470, 519.1552, 503.1782 and 553.1396 $g.mol^{-1}$, was further confirmed using electron impact mass spectrometry. The molecular ion peaks were observed at *m/z* 475.09, 519.14, 503.12 and 553.14 for compounds **4.2**–**4.5**, respectively.

Molecular Structure

Crystals suitable for single–crystal X−ray diffraction were grown by the slow evaporation of solutions of **4.2** and **4.3** in dichloromethane and acetone, respectively. Both compounds crystallised as red blocks in a triclinic crystal system with the centrosymmetric space group $P\bar{1}$. Selected bond lengths and angles are listed in Table 4.1, with selected crystallographic data tabulated in Table 4.2.

As expected, due to the electropositive nature of the silicon atom, less electron density is contributed to Si−C bond formation. Therefore, the terminal C−C bonds [C(22)−C(23) and C(23)−C(24)] of compound **4.2** are shorter than the corresponding C−Si bonds [C(24)−Si(1) and Si(1)−C(25)] of compound **4.3**, with lengths of ~1.53 and ~1.87 Å, respectively (Table 4.1). Furthermore, differences in C−N bond lengths have been noted for the bonds N(2)−C(9) and N(3)−C(22). Due to the proximity of the aromatic quinoline ring, resonance extends to the

N(2)−C(9) bond resulting in a bond length of 1.36 Å. This bond length is significantly shorter than 1.47 Å, which has been noted for the N(3)−C(22) bond of the side−chain (Table 4.1)

Table 4.1 Selected bond lengths (Å) and angles (°)

	4.2	**4.3**
Bond Lengths (Å)		
C(22)−C(23)	1.531(3)	−
C(24)−Si(1)	−	1.8722(19)
N(3)−C(22)	1.465	1.467(2)
N(2)-C(9)	1.366(3)	1.364(2)
C(23)−C(24)	1.538(3)	1.522
Si(1)−C(25)	−	1.872(3)
Hydrogen Bond Lengths (Å)		
N(2)−H(2)···N(3)	3.160(2)	2.993(2)
N(3)−H(3)···N(1)	3.404(3)	−
Bond Angles (°)		
C(9)−N(2)−C(10)	119.54(17)	120.85(14)
C(21)−N(3)−C(22)	111.53(17)	113.05(14)
N(3)−C(22)−C(23)	115.1(2)	111.44(16)
C(23)−C(24)−Si(1)	−	114.89(13)
Hydrogen Bond Angles (°)		
N(3)−C(22)−C(23)	145.9	155.7(19)
N(3)−H(3)···N(1)	159	−
Dihedral Bond Angles (°)		
C(10)−C(11)−C(12)−C(21)	−7.7(3)	1.5(2)
N(2)−C(10)−C(11)−C(12)	70.5(2)	67.39(19)
C(11)−C(12)−C(21)−N(3)	−77.4(2)	−74.4(2)

It is evident from the molecular structures, that both compounds **4.2** and **4.3** have a folded conformation due to intramolecular hydrogen bonding between the aromatic amine nitrogen N(2) and the aliphatic amine nitrogen N(3) (Figure 4.5). In both cases, the nitrogen atom N(2) acts as the H–donor and the nitrogen atom N(3) as the acceptor. This folded conformation has previously been observed for ferroquine derivatives, including compound **4.1**.[5,9–11,17] For compound **4.2**, the crystal data listed in Table 4.1 suggests that the compound could also fold

in a different manner due to hydrogen bonding between the quinoline nitrogen atom N(1) and the aliphatic amine nitrogen atom N(3).

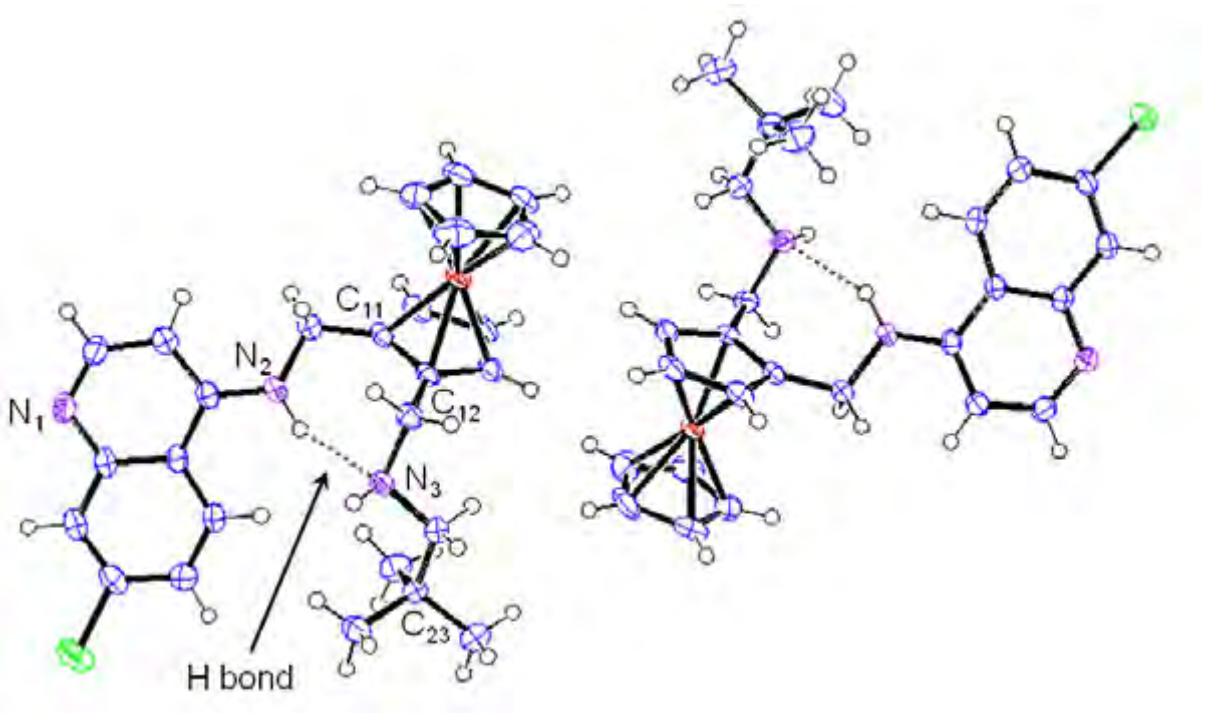

a)

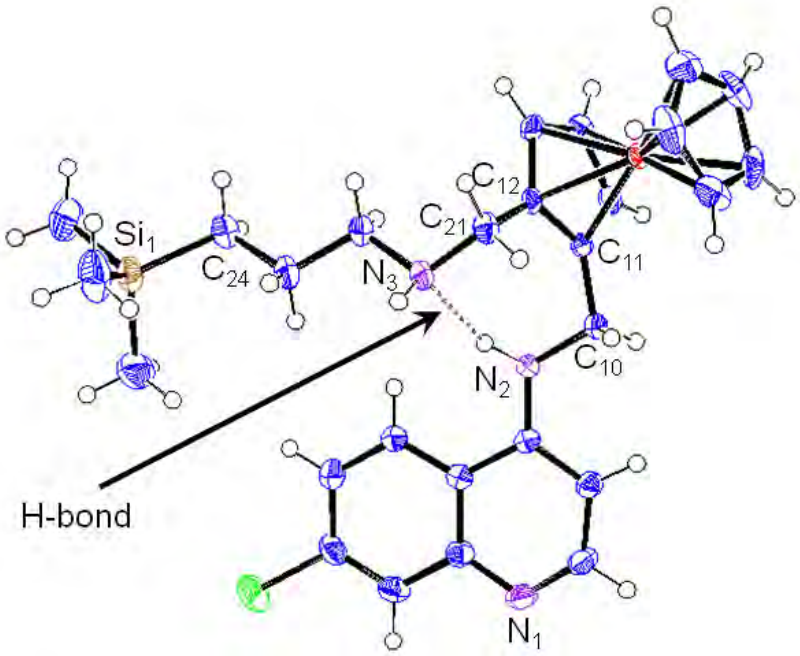

b)

Figure 4.5 ORTEP representations of compound **4.2** (**a**) and **4.3** (**b**) with ellipsoids drawn at the 50 % probability level.

Table 4.2 Crystal data of compounds **4.2** and **4.3.**

	4.2	**4.3**
Chemical formula	$C_{26}H_{30}ClFeN_3$	$C_{27}H_{34}ClFeN_3Si$
Formula weight	475.83	519.96
Crystal system	Triclinic	Triclinic
Space group	$P\bar{1}$	$P\bar{1}$
Crystal size (mm)	0.05 x 0.09 x 0.15	0.21 x 0.32 x 0.34
a, b, c (Å)	8.6284(12), 10.9159(15), 26.353(4)	6.6872(6), 7.7098(7), 25.388(2)
α, β, γ (°)	83.680(3), 84.639(3), 73.336(3)	92.4700(10), 94.337(2), 95.214(2)
V/Å^3	2358.4(6)	1298.13(19)
Z	4	2
T/K	173	173
D_c/g.cm^{-3}	1.340	1.330
μ/mm^{-1}	0.771	0.750
Scan range/°	1.96 < θ < 28.4	1.66 < θ < 27.2
Unique reflections	11751	5756
Reflections used [I > 2σ(I)]	8046	4992
R_{int}	0.057	0.035
R indices (all data)	0.0413, wR2 0.0903, S 1.03	0.0339, wR2 0.0809, S 1.03
Goodness-of-fit	1.026	1.027
Max, Min Δρ/e Å	−0.34; 0.40	−0.31; 0.33

Compound **4.3** was further reacted with $[RuCl_2(\eta^6\text{-}p\text{-}^iPrC_6H_4Me)]_2$, $[RuCl_2(\eta^6\text{-}p\text{-}C_6H_5O(CH_2)_2OH)]_2$ and $[RhCl_2(Cp^*)]_2$ to prepare heterobimetallic complexes with compound **4.3** binding in a monodentate mode *via* the quinoline nitrogen atom. Analyses of the solids (TLC and IR) confirmed the formation of the proposed complexes. As seen in Figure 4.6, when $[RuCl_2(\eta^6\text{-}p\text{-}^iPrC_6H_4Me)$(**4.3**)] was analysed by ^{1}H NMR spectroscopy in DMSO–d_6, no differences in chemical shifts were observed between that of the starting material and the new complex. The same trend was observed for $[RuCl_2(\eta^6\text{-}p\text{-}C_6H_5O(CH_2)_2OH)$(**4.3**)] and [RhCl$_2$(Cp*)(**4.3**)]. This suggests cleavage of the ruthenium–nitrogen bond. If the complex was stable in DMSO-d_6, even a slight shift should have been observed for the signal of the proton (H–2) adjacent to the quinoline C=N bond.

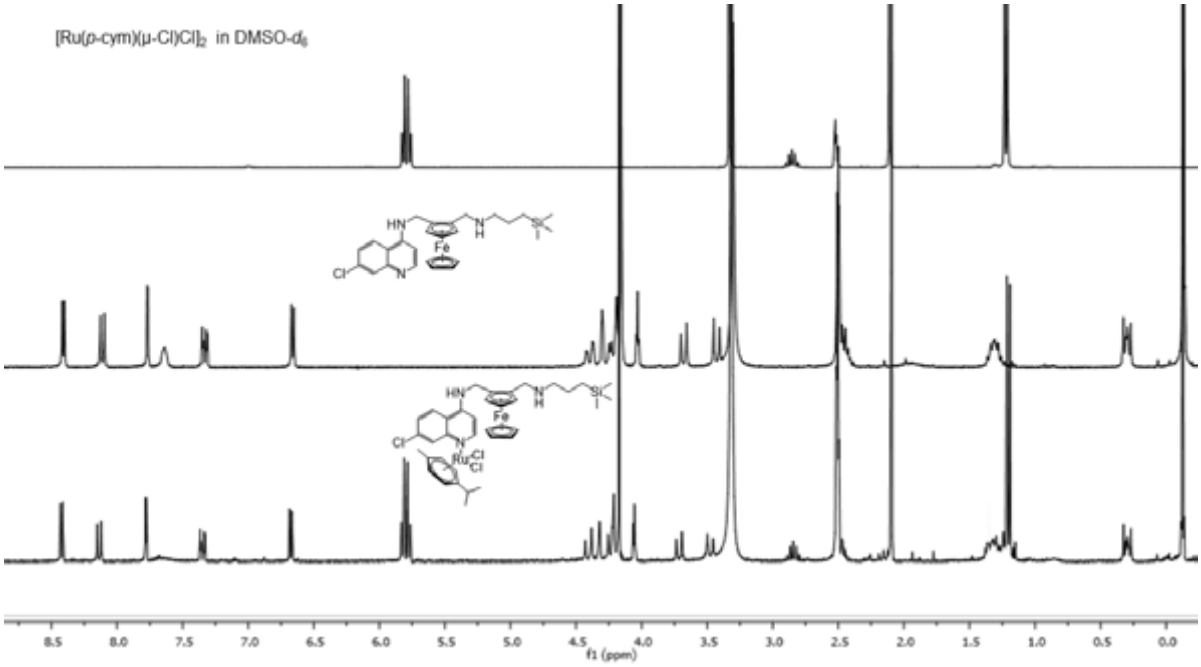

Figure 4.6 ^{1}H NMR spectra for $[RuCl_2(\eta^6\text{-}p\text{-}^{i}PrC_6H_4Me)]_2$, **4.3** and $[RuCl_2(\eta^6\text{-}p\text{-}^{i}PrC_6H_4Me)$(**4.3**)] in DMSO-$d_6$.

Patra *et al*. investigated a range of *N*-heterocyclic-$[Ru(\eta^6\text{-arene})Cl_2]$ complexes and noted similar observations when analysed in DMSO–d_6.[36] They observed that upon cleavage of the metal-nitrogen bond, the signal observed corresponds to the *N*-heterocyclic compound and the $[Ru(\eta^6\text{-arene})(DMSO)Cl_2]$ complex.[36] Therefore, preparations of these complexes were abandoned as stock solutions for biological assays are made using dimethyl sulfoxide.

4.2.2 Synthesis and Characterisation of Ferrocenyl−Containing Aminobenzothiazoles

Benzothiazole–based compounds which are analogous to those in Section 4.2.1 were prepared. All components, except the quinoline ring, were kept the same as in Section 4.2.1 which allows one to determine the contribution of the benzothiazole ring to any observed pharmacological activity.

Synthesis

6-Chloro-2-iodobenzothiazole (**4.6**) was prepared as described in Scheme 4.4, *via* a Sandmeyer–type reaction. As seen in Figure 4.7, the benzothiazole diazonium salt was prepared by the nucleophilic addition of the primary amine to the nitrosonium ion (prepared *in situ* from H_2SO_4 and $NaNO_2$).

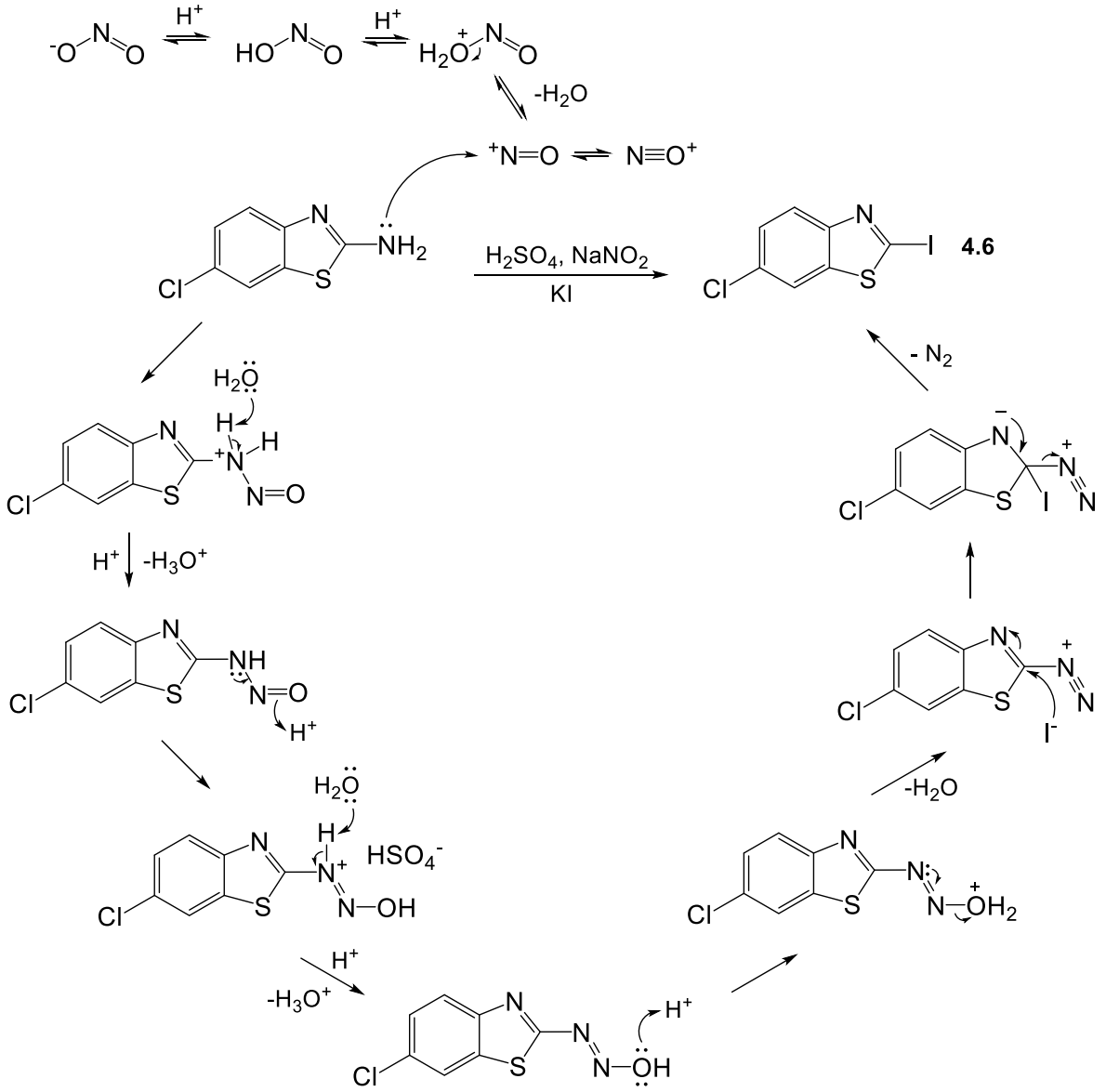

Figure 4.7 Mechanism for the formation of 6-chloro-2-iodobenzothiazole.

Further reaction of the stable diazonium salt was possible in the presence of a suitable nucleophile. Therefore, the desired compound **4.6** was prepared *via* a nucleophilic substitution reaction with iodide (from potassium iodide), which results in the liberation of N_2 gas (Figure 4.7).

Compound **4.7** was prepared *via* a nucleophilic substitution reaction, whereby 2-[(*N*,*N*-dimethylamino)methyl]ferrocenylmethylamine substitutes the iodide in the 2nd position as illustrated in Scheme 4.3. 2-[(*N*,*N*-Dimethylamino)methyl]ferrocenylmethylamine was prepared *via* published methods as seen in Scheme 4.1.[4]

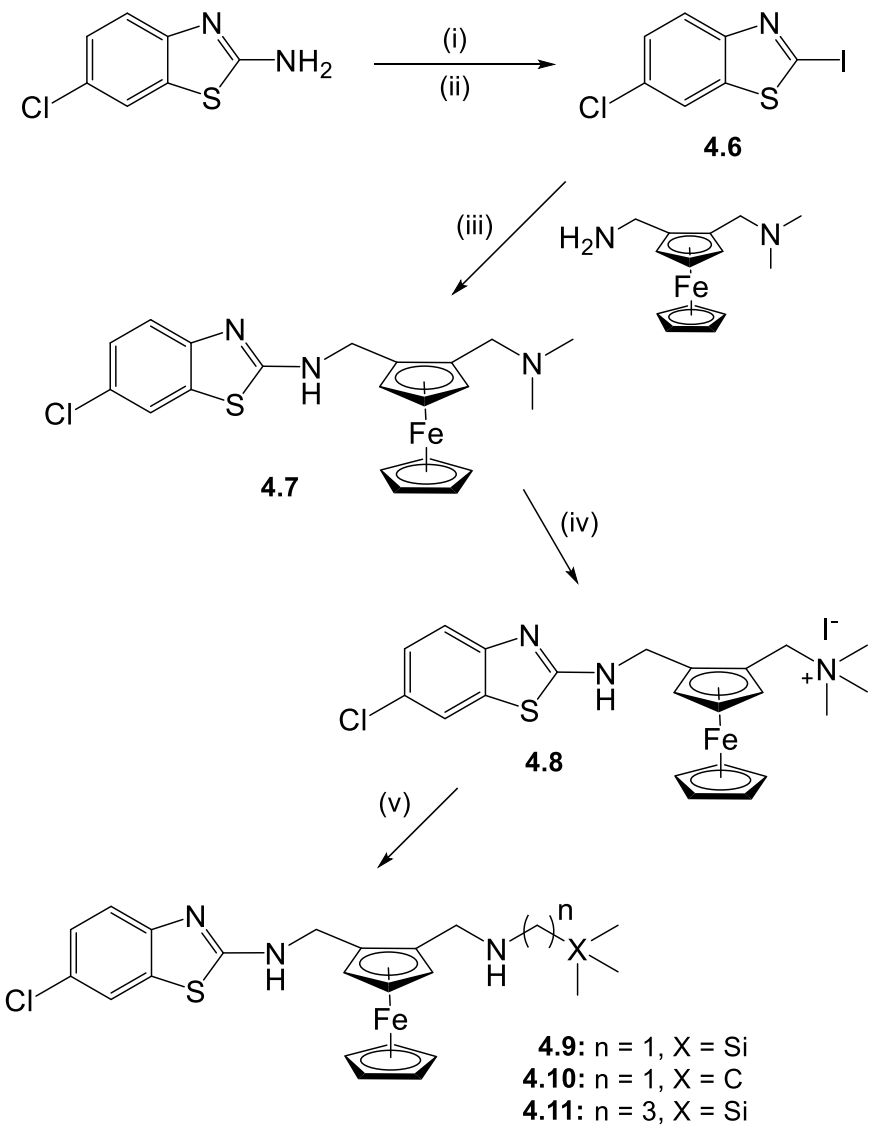

Scheme 4.3 The synthesis of a ferrocenyl−containing aminobenzothiazoles (**4.7**−**4.11**).
Reagents and conditions: (i) H_2SO_4, $NaNO_2$, 0˚C, 0.25 hr; (ii) KI, rt, 24 hr; (iii) THF, K_2CO_3, 30 ˚C, 3 days; (iv) Acetone, MeI, rt, 6 hr; (v) 8 eq. of (aminomethyl)trimethylsilane (**4.9**), 2,2'-dimethylpropan-1-amine (**4.10**) or (3-aminopropyl)trimethylsilane (**4.11**); CH_3CN, K_2CO_3, reflux, 2 days.

Attempts were made to prepare the ferrocenyl−containing aminobenzothiazole **4.7** *via* a Schiff base condensation reaction between 2-[(*N*,*N*-dimethylamino)methyl]ferrocenyl-carboxaldehyde and 2-amino-6-chlorobenzothiazole. The resulting imine compound was not stable and decomposition was accelerated when exposed to light. However, the stable compound **4.7** could be prepared in low yields, in a one–pot reductive amination reaction. This two part reaction [imine formation; imine reduction ($NaBH_4$)] was achieved when the reaction was carried out in dichloromethane (in the presence of a drying agent), with the exclusion of light and refluxing at 45 ˚C for 24 hr to prepare the imine (not isolated). The reduction of the imine was then carried out at room temperature (light excluded) with a reducing agent in

DCM:MeOH (2:1). No increase in overall yield was observed even after allowing 48 hr for imine formation. Lower yields were obtained when the reaction was carried out in purely alcoholic solvents or heated at higher temperatures, even in the presence of drying agents or the use of a Dean–Stark apparatus.

The quaternised compound **4.8** was prepared by reacting compound **4.7** with iodomethane. The ferrocenyl–containing aminobenzothiazoles (**4.9**–**4.11**) were prepared by the procedure outlined in Scheme 4.4. Nucleophilic substitution of the trimethylammonium group by amine–terminated organosilanes, (aminomethyl)trimethylsilane and (3-aminopropyl)trimethylsilane, as well as a corresponding carbon analogue 2,2'-dimethylpropan-1-amine, yielded the desired compounds.

Compounds **4.6**−**4.11** were isolated as orange or yellow solids in low to moderate yields (18−72 %). The compounds were thermally stable, melting between 130 and 180 ˚C, and were soluble in most organic solvents, such as chlorinated and alcoholic solvents.

Characterisation

Compounds **4.6**−**4.11** were fully characterised using NMR (^{1}H; ^{13}C{^{1}H}; COSY) spectroscopy, infrared (IR) spectroscopy and mass spectrometry (EI–MS; ESI−MS).

NMR Spectroscopy

The ^{1}H NMR spectra of compounds **4.6**, **4.7** and **4.9**−**4.11** were recorded in $CDCl_3$ and **4.8** in DMSO−d_6. It is evident from the ^{1}H NMR spectra for compounds **4.6** and **4.7** that the compounds were successfully synthesised due to the shifts observed for the signals of the aromatic protons (Figure 4.8). The conjugated system of the starting material 2-amino-6-chlorobenzothiazole results in the H−8 proton resonating upfield relative to H−5, due to the presence of the NH_2 group. However, formation of compound **4.6**, which contains the electron–withdrawing iodo substituent, results in a less conjugated system. This in turn results in H−8 resonating more downfield relative to H−5.

Furthermore, reacting compound **4.6** with 2-[(*N*,*N*-dimethylamino)methyl]ferrocenyl-methylamine reintroduces an electron−donating amine, which once again results in H−8 resonating upfield relative to H−5 (Figure 4.8). In addition to the shifts observed for the

aromatic signals, a broad signal observed at 8.31 ppm corresponds to the newly incorporated NH of compound **4.7**, which confirms formation of the desired compound.

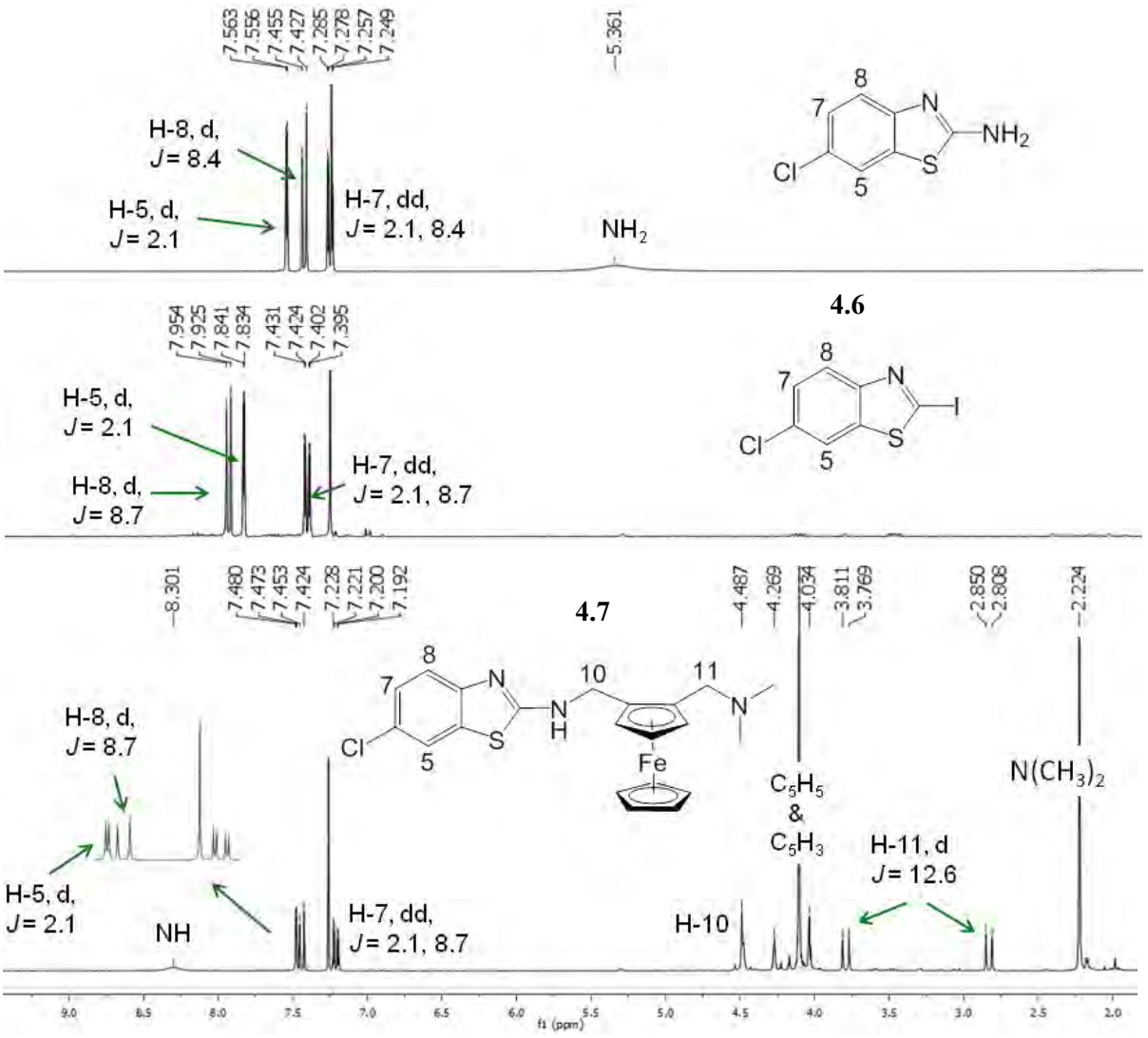

Figure 4.8 The ^{1}H NMR spectra of 2-amino-6-chlorobenzothiazole, compound **4.6** and compound **4.7**.

As seen with the aminoquinoline derivatives in Section 4.2.1, chiral compounds are produced due to the 1,2-disubstitution of the cyclopentadienyl ring of the ferrocenyl moiety. Therefore, the H−10 and H−11 protons are diastereotopic and experience geminal coupling. For the methylene protons H−11, two doublets are observed, each accounting for one proton (Figure 4.8).

Quaternisation of compound **4.7** was confirmed by the presence of a singlet at 2.96 ppm, which corresponds to the nine methyl protons of the trimethylammonium [–$N(CH_3)_3^+$] group. Upon substitution of the trimethylammonium group of compound **4.8** with the various amines, the

signal is now absent, and the signals for the protons of the incorporated amine side–chain are observed. This confirms preparation of compounds **4.9**−**4.11**.

The protons of the incorporated amine side–chain resonate in a similar manner to that observed for the aminoquinoline derivatives in Section 4.2.1. The H−12 protons of compounds **4.9** and **4.10** resonate as two doublets, while three signals were observed for the protons of the propyl chain of compound **4.11**. Additionally, singlets were observed for the methyl protons of the $Si(CH_3)_3$ and $C(CH_3)_3$ groups. The ferrocenyl and aromatic protons were observed in the expected regions 7.22−7.50 ppm and 4.05−4.28 ppm respectively, for compounds **4.9**−**4.11**.

The $^{13}C\{^1H\}$ NMR spectra for compounds **4.6**, **4.7** and **4.9**−**4.11** were recorded in $CDCl_3$ and compound **4.8** in DMSO−d_6. The aromatic carbon atoms were observed in the expected region between 119 and 151 ppm, with the remaining benzothiazole carbon C−2 resonating significantly downfield at ~166 ppm (**4.6**: 152.8 ppm) for the ferrocenyl–containing compounds (**4.7**−**4.11**). The ferrocenyl carbon atoms were also observed in the expected region (65–85 ppm). The CH_2 carbon atoms resonate upfield (14–53 ppm) with the carbons closer to the electropositive silicon being more shielded. As seen with the aminoquinoline derivatives (**4.1**−**4.4**), the $Si(CH_3)_3$ carbon atoms resonate significantly upfield at approximately –2 ppm, while the $C(CH_3)_3$ carbon atoms resonate at 28.1 and 31.3 ppm.

Infrared Spectroscopy and Mass Spectrometry

Infrared analysis of compounds **4.6**–**4.11** was carried out using ATR. The absorption band corresponding to the stretching frequency of the C=N (benzothiazole ring) of compound **4.6** was observed at 1588 cm^{-1}. Upon formation of the aminobenzothiazole compounds (**4.7**−**4.11**), the absorption band shifts slightly to a higher wavenumber around 1596 cm^{-1}.

Compounds **4.6**–**4.11** were calculated to have molecular masses of 294.8719, 439.0566, 580.9845, 497.0804, 481.1034 and 525.1116 $g.mol^{-1}$. The identity of compounds **4.6**, **4.7**, **4.9**−**4.11** was further confirmed using electron impact mass spectrometry. Compound **4.8** was identified using electrospray ionisation mass spectrometry. The molecular ion peaks were observed at *m/z* 294.82, 439.04, 497.01, 481.08 and 525.00 for compounds **4.6**, **4.7** and **4.9**−**4.11**, respectively. The mass spectrum for compound **4.8** revealed a peak at *m/z* 454.0808

corresponding to $[M]^+$, which is the positively charged fragment (excludes the iodide counter–ion).

4.2.3 Synthesis and Characterisation of Ferrocenylamines

In order to determine the contribution of the ferrocenyl moiety to the pharmacological activity, ferrocenyl compounds containing the amines used in Sections 4.2.1 and 4.2.2 were prepared.

Synthesis

Ferrocenylamines (**4.12**; **4.13**) were prepared *via* a reductive amination reaction. Ferrocenecarboxaldehyde was reacted with either (aminomethyl)trimethylsilane or 2,2'-dimethylpropan-1-amine *via* a Schiff–base condensation reaction, followed by the reduction of the imine with sodium borohydride (Scheme 4.4).

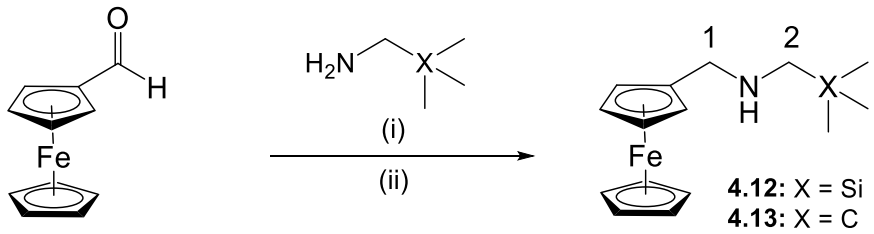

Scheme 4.4 The synthesis of ferrocenylamines.
Reagents and conditions: (i) (aminomethyl)trimethylsilane (**4.12**) or 2,2'-dimethylpropan-1-amine (**4.13**), DCM, 35 °C, 5 hr, in dark; (ii) $NaBH_4$, DCM−MeOH (v/v, 5:2), rt, overnight.

Compound **4.12** was isolated as a sticky orange solid, whereas compound **4.13** was isolated as an orange powder. The compounds were isolated in good yields (~95 %), with a melting point range of 55.2−57.2 ˚C for compound **4.13**.

Characterisation

The compounds were fully characterised using NMR (^1H; $^{13}C\{^1H\}$) spectroscopy, infrared spectroscopy and mass spectrometry (EI–MS).

NMR Spectroscopy

The ^1H NMR spectra for compounds **4.12** and **4.13** were recorded in $CDCl_3$. The expected ferrocenyl signals were observed. Two triplets (J ~1.6 Hz) each accounting for two protons were observed at 4.11 and 4.21 ppm, with a singlet corresponding to the unsubstituted cyclopentadienyl ring observed at 4.13 ppm. In addition to the ferrocenyl signals, two singlets

corresponding to the methylene protons were observed. The methylene protons (H−1) adjacent to the ferrocenyl moiety were observed at 3.52 ppm. As expected, the methylene protons (H−2) of compound **4.12** were more shielded (2.11 ppm) than those of the carbon analogue **4.13** (2.40 ppm).

The ferrocenyl, methylene and methyl carbons were all accounted for in the $^{13}C\{^{1}H\}$ NMR spectra.

Infrared Spectroscopy and Mass Spectrometry

Infrared spectral analysis of compounds **4.12** and **4.13** confirmed the absence of absorption bands for C=O (aldehyde) or C=N (imine) moieties. The presence of an absorption band for the newly incorporated NH was observed at 3093 and 3088 cm^{-1} for **4.12** and **4.13**, respectively.

The structure of the compounds **4.12** and **4.13** were further confirmed by electron impact mass spectrometry. Molecular ion peaks observed at *m/z* 301.09 and 285.02 correspond to compound **4.12** and **4.13**, respectively.

4.3 Summary

Ferroquine and its quaternised form were prepared *via* published methods. A series of ferrocenyl–containing aminoquinolines (**4.1**−**4.5**) were prepared *via* a nucleophilic substitution reaction. The quaternised form of ferroquine was reacted with various amines, such as (aminomethyl)trimethylsilane, 2,2'-dimethylpropan-1-amine, (3-aminopropyl)trimethylsilane, 4,4'-dimethylpentan-1-amine and (aminomethyl)dimethylphenylsilane. Compounds **4.1**−**4.5** were fully characterised using NMR (^{1}H; $^{13}C\{^{1}H\}$; COSY; HSQC) spectroscopy, infrared (IR) spectroscopy and electron impact mass spectrometry (EI–MS). The molecular structures of compounds **4.2** and **4.3** were determined using single–crystal X–ray diffraction. Both compounds crystallise in a folded conformation due to intramolecular hydrogen bonding between the nitrogen atoms on opposite sides of the ferrocenyl moiety. In the case of compound **4.2**, hydrogen bonding could also occur between the quinoline nitrogen and the NH of the side–arm.

Following on from the series of ferrocenyl–containing aminoquinolines, a series of benzothiazole–based compounds was prepared.

6-Chloro-2-iodobenzothiazole (prepared *via* a Sandmeyer–type reaction) was reacted with 2-[(*N*,*N*-dimethylamino)methyl]ferrocenylmethylamine in a nucleophilic substitution reaction to prepare the ferrocenyl–containing aminobenzothiazole **4.7**. This was followed by the quaternisation of compound **4.7** by reacting with iodomethane. The quaternised compound **4.8** was subsequently reacted with various amines, such as (aminomethyl)trimethylsilane, 2,2'-dimethylpropan-1-amine and (3-aminopropyl)trimethylsilane to afford compounds **4.9**−**4.11**, respectively. Compounds **4.7**−**4.11** were fully characterised using NMR (^{1}H; ^{13}C{^{1}H}; COSY) spectroscopy, infrared (IR) spectroscopy and mass spectrometry (Electron Impact; Electrospray Ionisation).

Ferrocenylamines **4.12** and **4.13** were prepared by a reductive amination reaction. The imine was prepared by reacting ferrocenecarboxaldehyde with either (aminomethyl)trimethylsilane or 2,2'-dimethylpropan-1-amine, which was then reduced to the amine. Compounds **4.12** and **4.13** were fully characterised using NMR (^{1}H; ^{13}C{^{1}H}) spectroscopy, infrared (IR) spectroscopy and electron impact mass spectrometry (EI−MS).

4.4 References

1 J. N. Burrows, E. Burlot, B. Campo, S. Cherbuin, S. Jeanneret, D. Leroy, T. Spangenberg, D. Waterson, T. N. Wells and P. Willis, *Parasitology*, 2014, **141**, 128–139.

2 D. A. Fidock, T. Nomura, A. K. Talley, R. A. Cooper, S. M. Dzekunov, M. T. Ferdig, L. M. Ursos, A. B. Sidhu, B. Naudé, K. W. Deitsch, X. Z. Su, J. C. Wootton, P. D. Roepe and T. E. Wellems, *Mol. Cell*, 2000, **6**, 861–871.

3 A. Ecker, A. M. Lehane, J. Clain and D. A. Fidock, *Trends Parasitol.*, 2012, **28**, 504–514.

4 C. Biot, G. Glorian, L. A. Maciejewski and J. S. Brocard, *J. Med. Chem.*, 1997, **40**, 3715–3718.

5 F. Dubar, T. J. Egan, B. Pradines, D. Kuter, K. K. Ncokazi, D. Forge, J. F. Paul, C. Pierrot, H. Kalamou, J. Khalife, E. Buisine, C. Rogier, H. Vezin, I. Forfar, C. Slomianny, X. Trivelli, S. Kapishnikov, L. Leiserowitz, D. Dive and C. Biot, *ACS Chem. Biol.*, 2011, **6**, 275–287.

6 A. Kreidenweiss, P. G. Kremsner, K. Dietz and B. Mordmüller, *Am. J. Trop. Med. Hyg.*, 2006, **75**, 1178–1181.

7 M. Henry, S. Briolant, A. Fontaine, J. Mosnier, E. Baret, R. Amalvict, T. Fusai, L.

Fraisse, C. Rogier and B. Pradines, *Antimicrob. Agents Chemother.*, 2008, **52**, 2755–2759.

8 C. Biot, D. Taramelli, I. Forfar-Bares, L. A. Maciejewski, M. Boyce, G. Nowogrocki, J. S. Brocard, N. Basilico, P. Olliaro and T. J. Egan, *Mol. Pharm.*, 2005, **2**, 185–193.

9 F. Dubar, J. Khalife, J. Brocard, D. Dive and C. Biot, *Molecules*, 2008, **13**, 2900–2907.

10 C. Biot, W. Castro, C. Botté and M. Navarro, *Dalton Trans.*, 2012, **41**, 6335–6349.

11 M. Navarro, W. Castro and C. Biot, *Organometallics*, 2012, **31**, 5715–5727.

12 W. A. Wani, E. Jameel, U. Baig, S. Mumtazuddin and L. T. Hun, *Eur. J. Med. Chem.*, 2015, **101**, 534–551.

13 M. A. L. Blackie and K. Chibale, *Met. Based. Drugs*, 2008, **2008**, 495123–495133.

14 C. Biot, W. Daher, C. M. N'Diaye, P. Melnyk, B. Pradines, N. Chavain, A. Pellet, L. Fraisse, L. Pelinski, C. Jarry, J. Brocard, J. Khalife, I. Forfar-Bares and D. Dive, *J. Med. Chem.*, 2006, **49**, 4707–4714.

15 C. Biot, L. Delhaes, H. Abessolo, O. Domarle, L. A. Maciejewski, M. Mortuaire, P. Delcourt, P. Deloron, D. Camus, D. Dive and J. . Brocard, *J. Organomet. Chem.*, 1999, **589**, 59–65.

16 C. Biot, B. Pradines, M.-H. Sergeant, J. Gut, P. J. Rosenthal and K. Chibale, *Bioorg. Med. Chem. Lett.*, 2007, **17**, 6434–6438.

17 Y. Li, C. de Kock, P. J. Smith, K. Chibale and G. S. Smith, *Organometallics*, 2014, **33**, 4345–4348.

18 P. F. Salas, C. Herrmann, J. F. Cawthray, C. Nimphius, A. Kenkel, J. Chen, C. De Kock, P. J. Smith, B. O. Patrick, M. J. Adam and C. Orvig, *J. Med. Chem.*, 2013, **56**, 1596–1613.

19 C. Biot, W. Daher, N. Chavain, T. Fandeur, J. Khalife, D. Dive and E. De Clercq, *J. Med. Chem.*, 2006, **49**, 2845–2849.

20 F. Bellot, F. Coslédan, L. Vendier, J. Brocard, B. Meunier and A. Robert, *J. Med. Chem.*, 2010, **53**, 4103–4109.

21 N. Chavain, E. Davioud-Charvet, X. Trivelli, L. Mbeki, M. Rottmann, R. Brun and C. Biot, *Bioorg. Med. Chem.*, 2009, **17**, 8048–8059.

22 R. Arancibia, F. Dubar, B. Pradines, I. Forfar, D. Dive, A. H. Klahn and C. Biot, *Bioorg. Med. Chem.*, 2010, **18**, 8085–8091.

23 L. Glans, D. Taylor, C. de Kock, P. J. Smith, M. Haukka, J. R. Moss and E. Nordlander, *J. Inorg. Biochem.*, 2011, **105**, 985–990.

24 S. Pomel, C. Biot, C. Bories and P. M. Loiseau, *Parasitol. Res.*, 2013, **112**, 665–669.

25 T. Stringer, D. Taylor, H. Guzgay, A. Shokar, A. Au, P. J. Smith, D. T. Hendricks, K. M. Land, T. J. Egan and G. S. Smith, *Dalton Trans.*, 2015, **44**, 14906–14917.

26 M. Müller, *Biochem. Pharmacol.*, 1986, **35**, 37–41.

27 F. Delmas, C. Di Giorgio, M. Robin, M. Gasquet, C. Detang, M. Costa, N. Azas, P. Timon-David and J.-P. Galy, *Antimicrob. Agents Chemother.*, 2002, **46**, 2588–2594.

28 P. C. Sharma, A. Sinhmar, A. Sharma, H. Rajak and D. P. Pathak, *J. Enzyme Inhib. Med. Chem.*, 2013, **28**, 240–266.

29 R. S. Keri, M. R. Patil, S. A. Patil and S. Budagumpi, *Eur. J. Med. Chem.*, 2015, **89**, 207–251.

30 G. Sadhasivam, K. Kulanthai, S. Rajamani and P. Perumal, *Bangladesh J. Pharmacol.*, 2016, **11**, 321–327.

31 S. Hout, N. Azas, A. Darque, M. Robin, C. Di Giorgio, M. Gasquet, J. Galy and P. Timon-David, *Parasitology*, 2004, **129**, 525–535.

32 D. S. B. Ongarora, J. Gut, P. J. Rosenthal, C. M. Masimirembwa and K. Chibale, *Bioorg. Med. Chem. Lett.*, 2012, **22**, 5046–5050.

33 K. Sampath and C. Jayabalakrishnan, *Arab. J. Chem.*, 2013.
DOI: 10.1016/j.arabjc.2013.12.017.

34 K. Sampath, S. Sathiyaraj and C. Jayabalakrishnan, *Med. Chem. Res.*, 2014, **23**, 958–968.

35 C. Biot, L. Delhaes, C. M. N'Diaye, L. A. Maciejewski, D. Camus, D. Dive and J. S. Brocard, *Bioorg. Med. Chem.*, 1999, **7**, 2843–2847.

36 M. Patra, T. Joshi, V. Pierroz, K. Ingram, M. Kaiser, S. Ferrari, B. Spingler, J. Keiser and G. Gasser, *Chem. - A Eur. J.*, 2013, **19**, 14768–14772.

CHAPTER 5

Pharmacological Evaluation of Organosilane Heterocycle−Based Compounds as Antiparasitic Agents

5.1 Introduction

As mentioned in Chapter 3 (Section 3.1), one approach to identifying potential antiparasitic lead compounds is based on whole–cell phenotypic screening, which initially involves *in vitro* evaluation against the parasite of interest and cytotoxicity studies against mammalian cell–lines. Furthermore, identification of potential effective lead compounds by means of *in vitro* evaluation is generally followed by determining how the compound exerts its pharmacological effects.

Mechanism of Action

The route by which an active compound exerts its pharmacological effects is of significance. Drugs may interact with receptors, enzymes, ion channels or the survival process used by the foreign microbe. Therefore, mechanisms involving the inhibition of haemozoin formation especially in case of antimalarial agents, the generation of reaction species [reactive oxygen species (ROS) or reactive nitrogen species (RNS)] or interactions with DNA to name a few, are studied.[1,2] In terms of haemozoin inhibition, the NP–40 β–haematin inhibition assay is used.[3] The neutral detergent NP–40 is used to mimic lipids and mediates β–haematin formation in the assay. Therefore, the amount of β–haematin can be quantified using the colorimetric pyridine ferrochrome method developed by Egan *et al*.[4]

Furthermore, when looking at ferroquine as an example, various components have been identified as being essential for the overall biological activity (Figure 5.1). As part of this project, the ferroquine derivatives prepared retained the ferrocene and 4-aminoquinoline cores, as well as a 7-chloro substituent. As seen in Figure 5.1, the importance of each component has been summarised.[5]

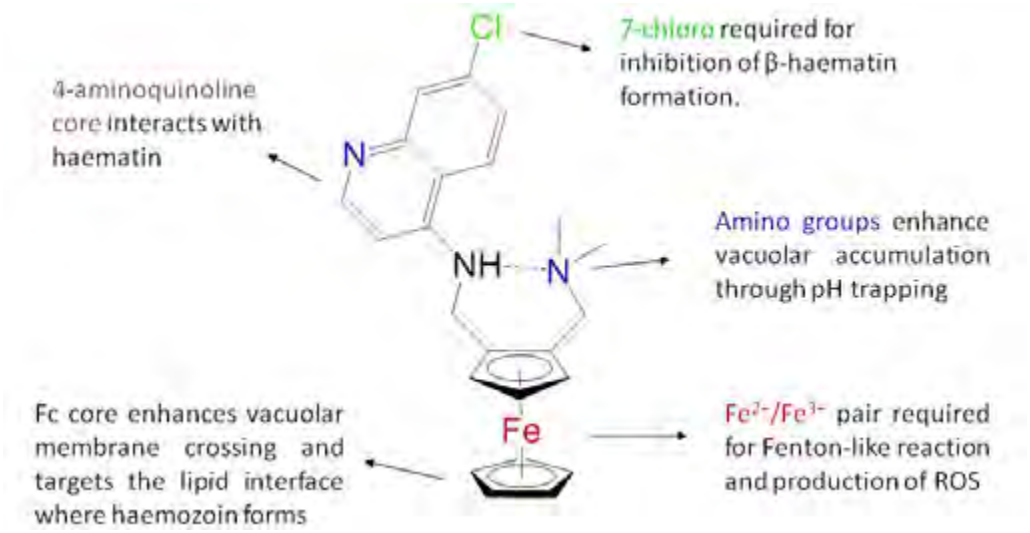

Figure 5.1 Proposed structure–activity relationship for ferroquine.[5]

However, in addition to identifying potential mechanisms of action, it is also important to determine the drug metabolism and pharmacokinetics profile of a potential drug lead.

In Vitro Models of Drug Metabolism

Metabolism, or biotransformation, generally refers to the process of converting a hydrophobic compound to a more hydrophilic form. This conversion, which is facilitated by enzymes (e.g. cytochrome P450 family[6]), allows either for the generation of the active compound, inactivation of the active compound or generation of potentially toxic compounds to be excreted (Figure 5.2). Metabolism of a compound can be divided into two phases.[7] The first phase of metabolism occurs in the hepatic system; however, compounds may be further metabolised (phase II) in tissues such as gastrointestinal epithelial, renal, skin, and lung tissues. Metabolic processes such as oxidation, reduction or hydrolysis may occur in phase I metabolism, whereas phase II metabolism involves conjugation of naturally occurring compounds to the metabolism product of phase I.[7]

Metabolic stability is defined as the percentage of parent compound lost over time in the presence of a metabolically active test system, i.e. enzyme. Therefore, metabolic stability assays are used to estimate the susceptibility of the test compound to metabolism. In general, if > 70 % of a compound remains after the incubation period then the compound is relatively stable, whereas < 30 % suggests that the compound is unstable. These assays employ the use of

liver models, such as liver microsomes, hepatocytes or liver slices, depending on the purpose of the assay.[8,9] In more high–throughput screenings, the use of microsomes is more applicable.

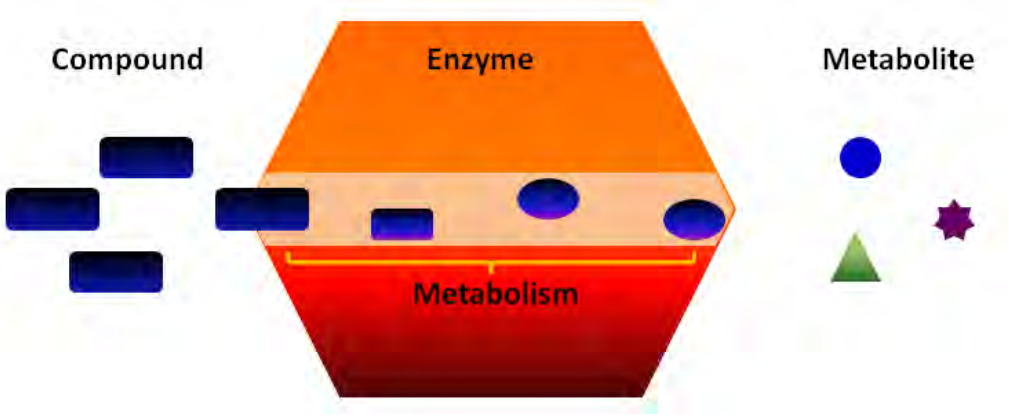

Figure 5.2 Diagram illustrating the metabolism of a compound.

If a compound displays good stability, another important concept to determine is the half–life of the compound. Half–life refers to the amount of time taken for the drug plasma concentration to reduce to half the initial concentration.[10] Knowing the half–life of the compound may assist in dosing plans, where a compound with a longer half–life may be administered at lower dosages and less frequently. In the case of drug toxicity or side effects, the half–life can be used to determine how long it will take for the drug to clear.

Furthermore, an important analysis tool for metabolic stability studies is liquid chromatography–tandem mass spectrometry technique (LC–MS/MS). Liquid chromatography is used to separate possible metabolites, whereas mass spectrometry is used to determine the masses of the metabolites and thus utilised to identify the metabolite.[11]

5.2 Pharmacological Evaluation of Ferrocenyl–Containing Aminoquinolines and Aminobenzothiazoles

The pharmacological activities of the synthesised ferrocenyl–containing aminoquinoline and aminobenzothiazole compounds (Figure 5.3) were evaluated through *in vitro* screening. The compounds were screened against the NF54 chloroquine–sensitive and Dd2 chloroquine–resistant *Plasmodium falciparum* strains, and their cytotoxicity evaluated against the Chinese Hamster Ovarian (CHO) cell–line. Selected compounds were also tested for their ability to inhibit β–haematin formation as a potential mechanism of action. Based on the data

for compounds screened against *P. falciparum* strains, compounds were selected for further *in vitro* testing in metabolic stability studies. Additionally, the antiparasitic activity of these ferrocenyl–containing aminoquinoline and aminobenzothiazole compounds was also determined against the metronidazole–sensitive G3 strain of *T. vaginalis*. Furthermore, the cytotoxicity of selected compounds were evaluated against the WHCO1 oesophageal cancer cell–line

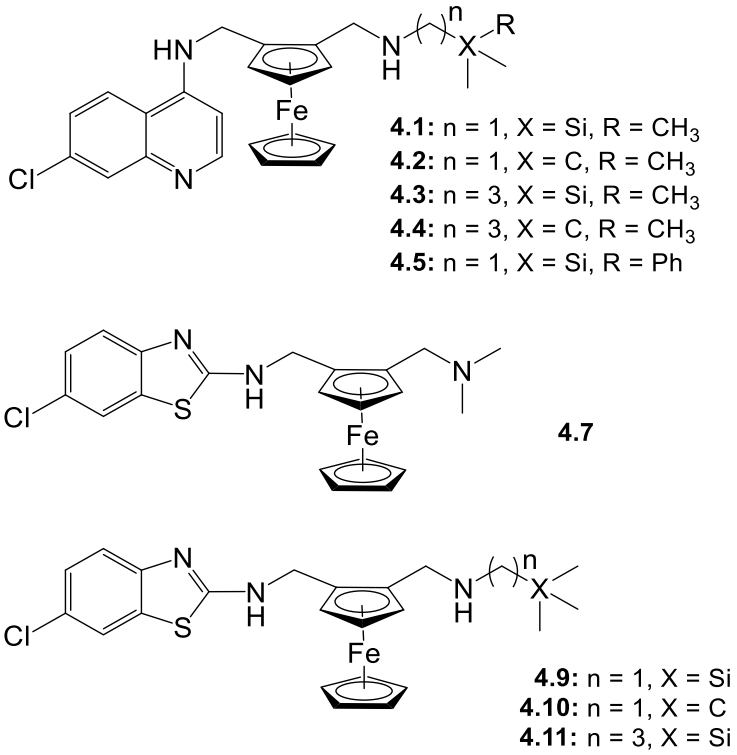

Figure 5.3 Ferrocenyl–containing aminoquinolines (**4.1**−**4.4**) and aminobenzothiazoles (**4.7**; **4.9**–**4.11**).

5.2.1 Predicting Lipophilicity

An important physicochemical characteristic to consider when searching for a compound suitable for *in vivo* models is the lipophilicity of the compound of interest. As mentioned in Chapter 4 (Section 4.1), there is a marked difference in the lipophilicity of ferroquine and chloroquine, which influences accumulation of the compound.[5] Therefore, the log*P* values of the ferrocenyl–containing aminoquinolines and aminobenzothiazoles were determined using the method described in Chapter 3.

The clog*P* values of the benzene–derivatives were determined using ChemBioDraw and listed in Table 5.1. These clog*P* values were used in combination with the fragmental constant approach to determine the log*P* value for the ferrocenyl−containing compounds.

Table 5.1 clog*P* values calculated for the benzene–derivatives using ChemBioDraw v13.0.

Compound	cLog*P*	Compound	cLog*P*
Derivative of 4.1	6.498	Derivative of 4.7	4.583
Derivative of 4.2	5.933	Derivative of 4.9	6.538
Derivative of 4.3	6.954	Derivative of 4.10	5.973
Derivative of 4.4	6.991	Derivative of 4.11	6.994
Derivative of 4.5	7.977		

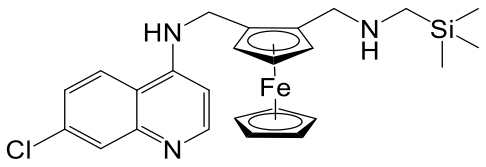

4.1

Prediction:

$\log P_{(\text{Fc derivative})} = \text{clog}P_{(\text{benzene derivative})} - f_{(C6H4)} + f_{(Fc\text{-}2H)}$

$= 6.498 - 1.476 + 2.252 = \mathbf{7.274}$

Table 5.2 Compilation of the estimated log*P* values for compounds **4.1**–**4.5**, **4.7** and **4.9**–**4.11**.

Compound	Log*P*	Compound	Log*P*
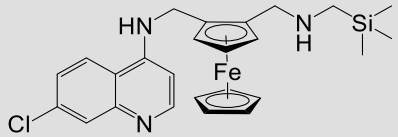 **4.1**	7.274	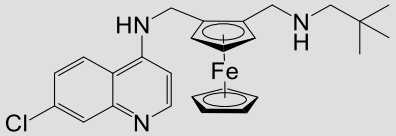 **4.2**	6.709
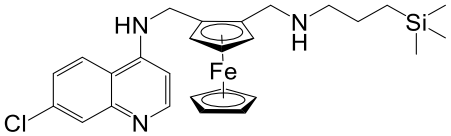 **4.3**	7.730	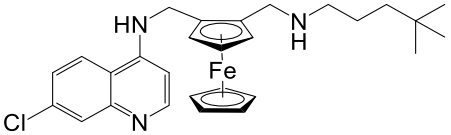 **4.4**	7.767
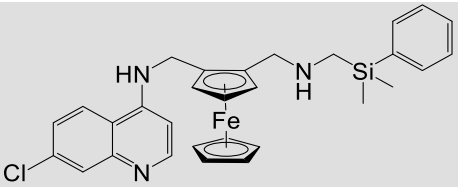 **4.5**	8.753	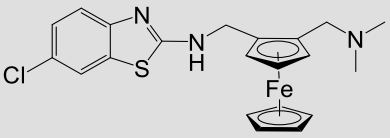 **4.7**	5.359
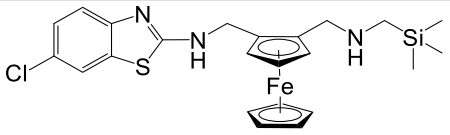 **4.9**	7.314	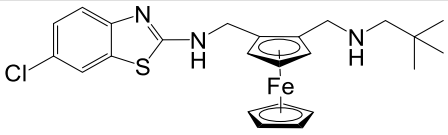 **4.10**	6.749
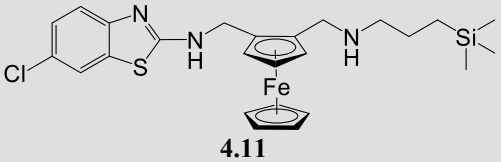 **4.11**	7.770		

The log*P* values of the remaining aminoquinolines and aminobenzothiazoles were calculated as illustrated above and the data listed in Table 5.2. The log*P* value for ferroquine (= 5.1[12]) and

the estimated value of the benzothiazole derivative (= 5.373) are relatively similar. Furthermore, with the incorporation of the amine side–chains, a significant increase of between 1.3 and 2.5 log*P* units was calculated. As expected, the estimated log*P* values also confirm that extending the side–chain from 1–carbon to 3–carbons increases the log*P* value (Table 5.2). A further increase in the log*P* value is generally observed for the silicon–containing compounds.

As further confirmation for this method, the log*P* values were calculated using only the fragmental approach. However, the fragmental approach could only be utilised for the carbon analogues due to a lack of fragmental data for silicon.

For compound **4.2**:

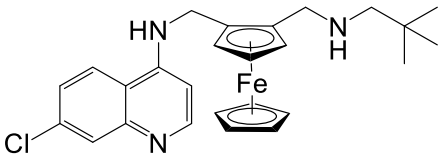

Fragments[13] to consider:

Cl + Quinolinyl-H + Fc-2H + NH_{ar} +NH_{aliph} + $3CH_2$ + $3CH_3$ + C

Log*P* = 0.933 + 1.617 + 2.252 + (−0.938) + (−1.814) + 3(0.519) + 3(0.724) + 0.110 = **5.889**

However, as mentioned in Chapter 3, the fragmental method employs correction factors (C_M = 0.219) when features such as hydrogen bonding are present.[13] It is also known from the crystal structures of compounds **4.1**–**4.3** (Chapter 4; Section 4.2.1) that the compounds experience intramolecular hydrogen bonding. As determined by Rekker *et al*.[13], one hydrogen bond is equivalent to three C_M.

Therefore, **log*P*** of compound **4.2** = 5.889 + $3C_M$

= **6.546**

Table 5.3 Comparison of estimated log*P* data.

Compound	Estimated LogP_1 (ChemBioDraw–fragment method)	Estimated LogP_2 (Fragmental method)	ΔLogP^a
4.2	6.709	6.546	0.163
4.4	7.767	7.584	0.183
4.7	5.359	5.356	0.003
4.10	6.749	6.532	0.217

[a]ΔLog*P* = estimated LogP_1 – estimated LogP_2

The log*P* values of compounds **4.4**, **4.7** and **4.10** were calculated using the above method and the values listed in Table 5.3. When comparing the estimated log*P* value calculated using the ChemBioDraw–fragmental method to that calculated using only the fragmental approach, the values are within a small error range. This confirms that the ChemBioDraw–fragmental method is suitable for estimating the log*P* values of these types of compounds.

5.2.2 Stability of compounds 4.3 and 4.11

As mentioned in Chapter 3, the stability of compounds in solution is important when evaluating the pharmacological activity. Therefore, as a model system for the stability of the aminoquinoline compounds, compound **4.3** was investigated and monitored by ^{1}H NMR spectroscopy over a 72 hr period at 37 °C. The ^{1}H NMR spectra for compound **4.3** were recorded in DMSO−d_6:D_2O (9:1, v/v; Figure 5.4a).

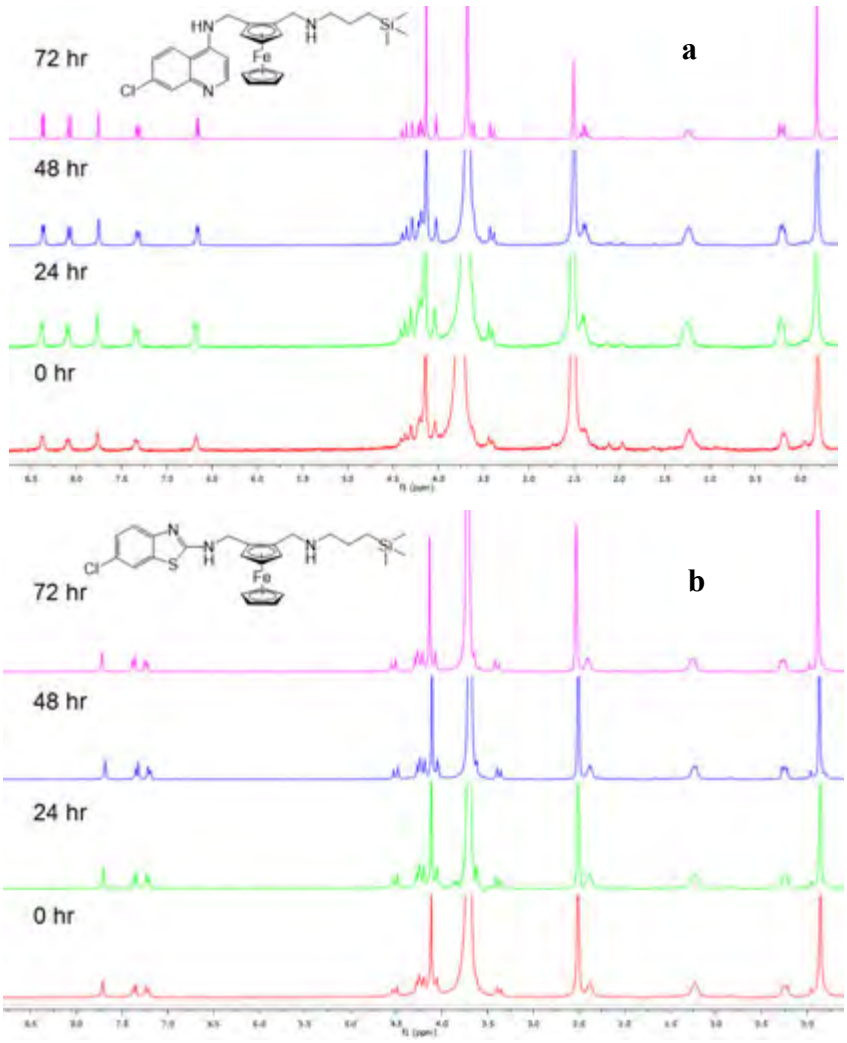

Figure 5.4 ^{1}H NMR spectra of compounds **4.3** (**a**) and compound **4.11** (**b**) in DMSO−d_6:D_2O (9:1, v/v) heated at 37 ˚C over 72 hr.

Similarly, the aminobenzothiazole compound **4.11** was also monitored in DMSO−d_6:D_2O (9:1, v/v; Figure 5.4b) under the conditions described above. As seen in Figure 5.4, the spectra remain unchanged over the study period, attesting to the stability of these compounds.

5.2.3 In Vitro Antiplasmodial and Cytotoxicity Studies

The ferrocenyl–containing aminoquinolines (**4.1**−**4.4**) and aminobenzothiazoles (**4.7**; **4.9**−**4.11**) were initially screened against the NF54 chloroquine–sensitive strain of *P. falciparum*. In addition to the ferrocenyl–containing heterocycles, 2-amino-6-chlorobenzothiazole (2-NH_2-6-ClBenz) and ferrocenylamines (**4.12**; **4.13**) were also evaluated to determine their contribution to any observed pharmacological activity. Chloroquine diphosphate (CQDP) and artesunate were used as the control drugs in this study. The IC_{50} values are illustrated in Figure 5.5 and Table 5.4.

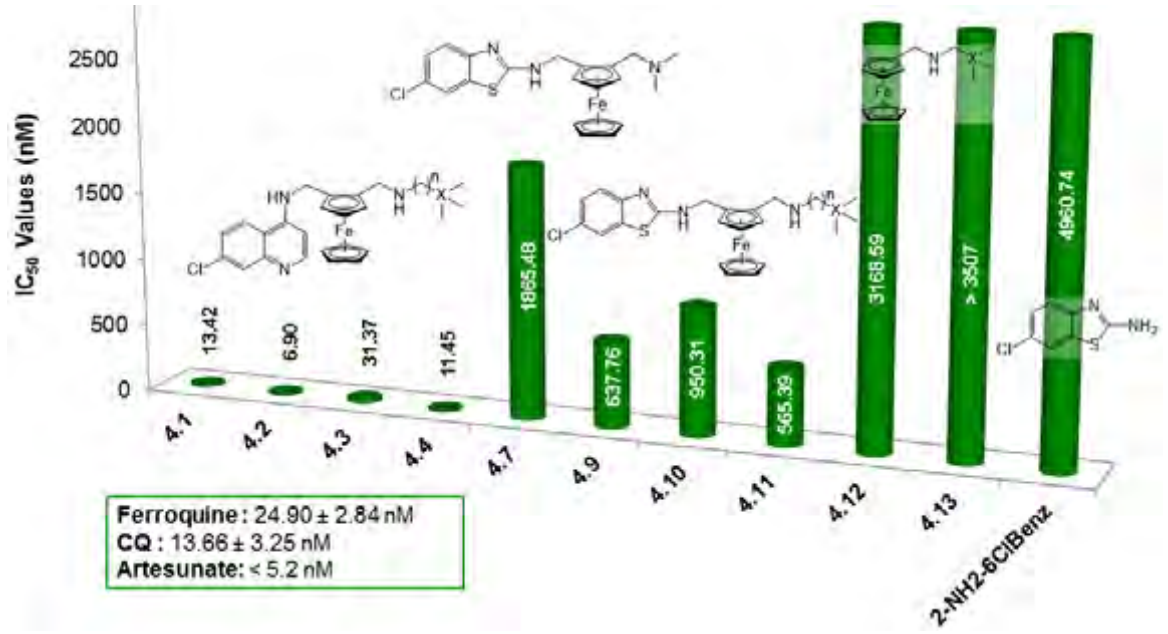

Figure 5.5 Antiplasmodial evaluation against the *P. falciparum* strain NF54.

As seen in Figure 5.5, the ferrocenyl–containing aminoquinolines (**4.1**−**4.4**) displayed pharmacological activities in the low nanomolar range (6.90–31.37 nM). The non–silicon derivatives (**4.2** & **4.4**) are slightly more potent than the silicon–containing analogues; however, when comparing compounds in the nanomolar range this difference is not significant. Therefore, against the chloroquine–sensitive strain the ferrocenyl–containing aminoquinolines display similar activities.

When comparing the IC_{50} data for ferroquine (IC_{50} = 24.90 nM) with its benzothiazole analogue **4.7** (IC_{50} = 1865.48 nM), the benzothiazole analogue is significantly less active than the quinoline analogue. Amongst the ferrocenyl–containing aminobenzothiazoles, an enhancement of activity is observed for the amine–terminated compounds (**4.9**−**4.11**) in comparison to compound **4.7**. Furthermore, the ferrocenyl−containing aminobenzothiazoles **4.9**−**4.11** displayed activity with IC_{50} values between 565.39 and 950.21 nM, where a slight enhancement of activity is observed for the silicon–containing analogues (Figure 5.5).

Table 5.4 Antiplasmodial and cytotoxicity data of selected compounds (**4.1**–**4.4**, **4.7** & **4.9**–**4.13**)

Compound		IC_{50} (nM) NF54	IC_{50} (nM) Dd2	IC_{50} (µM) CHO
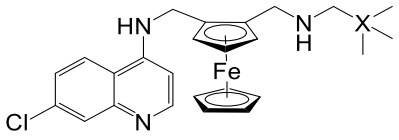	**4.1** (X=Si)	13.32 ± 2.46	13.40 ± 0.69	3.87 ± 1.43
	4.2 (X=C)	6.90 ± 0.86	13.87 ± 2.82	15.36 ± 0.90
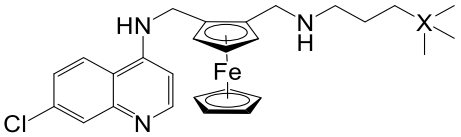	**4.3** (X=Si)	31.37 ± 10.45	27.13 ± 3.58	9.64 ± 1.25
	4.4 (X=C)	11.45 ± 0.79	35.57 ± 6.16	3.62 ± 0.32
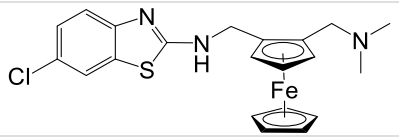	**4.7**	1865.48 ± 11.84	ND	16.90 ± 1.28
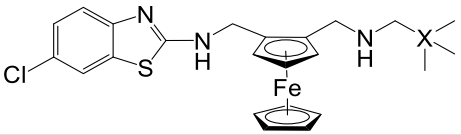	**4.9** (X=Si)	637.76 ± 195.15	718.24 ± 91.14	7.14 ± 0.44
	4.10 (X=C)	950.31 ± 72.37	163.80 ± 33.26	6.63 ± 1.91
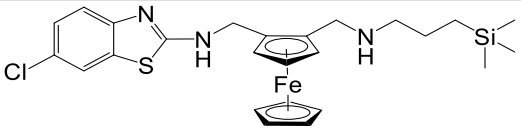	**4.11**	565.39 ± 9.98	415.17 ± 48.56	3.90 ± 0.78
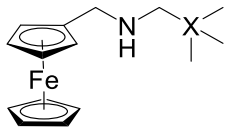	**4.12** (X=Si)	3168.59 ± 76.39	59.45 ± 10.30	276.01 ± 53.14
	4.13 (X=C)	> 3507	ND	212.90 ± 30.51
2-Amino-6-chlorobenzothiazole		4960.74 ± 790.69	ND	> 541.56
Ferroquine		24.90 ± 2.84	17.34 ± 5.90	24.44 ± 0.65
Chloroquine		13.66 ± 3.25	301.37 ± 9.07	ND
Artesunate		< 5.2	16.91 ± 2.86	ND
Emetine		ND	ND	0.23 ± 0.01

ND = not determined

Furthermore, when examining the data for 2-amino-6-chlorobenzothiazole and the ferrocenylamines (**4.12**; **4.13**), it is evident that on their own these components are not as effective against the sensitive parasitic strain. 2-Amino-6-chlorobenzothiazole (IC_{50} = 4960.74 nM) and the silicon–containing ferrocenylamine **4.12** (IC_{50} = 3168.59 nM) were significantly less potent than the ferrocenyl−containing aminoquinolines and aminobenzothiazoles, whereas the ferrocenylamine **4.13** was not effective at the highest tested concentration (> 1000 ng/mL).

Overall, when comparing the activity of the aminoquinolines (**4.1**−**4.4**) with their corresponding aminobenzothiazoles (**4.9**−**4.11**), the quinoline−based compounds displayed superior activity against the *P. falciparum* strain NF54. The aminoquinolines display similar activity to that of chloroquine and ferroquine.

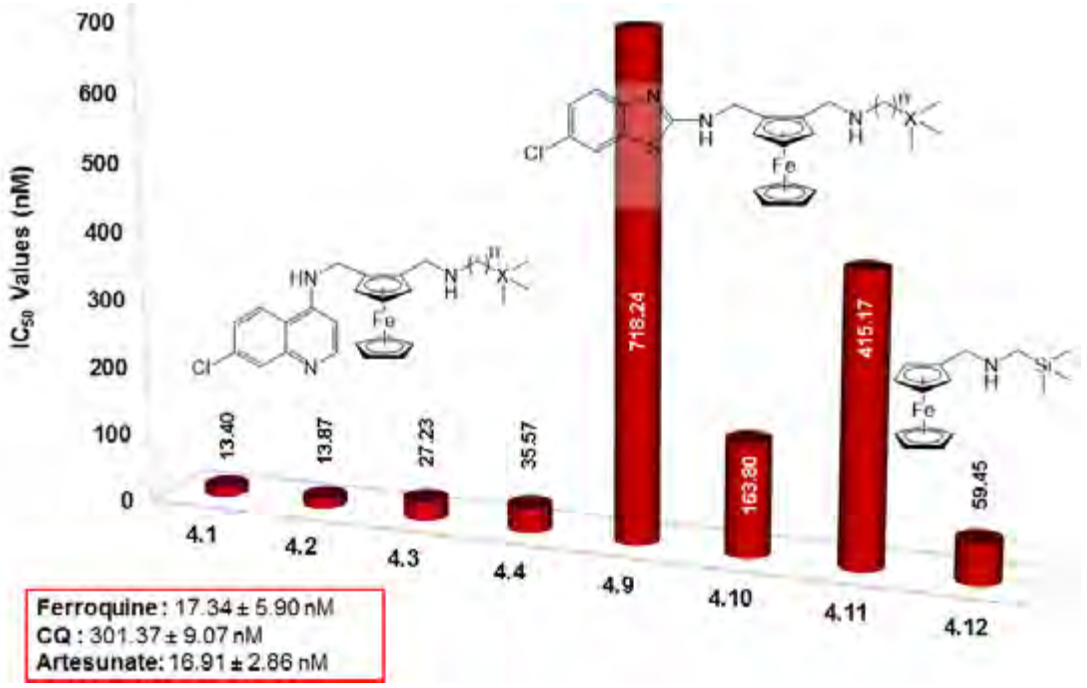

Figure 5.6 Antiplasmodial evaluation against Dd2 strain of *P. falciparum*.

Ideally, a lead compound would be more promising if it was also effective against the strain resistant to the known treatments. Therefore, the compounds were also evaluated against the chloroquine–resistant Dd2 strain of *P. falciparum* (Table 5.4 and Figure 5.7). The ferrocenyl–containing aminoquinolines (**4.1**–**4.4**) displayed similar IC_{50} values (13–36 nM) against the Dd2 strain, which was also comparable to that observed against the NF54 strain. The activity was also comparable to ferroquine. Furthermore, when compared to chloroquine

(IC_{50} = 179.10 nM), the ferrocenyl−containing aminoquinolines were more potent against the Dd2 strain.

The activity of the aminobenzothiazoles (**4.9–4.11**) varied with IC_{50} values of 718.24, 163.80 and 415.17 nM, respectively. When compared to the activity observed against the NF54 strain, the silicon–analogues displayed similar activity against both strains, whereas the carbon–analogue (**4.10**) was significantly more effective against the resistant strain. The carbon–analogue was also more effective against the resistant strain than chloroquine. Once again, the aminobenzothiazoles were not as effective as the aminoquinolines.

The ferrocenylamines (**4.12**, **4.13**) which displayed poor effects against the CQ–sensitive strain, exhibited significantly improved activity for compound **4.12** (IC_{50} value = 59.45 nM) against the CQ–resistant strain.

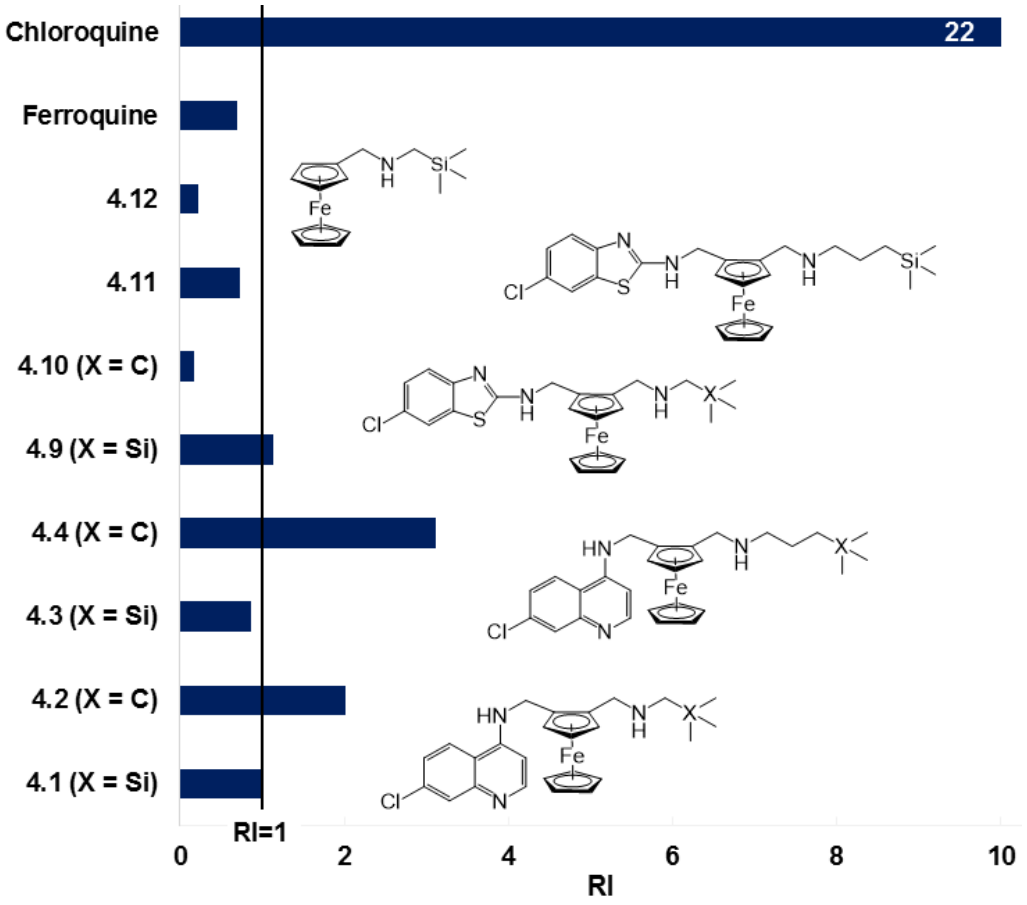

Figure 5.7 Resistance indices for tested compounds (**4.1–4.4**, **4.9–4.11**, **4.12**).

Furthermore, resistance indices [RI = $\frac{\text{IC50 (Dd2)}}{\text{IC50 (NF54)}}$] were calculated for the compounds (**4.1**−**4.4**, **4.9**–**4.12**) evaluated against the resistant strain (Figure 5.7). The black line in Figure 5.7 corresponds to a RI value of 1. The silicon–containing aminoquinolines (**4.1**, **4.3**), the ferrocenyl–containing aminobenzothiazoles (**4.9**–**4.11**), the silicon-containing ferrocenylamine (**4.12**) and ferroquine have RI values around or below 1. Furthermore, the aminobenzothiazoles had RI values significantly smaller than the aminoquinolines.

The synthesised compounds (**4.1**−**4.4**, **4.7**, **4.9**–**4.13**, **FQ**) were also screened for their cytotoxicity against the Chinese Hamster Ovarian (CHO) cell–line (Table 5.4). This data was used to calculate selectivity indices [SI = $\frac{\text{IC50 (CHO)}}{\text{IC50 (NF54) or (Dd2)}}$] which are represented in Figure 5.8.

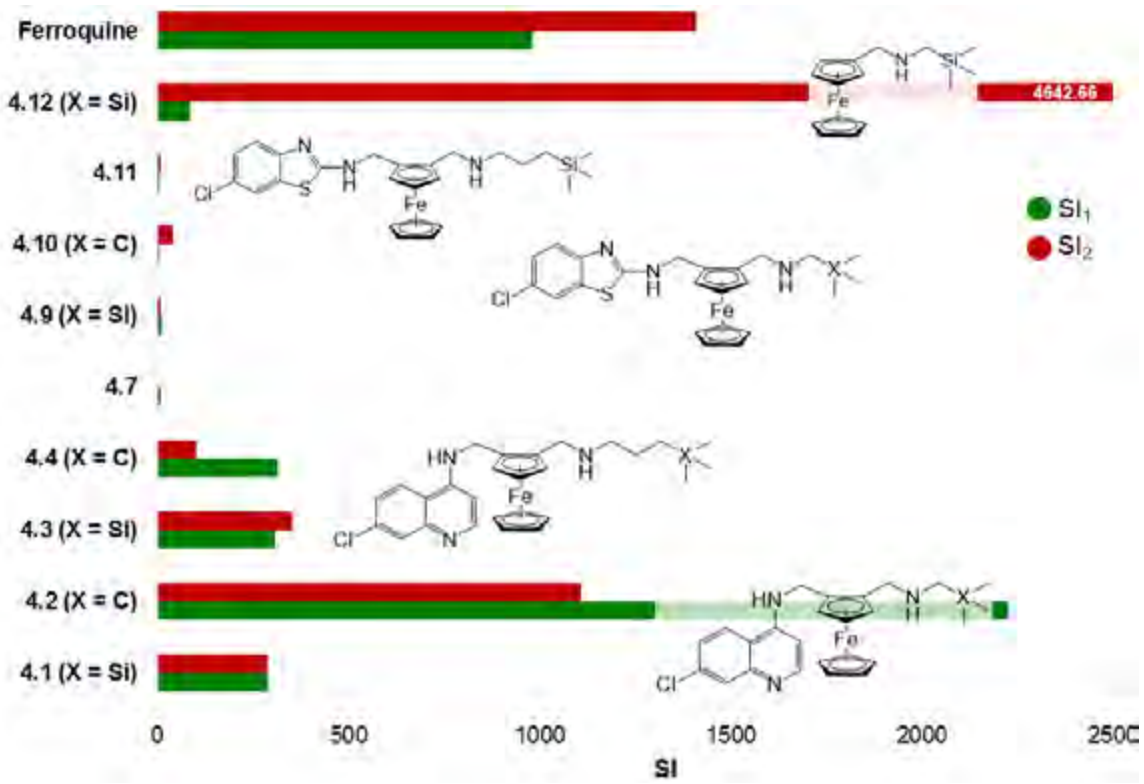

Figure 5.8 Selectivity indices calculated for the tested compounds (**4.1**−**4.4**, **4.7**, **4.9**–**4.12**, **FQ**). $SI_1 = IC_{50}(CHO)/ IC_{50}$ (NF54). $SI_2 = IC_{50}(CHO)/ IC_{50}$ (Dd2)

As seen in Figure 5.8, the aminoquinolines (SI = 288–2227) displayed greater selectivity towards parasitic strains than the corresponding aminobenzothiazole analogues (SI = 6.9–41). Amongst the two series of compounds, the carbon–analogues with the methylene spacer had

the largest SI values. On the other hand, the ferrocenylamine **4.12** displayed the greatest selectivity towards the CQ–resistant parasites.

As determined in Section 5.2.1, the log*P* values estimated for the quinoline– and benzothiazole–based compounds were fairly similar. Therefore, for the benzothiazole–based compounds the pharmacological activity is unlikely to be related to lipophilicity and possible accumulation at the target site.

Overall, the evaluated compounds displayed promising results and are good candidates for further testing.

5.2.4 β–Haematin Inhibition Studies

The NP−40 detergent mediated assay was used to establish if selected ferrocenyl–containing aminoquinolines and aminobenzothiazoles prepared in this study inhibit β–haematin (synthetic haemozoin) formation. It has been widely established that quinoline−based compounds inhibit the formation of β−haematin (and haemozoin). Ferrocenyl–containing aminoquinolines **4.3** and **4.4** were selected to determine if incorporation of silicon improves the effect on the observed β–haematin inhibitory activity. A preliminary study was done on the ferrocenyl–containing aminobenzothiazole **4.7** to determine if an analogous benzothiazole–based compound would inhibit β–haematin formation. Chloroquine was the control compound. The IC_{50} values for 4.3 and 4.4 are listed in Table 5.5 and Figure 5.9 illustrates the concentration dose–response curve for **4.7**.

Table 5.5 Tabulation of β–haematin inhibition activity of **4.3**, **4.4** and **CQ**

Compound		IC_{50} (μM) [95% confidence interval]
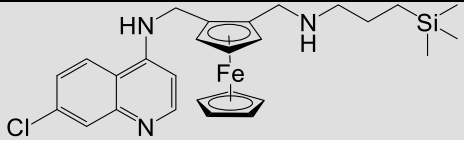	**4.3**	9.03 [8.125−10.03]
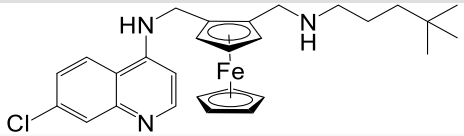	**4.4**	10.02 [9.143−10.98]
CQ		73.76 [71.32−76.28]

Compounds **4.3** and **4.4** are analogous ferrocenyl–containing aminoquinolines, and the effect of silicon on the inhibition of β–haematin formation was investigated. Both aminoquinolines **4.3** and **4.4** inhibited the formation of β–haematin with IC_{50} values of 9.03 and 10.02 μM, respectively. These IC_{50} values are significantly lower than that observed for chloroquine (73.76 μM), suggesting that these ferrocenyl−containing compounds are more effective inhibitors of β–haematin formation. Incorporation of silicon only has a moderate effect on the inhibition of β–haematin.

Compound **4.1** has previously been evaluated for its β–haematin inhibition activity, displaying inhibitory effects with an IC_{50} value of 16.2 μM.[14]. As seen for other ferrocenyl–containing aminoquinolines, the compounds probably binds to haematin *via* π–π stacking.[15] However, from the crystal structure of compound **4.3** (Figure 4.5), it can be seen that the propyl side–chain dangles either above or below the quinoline ring. Therefore, perhaps incorporation of the longer propyl side-chain further prevents the formation of β–haematin.

On the other hand, the aminobenzothiazole **4.7**, which is analogous to ferroquine had no effect on the inhibition of β–haematin formation (Figure 5.9). Therefore, the aminobenzothiazole–based compounds may exert their pharmacological effects *via* a different mechanism.

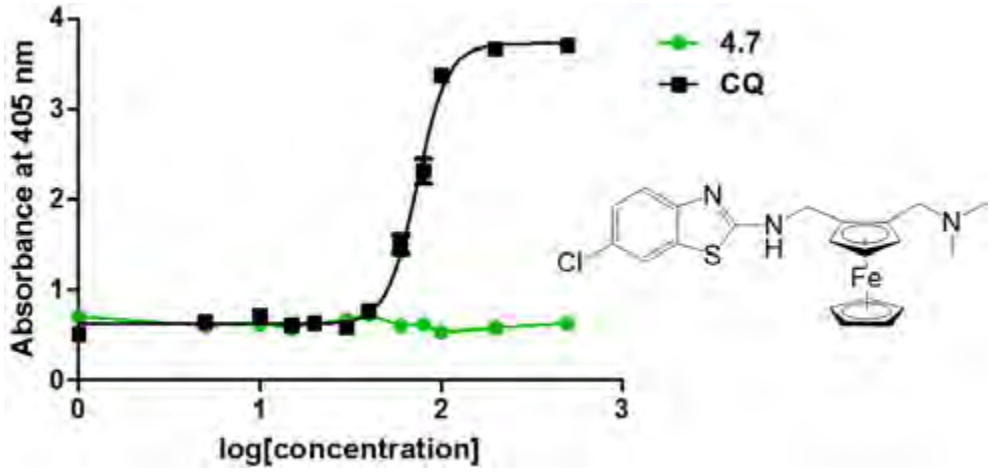

Figure 5.9 Concentration dose−response curves for NP−40 detergent mediated β–haematin assays of ferrocenyl–containing aminobenzothiazole **4.7** and chloroquine.

5.2.5 In Vitro Microsomal Metabolic Stability Studies

Due to the *in vitro* antiplasmodial activity observed, the microsomal stability of compounds **4.1**–**4.3** and ferroquine were assessed in human and mouse liver microsomes using the single point assay.[16] As seen in Figure 5.10, after 30 min incubation time at 0.40 mg protein/mL microsomes, compounds **4.1**–**4.3** were rapidly metabolised.

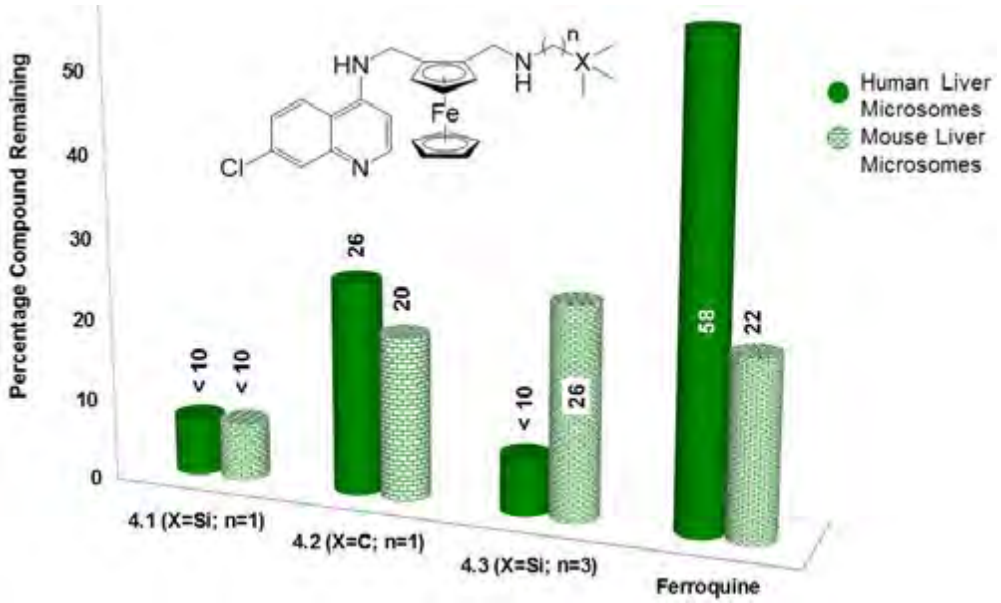

Figure 5.10 Percentage of compound (**4.1**–**4.3**, **FQ**) remaining after incubation with liver microsomes.

The compounds were unstable when incubated with both human and mouse liver microsomes. For the organosilane–containing compounds (**4.1**; **4.3**), less than 10 % of the parent compound remained after incubation in human liver microsomes. The same result was observed for compound **4.1** in mouse liver microsomes, with compound **4.3** metabolising more slowly. In general, the carbon–analogue metabolised more slowly than the silicon–containing analogues. Furthermore, compounds **4.2** and **4.3** are as unstable as ferroquine when incubated with mouse liver microsomes (Figure 5.10). When comparing ferroquine with compound **4.2**, ferroquine is significantly more stable when incubated with human liver microsomes and the incorporation of the amine side–chain (**4.2**) did not improve stability.

5.2.6 In Vitro Antitrichomonal Studies

In vitro antitrichomonal screening was carried out for the synthesised ferrocenyl–containing aminoquinoline and aminobenzothiazole compounds to determine general growth inhibition against the metronidazole–sensitive G3 strain of *Trichomonas vaginalis*. DMSO was employed as a control for the screening, and the antitrichomonal activity data is listed in Table 5.6.

Compounds **4.1**−**4.3** were tested at 50 µM concentration, while the remaining compounds were tested at 100 µM concentration. As seen in Table 5.6, the ferrocenyl–containing aminoquinolines and aminobenzothiazoles generally display good activity with parasite growth inhibition above 90 %. When analysing the data for aminoquinolines **4.1**−**4.3** (tested at 50 µM), the carbon analogue **4.2** was a more effective inhibitor (91.42 %) when compared to its silicon analogue **4.1** (24.33 %). However, when evaluating the corresponding aminobenzothiazoles **4.9** and **4.10**, similar inhibitory effects (99 %) were observed.

The ferrocenylamines **4.12** and **4.13**, along with 2-amino-6-chlorobenzothiazole, were screened to determine if the ferrocenyl, amine–side chain or benzothiazole moiety would be effective as is. The tested compounds were poor inhibitors of parasite growth, displaying effects below 40 %. Therefore, once again the different physicochemical properties of the ferrocenyl–containing aminoquinolines and aminobenzothiazoles, over their individual components, led to improved activities.

Table 5.6 Percentage growth inhibition of the G3 strain of *T. vaginalis*.

Compound		% Growth Inhibition ± SE
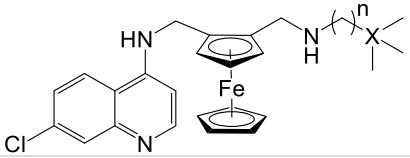	**4.1** (X=Si; n=1)	24.55 ± 2.14[a]
	4.2 (X=C; n=1)	91.42 ± 1.35[a]
	4.3 (X=Si; n=3)	77.08 ± 6.85[a]
	4.4 (X=C; n=3)	100[b]
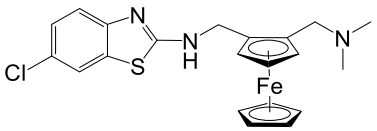	**4.7**	94.5 ± 7.91[b]
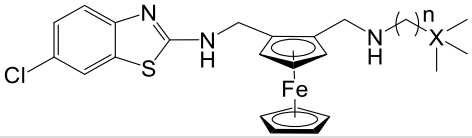	**4.9** (X=Si; n=1)	99.4 ± 1.09[b]
	4.10 (X=C; n=1)	99.3 ± 1.28[b]
	4.11 (X=Si; n=3)	90.5 ± 8.53[b]
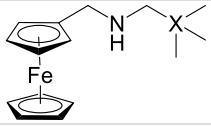	**4.12** (X=Si)	29.8 ± 20.4[b]
	4.13 (X=C)	27.9 ± 11.2[b]
2-Amino-6-chlorobenzothiazole		34.4 ± 13.7[b]
FQ		54.20 ± 1.45[a]

[a]Tested at 50 µM; [b]Tested at 100 µM.

The IC_{50} values were determined for compounds displaying percentage inhibitions above 90 % (Table 5.7). As seen in Table 5.7, the compounds displayed moderate activity in the

micromolar range, with the carbon analogue **4.4** being the most effect parasite growth inhibitor with an IC_{50} value of 8.30 μM. No definite trend could be observed when comparing compounds with methylene and propyl spacers. These compounds were not as effective as the FDA approved drug metronidazole (IC_{50} = 0.72 μM).

Table 5.7 Antitrichomonal data for the compounds (**4.2**; **4.4**; **4.7**; **4.9**; **4.11**)

Compound	IC_{50} (μM) G3 Strain
4.2 (X=C; n=1)	20.27
4.4 (X=C; n=3)	8.30
4.7	25.16
4.9 (X=Si; n=1)	38.07
4.11 (X=Si; n=3)	38.09
Metronidazole	0.72

5.2.7 In Vitro Antitumour Studies

Ferrocenyl–containing aminoquinoline and aminobenzothiazoles, along with 2-amino-6-chlorobenzothiazole and ferrocenylamines, were screened for their cytotoxicity against the WHCO1 oesophageal cancer cell–line. Ferrocenyl–containing aminoquinolines (**4.1**, **4.3**, **4.4**), ferrocenyl–containing aminobenzothiazoles (**4.9**, **4.10**) and the ferrocenylamine **4.12** were excluded from the assay due to poor solubility at the highest stock concentration. The results for the tested compounds are illustrated in Figure 5.11.

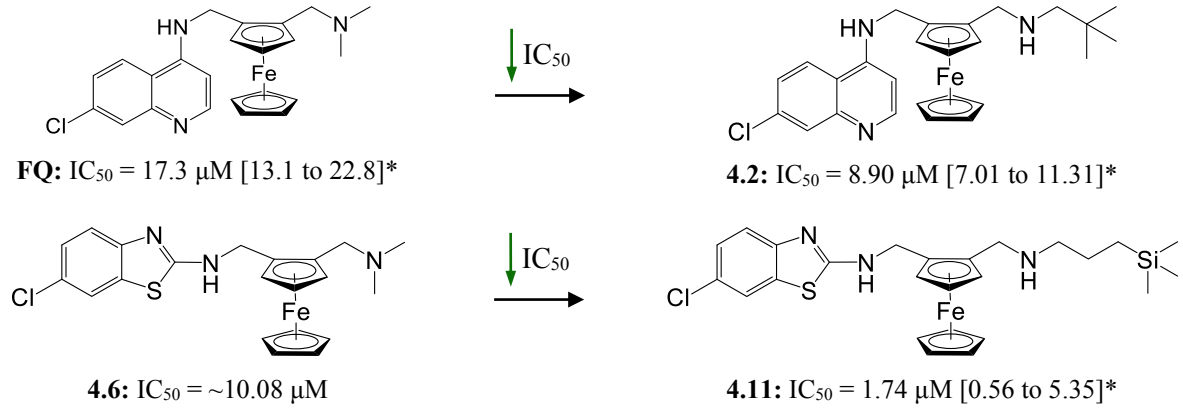

FQ: IC_{50} = 17.3 μM [13.1 to 22.8]*

4.2: IC_{50} = 8.90 μM [7.01 to 11.31]*

4.6: IC_{50} = ~10.08 μM

4.11: IC_{50} = 1.74 μM [0.56 to 5.35]*

Figure 5.11 Cytotoxicity of ferrocenyl–containing aminoquinolines (**FQ**; **4.2**) and aminobenzothiazole (**4.7**; **4.11**). *95 % Confidence Interval.

2-Amino-6-chlorobenzothiazole and the silicon–containing ferrocenylamine **4.12**, which were tested in order to identify active components, were not cytotoxic at the highest tested concentration. However, when evaluating the combination of the heterocyclic ring and

ferrocenyl moiety in the form of ferroquine and the analogous benzothiazole–based **4.7**, the compounds displayed significant cytotoxicity with IC_{50} values of 17.3 and 10.2 μM, respectively. A slight improvement was observed for the benzothiazole–based compound (**4.7**) when compared to the quinoline–based compound (**FQ**). Additionally, with the incorporation of an amine side–chain a further enhancement in activity was observed. Of the tested compounds, the silicon–containing benzothiazole–based compound **4.11** was the most potent with an IC_{50} value of 1.74 μM.

The screening of a larger group of ferrocenyl−containing aminoquinoline and aminobenzothiazoles would have to be conducted to definitively conclude if silicon–containing benzothiazole–based compounds are the most effective against the WHCO1 oesophageal cancer cell–line.

5.3 Summary

Ferrocenyl–containing aminoquinolines and aminobenzothiazoles were screened for the antiparasitic effects against *Plasmodium falciparum* and *Trichomonas vaginalis*. When tested against the NF54 CQS strain of *P. falciparum*, the aminoquinolines (**4.1**–**4.4**) were the most effective with activities in the low nanomolar range, whereas the corresponding aminobenzothiazoles (**4.7**; **4.9**–**4.11**) displayed activities in the low micromolar range. Furthermore, when evaluated against the Dd2 CQR strain, the aminoquinolines were once again more effective than the aminobenzothiazoles. However, the aminobenzothiazoles were generally more effective against the CQ–resistant strain than the CQ–sensitive strain, as is evidenced by the calculated RI values. Additionally, the aminoquinolines and aminobenzothiazole displayed selective antiparasitic activity.

The ferrocenyl–containing aminoquinolines (**4.3**; **4.4**) were effective inhibitors of β–haematin, displaying improved inhibitory effects when compared to chloroquine. On the other hand, the benzothiazole–based compound (**4.7**) was not at all effective at inhibiting the formation of β–haematin. Microsomal metabolic stability studies revealed that the ferrocenyl–containing aminoquinolines are metabolised more quickly than ferroquine. For this reason they are not expected to perform well *in vivo*. Future optimisation studies would benefit from metabolite identification studies as some of the metabolites may be pharmacologically active, and thus may contribute to *in vivo* activity.

When tested for antitrichomonal activity, the compounds were generally effective at inhibiting parasite growth with percentage inhibitions above 90 % and moderate IC_{50} values. Compounds with propyl spacers generally displayed better inhibitory effects than the corresponding compounds with a methylene spacer.

The cytotoxicity of the compounds was evaluated against the WHCO1 oesophageal cancer cell–line. Incorporation of the amine side–chain led to an improvement in cytotoxicity. Furthermore, the aminobenzothiazole compounds was found to be more cytotoxic than the aminoquinoline compounds.

5.4 References

1 P. Rawat, S. Goyal, N. Dhaliwal and S. Kumar, *Int. J. Pharm. Biomed. Sci.*, 2013, **4**, 1055–1059.

2 L. J. K. Boerner and J. M. Zaleski, *Curr. Opin. Chem. Biol.*, 2005, **9**, 135–144.

3 R. D. Sandlin, M. D. Carter, P. J. Lee, J. M. Auschwitz, S. E. Leed, J. D. Johnson and D. W. Wright, *Antimicrob. Agents Chemother.*, 2011, **55**, 3363–3369.

4 K. K. Ncokazi and T. J. Egan, *Anal. Biochem.*, 2005, **338**, 306–319.

5 C. Biot, D. Taramelli, I. Forfar-Bares, L. A. Maciejewski, M. Boyce, G. Nowogrocki, J. S. Brocard, N. Basilico, P. Olliaro and T. J. Egan, *Mol. Pharm.*, 2005, **2**, 185–193.

6 U. M. Zanger and M. Schwab, *Pharmacol. Ther.*, 2013, **138**, 103–141.

7 R. J. Flanagan, A. Taylor, I. D. Watson and R. Whelpton, *Fundamentals of Analytical Toxicology*, John Wiley & Sons, Ltd, West Sussex, 2007.

8 C. M. Masimirembwa, U. Bredberg and T. B. Andersson, *Clin. Pharmacokinet.*, 2003, **42**, 515–528.

9 J. Lee and X. Liu, *Curr. Drug Metab.*, 2007, **8**, 822–829.

10 J. Lin and A. Lu, *Pharmacol. Rev.*, 1997, **49**, 403–449.

11 C. Chen, F. J. Gonzalez and J. R. Idle, *Drug Metab. Rev.*, 2007, **39**, 581–597.

12 C. Biot, N. Chavain, F. Dubar, B. Pradines, X. Trivelli, J. Brocard, I. Forfar and D. Dive, *J. Organomet. Chem.*, 2009, **694**, 845–854.

13 R. Mannhold and R. Rekker, *Perspect. Drug Discov. Des.*, 2000, **18**, 1–18.

14 Y. Li, C. de Kock, P. J. Smith, K. Chibale and G. S. Smith, *Organometallics*, 2014, **33**, 4345–4348.

15 F. Dubar, J. Khalife, J. Brocard, D. Dive and C. Biot, *Molecules*, 2008, **13**, 2900–2907.

16 L. Di, E. H. Kerns, N. Gao, S. Q. Li, Y. Huang, J. L. Bourassa and D. M. Huryn, *J. Pharm. Sci.*, 2004, **93**, 1537–1544.

CHAPTER 6
Conclusions and Future Outlook

6.1 Summary and Conclusions

6.1.1 Synthesis

The first series of compounds prepared were ferrocenyl– and aryl–derived organosilane–based thiosemicarbazones, along with their ruthenium, rhodium and palladium complexes. Five new thiosemicarbazones (**2.3**–**2.5**) were prepared *via* a nucleophilic substitution reaction of a methanethiol group (dithiocarbamate) with the selected amine. These thiosemicarbazones were further reacted with $[Ru(\eta^6\text{-}p\text{-}^{i}PrC_6H_4Me)Cl_2]_2$ to synthesise two heterobimetallic complexes (**2.6a**–**b**) and three mononuclear complexes (**2.7a**–**b**; **2.8**). The thiosemicarbazones were also reacted with $[Rh(Cp^*)Cl_2]_2$ to prepare two heterobimetallic complexes (**2.9a**–**b**) and three mononuclear complexes (**2.10a**–**b**; **2.11**). The cationic complexes prepared above involved bidentate *N,S*–chelation of the thiosemicarbazone to the ruthenium or rhodium metal centre *via* dative bonds. Additionally, thiosemicarbazones (with a methyl group on the imine carbon) were selected as suitable for the preparation of neutral *ortho*–cyclopalladated complexes (**2.12**–**2.14**). The thiosemicarbazone was reacted with the palladium precursor *cis*–$[Pd(PTA)_2Cl_2]$, in the presence of trimethylamine as the base facilitating the abstraction of the proton on the ferrocenyl or aryl ring, to bring about C–H activation. These compounds were fully characterised using NMR (^1H, $^{13}C\{^1H\}$, $^{31}P\{^1H\}$, COSY, HSQC) spectroscopy, infrared spectroscopy and mass spectrometry [electron impact, electrospray ionisation].

The second series of compounds prepared were ferrocenyl–containing aminoquinolines (**4.1**–**4.5**). These compounds were ferroquine derivatives, whereby the terminal dimethylamine group was replaced with amine side–chains consisting of both organosilane and carbon analogues. This displacement was carried out *via* the quaternisation of the terminal dimethylamine group, followed by the substitution of the trimethylammonium $[-N(CH_3)_3^+]$ group with the amine. The third series of compounds prepared were ferrocenyl–containing aminobenzothiazoles (**4.9**–**4.11**), which were benzothiazole–based analogues of the second series. The benzothiazole–based analogue of ferroquine (**4.7**) was prepared by reacting 6-chloro-2-iodobenzothiazole with 2-[(*N*,*N*-dimethylamino)methyl]-ferrocenylmethylamine in a substitution reaction. The terminal dimethylamine group of compound **4.7** was quaternised

(compound **4.8**) using iodomethane, and the resulting trimethylammonium [–$N(CH_3)_3^+$] group substituted with the appropriate amine side–chains to prepare the desired compounds. The compounds were fully characterised using NMR (^1H; $^{13}C\{^1H\}$; COSY; HSQC) spectroscopy, infrared spectroscopy and mass spectrometry (Electron Impact; Electrospray Ionisation). The preparation of the ferrocenyl–containing aminoquinolines (**4.2**; **4.3**) was further confirmed by the molecular structures of the two compounds which were determined using single–crystal X–ray diffraction. As seen with ferroquine[1] and the previously reported compound **4.1**[2], both compounds **4.2** and **4.3** also crystallised in a folded conformation due to intramolecular hydrogen bonding between the nitrogen atoms on opposite sides of the ferrocenyl moiety. Therefore, these ferrocenyl–containing heterocyclic compounds can be synthesised successfully, and in good yields, *via* a halide substitution reaction, as opposed to the lower yielding reductive amination method.

6.1.2 Pharmacological Evaluation

The thiosemicarbazones, along with the ruthenium, rhodium and palladium complexes, were screened for their *in vitro* antiplasmodial activity against the chloroquine–sensitive NF54 and chloroquine–resistant Dd2 strains. The thiosemicarbazone compounds generally displayed activities in the low micromolar range. Overall, the cyclopalladated thiosemicarbazone complexes were the most effective against both strains. In general, the organosilane derivatives also showed selectivity towards the parasites. The cyclopalladated complexes (**2.12**–**2.14**) were not tested for their ability to inhibit the formation of β–haematin as previous studies of similarly structured square–planar cyclopalladated[3] and cycloplatinated[4] complexes did not inhibit β–haematin formation. Therefore, the rhodium complexes which also displayed promising activities were evaluated for their ability to inhibit the formation of β–haematin. The rhodium complexes displayed inhibitory effects, whereas the metal–free compound was ineffective. Therefore, due to the *in vitro* activities noted, the incorporation of thiosemicarbazone in compounds to be evaluated as antiplasmodial agents still has merit for future studies.

Cyclopalladated complex **2.13**, which displayed good *in vitro* antiplasmodial activity, was chosen for *in vivo* evaluation in a *Plasmodium berghei* mouse model. The compound was administered orally using a HPMC:DMSO vehicle at concentrations of 10, 30 and 50 mg/kg. As the compound did not display any signs of toxicity at the highest tested concentration (50

mg/kg), compound **2.13** was evaluated at a 50 mg/kg concentration in a *P. berghei* infected mouse model. The compound was found to be inactive, where no reduction in parasitaemia was observed. Attempts were also made to develop as HPLC–UV method to analyse blood samples collected during the study. However, this proved unsuccessful due to inconsistent observations. There was also an interest in determining how effective these compounds are against another parasite. Therefore, the thiosemicarbazone compounds were also screened for their antitrichomonal activity against the metronidazole–sensitive G3 strain of *Trichomonas vaginalis*. The ruthenium (**2.6**–**2.8**) and rhodium (**2.9**–**2.11**) complexes displayed growth inhibitions above 90 %, whereas the dithiocarbamates (**2.1**; **2.2**), thiosemicarbazones (**2.3**–**2.5**) and the cyclopalladated complexes (**2.12**–**2.14**) had no significant effect. Furthermore, within the thiosemicarbazone and rhodium thiosemicarbazone series, the carbon analogues were less effective inhibitors of parasite growth than the organosilanes. The IC_{50} values were determined for complexes displaying inhibitions above 90 %. The ruthenium (**2.6b**; **2.7a**; **2.7b**) and rhodium (**2.9a**; **2.10a**) complexes displayed moderate IC_{50} values (7–35 μM), with the rhodium complexes appearing to be more effective inhibitors of G3 parasite growth compared to the ruthenium complexes. Therefore, perhaps the geometry of the ruthenium and rhodium complexes influences how the complexes exert their effects when compared to that observed for the square–planar palladium complex.

Preliminary antitumour activities of selected ferrocenyl–containing thiosemicarbazone compounds were determined against cisplatin–sensitive (A2780) and cisplatin–resistant (A2780*cis*R) human ovarian carcinoma cell–lines, as well as non–tumourigenic human fibroblast skin cells (KMST–6). The compounds displayed moderate activities (18–150 μM) and did not show any selectivity between the tumourigenic and non–tumourigenic cell–lines. Therefore, these types of ferrocenyl-derived thiosemicarbazone compounds may not be suitable for these cell–lines.

The ferrocenyl–containing aminoquinolines (**4.1**–**4.4**) and aminobenzothiazoles (**4.7**; **4.9**–**4.11**) were also screened against the NF54 and Dd2 strains of *Plasmodium falciparum*. The aminoquinolines and aminobenzothiazoles displayed activities in nanomolar and micromolar ranges, respectively. For the aminoquinolines, similar activities were observed against both strains. On the other hand, the aminobenzothiazoles were more effective against the CQ–resistant strain. Therefore, with resistance index values close to or below 1, these

ferrocenyl–containing aminoquinolines and aminobenzothiazoles may exert their effects *via* a different mechanism to that of chloroquine.

In terms of potential mechanisms of action, chloroquine is a known inhibitor of haemozoin formation. The same applies for ferroquine. The inhibition of β–haematin, synthetic form of haemozoin, is also seen for the ferrocenyl–containing aminoquinolines (**4.3**; **4.4**), but not for the aminobenzothiazole **4.7**. Therefore, it is possible that the mechanisms of action for the aminoquinolines are similar to that of chloroquine and ferroquine. Similar to ferroquine, the aminoquinolines may also be able to overcome the resistance mechanism, and thus are able to accumulate in the digestive vacuole where they exert their effects.

Metabolic stability studies conducted on the ferrocenyl–containing aminoquinolines (**4.1**–**4.3**) revealed that the compounds metabolise more rapidly than ferroquine. It has also been observed that the organosilane derivatives metabolised more rapidly than the carbon analogue. When comparing the C–C and C–Si σ–bonds, it is known that due to the larger atom size of silicon in comparison to carbon that the bond C–Si is longer and thus weaker. This was also confirmed by the crystal data for compounds **4.1**[2] and **4.3**. Additionally, due to the more electropositive nature of silicon, it is more susceptible to nucleophilic attack. This may result in a more degradable compound. Daher *et al*. analysed ferroquine and its metabolites.[5] They identified metabolism products with a free terminal amine (loss of methyl groups), a hydroxylation product, a N–oxidation product and 4-amino-7-chloroquinoline. These metabolites were found to be less effective than ferroquine when screened against two strains (3D7 and W2) of *P. falciparum*. However, it would be interesting to determine the activity of these metabolites against the NF54 and Dd2 strains. Therefore, identification of the metabolism products for compounds **4.1**–**4.3** may shed light on whether or not the C–Si bond is the first site of metabolism.

The ferrocenyl–containing aminoquinolines and aminobenzothiazoles were effective inhibitors of *T. vaginalis* parasite growth with percentage inhibitions above 90 % and moderate IC_{50} values. On the other hand, the ferrocenylamines and 2-amino-6-chlorobenzothiazole, which are essentially the components the aminoquinolines and aminobenzothiazoles consist of, were poor inhibitors of *T. vaginalis* growth. FDA approved treatments for trichomoniasis are primarily 5-nitroimidazole-based compounds which exert their pharmacological effects through the

reduction of the nitro groups and formation of nitro radical−ion intermediates which are able to interact with DNA.[6] Therefore, it would be interesting to determine by which mechanism these ferrocenyl–containing aminoquinolines and aminobenzothiazoles exert their pharmacological effects against trichomonads.

When screened for cytotoxicity against the WHCO1 oesophageal cancer cell–line, the compounds containing the amine side–chain were more cytotoxic than ferroquine and its benzothiazole analogue. Furthermore, the aminobenzothiazoles were found to be more cytotoxic than the aminoquinolines.

6.2 Future Outlook

Although the pharmacological activities observed for the thiosemicarbazone compounds, ferrocenyl–containing aminoquinolines and ferrocenyl–containing aminobenzothiazoles proved to be promising, they could be improved upon. However, understanding how these compounds exert their pharmacological activities may assist in designing new compounds with improved activities.

Mechanisms of action such as β–haematin inhibition, cysteine protease inhibition, DNA interactions, mitochondrial interactions or generation of reactive species, to name a few, may give preliminary information on how a compound may exert its pharmacological effects. However, despite many of these studies being conducted in closed systems, they may point researchers in a direction to investigate within cells and mammalian systems as there are various other factors that may either contribute to observed activity or prevent the compound from displaying any pharmacological effects. Based on the results stated in Chapter 3 (Section 3.2.3), the rhodium thiosemicarbazone complexes inhibited the formation of β–haematin. Hence, it would be interesting to computationally model the interaction between the rhodium complexes and β-haematin to determine how the rhodium complexes inhibits β-haematin formation. Based on the β–haematin inhibition assay, the aminoquinolines inhibit the formation of β–haematin, whereas the aminobenzothiazoles does not inhibit β–haematin formation. Modelling studies of quinoline compounds have shown that the quinoline ring π-stacks with the β–haematin to prevent dimerization.[1] Therefore, it would be interesting to model the benzothiazole compound to determine why a similar inhibition mechanism does not occur.

Furthermore, as mentioned in Chapter 3 (Section 3.2.6) preliminary method development work was carried out for compound **2.13** using HPLC–UV. One of the drawbacks to using protein precipitation or liquid–liquid extraction methods, is the possibility of protein binding, which may have been the case for this work. Therefore, future studies involving either inductively coupled plasma mass spectrometry (ICP−MS) analysis of the precipitated proteins or protein binding studies may prove or disprove that idea. Furthermore, developing a procedure to extract complexes by disrupting protein–complex binding without affecting the complex, as well as developing a HPLC–UV or HPLC–MS method which can be applied to coordination and organometallic complexes would be useful.

As mentioned before, developing new compounds with improved physico–chemical properties may lead to compounds with improved pharmacological activities. It would be interesting to evaluate cycloruthenated and cyclorhodated thiosemicarbazone complexes to determining if the *ortho*–cyclometalated versions display improved activity over the *N,S*–chelated complexes reported herein. It would also be interesting to determine if the cyclorhodated complexes display β–haematin formation inhibition. Preparing metabolically stable quinoline– and benzothiazole–based hybrid compounds containing other organometallic moieties with improved aqueous solubility may be an avenue to investigate.

6.3 References

1 F. Dubar, J. Khalife, J. Brocard, D. Dive and C. Biot, *Molecules*, 2008, **13**, 2900–2907.

2 Y. Li, C. de Kock, P. J. Smith, K. Chibale and G. S. Smith, *Organometallics*, 2014, **33**, 4345–4348.

3 L. Barnard, Honours Dissertation, University of Cape Town, 2014.

4 P. Chellan, K. M. Land, A. Shokar, A. Au, S. H. An, C. M. Clavel, P. J. Dyson, C. de Kock, P. J. Smith, K. Chibale and G. S. Smith, *Organometallics*, 2012, **31**, 5791–5799.

5 W. Daher, L. Pelinski, S. Klieber, F. Sadoun, V. Meunier, M. Bourrié, C. Biot, F. Guillou, G. Fabre, J. Brocard, L. Fraisse, J.-P. Maffrand, J. Khalife and D. Dive, *Drug Metab. Dispos.*, 2006, **34**, 667–682.

6 M. Müller, *Biochem. Pharmacol.*, 1986, **35**, 37–41.

CHAPTER 7

Experimental Section

7.1 General remarks

All reagents and solvents were purchased from commercial suppliers. All reagents were purchased from Aldrich and used without further purification. Palladium(II) chloride, ruthenium(III) trichloride trihydrate and rhodium(III) trichloride trihydrate were kindly donated by Anglo American Platinum Limited. Methyl hydrazinecarbodithioate[1], Schiff base dithiocarbamates [ferrocenyl[2] (**2.1a**), acetylferrocenyl[3] (**2.1b**), 3,4-dichloroacetophenone[4] (**2.2b**)], $[Ru(\eta^6\text{-}p\text{-}^iPrC_6H_4Me)Cl_2]_2$[5], $[Rh(Cp^*)Cl_2]_2$[6] and *cis*−$[Pd(PTA)_2Cl_2]$[7] were synthesised by means of published methods. 2-[(*N*,*N*-dimethylamino)methyl]ferrocene carboxaldehyde, 2-[(*N*,*N*-dimethylamino)methyl]ferrocene oxime, 2-[(*N*,*N*-dimethylamino)methyl]ferrocene-methylamine, ferroquine and quaternised ferroquine were also prepared *via* published methods.[4,8] Nuclear magnetic resonance (NMR) spectra were recorded on either a Varian Mercury 300 spectrometer (^1H at 300.08 MHz), a Bruker 400 Biospin GmbH spectrometer (^1H at 400.20 MHz, $^{13}C\{^1H\}$ at 100.60 MHz, $^{31}P\{^1H\}$ at 161.80 MHz) or a Bruker 600 FT spectrometer (^1H at 600.100 MHz, $^{13}C\{^1H\}$ at 150.60 MHz) at ambient temperature using the residual solvent peak as internal standard for ^1H NMR and ^{13}C NMR. Infrared (IR) spectra were determined using a either a Perkin–Elmer Spectrum 100 FT–IR or a Bruker FT–IR spectrometer, and were recorded either using KBr pellets or ATR. Elemental analyses (C, H and N) were recorded on a Thermo Flash 1112 Series CHNS–O Analyser. Mass spectrometry was either carried out on a JEOL GCmateII and data were recorded using Electron Impact (EI) mode or on a Waters API Quattro Micro triple quadrupole mass spectrometer (samples injected into a stream of 50% acetonitrile and 0.1% formic acid) and data recorded using Electrospray Ionisation (ESI) mass spectrometry in the positive mode. Melting points were determined on the Büchi Melting Point apparatus B–540. Purity of selected compounds was checked using an analytical Agilent HPLC 1260 equipped with an Agilent DAD 1260 UV/vis detector and a X Bridge C18 column (2.5 μM, 50 mm x 3 mm). The compounds were eluted using a mixture of solvent A (10 mM NH_4OAc/H_2O) and solvent B (10 mM NH_4OAc/MeOH) at a flow rate of 0.9 mL/min. The gradient elution conditions were as follows: 10% solvent B between 0 and 1 min, 10−95% solvent B between 1 and 3 min, 95% solvent B between 3 and 5 min.

Single–crystal X–ray diffraction data were collected on a Bruker KAPPA APEX II DUO diffractometer using graphite–monochromated Mo–Kα radiation (χ = 0.71073 Å). The

7.2 Organosilane thiosemicarbazones

7.2.1 Schiff base dithiocarbamates

3,4-Dichlorobenzaldamine Schiff base dithiocarbamates (**2.2a**)

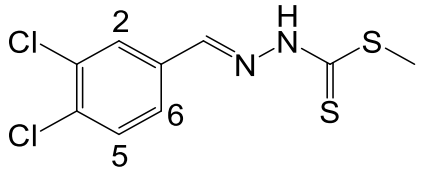

Methyl hydrazinecarbodithioate (1.01 g, 8.28 mmol) was suspended in dry isopropanol (5.00 mL), after which the 3,4-dichlorobenzaldehyde (1.45 g, 8.29 mmol) was dissolved in iso-propanol (10.0 mL) was added. The pale yellow mixture was heated at 70 ˚C for 24 hr, during which the starting material dissolved followed by the precipitation of a solid. The solid was collected by suction filtration and washed with cold isopropanol. Compound **2.2a** was isolated as an off–white powder (1.58 g, 68 %). **m.p.:** 200.9–201.4 ˚C. **^{1}H NMR (399.95 MHz, DMSO–*d*$_6$):** δ (ppm) = 13.4 (s, 1H, NH); 8.21 (s, 1H, HC=N); 7.94 (s, 1H, H–2); 7.71 (m, 2H, H–5 & H–6); 2.53 (s, 3H, SCH_3). **^{13}C{^{1}H} NMR (100.64 MHz, DMSO–*d*$_6$):** δ (ppm) = 199.0 (C=S); 143.4 (C=N); 134.2; 132.8; 131.8; 131.1; 128.7; 127.0; 16.7 (SCH_3). **FT–IR (KBr, cm^{-1}):** ν = 1586 (m, C=N); 812 (s, C=S). **EI^{+}–MS** (277.9504 g.mol^{-1})**:** *m/z* 277.94 ([M]$^{+}$, 100%). **Elemental analysis** for $C_9H_8Cl_2N_2S_2$ (277.95 g.mol^{-1}): Found C 38.77, H 2.82, N 9.46 %; Calculated C 38.72, H 2.89, N 10.03 %.

7.2.2 Functionalised thiosemicarbazones

Ferrocenyl–((trimethylsilyl)methyl) thiosemicarbazone (**2.3a**)

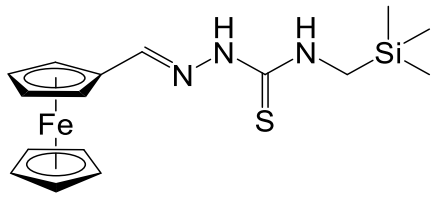

An excess of (aminomethyl)trimethylsilane (0.220 mL, 1.64 mmol) was added to the flask under N_2. Compound **2.1a** (0.500 g, 1.57 mmol) and dry ethanol (10.0 mL) was added to the silane. The reaction mixture was heated at 70 ˚C under argon for 22 hr, cooled to room temperature and added water (10.0 mL). The compound was extracted using DCM (20.0 mL) and washed with H_2O (6 x 30.0 mL). The organic layer was collected, dried over $MgSO_4$ and the solvent removed. The resulting solid was suspended in minimum diethyl ether, stirred in pentane and collected by suction filtration. Compound **2.3a** was obtained as a light brown solid (0.199 g, 34 %). **m.p.:**

117.5 ˚C (Decomposition w/o melting). **^{1}H NMR (300.08 MHz, $CDCl_3$):** δ (ppm) = 9.22 (s, 1H, NNH); 7.68 (s, 1H, HC=N); 7.32 (br s, 1H, NH); 4.57 (t, $^3J_{HH}$ = 2.00 Hz, 2H, C_5H_4); 4.42 (t, $^3J_{HH}$ = 2.00 Hz, 2H, C_5H_4); 4.21 (s, 5H, C_5H_5); 3.26 (d, $^3J_{HH}$ = 5.60 Hz, 2H, CH_2); 0.18 (s, 9H, $Si(CH_3)_3$). **^{13}C{^{1}H} NMR (100.64 MHz, $CDCl_3$):** δ (ppm) = 166.4 (C=S); 143.1 (C=N); 78.0, 70.5, 69.3, 67.6 (Fc); 34.9 (CH_2); –2.48 ($Si(CH_3)_3$). **IR (KBr, cm^{-1}):** ν = 1606 (s, C=N); 1245 (m, Si-CH_3); 856 (m, C=S). **EI$^+$−MS** (373.0724 g.mol^{-1})**:** *m/z* 373.07 ([M]$^+$, 100 %). **Elemental analysis** for $C_{16}H_{23}FeN_3SiS$ (373.07 g.mol^{-1}): Found C 51.10, H 6.38, N 11.30 %; Calculated C 51.47, H 6.21, N 11.25 %.

Ferrocenylethylidene-((trimethylsilyl)methyl) thiosemicarbazone (**2.3b**)

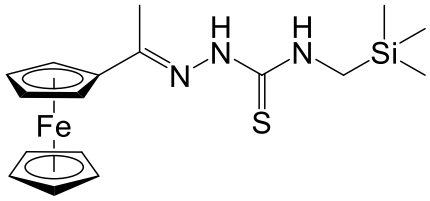

An excess of (aminomethyl)trimethylsilane (0.0900 mL, 0.672 mmol) was added to the flask under N_2. Compound **2.1b** (0.202 g, 0.609 mmol) and dry ethanol (15.0 mL) was added to the silane. The reaction mixture was heated at 70 ˚C under argon for 7 hr and stirred overnight at room temperature. Water (10.0 mL) was added to the flask, precipitating a solid. The solid was collected by suction filtration and washed with water, followed by minimal ethanol. Compound **2.3b** was isolated as an orange-brown solid (0.165 g, 70 %). **m.p.:** 125.0–126.2 ˚C. **^{1}H NMR (300.07 MHz, DMSO–*d*$_6$):** δ (ppm) = 9.88 (s, 1H, NNH); 7.95 (t, $^3J_{HH}$ = 5.70 Hz, 1H, NH); 4.74 (t, $^3J_{HH}$ = 1.80 Hz, 2H, C_5H_4); 4.38 (t, $^3J_{HH}$ = 1.80 Hz, 2H, C_5H_4); 4.17 (s, 5H, C_5H_5); 3.18 (d, $^3J_{HH}$ = 6.00 Hz, 2H, CH_2); 2.19 (s, 3H, CH_3); 0.10 (s, 9H, $Si(CH_3)_3$). **^{13}C{^{1}H} NMR (100.64 MHz, $CDCl_3$):** δ (ppm) = 178.1 (C=S); 148.0 (C=N); 82.5; 70.3; 69.3; 66.8 (Fc); 34.7 (CH_2); 14.2 (CH_3); –2.50 ($Si(CH_3)_3$). **FT–IR (KBr, cm^{-1}):** ν = 1600 (m, C=N); 1243 (m, Si-CH_3); 851 (s, C=S). **EI$^+$−MS:** *m/z* 387.04 ([M]$^+$, 100 %). **Elemental analysis** for $C_{17}H_{25}FeN_3SiS$ (387.07 g/mol): Found C 52.42, H 6.87, N 11.07 %; Calculated C 52.71, H 6.50, N 10.85 %.

General procedure for the synthesis of compounds 2.4a−b

An excess of (aminomethyl)trimethylsilane was added to the flask under N_2. The thiosemicarbazone thioester and dry ethanol (15.0 mL) was added to the silane. The reaction mixture was refluxed under argon for 24 hr, after which water (10.0 mL) was added to the flask, precipitating a solid. The ethanol was removed, and the white solid was collected by suction filtration and washed with water, followed by a minimal volume of ethanol.

3,4-Dichlorobenzylidene-(trimethylsilyl)methyl thiosemicarbazone (**2.4a**)

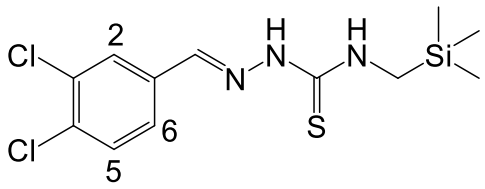

(Aminomethyl)trimethylsilane (0.270 mL, 2.02 mmol), compound **2.2a** (0.500 g, 1.82 mmol). Compound **2.4a** was obtained as an off-white solid (0.375 g, 62 %). **m.p.:** 141.2–143.1 ˚C. **^{1}H NMR (300.07 MHz, $CDCl_3$):** δ (ppm) = 9.84 (s, 1H, NNH); 7.78 (s, 1H, HC=N); 7.69 (d, $^{3}J_{HH}$ = 1.80 Hz, 1H, H–2); 7.48 (d, $^{3}J_{HH}$ = 8.40 Hz, 1H, H–5); 7.41 (dd, $^{3}J_{HH}$ = 1.80, 8.40 Hz, 1H, H–6); 7.38 (br s, 1H, NH); 3.28 (d, $^{3}J_{HH}$ = 6.00 Hz, 2H, CH_2); 0.18 (s, 9H, $Si(CH_3)_3$). **^{13}C{^{1}H} NMR (100.64 MHz, $CDCl_3$):** δ (ppm) = 177.7 (C=S); 139.3 (C=N); 134.1; 133.6; 133.3; 130.9; 128.5; 126.0; 35.0 (CH_2); –2.44 ($Si(CH_3)_3$). **FT–IR (KBr, cm^{-1}):** ν = 1602 (s, C=N); 1250 (m, Si-CH_3); 854 (s, C=S). **EI^{+}–MS** (333.0286 g.mol^{-1})**:** *m/z* 333.00 ($[M]^{+}$, 76 %); 317.9801 ($[M–CH_3]^{+}$, 100 %). **Elemental analysis** for $C_{12}H_{17}Cl_2N_3SiS$ (333.03 g.mol^{-1}): Found (%) C 43.04, H 5.18, N 12.47; Calculated (%) C 43.24, H 5.14, N 12.62.

3,4-Dichlorophenylethylidene-((trimethylsilyl)methyl) thiosemicarbazone (**2.4b**)

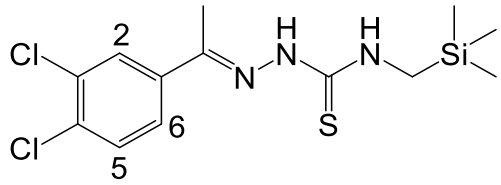

(Aminomethyl)trimethylsilane (0.250 mL, 1.87 mmol), compound **2.2b** (0.501 g, 1.71 mmol). Compound **2.4b** was obtained as a white solid (0.492 g, 83 %). **m.p.:** 153.8–156.7 ˚C. **^{1}H NMR (300.07 MHz, DMSO–d_6):** δ (ppm) = 10.2 (s, 1H, NNH); 8.41 (t, $^{3}J_{HH}$ = 5.70 Hz, 1H, NH); 8.13 (d, $^{3}J_{HH}$ = 2.40 Hz, 1H, H–2); 7.85 (dd, $^{3}J_{HH}$ = 2.40, 8.40 Hz, 1H, H–6); 7.65 (d, $^{3}J_{HH}$ = 8.40 Hz, 1H, H–5); 3.24 (d, $^{3}J_{HH}$ = 6.30 Hz, 2H, CH_2); 2.28 (s, 3H, CH_3); 0.10 (s, 9H, $Si(CH_3)_3$). **^{13}C{^{1}H} NMR (100.64 MHz, DMSO–d_6):** δ (ppm) = 177.3 (C=S); 144.3 (C=N); 138.4; 131.4; 131.2; 130.2; 127.9; 126.4; 34.5 (CH_2); 13.7 (CH_3); –1.84 ($Si(CH_3)_3$). **FT–IR (KBr, cm^{-1}):** ν = 1616 (s, C=N); 1252 (m, Si-CH_3); 846 (s, C=S). **EI^{+}–MS** (347.0442 g.mol^{-1})**:** *m/z* 347.02 ($[M]^{+}$, 31 %); 331.9837 ($[M–CH_3]^{+}$, 89 %). **Elemental analysis** for $C_{13}H_{19}Cl_2N_3SiS$ (347.04 g.mol^{-1}): Found C 44.78, H 5.77, N 11.71 %; Calculated C 44.82, H 5.50, N 12.06 %.

3,4-Dichloroacetophenone(neopentyl) thiosemicarbazone (**2.5**)

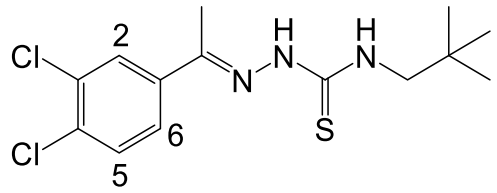

2,2'–Dimethylpropan-1-amine (0.210 mL, 1.79 mmol) was added to the flask under N_2. Compound **2.2b** (0.501 g, 1.71 mmol) and dry ethanol (20.0 mL) was added to the amine. The yellow reaction mixture was heated at 70 ˚C for 48 hr. Water (10.0 mL) was added and the precipitate was collected by suction filtration. The solid was washed with water followed by minimal ethanol ad dried. Compound **2.5** was isolated as a white solid (0.471 g, 83 %). **m.p.:** 192.2–193.0 ˚C. **^{1}H NMR (399.95 MHz, $CDCl_3$):** δ (ppm) = 8.63 (s, 1H, NNH); 7.77 (d, $^3J_{HH}$ = 1.60 Hz, 1H, H–2); 7.74 (br s, 1H, NH); 7.50 (m, 2H, H–5 & H–6); 3.60 (d, $^3J_{HH}$ = 5.60 Hz, 2H, CH_2); 2.26 (s, 3H, CH_3); 1.04 (s, 9H, $C(CH_3)_3$). **^{13}C{^{1}H} NMR (100.64 MHz, $CDCl_3$):** δ (ppm) = 178.4 (C=S); 143.7 (C=N); 137.4; 133.7; 133.0; 130.6; 128.0; 125.1; 55.8 (CH_2); 32.2 ($\underline{C}(CH_3)_3$); 27.4 ($C(\underline{C}H_3)_3$); 13.3 (CH_3). **FT–IR (KBr, cm^{-1}):** ν = 1615 (s, C=N); 858 (m, C=S). **EI$^+$–MS** (331.0672 g.mol^{-1})**:** *m/z* 330.98 ($[M]^+$, 64 %). **Elemental analysis** for $C_{14}H_{19}Cl_2N_3S$ (331.07 g.mol^{-1}): Found C 50.42, H 5.86, N 12.63 %; Calculated C 50.60, H 5.76, N 12.64 %.

7.2.3 Thiosemicarbazone Ruthenium(II) Complexes

General method:

The ruthenium dimer $[Ru(\eta^6\text{-}p\text{-}^iPrC_6H_4Me)Cl_2]_2$ was dissolved in DCM (5.00 mL) followed by the addition of two equivalents of the organosilane thiosemicarbazone. The reaction mixture was stirred at room temperature for 4 hr. The solvent was reduced (~1 mL) and added to stirring diethyl ether to precipitate a solid. The solid was collected by suction filtration and washed with diethyl ether.

*[Ru(II)Cl(η^6–$MeC_6H_4{}^iPr$)(**2.3a**)]Cl* (**2.6a**)

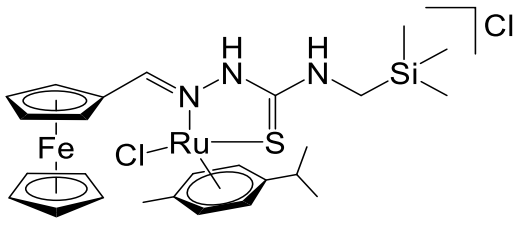

Ruthenium dimer (0.0500 g, 0.0816 mmol), Compound **2.3a** (0.0650 g, 0.174 mmol). Compound **2.6a** was isolated as an orange-red powder (0.0678 g, 61 %). **m.p.:** 102.9 ˚C (Decomp. without melting). **^{1}H NMR (300.07 MHz, $CDCl_3$):** δ (ppm) = 8.68 (br s, 1H, NH); 8.60 (s, 1H, HC=N); 6.06 (s, 1H, C_5H_4); 5.52 (d, $^3J_{HH}$ = 6.00 Hz, 1H, *p*–cym); 5.20 (br s, 2H, *p*–cym); 5.13 (d, $^3J_{HH}$ = 6.00 Hz, 1H, *p*–cym);

4.65 (br s, 3H, C_5H_4); 4.34 (s, 5H, C_5H_5); 2.99 (t, $^3J_{HH}$ = 6.30 Hz, 2H, CH_2); 2.66 (m, 1H, C<u>H</u>$(CH_3)_2$); 2.13 (s, 3H, $CH_{3(p\text{-cym})}$); 1.19 (d, $^3J_{HH}$ = 6.90 Hz, 3H, CH(C<u>H</u>$_3)_2$); 1.14 (d, $^3J_{HH}$ = 6.90 Hz, 3H, CH(C<u>H</u>$_3)_2$); 0.21 (s, 9H, $Si(CH_3)_3$). **$^{13}C\{^1H\}$ NMR (100.64 MHz, $CDCl_3$):** δ (ppm) = 158.6 (C=N); 101.6 (p–$cym_{quatern.}$); 88.5, 87.3, 83.8, 81.6 (p–cym); 70.0–72.6 (Fc); 36.1 (CH_2); 30.5 (<u>C</u>H$(CH_3)_2$); 22.7 (CH(<u>C</u>H$_3)_2$); 21.7 (CH(<u>C</u>H$_3)_2$); 18.5 ($CH_{3(p\text{-cym})}$); –2.56 ($Si(CH_3)_3$). **FT–IR (KBr, cm^{-1}):** ν = 1633 (w, C=N); 860 (s, C=S). **ESI^+–HRMS** (678.9866 $g.mol^{-1}$)**:** *m/z* 608.0793 ($[M–H–Cl]^+$, 40 %); 304.5437 ($[M–Cl]^{2+}$, 100 %). **Elemental analysis** for $C_{26}H_{37}Cl_2FeN_3RuSiS.¼C_5H_{12}$ (697.01 $g.mol^{-1}$): Found (%) C 46.88, H 5.72, N 5.92; Calculated (%) C 46.91, H 5.78, N 6.03.

*[Ru(II)Cl(η^6–$MeC_6H_4{}^iPr$)(**2.3b**)]Cl* (**2.6b**)

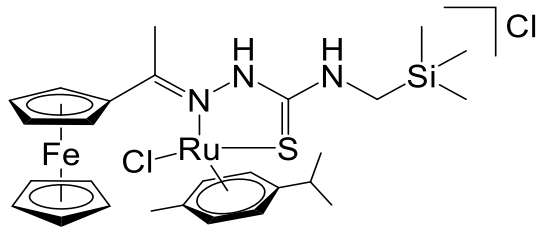

Ruthenium dimer (0.0383 g, 0.0625 mmol); Compound **2.3b** (0.0506 g, 0.131 mmol). Compound **2.6b** was isolated as a red powder (0.0598 g, 69 %). **m.p.:** 183.8 ˚C (Decomp. with melting). **^1H NMR (399.95 MHz, $CDCl_3$):** δ (ppm) = 12.4 (s, 1H, NNH); 10.3 (t, $^3J_{HH}$ = 6.00 Hz, 1H, NH); 6.28 (s, 1H, C_5H_4); 5.37 (d, $^3J_{HH}$ = 6.00 Hz, 1H, p–cym); 4.89 (d, $^3J_{HH}$ = 6.00 Hz, 1H, p–cym); 4.81 (d, $^3J_{HH}$ = 5.60 Hz, 1H, p–cym); 4.74 (d, $^3J_{HH}$ = 6.00 Hz, 1H, p–cym); 4.65 (d, $^3J_{HH}$ = 6.00 Hz, 2H, C_5H_4); 4.56 (s, 1H, C_5H_4); 4.29 (s, 5H, C_5H_5); 3.05 (m, 5H, CH_3 & CH_2); 2.57 (m, 1H, C<u>H</u>$(CH_3)_2$); 2.07 (s, 3H, $CH_{3(p\text{-cym})}$); 1.13 (d, $^3J_{HH}$ = 6.80 Hz, 3H, CH(C<u>H</u>$_3)_2$); 1.08 (d, $^3J_{HH}$ = 6.80 Hz, 3H, CH(C<u>H</u>$_3)_2$); 0.23 (s, 9H, $Si(CH_3)_3$). **$^{13}C\{^1H\}$ NMR (100.64 MHz, $CDCl_3$):** δ (ppm) = 178.5 (C=S); 168.2 (C=N); 102.2, 102.1 (p-$cym_{quatern.}$); 89.5, 87.3 (p-cym); 86.5 ($Fc_{quatern.}$); 84.1, 81.3 (p-cym); 72.9, 71.9, 71.4, 70.5, 69.8 (Fc); 36.6 (CH_2); 30.5 (<u>C</u>H$(CH_3)_2$); 27.7 (CH_3); 22.8 (CH(<u>C</u>H$_3)_2$); 21.4 (CH(<u>C</u>H$_3)_2$); 18.4 ($CH_{3(p\text{-cym})}$); –2.26 ($Si(CH_3)_3$). **FT–IR (ATR, cm^{-1}):** ν = 1624 (w, C=N); 858 (s, C=S). **ESI^+–HRMS** (693.0392 $g.mol^{-1}$)**:** *m/z* 622.0960 ($[M–H–Cl]^+$, 100 %); 311.5522 ($[M–Cl]^{2+}$, 98 %). **Elemental analysis** for $C_{27}H_{39}Cl_2FeN_3RuSiS$ (693.04 $g.mol^{-1}$): Found C 46.48, H 5.97, N 5.62 %; Calculated C 46.75, H 5.66, N 6.05 %.

*[Ru(II)Cl(η⁶–MeC₆H₄ⁱPr)(**2.4a**)]Cl* (**2.7a**)

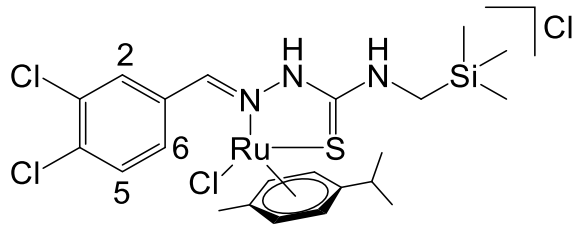

Ruthenium dimer (0.0765 g, 0.125 mmol); Compound **2.4a** (0.0860 g, 0.257 mmol). Compound **2.7a** was isolated as a light orange powder (0.115 g, 72 %). **m.p.:** 156.1 ˚C (Decomp. with melting). **^{1}H NMR (399.95 MHz, $CDCl_3$):** δ (ppm) = 8.91 (br s, 1H, NH); 8.77 (s, 1H, HC=N); 8.67 (s, 1H, H–2); 7.88 (d, $^{3}J_{HH}$ = 8.40 Hz, 1H, H–5); 7.64 (d, $^{3}J_{HH}$ = 8.40 Hz, 1H, H–6); 5.49 (d, $^{3}J_{HH}$ = 5.70 Hz, 1H, *p*–cym); 4.98 (d, $^{3}J_{HH}$ = 6.00 Hz, 1H, *p*–cym); 4.90 (d, $^{3}J_{HH}$ = 6.00 Hz, 1H, *p*–cym); 4.86 (d, $^{3}J_{HH}$ = 5.70 Hz, 1H, *p*–cym); 3.03 (d, $^{3}J_{HH}$ = 6.00 Hz, 2H, CH_2); 2.64 (m, 1H, C<u>H</u>$(CH_3)_2$); 2.12 (s, 3H, $CH_{3(p\text{-cym})}$); 1.18 (d, $^{3}J_{HH}$ = 6.90 Hz, 3H, CH(C<u>H</u>$_3)_2$); 1.12 (d, $^{3}J_{HH}$ = 6.90 Hz, 3H, CH(C<u>H</u>$_3)_2$); 0.18 (s, 9H, $Si(CH_3)_3$). **^{13}C{^{1}H} NMR (100.64 MHz, $CDCl_3$):** δ (ppm) = 177.7 (C=S); 156.4 (C=N); 136.2; 133.4; 132.7; 132.6; 130.9; 129.8; 104.2, 103.7 (*p*-$cym_{quatern.}$); 88.5, 88.2, 82.7, 81.2 (*p*-cym); 36.5 (CH_2); 30.8 (<u>C</u>H$(CH_3)_2$); 22.9 (CH(<u>C</u>H$_3)_2$); 21.5 (CH(<u>C</u>H$_3)_2$); 18.7 ($CH_{3(p\text{-cym})}$); –2.49 ($Si(CH_3)_3$). **FT–IR (KBr, cm^{-1}):** ν = 1630 (s, C=N); 856 (s, C=S). **ESI^{+}–HRMS** (638.9808 g.mol^{-1})**:** *m/z* 568.0345 ($[M–H–Cl]^{+}$, 100 %); 284.5207 ($[M–Cl]^{2+}$, 57 %). **Elemental analysis** for $C_{22}H_{31}Cl_4N_3RuSiS.H_2O$ (658.56 g.mol^{-1}): Found 40.06, 4.77, 5.94 %; Calculated C 40.13, H 5.05, N 6.38 %.

*[Ru(II)Cl(η⁶–MeC₆H₄ⁱPr)(**2.4b**)]Cl* (**2.7b**)

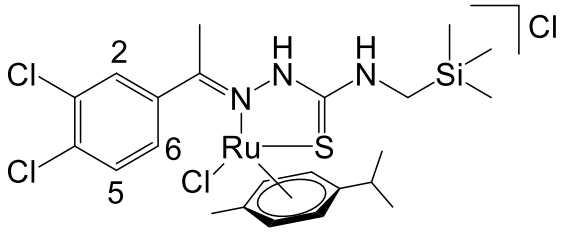

Ruthenium dimer (0.0495 g, 0.0808 mmol); Compound **2.4b** (0.0561 g, 0.161 mmol). Compound **2.7b** was isolated as an orange powder (0.0883 g, 84 %). **m.p.:** 190.8 ˚C (Decomp. with melting). **^{1}H NMR (300.07 MHz, $CDCl_3$):** δ (ppm) = 12.7 (s, 1H, NNH); 10.4 (br s, 1H, NH); 8.23 (s, 1H, H–2); 7.68 (m, 2H, H–5 & H–6); 5.32 (d, $^{3}J_{HH}$ = 6.30 Hz, 1H, *p*–cym); 4.90 (d, $^{3}J_{HH}$ = 6.00 Hz, 1H, *p*–cym); 4.71 (d, $^{3}J_{HH}$ = 6.30 Hz, 1H, *p*–cym); 4.10 (d, $^{3}J_{HH}$ = 5.40 Hz, 1H, *p*–cym); 3.07 (d, $^{3}J_{HH}$ = 5.40 Hz, 2H, CH_2); 2.93 (s, 3H, CH_3); 2.65 (m, 1H, C<u>H</u>$(CH_3)_2$); 2.06 (s, 3H, $CH_{3(p\text{-cym})}$); 1.16 (d, $^{3}J_{HH}$ = 6.90 Hz, 3H, CH(C<u>H</u>$_3)_2$); 1.10 (d, $^{3}J_{HH}$ = 6.60 Hz, 3H, CH(C<u>H</u>$_3)_2$); 0.22 (s, 9H, $Si(CH_3)_3$). **^{13}C{^{1}H} NMR (100.64 MHz, $CDCl_3$):** δ (ppm) = 178.5 (C=S); 165.9 (C=N); 141.2; 134.7; 133.2; 131.5; 130.6; 128.1; 105.9, 102.5 (*p*-$cym_{quatern.}$); 88.9, 88.1, 84.0, 82.5 (*p*-cym);

36.8 (CH_2); 30.6 ($\underline{C}H(CH_3)_2$); 26.8 (CH_3); 23.5 ($CH(\underline{C}H_3)_2$); 21.1 ($CH(\underline{C}H_3)_2$); 18.7 ($CH_{3(p\text{-cym})}$); –2.30 ($Si(CH_3)_3$). **FT–IR (KBr, cm^{-1}):** ν = 1633 (s, C=N); 866 (s, C=S). **ESI$^+$−HRMS** (654.0042 g.mol^{-1})**:** *m/z* 582.0500 ([M–H–Cl]$^+$, 100 %); 291.5291 ([M–Cl]$^{2+}$, 42 %). **Elemental analysis** for $C_{23}H_{33}Cl_4N_3RuSiS$ (654.00 g.mol^{-1}): Found C 42.37, H 5.27, N 6.14 %; Calculated C 42.20, H 5.08, N 6.42 %.

*[Ru(II)Cl(η^6–MeC$_6$H$_4$^{i}Pr)(**2.5**)]Cl* (**2.8**)

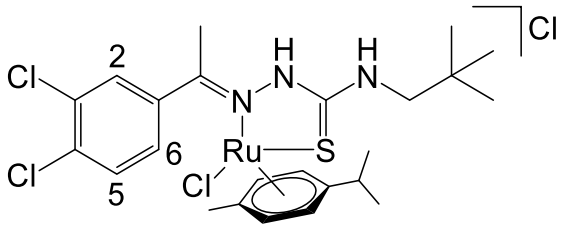

Ruthenium dimer (0.0515 g, 0.0841 mmol); Compound **2.5** (0.0575 g, 0.173 mmol). Compound **2.8** was obtained as an orange powder (0.0896 g, 83 %). **m.p.:** 197.7 ˚C (Decomp. without melting). **^{1}H NMR (399.95 MHz, CDCl$_3$):** δ (ppm) = 12.99 (s, 1H, NNH); 10.4 (s, 1H, NH); 8.22 (s, 1H, H–2); 7.68 (m, 2H, H–5 & H–6); 5.32 (d, $^3J_{HH}$ = 5.60 Hz, 1H, *p*–cym); 4.92 (d, $^3J_{HH}$ = 5.60 Hz, 1H, *p*–cym); 4.73 (d, $^3J_{HH}$ = 6.40 Hz, 1H, *p*–cym); 4.10 (d, $^3J_{HH}$ = 5.60 Hz, 1H, *p*–cym); 3.41 (m, 2H, CH_2); 2.96 (s, 3H, CH_3); 2.65 (m, 1H, $C\underline{H}(CH_3)_2$); 2.06 (s, 3H, $CH_{3(p\text{-cym})}$); 1.17 (d, $^3J_{HH}$ = 7.20 Hz, 3H, $CH(C\underline{H}_3)_2$); 1.11 (d, $^3J_{HH}$ = 6.80 Hz, 3H, $CH(C\underline{H}_3)_2$); 1.08 (s, 9H, $C(CH_3)_3$). **^{13}C{^{1}H} NMR (100.64 MHz, CDCl$_3$):** δ (ppm) = 178.46 (C=S); 166.85 (C=N); 141.24; 134.83; 133.29; 131.50; 130.64; 128.18; 106.14, 102.73 (p-cym$_{quaternary}$); 89.00, 88.02, 84.07, 82.47 (*p*-cym); 57.81 (CH_2); 32.50 ($\underline{C}(CH_3)_3$); 30.63 ($\underline{C}H(CH_3)_2$); 27.13 (CH_3); 23.54 ($CH(\underline{C}H_3)_2$); 22.26 ($C(\underline{C}H_3)_3$); 21.15 ($CH(\underline{C}H_3)_2$); 18.73 ($CH_{3(p\text{-cym})}$). **FT–IR (ATR, cm^{-1}):** ν = 1633 (s, C=N); 857 (s, C=S). **ESI$^+$−HRMS** (638.0242 g.mol^{-1})**:** *m/z* 568.0828 ([M+H–Cl]$^+$, 100 %); 284.5441 ([M–Cl]$^{2+}$, 68 %). **Elemental analysis** for $C_{24}H_{33}Cl_4N_3RuS.½C_5H_{12}$ (673.05 g.mol^{-1}): Found (%) C 47.53 H 5.46 N 6.80; Calculated (%) C 47.25, H 5.84, N 6.24.

7.2.4 Thiosemicarbazone Rhodium(III) Complexes

General method:

The rhodium dimer $[Rh(Cp^*)Cl_2]_2$ was dissolved in DCM (5.00 mL), followed by the addition of two equivalents of the ligand. The solution was stirred at room temperature for 4 hr. The solvent was reduced (~1 mL) and the contents added to stirring pentane to precipitate a solid. The solid was collected by suction filtration and washed with pentane.

[Rh(III)Cl(Cp)(**2.3a**)]Cl* (**2.9a**)

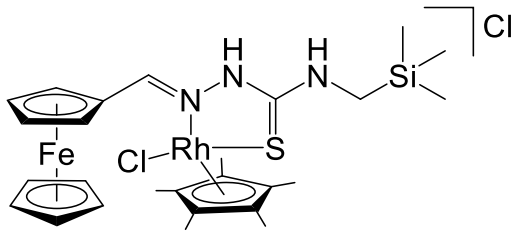

Rhodium dimer (0.0404 g, 0.0654 mmol); Compound **2.3a** (0.0486 g, 0.130 mmol). Compound **2.9a** was isolated as a red solid (0.0730 g, 82 %). **m.p.:** 132.8 ˚C (Decomp. w/o melting). **^{1}H NMR (399.95 MHz, $CDCl_3$):** δ (ppm) = 8.75 (s, 1H, NH); 8.62 (s, 1H, HC=N); 6.25 (s, 1H, C_5H_4); 4.64 (s, 1H, C_5H_4); 4.60 (s, 2H, C_5H_4); 4.34 (s, 5H, C_5H_5); 2.99 (m, 2H, CH_2); 1.51 (s, 15H, Cp*); 0.24 (s, 9H, $Si(CH_3)_3$). **^{13}C{^{1}H} NMR (100.64 MHz, $CDCl_3$):** δ (ppm) = 176.2 (C=S); 158.5 (C=N); 97.3 (d, $^{1}J_{RhC}$ = 7.45 Hz, $Cp^*_{quatern.}$); 75.6, 74.1, 73.2, 72.3, 70.4, 69.1 (Fc); 36.3 (CH_2); 9.48 ($CH_{3(Cp^*)}$); –2.42 ($Si(CH_3)_3$). **FT–IR (KBr, cm^{-1}):** ν = 1636 (w, C=N; 856 (s, C=S). **ESI^{+}–HRMS** (681.0254 g.mol^{-1})**:** *m/z* 610.0873 ($[M–H–Cl]^{+}$, 88 %); 305.5477 ($[M–Cl]^{2+}$, 100 %). **Elemental analysis** for $C_{26}H_{38}Cl_2N_3FeRhSiS.½H_2O$ (690.04 g.mol^{-1}): Found C 45.11, H 5.55, N 5.41 %; Calculated C 45.21, H 5.70, N 6.09 %.

[Rh(III)Cl(Cp)(**2.3b**)]Cl* (**2.9b**)

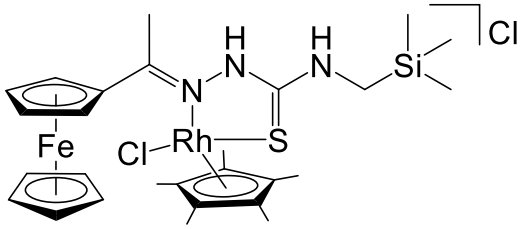

Rhodium dimer (0.0556 g, 0.0900 mmol); Compound **2.3b** (0.0683 g, 0.176 mmol). Compound **2.9b** was obtained as an orange powder (0.0962 g, 78 %). **^{1}H NMR (399.95 MHz, Acetone–d_6):** δ (ppm) = 10.90 (s, 1H, NNH); 7.86 (s, 1H, NH); 4.69 (t, $^{3}J_{HH}$ = 1.80 Hz, 2H, C_5H_4); 4.38 (t, $^{3}J_{HH}$ = 1.80 Hz, 2H, C_5H_4); 4.18 (s, 5H, C_5H_5); 3.31 (d, $^{3}J_{HH}$ = 6.30 Hz 2H, CH_2); 2.40 (s, 3H, CH_3); 1.62 (s, 15H, Cp*); 0.21 (s, 9H, $Si(CH_3)_3$). **^{13}C{^{1}H} NMR (100.64 MHz, Acetone–d_6):** δ (ppm) = 172.88 (C=S); 153.18 (C=N); 94.58 (d, $^{1}J_{RhC}$ = 7.75 Hz, $Cp^*_{quatern.}$); 82.59, 70.18, 69.41, 67.35 (Fc); 34.51 (CH_2); 17.06 (CH_3); 8.16 ($CH_{3(Cp^*)}$); –2.81 ($Si(CH_3)_3$). **FT–IR (KBr, cm^{-1}):** ν = 1638 (w, C=N); 856 (s, C=S). **ESI^{+}–HRMS** (695.0480 g.mol^{-1})**:** *m/z* 624.1039 ($[M–H–Cl]^{+}$, 25 %); 312.5549 ($[M–Cl]^{2+}$, 100 %). **Elemental analysis** for $C_{27}H_{40}Cl_2N_3FeRhSiS.½H_2O$ (704.05 g.mol^{-1}): Found (%) C 46.00, H 6.13, N 5.27; Calculated (%) C 46.02, H 5.87, N 5.97.

[Rh(III)Cl(Cp)(**2.4a**)]Cl* (**2.10a**)

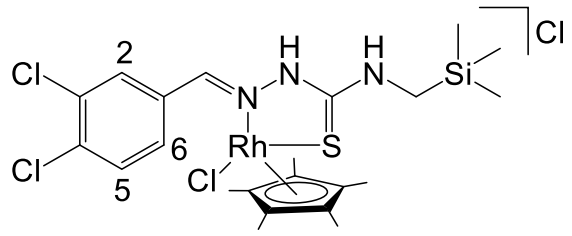

Rhodium dimer (0.0410 g, 0.0663 mmol); Compound **2.4a** (0.0445 g, 0.133 mmol). Compound **2.10a** was isolated as a red powder (0.0796 g, 93 %). **m.p.:** 205.4 ˚C (Decomp. w/o melting). **^{1}H NMR (399.95 MHz, $CDCl_3$):** δ (ppm) = 11.55 (s, 1H, NNH); 7.94 (s, 1H, HC=N); 7.67 (d, $^{3}J_{HH}$ = 2.00 Hz, 1H, H–2); 7.44 (d, $^{3}J_{HH}$ = 8.80 Hz, 1H, H–5); 7.36 (dd, $^{4}J_{HH}$ = 1.60 Hz, $^{3}J_{HH}$ = 8.00 Hz, 1H, H–6); 7.10 (br s, 1H, NH); 3.20 (d, $^{4}J_{HH} = J_{HH}$ = 5.60 Hz, 2H, CH_2); 1.70 (s, 15H, Cp*); 0.20 (s, 9H, $Si(CH_3)_3$). **^{13}C{^{1}H} NMR (100.64 MHz, $CDCl_3$):** δ (ppm) = 173.95 (C=S); 143.57 (C=N); 134.30; 133.61; 133.20; 130.81; 128.53; 126.66; 95.43 (d, $^{1}J_{RhC}$ = 8.05 Hz, $Cp^*_{quatern.}$); 34.80 (CH_2); 8.89 ($CH_{3(Cp^*)}$); –2.41 ($Si(CH_3)_3$). **FT–IR (KBr, cm^{-1}):** ν = 1638 (w, C=N); 856 (s, C=S). **ESI^{+}–HRMS** (640.9886 g.mol^{-1})**:** *m/z* 570.0446 ([M–H–Cl]$^{+}$, 100 %); 285.5261 ([M–Cl]$^{2+}$, 30 %). **Elemental analysis** for $C_{22}H_{32}Cl_4N_3RhSiS.½H_2O$ (649.99 g.mol^{-1}): Found (%) C 40.24, H 5.26, N 6.11; Calculated (%) C 40.62, H 5.12, N 6.46.

[Rh(III)Cl(Cp)(**2.4b**)]Cl* (**2.10b**)

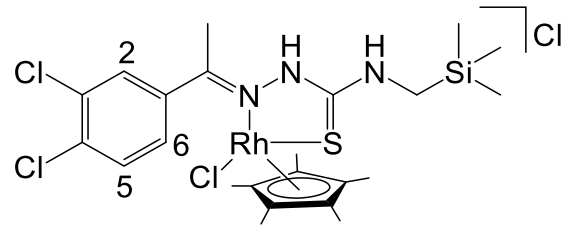

Rhodium dimer (0.0490 g, 0.0793 mmol); Compound **2.4b** (0.0552 g, 0.158 mmol). Compound **2.10b** was obtained as an orange solid (0.0839 g, 80 %). **m.p.** 112.7 ˚C (Decomp. w/o melting). **^{1}H NMR (399.95 MHz, $CDCl_3$):** δ (ppm) = 10.9 (s, 1H, NNH); 7.73 (m, 1H, H–2); 7.43 (m, 2H, H–5 & H–6); 7.39 (t, $^{3}J_{HH}$ = 5.20 Hz, 1H, NH); 3.16 (d, $^{3}J_{HH}$ = 5.60 Hz, 2H, CH_2); 2.52 (s, 3H, CH_3); 1.69 (s, 15H, Cp*); 0.19 (s, 9H, $Si(CH_3)_3$). **^{13}C{^{1}H} NMR (100.64 MHz, $CDCl_3$):** δ (ppm) = 174.3 (C=S); 149.4 (C=N); 137.9; 133.5; 132.7; 130.3; 128.2; 125.5; 95.2 (d, $^{1}J_{RhC}$ = 8.09 Hz, $Cp^*_{quatern.}$); 34.5 (CH_2); 16.7 (CH_3); 8.78 ($CH_{3(Cp^*)}$); –2.48 ($Si(CH_3)_3$). **FT–IR (KBr, cm^{-1}):** ν = 1629 (w, C=N); 858 (s, C=S). **ESI^{+}–HRMS** (655.0042 g.mol^{-1})**:** *m/z* 584.0607 ([M–H–Cl]$^{+}$, 100 %); 292.5339 ([M–Cl]$^{2+}$, 98 %). **Elemental analysis** for $C_{23}H_{34}Cl_4N_3RhSiS.½H_2O$ (664.01 g.mol^{-1}): Found (%) C 41.42, H 5.08, N 6.26; Calculated (%) C 41.57, H 5.31, N 6.33.

[Rh(III)Cl(Cp)(**2.5**)]Cl* (**2.11**)

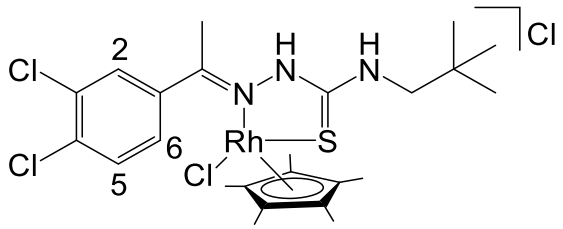

Rhodium dimer (0.0500 g, 0.0809 mmol); Compound **2.5** (0.0546 g, 0.164 mmol). Compound **2.11** was obtained as an orange solid (0.0741 g, 80 %). **m.p.:** 118.5 ˚C (Decomp. with melting). **^{1}H NMR (399.95 MHz, $CDCl_3$):** δ (ppm) = 10.9 (s, 1H, NNH); 7.71 (m, 1H, H–2); 7.54 (t, $^{3}J_{HH}$ = 6.40 Hz, 1H, NH); 7.44 (m, 2H, H–5 & H–6); 3.49 (d, $^{3}J_{HH}$ = 5.60 Hz, 2H, CH_2); 2.53 (s, 3H, CH_3); 1.68 (s, 15H, Cp*); 1.03 (s, 9H, $C(CH_3)_3$). **^{13}C{^{1}H} NMR (100.64 MHz, $CDCl_3$):** δ (ppm) = 173.7 (C=S); 149.8 (C=N); 137.9; 133.6; 132.8; 130.4; 128.3; 125.5; 95.4 (d, $^{1}J_{RhC}$ = 8.05 Hz, $Cp^*_{quatern.}$); 55.5 (CH_2); 31.9 ($\underline{C}(CH_3)_3$); 27.5 ($C(\underline{C}H_3)_3$); 16.9 (CH_3).8.79 ($CH_{3(Cp^*)}$). **FT–IR (ATR, cm^{-1}):** ν = 1624 (w, C=N); 853 (s, C=S). **ESI^{+}–HRMS** (639.0272 g.mol^{-1})**:** *m/z* 568.0739 ($[M–H–Cl]^{+}$, 100 %); 283.5399 ($[M–Cl]^{2+}$, 62 %). **Elemental analysis** for $C_{24}H_{34}Cl_4N_3RhS.H_2O$ (648.03 g.mol^{-1}): Found (%) C 44.10, H 5.44, N 6.18; Calculated (%) C 44.44, H 5.44, N 6.48.

7.2.5 Thiosemicarbazone Palladium(II) Complexes

General procedure

The thiosemicarbazone was dissolved in ethanol, followed by the addition of triethylamine (0.20 mL), and stirred for approximately 10 minutes. The palladium precursor *cis*–$[Pd(PTA)_2Cl_2]$ was added and the reaction mixture refluxed for 24 hr. The resulting solid was collected by suction filtration. If another phosphorus species was present, the solid was purified by washing the solid with a minimal volume of hot methanol to remove phosphorus impurity.

*[Pd(PTA)(**2.3b**)]* (**2.12**)

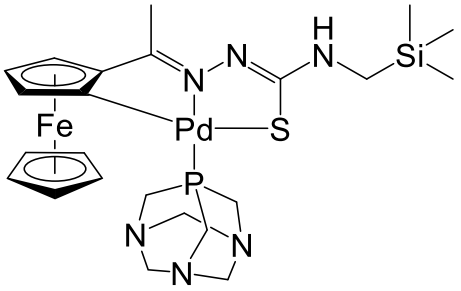

cis–$[Pd(PTA)_2Cl_2]$ (0.0525 g, 0.107 mmol); Compound **2.3b** (0.0738 g, 0.106 mmol). Compound **2.12** was isolated as a red powder (0.0434 g, 63 %). **m.p.:** 266.8 ˚C (Decomp. w/o melting). **^{1}H NMR (399.95 MHz, DMSO–d_6):** δ (ppm) = 6.56 (t, J_{HH} = 6.00 Hz, 1H, NH); 4.65 (d,

$^{4}J_{PH}$ = 12.40 Hz, 3H, $NCH_{2(eq)}N$); 4.44 (m, 4H, $NCH_{2(ax)}N$ & C_5H_3); 4.38 (d, J_{HH} = 2.40 Hz, 1H, C_5H_3); 4.32 (t, J_{HH} = 2.00 Hz, 1H, C_5H_3); 4.24 (s, 6H, PCH_2N); 4.11 (s, 5H, C_5H_5); 2.79 (d, J_{HH} = 6.00 Hz, 2H, CH_2); 2.14 (s, 3H, CH_3); 0.038 (s, 9H, $Si(CH_3)_3$). **$^{13}C\{^{1}H\}$ NMR (100.64 MHz, DMSO–*d*$_6$):** δ (ppm) = 163.0 (C=N); 99.5 (d, $^{2}J_{CP}$ = 12.9 Hz, C–Pd); 95.2 (C–CN); 75.4 (Fc); 72.5 (d, $^{3}J_{CP}$ = 6.74 Hz, NCH_2N); 69.8, 68.5, 66.7 (Fc); 52.7 (d, $^{1}J_{CP}$ = 16.1 Hz, PCH_2N); 37.3 (CH_2); 13.4 (CH_3); –1.35 ($Si(CH_3)_3$). **$^{31}P\{^{1}H\}$ NMR (162.01 MHz, DMSO–*d*$_6$):** δ (ppm) = –41.6. **FT–IR (KBr, cm^{-1}):** ν = 1570 (s, C=N), 1530 (s, C=N); 807 (s, C–S). **EI^{+}–MS** (648.0520 g.mol^{-1})**:** *m/z* 647.97 ($[M]^{+}$, 75 %). **Elemental analysis** for $C_{23}H_{35}FeN_6PdPSiS$ (648.05 g.mol^{-1}): Found C 42.13, H 5.53, N 13.03 %; Calculated C 42.57, H 5.44, N 12.95 %.

*[Pd(PTA)(**2.4b**)]* (**2.13**)

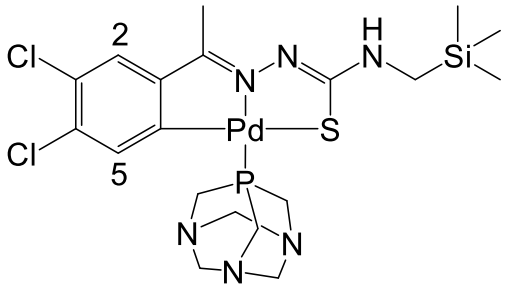

cis–$[Pd(PTA)_2Cl_2]$ (0.107 g, 0.218 mmol); Compound **2.4b** (0.0761 g, 0.218 mmol). Compound **2.13** was obtained as a yellow powder (0.0634 g, 48 %). **m.p.:** 240.2 ˚C (Decomp. with melting). **^{1}H NMR (300.07 MHz, DMSO–*d*$_6$):** δ (ppm) = 7.25 (m, 2H, H–2 & NH); 7.11 (d, J_{HH} = 3.60 Hz, 1H, H–5); 4.58 (d, $^{4}J_{PH}$ = 12.6 Hz, 3H, $NCH_{2(eq)}N$); 4.44 (d, $^{4}J_{PH}$ = 12.9 Hz, 3H, $NCH_{2(ax)}N$); 4.27 (s, 6H, PCH_2N); 2.86 (d, J_{HH} = 6.00 Hz, 2H, CH_2); 2.23 (s, 3H, CH_3); 0.039 (s, 9H, $Si(CH_3)_3$). **$^{13}C\{^{1}H\}$ NMR (100.64 MHz, DMSO–*d*$_6$):** δ (ppm) = 163.3 (d, J_{CP} = 7.04 Hz, C=N); 153.2 (Ar–C); 136.3 (d, J_{CP} = 8.05 Hz, C–Pd); 130.3, 127.0, 126.9, 126.6 (Ar–C); 72.4 (d, $^{3}J_{CP}$ = 7.18 Hz, NCH_2N); 51.5 (d, $^{1}J_{CP}$ = 15.4 Hz, PCH_2N); 37.9 (CH_2); 13.5 (CH_3); –1.39 ($Si(CH_3)_3$). **$^{31}P\{^{1}H\}$ NMR (121.47 MHz, DMSO–*d*$_6$):** δ (ppm) = –49.6. **FT–IR (KBr, cm^{-1}):** ν = 1578 (s, C=N), 1560 (s, C=N); 807 (s, C–S). **EI^{+}–MS** (608.0082 g.mol^{-1})**:** *m/z* 607.99 ($[M+H]^{+}$, 1.8 %). **Elemental analysis** for $C_{19}H_{29}Cl_2N_6PdPSiS$ (608.01 g.mol^{-1}): Found C 37.10, H 4.86, N 13.16 %; Calculated C 37.50, H 4.81, N 13.82 %.

*[Pd(PTA)(**2.5**)]* (**2.14**)

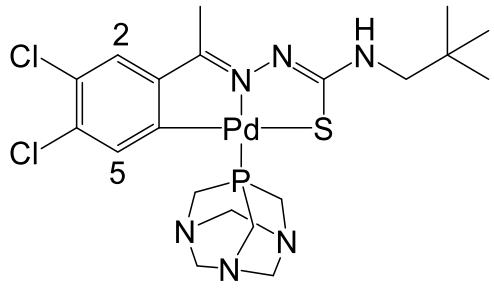

cis–[Pd(PTA)$_2$Cl$_2$] (0.147 g, 0.299 mmol); Compound **2.5** (0.0997 g, 0.300 mmol). Compound **2.14** was isolated as a yellow powder (0.0926 g, 52 %). **m.p.:** 242.1 ˚C (Decomp. with melting). **^{1}H NMR (399.95 MHz, DMSO–*d*$_6$):** δ (ppm) = 7.26 (s, 1H, H–2); 7.17 (br s, 1H, NH); 7.11 (d, J_{HH} = 3.60 Hz, 1H, H–5); 4.58 (d, $^4J_{PH}$ = 12.8 Hz, 3H, NCH$_{2(eq)}$N); 4.45 (d, $^4J_{PH}$ = 12.8 Hz, 3H, NCH$_{2(ax)}$N); 4.28 (s, 6H, PCH$_2$N); 3.14 (d, J_{HH} = 6.40 Hz, 2H, CH$_2$); 2.24 (s, 3H, CH$_3$); 0.88 (s, 9H, C(CH$_3$)$_3$). **^{13}C{^{1}H} NMR (100.64 MHz, CDCl$_3$):** δ (ppm) = 165.5 (Ar–C); 161.6 (d, J_{CP} = 7.4 Hz, C=N); 152.3 (Ar–C); 135.7 (d, $^2J_{CP}$ = 8.76 Hz, C–Pd); 131.7, 128.1, 127.2 (Ar–C); 72.4 (d, $^3J_{CP}$ = 7.18 Hz, NCH$_2$N); 58.0 (CH$_2$); 51.5 (d, $^1J_{CP}$ = 15.4 Hz, PCH$_2$N); 32.3 (C(CH$_3$)$_3$); 27.3 (C(CH$_3$)$_3$); 13.4 (CH$_3$). **^{31}P{^{1}H} NMR (121.47 MHz, DMSO–*d*$_6$):** δ (ppm) = –49.6. **FT–IR (KBr, cm^{-1}):** ν = 1582 (s, C=N), 1558 (s, C=N); 801 (s, C–S). **EI$^+$–MS** (592.0312 g.mol^{-1})**:** *m/z* 592.09 ([M]$^+$, 1.5 %). **Elemental analysis** for $C_{20}H_{29}Cl_2N_6PdPS$ (592.03 g.mol^{-1}): Found C 40.31, H 5.06, N 14.27 %; Calculated C 40.45, H 4.92, N 14.15 %.

7.3 Ferrocenyl–Containing Aminoquinolines

General method

Quaternised ferroquine was refluxed in acetonitrile (20.0 mL), with 8 equivalents of various amines in the presence of K_2CO_3 (2 eq.), for 3 days. The cooled solution was diluted using chloroform:H_2O (1:1; 60.0 mL) and extracted using chloroform (2 x 40.0 mL). The organic layer was dried over Na_2SO_4 and the solvent removed. The compound was purified using silica gel chromatography, eluting with ethyl acetate: petroleum ether: triethylamine (7:2:1). Previously published compound **4.1** was prepared following the method described above.

7-Chloro-4-[2-(N'-substituted aminomethyl)-N-ferrocenylmethyl(aminomethyl)trimethyl-silane]quinoline (**4.1**)

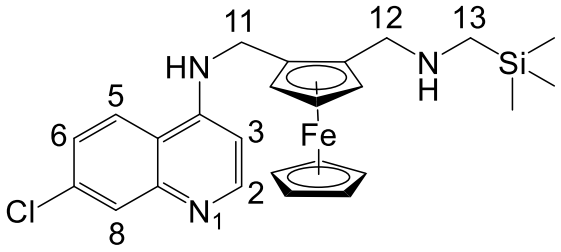

Quaternised ferroquine (0.307 g, 0.534 mmol); (aminomethyl)trimethylsilane (0.560 mL, 4.18 mmol). Compound **4.1** was isolated as an orange solid (0.218 g, 83 %). R_f value = 0.63. **m.p.:** 154.6–156.5 ˚C. **^{1}H NMR (300.08 MHz, $CDCl_3$):** δ (ppm) = 8.55 (d, $^3J_{HH}$ = 5.40 Hz, 1H, H–2); 7.94 (d, $^4J_{HH}$ = 2.40 Hz, 1H, H–8); 7.71 (d, $^3J_{HH}$ = 9.00 Hz, 1H, H–5); 7.26 (dd, $^4J_{HH}$ = 2.40 Hz, $^3J_{HH}$ = 9.00 Hz, 1H, H–6); 6.55 (br s, 1H, NH); 6.50 (d, $^3J_{HH}$ = 5.40 Hz, 1H, H–3); 4.37 (d, $^3J_{HH}$ = 13.20 Hz, 1H, H–11); 4.28 (m, 1H, C_5H_3); 4.24 (m, 1H, C_5H_3); 4.15 (m, 6H, C_5H_5 & H–11); 4.12 (t, $^3J_{HH}$ = 2.40 Hz, 1H, C_5H_3); 3.76 (d, $^3J_{HH}$ = 12.30 Hz, 1H, H–12); 3.49 (d, $^3J_{HH}$ = 12.30 Hz, 1H, H–12); 2.21 (d, $^3J_{HH}$ = 13.80 Hz, 1H, H–13); 2.11 (d, $^3J_{HH}$ = 13.80 Hz, 1H, H–13); 0.046 (s, 9H, $Si(CH_3)_3$). **Elemental analysis** for $C_{25}H_{30}ClFeN_3Si$ (491.11 g/mol): Found C 61.13, H 6.25, N 8.71 %; Calculated C 61.08, H 6.15, N 8.55 %.

7-Chloro-4-[2-(N'-substituted aminomethyl)-N-ferrocenylmethyl(amino-2,2'-dimethylpropyl)] quinoline (**4.2**)

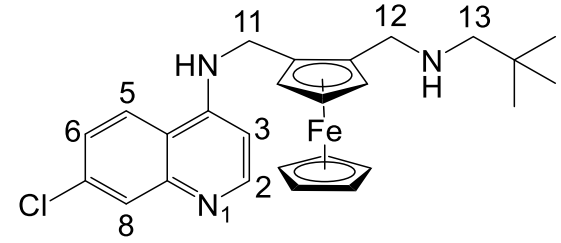

Quaternised ferroquine (0.201 g, 0.350 mmol); 2,2'–dimethylpropan-1-amine (0.340 mL, 2.90 mmol). Compound **4.2** was obtained as an orange solid (0.111 g, 67 %). R_f value = 0.52. **m.p.:** 143.1–144.9 ˚C. **^{1}H NMR (300.08 MHz, $CDCl_3$):** δ (ppm) = 8.56 (d, $^3J_{HH}$ = 5.70 Hz, 1H, H–2); 7.94 (d, $^4J_{HH}$ = 2.01 Hz, 1H, H–8); 7.72 (d, $^3J_{HH}$ = 9.00 Hz, 1H, H–5); 7.26 (dd, $^4J_{HH}$ = 2.10 Hz, $^3J_{HH}$ = 8.70 Hz, 1H, H–6); 6.46 (d, $^3J_{HH}$ = 5.10 Hz, 1H, H–3); 6.20 (br s, 1H, NH); 4.35–4.40 (m, 1H, H–11); 4.27–4.28 (m, 1H, C_5H_3); 4.23–4.24 (m, 1H, C_5H_3); 4.14–4.21 (m, 2H, C_5H_5 & H–11); 4.12 (t, $^3J_{HH}$ = 2.40 Hz, 1H, C_5H_3); 3.72 (d, $^3J_{HH}$ = 12.40 Hz, 1H, H–12); 3.51 (d, $^3J_{HH}$ = 12.40 Hz, 1H, H–12); 2.46 (d, $^3J_{HH}$ = 11.70 Hz, 1H, H–13); 2.39 (d, $^3J_{HH}$ = 11.40 Hz, 1H, H–13); 0.91 (s, 9H, $C(CH_3)_3$). **^{13}C{^{1}H} NMR (100.64 MHz, $CDCl_3$):** δ (ppm) = 152.1, 149.7, 149.3, 134.7, 128.6, 124.9, 121.9, 117.4, 99.2 (C_{Ar}); 86.1, 83.2 ($Fc_{quat.}$); 70.3, 69.8, 69.1, 66.4 (Fc); 62.5, 49.2, 42.0 (CH_2); 31.5 ($\underline{C}(CH_3)_3$); 27.9 ($C(\underline{C}H_3)_3$). **FT–IR (ATR, cm^{-1}):** ν = 3270 (br, N–H); 2948 (w,

N–H); 1611 (w, C=N); 1577 (s, C=C). **EI$^+$−MS** (475.1470 g.mol^{-1})**:** *m/z* 475.09 ([M]$^+$, 81 %). **Elemental analysis** for $C_{26}H_{30}ClFeN_3$ (475.15 g.mol^{-1}): Found C 65.30, H 6.59, N 8.32 %; Calculated C 65.66, H 6.36, N 8.84 %.

7-Chloro-4-[2-(N'-substituted aminomethyl)-N-ferrocenylmethyl(aminopropyl)trimethyl-silane]quinoline (**4.3**)

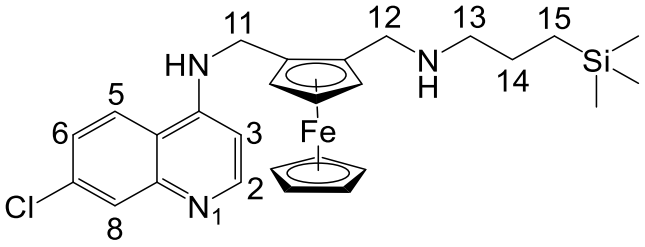

Quaternised ferroquine (0.199 g, 0.347 mmol); (3-aminopropyl)trimethylsilane (0.450 mL, 2.74 mmol). Compound **4.3** was isolated as a yellow solid (0.129 g, 72 %). R_f value = 0.36. **m.p.:** 149.4–150.9 ˚C. **^{1}H NMR (300.08 MHz, $CDCl_3$):** δ (ppm) = 8.54 (d, $^3J_{HH}$ = 5.40 Hz, 1H, H–2); 7.92 (d, $^4J_{HH}$ = 2.10 Hz, 1H, H–8); 7.81 (d, $^3J_{HH}$ = 9.00 Hz, 1H, H–5); 7.24 (dd, $^4J_{HH}$ = 2.40 Hz, $^3J_{HH}$ = 9.00 Hz, 1H, H–6); 6.48 (d, $^3J_{HH}$ = 5.40 Hz, 1H, H–3); 4.38 (d, $^3J_{HH}$ = 13.20 Hz, 1H, H–11); 4.29–4.30 (m, 1H, C_5H_3); 4.22–4.24 (m, 1H, C_5H_3); 4.17–4.20 (m, 6H, C_5H_5 & H–11); 4.10 (t, $^3J_{HH}$ = 2.40 Hz, 1H, C_5H_3); 3.71 (d, $^3J_{HH}$ = 12.30 Hz, 1H, H–12); 3.53 (d, $^3J_{HH}$ = 12.30 Hz, 1H, H–12); 2.60–2.70 (m, 2H, H–13); 1.46–1.59 (m, 2H, H–14); 0.42 (t, $^3J_{HH}$ = 8.40 Hz, 2H, H–15); −0.036 (s, 9H, $Si(CH_3)_3$). **^{13}C{^{1}H} NMR (100.64 MHz, $CDCl_3$):** δ (ppm) = 152.1, 150.1, 149.4, 134.7, 128.4, 124.7, 122.6, 117.8, 98.9 (C_{Ar}); 85.6, 83.5 ($Fc_{quat.}$); 70.7, 70.2, 69.2, 66.1 (Fc); 53.4, 47.8, 42.4, 24.2, 14.2 (CH_2); –1.74 ($Si(CH_3)_3$). **FT–IR (ATR, cm^{-1}):** ν = 3198 (br, N–H); 2954 (w, N–H); 1611 (w, C=N); 1570 (s, C=C). **EI$^+$−MS** (519.1552 g.mol^{-1})**:** *m/z* 519.14 ([M]$^+$, 49 %). **Elemental analysis** for $C_{27}H_{34}ClFeN_3Si$ (519.15 g.mol^{-1}): Found C 62.13, H 6.82, N 7.99 %; Calculated C 62.41, H 6.60, N 8.09 %.

7-Chloro-4-[2-(N'-substituted aminomethyl)-N-ferrocenylmethyl(amino-4,4'-dimethylpentyl)]quinoline (**4.4**)

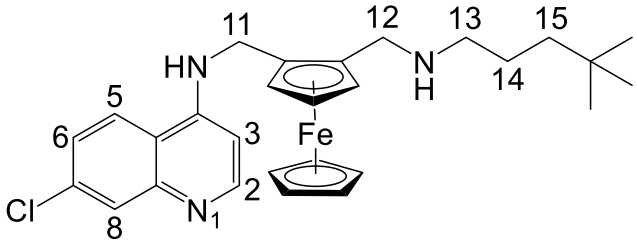

Quaternised ferroquine (0.194 g, 0.337 mmol); 4,4'-dimethylpentan-1-amine (0.380 mL, 2.64 mmol). Compound **4.4** was isolated as a yellow solid (0.144 g, 85 %). R_f value = 0.28. **m.p.:** 143.1–144.5 ˚C. **^{1}H NMR (300.08 MHz, $CDCl_3$):** δ (ppm) = 8.55 (d, $^3J_{HH}$

= 5.40 Hz, 1H, H–2); 7.92 (d, $^4J_{HH}$ = 2.40 Hz, 1H, H–8); 7.80 (d, $^3J_{HH}$ = 9.00 Hz, 1H, H–5); 7.25 (dd, $^4J_{HH}$ = 2.40 Hz, $^3J_{HH}$ = 9.00 Hz, 1H, H–6); 7.20 (br s, 1H, NH); 6.48 (d, $^3J_{HH}$ = 5.40 Hz, 1H, H–3); 4.37 (d, $^3J_{HH}$ = 12.90 Hz, 1H, H–11); 4.27–4.28 (m, 1H, C_5H_3); 4.20–4.21 (m, 1H, C_5H_3); 4.13–4.18 (m, 6H, C_5H_5 & H–11); 4.10 (t, $^3J_{HH}$ = 2.40 Hz, 1H, C_5H_3); 3.70 (d, $^3J_{HH}$ = 12.00 Hz, 1H, H–12); 3.53 (d, $^3J_{HH}$ = 12.00 Hz, 1H, H–12); 2.55–2.66 (m, 2H, H–13); 1.40–1.53 (m, 2H, H–14); 1.11 (t, $^3J_{HH}$ = 8.70 Hz, 2H, H–15); 0.85 (s, 9H, $C(CH_3)_3$). **$^{13}C\{^1H\}$ NMR (100.64 MHz, $CDCl_3$):** δ (ppm) = 152.1, 150.1, 149.4, 134.6, 128.5, 124.7, 122.6, 117.8, 98.9 (C_{Ar}); 85.6, 83.5 ($Fc_{quat.}$); 70.4, 70.2, 69.2, 66.1 (Fc); 50.9, 47.9, 42.4, 41.6 (CH_2); 30.1 ($\underline{C}(CH_3)_3$); 29.3 ($C(\underline{C}H_3)_3$); 25.0 (CH_2). **FT–IR (ATR, cm^{-1}):** ν = 3258 (br, N–H); 2956 (w, N–H); 1611 (w, C=N); 1578 (s, C=C). **EI$^+$–MS** (503.1782 g.mol^{-1})**:** *m/z* 503.12 ($[M]^+$, 78 %). **Elemental analysis** for $C_{28}H_{34}ClFeN_3$ (503.18 g.mol^{-1}): Found C 66.73, H 6.77, N 8.08 %; Calculated C 66.78, H 6.81, N 8.35 %.

7-Chloro-4-[2-(N'-substituted aminomethyl)-N-ferrocenylmethyl(aminomethyl)dimethylphenyl-silane]quinoline (**4.5**)

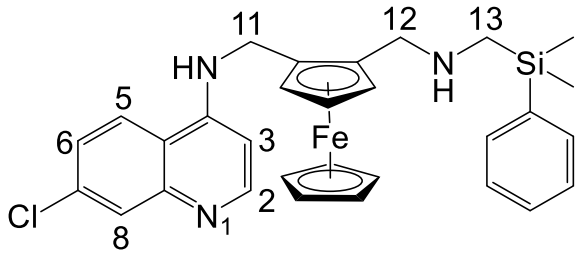

Quaternised ferroquine (0.101 g, 0.176 mmol); (aminomethyl)dimethylphenylsilane (0.25 mL, 1.39 mmol). Compound **4.5** was isolated as a yellow solid (0.0470 g, 48 %). R_f value = 0.66. **m.p.:** 157.0–159.4 ˚C. **^{1}H NMR (400.22 MHz, $CDCl_3$):** δ (ppm) = 8.52 (d, $^3J_{HH}$ = 5.40 Hz, 1H, H–2); 7.92 (d, $^4J_{HH}$ = 2.10 Hz, 1H, H–8); 7.56 (d, $^3J_{HH}$ = 9.00 Hz, 1H, H–5); 7.49–7.52 (m, 2H, Ph); 7.32–7.34 (m, 3H, Ph); 7.16 (dd, $^4J_{HH}$ = 2.10 Hz, $^3J_{HH}$ = 9.00 Hz, 1H, H–6); 6.50 (br s, 1H, NH); 6.46 (d, $^3J_{HH}$ = 5.40 Hz, 1H, H–3); 4.27–4.33 (m, 2H, C_5H_3 & H–11); 4.15–4.20 (m, 2H, C_5H_3 & H–11); 4.09–4.11 (m, 6H, C_5H_3 & C_5H_5); 3.75 (d, $^3J_{HH}$ = 12.60 Hz, 1H, H–12); 3.44 (d, $^3J_{HH}$ = 12.60 Hz, 1H, H–12); 2.46 (d, $^3J_{HH}$ = 14.00 Hz, 1H, H–13); 2.37 (d, $^3J_{HH}$ = 14.00 Hz, 1H, H–13); 0.34 (s, 6H, $Si(CH_3)_2$). **$^{13}C\{^1H\}$ NMR (100.64 MHz, $CDCl_3$):** δ (ppm) = 151.5, 149.4, 148.7, 136.9, 134.3, 133.2, 129.0, 128.0, 127.6, 124.6, 121.5, 117.1, 98.6 (C_{Ar}); 84.8, 82.9 ($Fc_{quat.}$); 70.0, 69.4, 68.7, 66.0 (Fc); 51.6, 41.6, 38.8 (CH_2); –3.99 ($Si(CH_3)$). **FT–IR (ATR, cm^{-1}):** ν = 3298 (br, N–H); 2948 (w, N–H); 1609 (w, C=N); 1578 (s, C=C). **EI$^+$–MS** (553.1396 g.mol^{-1})**:** *m/z* 553.14 ($[M]^+$, 12 %); 389.07 ($[M–NHCH_2Si(CH_3)_2Ph]^+$, 39.5 %); 388.03 ($[M–H–NHCH_2Si(CH_3)_2Ph]^+$, 100 %). **Elemental analysis** for $C_{30}H_{32}ClFeN_3Si·½H_2O$ (562.14 g.mol^{-1}): Found C 63.79, H 5.87, N 7.38 %; Calculated C 64.04, H 5.92, N 7.47 %.

7.4 Ferrocenyl−Containing Aminobenzothiazoles

6–Chloro–2–iodobenzothiazole (**4.6**)

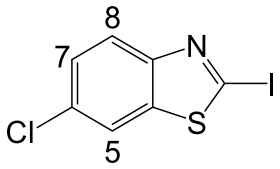

2-Amino-6-chlorobenzothiazole (0.325 g, 1.76 mmol) was dissolved in 3 M H_2SO_4 (25.0 mL) and cooled to 0˚C. Sodium nitrite (0.366 g, 5.30 mmol) was added to the yellow solution over 0.25 hr. Potassium iodide (0.332 g, 2.00 mmol) was added to the orange solution at 0˚C and allowed to stir at ambient temperature for 24 hr. The contents were diluted with H_2O/Et_2O (60.0 mL; 1:1), extracted using ethyl acetate (2 x 30.0 mL), collected the organic layer which was dried over Na_2SO_4 and the solvent was removed. The crude solid was purified using silica column chromatography [Ethyl acetate: Hexane (4:1)]. R_f = 0.88. Compound **4.6** was obtained as an orange solid (0.243 g, 47 %). **m.p.** 141.1–143.4 ˚C. **^{1}H NMR (300.08 MHz, $CDCl_3$):** δ (ppm) = 7.94 (d, $^3J_{HH}$ = 8.70 Hz, 1H, H–8); 7.84 (d, $^3J_{HH}$ = 2.40 Hz, 1H, H–5); 7.41 (dd, $^4J_{HH}$ = 2.40 Hz, $^3J_{HH}$ = 8.70 Hz, 1H, H–7). **^{13}C{^{1}H} NMR (100.64 MHz, $CDCl_3$):** δ (ppm) = 152.8; 140.2; 132.1; 127.2; 123.2; 120.1; 105.8. **FT–IR (ATR, cm^{-1}):** ν = 1588 (s, C=N); 1546 (m, C=C). **EI$^+$−MS** (294.8719 g.mol^{-1})**:** *m/z* 294.82 ([M]$^+$, 100 %).

6–Chloro–N–[(2–(dimethylaminomethyl)ferrocenylmethylamino)benzo[d]thiazole (**4.7**)

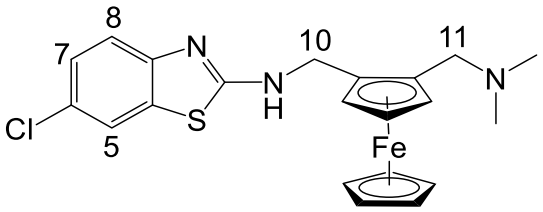

2-[(*N*,*N*-dimethylamino)methyl]ferrocene-methylamine (0.178 g, 0.652 mmol) was dissolved in THF (6.00 mL), followed by the addition K_2CO_3 and 2-iodo-6-chloro-benzothiazole (0.158 g, 0.536 mmol). The orange solution was heated at 30 ˚C for 3 days, after which water (20.0 mL) was added. The compound was extracted using DCM (2 x 20.0 mL), the organic layer was collected and dried over Na_2SO_4. The crude product was purified using silica column chromatography: Initially flush with diethyl ether to remove unreacted 2-iodo-6-chlorobenzothiazole, followed by the elution of compound **4.7** using Ethyl acetate: Hexane: Et_3N (75: 20: 5). R_f = 0.43. Compound **4.7** was isolated as an orange hydroscopic solid (0.128 g, 54 %). **^{1}H NMR (300.08 MHz, $CDCl_3$):** δ (ppm) = 8.31 (br s, 1H, NH); 7.48 (d, $^4J_{HH}$ = 2.10 Hz, 1H, H–5); 7.45 (d, $^3J_{HH}$ = 8.70 Hz, 1H, H–8); 7.22 (dd, $^4J_{HH}$ = 2.10 Hz, $^3J_{HH}$ = 8.70 Hz, 1H, H–7); 4.50 (br s, 2H, H–10); 4.28 (t, $^3J_{HH}$ = 1.80 Hz, 1H, C_5H_3); 4.10–4.12 (m, 6H, C_5H_3 & C_5H_5); 4.04 (t, $^3J_{HH}$ = 2.70 Hz, 1H, C_5H_3); 3.80 (d, $^3J_{HH}$ = 12.60 Hz, 1H, H–11); 2.84 (d,

$^{3}J_{HH}$ = 12.60 Hz, 1H, H–11); 2.23 (s, 6H, $N(CH_3)_2$). **$^{13}C\{^{1}H\}$ NMR (100.64 MHz, $CDCl_3$):** δ (ppm) = 166.7, 151.6, 131.8, 126.3, 126.1, 120.3, 119.2 (C_{Ar}); 84.1, 83.8 ($Fc_{quat.}$); 71.1, 70.3, 69.2, 65.8 (Fc); 58.1 (CH_2); 44.5 ($N(CH_3)_2$). **FT–IR (ATR, cm^{-1}):** ν = 3182 (br, N-H); 1597 (s, C=N); 1536 (s, C=C). **EI^{+}−MS** (439.0566 $g.mol^{-1}$)**:** *m/z* 439.04 ($[M]^{+}$, 86 %). **LCMS** for $C_{21}H_{22}ClFeN_3S$ (439.0566 $g.mol^{-1}$): *m/z* 440.1 $[M+H]^{+}$, t_R = 3.832 min, > 99 %.

N,N,N–Trimethyl{2–N'–(6–benzothiazolyl)aminomethyl}ferrocenylmethylammonium iodide (**4.8**)

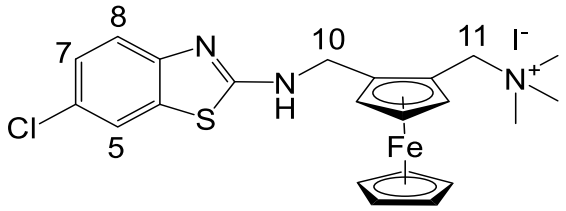

Compound **4.7** (0.172 g, 0.391 mmol) was dissolved in acetone (2.50 mL), followed by the addition of iodomethane. The contents were stirred at room temperature for 6 hr. The resulting solid was collected by suction filtration and washed with acetone. Compound **4.8** was isolated as a yellow solid (0.0420 g, 18 %). **m.p.:** 181.3 ˚C (Decomp. w/o melting). **^{1}H NMR (300.08 MHz, DMSO–d_6):** δ (ppm) = 8.22 (t, $^{3}J_{HH}$ = 5.10 Hz, 1H, NH); 7.81 (d, $^{4}J_{HH}$ = 2.10 Hz, 1H, H–5); 7.40 (d, $^{3}J_{HH}$ = 8.70 Hz, 1H, H–8); 7.26 (dd, $^{4}J_{HH}$ = 2.40 Hz, $^{3}J_{HH}$ = 8.70 Hz, 1H, H–7); 4.64 (d, $^{3}J_{HH}$ = 13.8 Hz, 1H, H–10); 4.60–4.61 (m, 1H, C_5H_3); 4.57–4.58 (m, 1H, C_5H_3); 4.39−4.55 (m, 4H, H–10 & H–11 & C_5H_3); 4.25 (s, 5H, C_5H_5); 2.96 (s, 9H, $N(CH_3)_3$). **$^{13}C\{^{1}H\}$ NMR (100.64 MHz, $CDCl_3$):** δ (ppm) = 166.6, 151.7, 132.7, 126.2, 125.3, 121.2, 119.4 (C_{Ar}); 87.2, 73.1 ($Fc_{quat.}$); 72.8, 71.5, 70.3, 69.9 (Fc); 64.1 (CH_2); 52.0($N(CH_3)_3$); 41.8 (CH_2). **FT–IR (ATR, cm^{-1}):** ν = 3218 (m, N–H); 1596 (s, C=N); 1558 (s, C=C). **ESI^{+}−HRMS** (580.9845 $g.mol^{-1}$)**:** *m/z* 454.0808 ($[M]^{+}$, 57 %), 395.0078 ([M−$N(CH_3)_3$, 100 %). **Elemental analysis** for $C_{22}H_{25}ClFeN_3SI$ (580.97 $g.mol^{-1}$): Found C 45.02, H 4.75, N 6.52 %; Calculated C 45.44, H 4.34, N 7.23 %.

General method for the synthesis of compounds 4.9−4.11

The amine was added to the flask under N_2, and dissolved in acetonitrile (15.0 mL). Compound **4.8** and K_2CO_3 (3 eq.) was added to the amine solution and the contents refluxed for 48 hr (monitored by TLC). Reaction mixture was cooled to room temperature and H_2O (30.0 mL) added. The compound was extracted using DCM (2 x 30.0 mL), the yellow organic layer collected and dried over Na_2SO_4. The compound was purified using silica column chromatography [ethyl acetate: petroleum ether: Et_3N (7:2.5:0.5)]. The second yellow band was collected.

6-Chloro-2-[2-(N'-substituted aminomethyl)-N-ferrocenylmethyl(aminomethyl)trimethylsilane] benzo[d]thiazole (**4.9**)

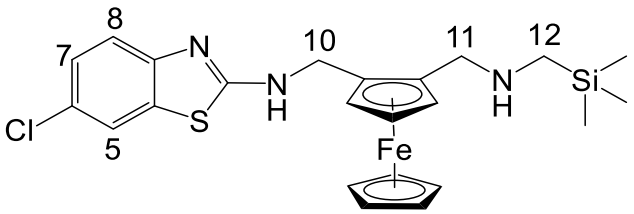

Compound **4.8** (0.0867 g, 0.149 mmol); (aminomethyl)trimethylsilane (0.160 mL, 1.19 mmol). R_f = 0.45. Compound **4.9** was isolated as a yellow solid (0.0465 g, 63 %). **m.p.:** 130.5−132.8 ˚C. **^{1}H NMR (300.08 MHz, $CDCl_3$):** δ (ppm) = 7.83 (br s, 1H, NH); 7.50 (d, $^3J_{HH}$ = 1.80 Hz, 1H, H–8); 7.46 (d, $^3J_{HH}$ = 8.70 Hz, 1H, H–5); 7.22 (dd, $^4J_{HH}$ = 2.10 Hz, $^3J_{HH}$ = 8.40 Hz, 1H, H–7); 4.46−4.57 (m, 2H, H–10); 4.28−4.29 (m, 1H, C_5H_3); 4.16−4.17 (m, 1H, C_5H_3); 4.12 (s, 5H, C_5H_5); 4.06 (t, $^3J_{HH}$ = 2.40 Hz, 1H, C_5H_3); 3.80 (d, $^3J_{HH}$ = 12.30 Hz, 1H, H–11); 3.43 (d, $^3J_{HH}$ = 12.30 Hz, 1H, H–11); 2.16 (d, $^3J_{HH}$ = 13.60 Hz, 1H, H–12); 2.07 (d, $^3J_{HH}$ = 13.60 Hz, 1H, H–12); 0.10 (s, 9H, $Si(CH_3)_3$). **^{13}C{^{1}H} NMR (100.64 MHz, $CDCl_3$):** δ (ppm) = 166.3, 151.4, 131.8, 126.3, 126.1, 120.3, 119.3 (C_{Ar}); 84.8, 83.9 ($Fc_{quat.}$); 70.6, 70.1, 69.1, 66.0 (Fc); 52.6, 43.9, 40.2 (CH_2); −2.31 ($Si(CH_3)_3$). **FT–IR (ATR, cm^{-1}):** ν = 3185 (w, N-H); 1594 (w, C=N); 1557 (s, C=C). **EI$^+$−MS** (497.0804 g.mol^{-1})**:** *m/z* 497.01 ($[M]^+$, 100 %). **LCMS** for $C_{23}H_{28}ClFeN_3SiS$ (497.05 g.mol^{-1}): *m/z* 498.1 $[M+H]^+$, t_R = 4.340 min, > 99 %.

6-Chloro-2-[2-(N'-substituted aminomethyl)-N-ferrocenylmethyl(amino-2,2'-dimethylpropyl)]-benzo[d]thiazole (**4.10**)

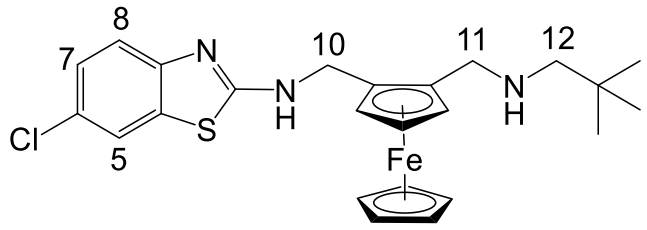

Compound **4.8** (0.0756 g, 0.130 mmol); 2,2'dimethylpropan-1-amine (0.120 mL, 1.02 mmol). R_f = 0.54. Compound **4.10** was isolated as a yellow solid (0.0452 g, 72 %). **m.p.:** 144.2−146.4 ˚C. **^{1}H NMR (300.08 MHz, $CDCl_3$):** δ (ppm) = 7.70 (br s, 1H, NH); 7.48 (d, $^3J_{HH}$ = 2.10 Hz, 1H, H–8); 7.46 (d, $^3J_{HH}$ = 8.70 Hz, 1H, H–5); 7.22 (dd, $^4J_{HH}$ = 2.10 Hz, $^3J_{HH}$ = 8.70 Hz, 1H, H–7); 4.59 (d, $^3J_{HH}$ = 13.80 Hz, 1H, H–10); 4.50 (d, $^3J_{HH}$ = 13.80 Hz, 1H, H–10); 4.28−4.29 (m, 1H, C_5H_3); 4.15−4.16 (m, 1H, C_5H_3); 4.12 (s, 5H, C_5H_5); 4.06 (t, $^3J_{HH}$ = 2.40 Hz, 1H, C_5H_3); 3.77 (d, $^3J_{HH}$ = 12.30 Hz, 1H, H–11); 3.45 (d, $^3J_{HH}$ = 12.30 Hz, 1H, H–11); 2.46 (d, $^3J_{HH}$ = 11.10 Hz, 1H, H–12); 2.37 (d, $^3J_{HH}$ = 11.10 Hz, 1H, H–12); 0.97 (s, 9H, $C(CH_3)_3$). **^{13}C{^{1}H} NMR (100.64 MHz, $CDCl_3$):** δ (ppm) = 166.3, 151.4, 131.9, 126.3, 126.1, 120.3, 119.3 (C_{Ar}); 85.2, 83.9 ($Fc_{quat.}$); 70.5, 70.1, 69.1, 65.9 (Fc); 62.3, 49.0, 43.8 (CH_2); 31.3 ($\underline{C}(CH_3)_3$); 28.1 ($C(\underline{C}H_3)_3$).

FT-IR (ATR, cm^{-1}): ν = 3198 (br, N-H); 1597 (w, C=N); 1543 (s, C=C). **EI$^+$−MS** (481.1034 g.mol^{-1})**:** *m/z* 481.08 ([M]$^+$, 73 %). **LCMS** for $C_{24}H_{28}ClFeN_3S$ (481.1034 g.mol^{-1}): *m/z* 482.1 [M+H]$^+$, t_R = 4.207 min, > 99 %.

6–Chloro–2–[2–(N'–substituted aminomethyl)–N–ferrocenylmethyl(aminopropyl)trimethyl–silane]benzo[d]thiazole (**4.11**)

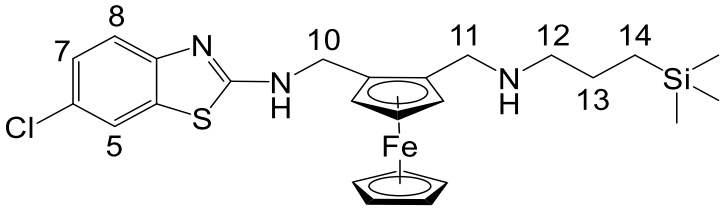

Compound **4.8** (0.0709 g, 0.122 mmol); 3-aminopropyl(trimethyl)-silane (0.180 mL, 1.07 mmol). R_f = 0.66. Compound **4.11** was isolated as a yellow hydroscopic solid (0.0334 g, 52 %). **^{1}H NMR (300.08 MHz, $CDCl_3$):** δ (ppm) = 8.42 (br s, 1H, NH); 7.49 (d, $^3J_{HH}$ = 2.10 Hz, 1H, H−8); 7.45 (d, $^3J_{HH}$ = 8.40 Hz, 1H, H−5); 7.22 (dd, $^4J_{HH}$ = 2.10 Hz, $^3J_{HH}$ = 8.40 Hz, 1H, H−7); 4.45−4.55 (m, 2H, H−10); 4.26−4.28 (m, 1H, C_5H_3); 4.11−4.14 (m, 6H, C_5H_3 & C_5H_5); 4.05 (t, $^3J_{HH}$ = 2.40 Hz, 1H, C_5H_3); 3.72 (d, $^3J_{HH}$ = 12.30 Hz, 1H, H−11); 3.48 (d, $^3J_{HH}$ = 12.30 Hz, 1H, H−11); 2.56−2.71 (m, 2H, H−12); 1.49−1.60 (m, 2H, H−13); 0.51 (t, $^3J_{HH}$ = 9.00 Hz, 2H, H−14); 0.017 (s, 9H, $Si(CH_3)_3$). **^{13}C{^{1}H} NMR (100.64 MHz, $CDCl_3$):** δ (ppm) = 166.3, 151.5, 131.8, 126.3, 126.1, 120.3, 119.2 (C_{Ar}); 85.1, 83.8 ($Fc_{quat.}$); 70.4, 70.2, 69.1, 65.9 (Fc); 52.6, 47.8, 43.9, 24.5, 14.3 (CH_2); −1.68 ($Si(CH_3)_3$). **FT−IR (ATR, cm^{-1}):** ν = 3190 (br, N−H); 1597 (s, C=N); 1562 (s, C=C). **EI$^+$−MS** (525.1116 g.mol^{-1})**:** *m/z* 525.00 ([M]$^+$, 93 %). **LCMS** for $C_{25}H_{32}ClFeN_3SiS$ (525.1116 g.mol^{-1}): *m/z* 526.1 [M+H]$^+$, t_R = 4.710 min, > 99 %.

7.5 Ferrocenylamines

General method for preparation of compounds 4.12 and 4.13

The amine (1 eq.) was added to the Schlenk flask under N_2, followed by the addition of ferrocenecarboxaldehyde and DCM (5.00 mL). The contents were heated at 35 ˚C for 5 hrs with the exclusion of light. The red solution was cooled to room temperature and MeOH (2.00 mL) added. $NaBH_4$ was slowly added to the solution, and the resulting orange solution was stirred at room temperature overnight. Water (20.0 mL) was added and the compound extracted using DCM (2 x 20.0 mL). The organic layer was collected, dried over Na_2SO_4 and the solvent removed.

N−(ferrocenylmethyl)−N−(trimethylsilyl)methanamine (**4.12**)

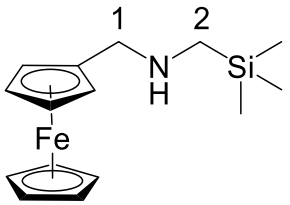

Ferrocenecarboxaldehyde (0.145 g, 0.678 mmol); (aminomethyl)trimethylsilane (0.100 mL, 0.747 mmol); $NaBH_4$ (0.0509 g, 1.34 mmol). Compound **4.12** was isolated as a sticky orange solid (0.196 g, 96 %). **^{1}H NMR (300.08 MHz, $CDCl_3$):** δ (ppm) = 4.21 (t, $^3J_{HH}$ = 1.50 Hz, 2H, C_5H_4); 4.12 (s, 5H, C_5H_5); 4.11 (t, $^3J_{HH}$ = 1.50 Hz, 2H, C_5H_4); 3.52 (s, 2H, H–1); 2.11 (s, 2H, H–2); 0.057 (s, 9H, $Si(CH_3)_3$). **^{13}C{^{1}H} NMR (100.64 MHz, $CDCl_3$):** δ (ppm) = 87.1 ($Fc_{quat.}$); 68.5, 68.3, 67.6 (Fc); 53.4, 40.0 (CH_2); −2.51 ($Si(\underline{C}H_3)_3$). **FT−IR (ATR, cm^{-1}):** ν = 3093 (br, N−H). **EI$^+$−MS** (301.0944 g.mol^{-1})**:** *m/z* 301.09 ([M]$^+$, 73 %). **Elemental analysis** for $C_{15}H_{23}FeNSi{\cdot}½H_2O$ (307.04 g.mol^{-1}): Found C 58.75, H 7.55, N 4.19 %; Calculated C 58.62, H 7.77, N 4.56 %.

*N−(ferrocenylmethyl)−N−2,2−dimethylpropan−1−amin*e (**4.13**)

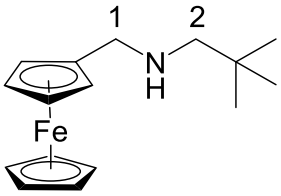

Ferrocenecarboxaldehyde (0.149 g, 0.696 mmol); 2,2'-dimethylpropan-1-amine (0.0900 mL, 0.768 mmol); $NaBH_4$ (0.0578 g, 1.53 mmol). Compound **4.13** was isolated as an orange solid (0.188 g, 95 %). **m.p.:** 55.2−57.2 ˚C. **^{1}H NMR (300.08 MHz, $CDCl_3$):** δ (ppm) = 4.21 (t, $^3J_{HH}$ = 1.80 Hz, 2H, C_5H_4); 4.13 (s, 5H, C_5H_5); 4.11 (t, $^3J_{HH}$ = 1.80 Hz, 2H, C_5H_4); 3.52 (s, 2H, H–1); 2.40 (s, 2H, H–2); 0.93 (s, 9H, $C(CH_3)_3$). **^{13}C{^{1}H} NMR (100.64 MHz, $CDCl_3$):** δ (ppm) = 87.8 ($Fc_{quat.}$); 68.4, 68.3, 67.5 (Fc); 62.2, 49.9 (CH_2); 31.5 ($\underline{C}(CH_3)_3$); 27.8 ($C(\underline{C}H_3)_3$). **FT−IR (ATR, cm^{-1}):** ν = 3088 (br, N−H). **EI$^+$−MS** (285.1174 g.mol^{-1})**:** *m/z* 285.02 ([M]$^+$, 79 %). **Elemental analysis** for $C_{16}H_{23}FeN{\cdot}⅛H_2O$ (288.71 g.mol^{-1}): Found C 66.83, H 8.46, N 4.63 %; Calculated C 66.50, H 8.17, N 4.85 %.

7.6 DMSO and Aqueous Media Stability Studies

A stability of the cyclopalladated complex **2.13** was monitored by NMR spectroscopy in DMSO−d_6 and DMSO−d_6:D_2O (9:1, v/v) and the stability of the ferrocenyl−containing aminoquinoline **4.3** and aminobenzothiazole **4.11** was monitored in DMSO−d_6:D_2O (9:1, v/v). The ^{1}H NMR spectra were recorded at 0 hr. The solution was warmed at 37 ˚C, and the stability monitored by ^{1}H NMR spectroscopy at 24, 48 and 72 hr time intervals to confirm stability of compound during the *in vitro* assay time period.

7.7 Pharmacological Studies

7.7.1 Antiplasmodial Assay

Continuous *in vitro* cultures of asexual erythrocyte stages of *P. falciparum* were maintained using a modified method of Trager and Jensen.[9] Quantitative assessment of antiplasmodial activity *in vitro* was determined *via* the parasite lactate dehydrogenase assay using a modified method described by Makler.[10] Antiplasmodial assay was conducted according to previously published methods.[10] A full dose-response was performed for all compounds to determine the concentration inhibiting 50% of parasite growth (IC_{50} value). Test samples were tested at a starting concentration of 100 μg/ml, which was then serially diluted 2-fold in complete medium to give 10 concentrations; with the lowest concentration being 0.2 μg/ml. Reference drugs were tested at a starting concentration of 1000 ng/ml. Active compounds were retested at starting concentrations of 10 μg/ml or 1000 ng/ml. The highest concentration of solvent to which the parasites were exposed had no measurable effect on the parasite viability (data not shown). The IC_{50} values were obtained using a non-linear dose-response curve fitting analysis via Graph Pad Prism v.4.0 software.

7.7.2 Cytotoxicity Assay

The MTT-assay is used as a colorimetric assay for cellular growth and survival, and compares well with other available assays.[11,12] The test samples were tested in triplicate on one occasion. The same stock solutions prepared for the antiplasmodial activity testing were used for the cytotoxicity tests. Dilutions were prepared on the day of the experiment in complete medium. Emetine was used as the reference drug. The initial concentration of emetine was 100 μg/ml, which was serially diluted in complete medium with 10-fold dilutions to give 6 concentrations, the lowest being 0.001 μg/ml. The same dilution technique was applied to the all test samples. The highest concentration of solvent to which the cells were exposed to had no measurable effect on the cell viability (data not shown). The IC_{50} values were obtained from full dose response curves, using a non-linear dose-response curve fitting analysis via GraphPad Prism v.4 software.

7.7.3 β−Haematin Inhibition Assay

The β-haematin inhibition assay was adapted from the method described by Wright and co-workers.[13] Compounds were prepared as a 10 mM stock solution in DMSO. The samples were tested at various concentrations between 5 and 500 μM. The stock solution was serially diluted

to give 12 concentrations in a 96 well flat-bottom assay plate. NP-40 detergent was added to mediate the formation of β-haematin (305.5 μM). A 25 mM stock solution of haematin was prepared by dissolving haemin (16.3 mg) in dimethyl sulfoxide (1 mL). A 177.76 μL aliquot of haematin stock was suspended in 20 ml of a 2 M acetate buffer at pH 4.7. The suspension was then added to the plate to give a final haematin concentration of 100 μM. The plate was then incubated for 16 hours at 37°C. The assay was analysed using the pyridine-ferrochrome method developed by Ncokazi and Egan.[14] 32 μL of a solution of 50% pyridine, 20% acetone, 20% water and 10% 2M HEPES buffer (pH 7.4) was added to each well. To this, 60 μL acetone was added to each well and mixed. The absorbance of the resulting complex was measured at 405 nm on a SpectraMax 340PC plate reader. The IC_{50} values were obtained using a non-linear dose-response curve fitting analysis *via* GraphPad Prism v.5.00 software.

7.7.4 Metabolic Stability Study

A single-point microsomal stability assay was conducted in 96-well format to determine the microsomal clearance of the compounds.[17] Test compounds and controls were prepared from 10 mM DMSO stock solutions. 0.40 mg protein/mL microsomes (pooled Human mixed gender, male Mouse BALB/c; Xenotech) were incubated with 1 μM test compound at 37 °C. Metabolic reactions were initiated by the addition of NADPH and the plates were incubated for 30 min. The reactions were quenched with acetonitrile containing carbamazepine as internal standard. The centrifuged and filtered samples were analysed by HPLC–MS/MS and the analyte:internal standard ratio at T30 compared to that at T0 to determine % compound remaining. Control standards (midazolam and propranolol) were included in the assay to provide quality control and an indication of the metabolic capacity of the microsomes used.

7.7.5 Antitrichomonal Assay

Cultures of the G3 strain of *T. vaginalis* were grown in 5 ml complete TYM Diamond's media in a 37 ^{o}C incubator for 24 hr. 50 mM stocks of the compounds were made by dissolving in DMSO and were screened against G3 strain of *T. vaginalis*. Untreated cells and those inoculated with 5 μl DMSO (0.1%) were used as controls. 5 μL of 50 mM stocks of the compound library were inoculated for a final concentration of 50 μM. Results were calculated based on cell counts utilising a haemocytometer after 24 hr. IC_{50} values were determined using serial dilution of the compounds and the calculated IC_{50} values confirmed using the same assay described above.

7.7.6 Antitumour Assay

Cytotoxicity (WST-1) Assay

Human A2780 and A2780*cis*R ovarian cancer cells and KMST–6 human fibroblast skin cells were obtained from the European Collection of Cell Cultures (Salisbury, UK). A2780 and A2780cisR cells were grown routinely in RPMI−1640 medium and the KMST−6 cells in DMEM medium. Both media supplemented with 10% fetal calf serum (FCS) and antibiotics (Penicillin Streptomycin) at 37 °C and 5% CO_2. Cytotoxicity was determined using the WST-1 [(4-[3-(4-Iodophenyl)-2-(4-nitrophenyl)-2H-5-tetrazolio)-1,3-benzene disulfonate] assay. Cells were seeded in 96-well plates as monolayers with 100 µL of cell solution (approximately 5 000 cells) per well and pre–incubated for 24 hr in medium supplemented with 10% FCS. Compounds were prepared as DMSO solutions, dissolved in the culture medium and serially diluted to the appropriate concentration, to give a final DMSO concentration of 0.5%. 100 µL of drug solution was added to each well and the plates were incubated for another 24 hr. Subsequently, WST-1 (10 µL solution) was added to the cells and the plates were incubated for a further 3 hr. The WST-1 tetrazolium salt is cleaved to a soluble formazan by a cellular mechanism, succinate-tetrazolium reductase system (EC 1.3.99.1), which occurs primarily at the cell surface. This bioreduction depends largely on the cellular production of NAD(P)H within metabolically intact and viable cells. The optical density, directly proportional to the number of surviving cells, was quantified at 450 nm, and background correction was performed at 600 nm, using a multiwell plate reader and the fraction of surviving cells was calculated from the absorbance of untreated control cells. Evaluation is based on means from three microcultures per concentration level and analysed via GraphPad Prism v.5.00 software.

Cytotoxicity (MTT) Assay

The oesophageal cancer cell–line WHCO1, derived from a primary oesophageal squamous cell carcinoma, was provided by Professor Rob Veale (University of the Witwatersrand, Johannesburg, South Africa). IC_{50} determinations were carried out using an MTT (3-(4,5-dimethylthiazol-2-yl)-2,5-diphenyltetrazolium bromide) assay.[15] 3000 cells were seeded per well in 96–well plates. Plates were incubated at 37 °C under 5% CO_2 (24 hours), after which aqueous DMSO solutions of each compound (10 µL, with a constant final concentration of DMSO of 0.2%) were plated at various concentrations. After 48 hours incubation, observations were made, and MTT (10 µL) solution added to each well. After 4 hours of incubation, solubilisation solution (100 µL) was added to each well, and incubated overnight. Plates were

read at 595 nm on a BioTek microplate reader, and IC50 values calculated using Graph Pad Prism v.4.0. Package of GraphPad Software, San Diego, USA.

7.7.7 ***Plasmodium Berghei infected Mouse Model***

Ethics statement

Animal experiments were performed at the animal unit of the PK laboratory of the University of Cape Town, division of clinical pharmacology following the grant of ethical approval from the Animal Research Ethics Committee of the Faculty of Health Sciences of the University of Cape Town (project no. 013/028).

Environmental Conditions for the Animals

Male C57BL/6 mice 12 to 16 weeks old, weighing 25 to 35 g were obtained from the University of Cape Town`s animal unit. They were kept in cages (a maximum of 5 mice per cage) in a temperature−controlled room with a 12 hr day/night light cycle. Ample dried food and water were supplied, and their sanitation was monitored daily. The animals were acclimatised to the test environment for 3 to 4 days before the experiment started.

In Vivo Toxicity Evaluation

Three healthy male C57BL/6 mice ($mass_{average}$ = 35 g) were administered doses of compound **2.13** which were prepared in HPMC:DMSO (9:1; v/v). Each mouse received the dosage *via* oral gavage at their respective dose concentration and volumes as shown below:

M_1: 270 µL of 50 mg/kg (6.47 mg/mL)
M_2: 280 µL of 30 mg/kg (3.81 mg/mL)
M_3: 250 µL of 10 mg/kg (1.40 mg/mL)

The mice received the above specified dose four times (0, 24, 48 & 72 hr) during the course of the experiment, and the weight of the mice monitored throughout.

In Vivo Efficacy Evaluation

Plasmodium berghei transfected with green fluorescence protein (strain ANKA), a chloroquine−sensitive strain, was stored in liquid nitrogen. Parasites were thawed and administered intraperitoneally (IP) to infect two donor mice a week before the experiment

commenced. Then the parasite−infected red blood cells (RBCs) were collected into heparinised tubes by tail bleeding and the parasitaemia was determined using flow cytometry (≥ 15%). Finally, each of the test animals received 200 µl of the *P. berghei*−infected RBCs (1×10^7 per 200µl PBS) IP to infect them with the parasite. There were three animals per dose group, and each of them received the dosage *via* oral gavage at their respective dose concentration and volumes as shown below:

Group A: the negative control group received 200 µL of the drug vehicle alone (placebo).

Group B: the test group received 200 µL of 50 mg/kg (6.33 mg/ml) of compound **2.13** in HPMC: DMSO (9:1; v/v). Average mass of mice = 25 g.

Group C: the positive control group received 240 µL of 20 mg/kg CQ (2.50 mg/ml, free base) in H_2O. Average mass of mice = 30 g.

The volumes were adjusted relative to the weight of the mouse.

The test compound was administered to the animals once a day for four days. The first dose was administered 2 hr after infection, followed by the second, third and fourth dose at intervals of 24 hr. Blood samples were collected *via* tail bleeding in tubes containing PBS on day 5, and % parasitaemia was determined with FACSCalibur™ using the software CellQuestPro.[16]

7.8 References

1 D. L. Klayman, J. F. Bartosevich, T. S. Griffin, C. J. Mason and J. P. Scovill, *J. Med. Chem.*, 1979, **22**, 855–862.

2 G. Zhao and C. Yuan, *Transit. Met. Chem.*, 1994, **19**, 218–220.

3 B. K. Srivastava, S. K. Srivastava, O. P. Pandey and S. K. Sengupta, *Indian J. Chem. A Inorg. Bioinorg. Phys. Theor. Anal. Chem.*, 1996, **35A**, 57–59.

4 C. Biot, B. Pradines, M.-H. Sergeant, J. Gut, P. J. Rosenthal and K. Chibale, *Bioorg. Med. Chem. Lett.*, 2007, **17**, 6434–6438.

5 M. Bennett and A. Smith, *J. Chem. Soc., Dalton Trans.*, 1974, 233–241.

6 C. White, A. Yates and P. M. Mailtlis, *Inorg. Synth.*, 1992, **29**, 228–234.

7 A. M. M. Meij, S. Otto and A. Roodt, *Inorg. Chim. Acta*, 2005, **358**, 1005–1011.

8 C. Biot, L. Delhaes, C. M. N'Diaye, L. A. Maciejewski, D. Camus, D. Dive and J. S. Brocard, *Bioorg. Med. Chem.*, 1999, **7**, 2843–2847.

9 W. Trager and J. B. Jensen, *Science*, 1976, **193**, 673–675.

10 M. T. Makler, J. M. Ries, J. A. Williams, J. E. Bancroft, R. C. Piper, B. L. Gibbins and D. J. Hinrichs, *Am. Soc. Trop. Med. Hyg.*, 1993, **48**, 739–741.

11 T. Mosmann, *J. Immunol. Methods*, 1983, **65**, 55–63.

12 L. V. Rubinstein, R. H. Shoemaker, K. D. Paull, R. M. Simon, S. Tosini, P. Skehan, D. A. Scudiero, A. Monks and M. R. Boyd, *J. Natl. Cancer Inst.*, 1990, **82**, 1113–1118.

13 R. D. Sandlin, M. D. Carter, P. J. Lee, J. M. Auschwitz, S. E. Leed, J. D. Johnson and D. W. Wright, *Antimicrob. Agents Chemother.*, 2011, **55**, 3363–3369.

14 K. K. Ncokazi and T. J. Egan, *Anal. Biochem.*, 2005, **338**, 306–319.

15 J. van Meerloo, G. J. L. Kaspers and J. Cloos, in *Cancer Cell Culture: Methods and Protocols (Methods in Molecular Biology)*, ed. I. A. Cree, Human Press, 2nd edition, 2011, vol. 731, pp. 237–245.

16 B. Franke-Fayard, H. Trueman, J. Ramesar, J. Mendoza, M. van der Keur, R. van der Linden, R. E. Sinden, A. P. Waters and C. J. Janse, *Mol. Biochem. Parasitol.*, 2004, **137**, 23–33.

17 L. Di, E. H. Kerns, N. Gao, S. Q. Li, Y. Huang, J. L. Bourassa and D. M. Huryn, *J. Pharm. Sci.*, 2004, **93**, 1537–1544.